Breaching of river levees: analytical flow modelling and experimental hydro-morphodynamic investigations

Dissertation

submitted to and approved by the

Faculty of Architecture, Civil Engineering and Environmental Sciences
University of Braunschweig – Institute of Technology

and the

Faculty of Engineering
University of Florence

in candidacy for the degree of a
Doktor-Ingenieur (Dr.-Ing.) /
Dottore di Ricerca in Mitigation of Risk due to Natural Hazards on Structures and Infrastructures[*)]

by

Giovanni Michelazzo
Born 16 April 1983
from Florence, Italy

Submitted on	16 September 2013
Oral examination on	7 November 2013
Professorial advisors	Prof. Hocine Oumeraci Prof. Enio Paris

2014

*) Either the German or the Italian form of the title may be used.

To Laura

Preface

Working on a scientific research project is not an easy task. Several qualities from the candidate and surrounding conditions are required in order to perform a research project that is worth.

Attitude to the scientific research implies that one has a good basic knowledge of the subjects that will be studied, the capacity of analysing new topics, the determination and patience in looking for the aim of the study, the ability to propose solutions and to foresee likely problems and drawbacks.

A sound research originates from a good idea that is based on the knowledge of the international literature about the proposed object. Scientific research makes sense only if it brings novelties with respect to the current knowledge.

The initial idea has to be formulated in an overall framework: a kind of roadmap is necessary in order to avoid to get lost in the immense land of the science.

Moreover, one of the most important thing, when dealing with physical phenomenon, is to be able to understand which parts of the phenomenon are actually relevant according to the main purpose of the project, and how, where and when to observe them.

Final achievements of a research are always the result of the efforts of a working group. A team of people has been involved in the three-years project of the present PhD and my thanks are for all of them.

Prof. E. Paris and Prof. H. Oumeraci have been a constant and fundamental guide during all the phases: from the initial literature review, to the definition and update of the methodology, from the full support of the laboratory investigations to the analysis and interpretation of the results. They have pursued me toward an interesting and valid project.

I am also grateful to Prof. Luca Solari and Dr. Andreas Kortenhaus, who often gave me useful hints to solve problems and to improve my work.

A special thanks to Prof. L. Nagy, who offered me the possibility to collect data about real breaching events at the University of Techniques of Budapest.

Both the Department of Civil and Environmental Engineering of Florence (DICEA) and of Leichtweiß-Institute of Braunschweig (LWI) supported me in many steps of this path. I feel grateful to: the colleagues for the scientific, but not only, discussions; the workshop people (Mauro and Muzio in Florence; Jochen, Bernd, Rainer, Bernd and Uwe in Braunschweig) for the prompt and accurate work in the lab; the secretaries (Serena and Gabi) for the support in administrative and organisational issues.

I hope that this research will contribute to advance the understanding of the phenomenon of levee breaching, and that it will help for the mitigation of the tragic consequences that flood risk still has on the human community.

Abstract

Breaching of river levees often causes catastrophic damages to the hinterland which is supposed to be protected by the levees. The breaching process has been studied during the last decades mainly with reference to the case of dams and sea dikes, while specific knowledge and modelling tools are missing to address the case of river levees.

A new process-oriented approach was developed in the present study in order to advance the knowledge about the processes associated with the breaching of river levees and to investigate the physical conditions that determine a final configuration of the breach. The interaction between breach development and river hydro-morphodynamics was considered to be the key to understand the levee breaching process.

The river-breach system has been analysed by means of two series of laboratory experiments and an analytical model of the river flow, which give complementary descriptions about the breaching process. Results from the fixed bed laboratory investigations highlight the hydrodynamic processes that take place in a channel when a lateral outflow occurs (as in case of a levee breach). The movable bed investigations provide one of the few existing laboratory experiments reproducing a non-cohesive levee breach together with the river flow until an equilibrium stage is achieved. A simple overall picture of the hydrodynamic processes and a new interpretation of the breaching at the equilibrium stage are given by the analytical flow model.

This research provides the necessary knowledge about the breaching process of river levees in order to support more process-oriented approaches for the assessment of the breach features that can develop in a river levee. The application of the results to real case data shows that the research direction is appropriate and it pushes toward future research studies.

Sommario

Il collasso di argini fluviali durante eventi di piena è causa di frequenti inondazioni dei territori circostanti la cui protezione si basa proprio sull'affidabilità dei rilevati arginali. Il processo di formazione e sviluppo di una breccia in un argine (*breaching* in letteratura scientifica) è stato oggetto di studi negli ultimi decenni. D'altronde, le conoscenze e i modelli finora sviluppati si sono concentrati sulle casistiche di dighe di invasi e di dighe costiere, mentre scarsi sono i contributi riguardanti il caso specifico di argini fluviali.

Il presente lavoro di ricerca ha sviluppato un nuovo approccio di studio finalizzato ad una più profonda comprensione dei processi fisici associati allo sviluppo di una breccia fluviale fino al raggiungimento di uno stato di equilibrio nel processo di rottura. Il punto chiave focalizzato dalla ricerca riguarda l'interazione tra lo sviluppo della rotta e i meccanismi idro-morfodinamici del corso d'acqua.

L'approccio del lavoro è stato di natura sia sperimentale che modellistica. In particolare, lo svolgimento di due campagne sperimentali in canaletta di laboratorio in condizioni di fondo fisso e fondo mobile e l'implementazione di un modello analitico unidimensionale hanno fornito degli elementi per un'analisi integrata del processo di breccia. Gli esperimenti di laboratorio a fondo fisso hanno fornito una chiave di comprensione dell'idrodinamica del campo di moto in presenza di uno sfioro laterale di portata (rappresentativo della breccia arginale), mentre gli esperimenti a fondo mobile hanno riprodotto la rottura di un argine in materiale sciolto a scala di laboratorio fino al raggiungimento di uno stato di equilibrio dell'intero sistema fisico. Questi ultimi sono tra i pochi esperimenti esistenti, nella letteratura scientifica internazionale, riguardanti lo studio di brecce fluviali in condizioni di equilibrio stazionario e fondo mobile. Infine, l'impiego di un modello unidimensionale semplificato ha consentito di simulare i principali aspetti idrodinamici del problema ed ha fornito una prima interpretazione teorica sull'esistenza di un equilibrio nel sistema breccia-fiume.

La presente ricerca fornisce una solida base per la conoscenza e lo studio del processo di formazione e sviluppo di una breccia in un argine fluviale in materiale sciolto. I dati, le analisi e gli strumenti forniti potranno essere utilizzati come base di partenza per sviluppare nuovi e sempre più realistici approcci di valutazione delle caratteristiche finali di una breccia arginale, informazioni, queste, fondamentali per la stima delle potenziali conseguenze avverse in caso di scenari d'esondazione. L'applicazione dei risultati ad alcuni casi reali mostra come l'approccio sia appropriato per fornire delle valutazioni realistiche e incoraggia futuri lavori di ricerca.

Kurzfassung

Der Bruch von Flussdeichen ist oft mit dramatischen Folgen verbunden. Die bisherigen Untersuchungen über den Deichbruch erfolgten vorwiegend im Seedeich- und Dammbau, so dass heute die wissenschaftlichen Grundlagen und Modelle für die Beschreibung des Bruches von Flussdeichen nicht im ausreichenden Maße vorliegen. In dieser Studie wurde ein neues Verfahren entwickelt, das dazu beiträgt, das Grundlagenwissen hinsichtlich der beteiligten Prozesse wesentlich zu erweitern und die Bedingungen, die den Endzustand des Deichbruches entscheidend bestimmen, genauer zu untersuchen. Dabei wird davon ausgegangen, dass der Schlüssel zum Verständnis der hierfür verantwortlichen Prozesse in eine genaue Untersuchung der Interaktion zwischen Deichbruch und hydro-morphodynamischen Veränderungen im Fluss selbst besteht. Deshalb wurde das "Fluss-Deichbruch-System" durch zwei verschiedene Laborexperimente (Modell mit fester Sohle und Modell mit beweglicher Sohle) und ein analytisches Strömungsmodell untersucht, die sich zur Beschreibung des Deichbruchprozesses ideal ergänzen.

Das analytische Strömungsmodell, zusammen mit den Laborergebnissen, ermöglicht die Bestimmung eines vereinfachten Gesamtbildes der beteiligten hydrodynamischen Prozesse sowie eine neue Interpretation des Deichbruches beim Erreichen des Gleichgewichtzustands zwischen Fluss und Deichbruch.

Die Ergebnisse dieser Studie stellen einen wesentlichen Beitrag zu den wissenschaftlichen Grundlagen über die Prozesse beim Bruch von Flussdeichen dar, die für künftige detailliertere und mehr prozessbasierte Verfahren und Vorhersagemodelle benötigt werden. Die praktische Anwendung der Ergebnisse für einige reale Fallstudien aus früheren Deichbrüchen unterstreicht die Richtigkeit der hier verwendeten Forschungsansätze und die Notwendigkeit für weitere Studien in diese Richtung.

Table of Contents

List of Figures iv

List of Tables xi

List of Symbols xii

1 Introduction 1

1.1 Problem definition and motivations 1
1.2 Objectives 2
1.3 Methodology 2

2 Levee breaching processes and modelling: state-of-the-art review and specification of objectives and methodology 5

2.1 Causes of breach initiation 5
2.1.1 Morphological and hydraulic boundary conditions 6
2.1.2 Initial conditions: overtopping and seepage flow 8
2.1.3 Implications for the present study 9
2.2 Review of breaching parameters 9
2.2.1 Geometrical parameters 10
2.2.2 Temporal parameters 14
2.2.3 Breach initiation 15
2.2.4 Breach location 15
2.2.5 Implications for the present study 16
2.3 Breaching processes 16
2.3.1 Breaching induced by overtopping 16
2.3.2 Breaching induced by seepage 19
2.3.3 Implications for the present study 21
2.4 Hydrodynamic processes 22
2.4.1 Hydrodynamics of flow through the breach 22
2.4.2 Hydrodynamics of flow along the breach 23
2.4.3 Implications for the present study 25
2.5 Sediment transport processes and models 25
2.5.1 Sediment transport processes 25
2.5.2 Sediment transport models 26
2.5.3 Implications for the present study 28
2.6 Available breach models 28
2.6.1 Classification of available breach models 29
2.6.2 Limitations and uncertainties of available breach models 33
2.6.3 Implications for the present study 34
2.7 Specification of objectives and methodology 34
2.7.1 Objectives 34
2.7.2 Methodology and procedure 35

3 Fixed bed laboratory investigations 37

3.1 Experimental set-up 37
3.1.1 Experimental facilities 37
3.1.2 Measuring techniques and observations 41
3.2 Testing programme and test procedure 44
3.2.1 Test series 44
3.2.2 Test procedure 47
3.3 Measured data and experimental results 47

3.3.1 Spatial reference system 48
3.3.2 Measured data post-processing 48
3.3.3 Experimental results for each test series 51
3.4 Data analysis with a focus on process understanding 62
3.4.1 Analysis of the flow hydrodynamics 62
3.4.2 Analysis of the three-dimensional zones 64
3.4.3 Analysis of the De Marchi hypothesis 67
3.4.4 Computational analysis of the flow along the side weir 69
3.4.5 Characteristic parameters of the main flow 75
3.5 Summary and concluding remarks 85

4 Movable bed laboratory investigations 89

4.1 Experimental set-up 89
4.1.1 Experimental facilities 89
4.1.2 Measuring techniques and observations 93
4.2 Testing programme and test procedure 96
4.2.1 Test series 96
4.2.2 Test procedure 99
4.3 Measured data and experimental results 99
4.3.1 Spatial reference system 100
4.3.2 Measured data post-processing 101
4.3.3 Experimental results for each test series 104
4.4 Data analysis with a focus on process understanding 116
4.4.1 Analysis of breach discharge 118
4.4.2 Analysis of breach length 121
4.4.3 Analysis of river hydrodynamics 122
4.4.4 Analysis of sediment transport processes 127
4.4.5 Analysis of the breach morphology 132
4.5 Summary and concluding remarks 137

5 Analytical flow modelling 141

5.1 Hydrodynamic features of the flow along the breach 141
5.2 The De Marchi's analytical model 146
5.2.1 Mathematical formulation 146
5.2.2 New form of the De Marchi solution 149
5.2.3 Model implementation in subcritical flow 151
5.3 Application of the proposed model to laboratory and field data 157
5.3.1 Application to available laboratory data 157
5.3.2 Application to real river levee breach data 159
5.3.3 Subcritical limitation of the breach features 167
5.4 Summary and concluding remarks 171

6 Conceptual model of a levee breaching 175

6.1 Inception of the breaching (stage 1) 175
6.2 Progressive erosion of downstream side (stage 2) 177
6.3 Progressive erosion of upstream side (stage 3) 180
6.4 Final breach configuration (stage 4) 185
6.5 Summary of breaching stages 1-4 189
6.6 Summary and concluding remarks 191

7 Summary, conclusions and recommendations 193

7.1 Summary of key results 193
7.2 Applicability of the results 195
7.3 Future research 195

References 197
Annex A 205

List of Figures

Figure 2.1: Definitions of terms associated with river levees. 7

Figure 2.2: Levee breach as pathway between risk-source and risk-receptors. 7

Figure 2.3: Common failure mechanisms of the breaching of a flood embankment (Morris et al., 2007). 8

Figure 2.4: Californian levee (from Nagy and Tóth, 2005). 11

Figure 2.5: Plan view (plane xy) of a breach developed upon a river levee. 11

Figure 2.6: Definition of terms associated with levee breaches (section view yz). 12

Figure 2.7: Definition of terms associated with levee breaches (frontal view xz). 12

Figure 2.8: Stages of breach growth initiated by overtopping: a) initial levee; b) start of stage 1; c) end of stage 1; d) stage 2; e) stage 3; f) stage 4. 17

Figure 2.9: Breaching processes in laboratory test on homogeneous non-cohesive embankment (Hassan et al., 2004). 18

Figure 2.10: Breaching processes observed for cohesive material (Hassan et al., 2004). 19

Figure 2.11: Schematic representation of seepage and underseepage flow. 19

Figure 2.12: Stages of breach growth initiated by piping: a) stage 1; b) stage 2; c) stage 3; d) stage 4. 20

Figure 3.1: Sketch of the experimental apparatus (plan view: the dimensions are in mm). 39

Figure 3.2: Cross section A-A' of the flume (the dimensions are in mm) 39

Figure 3.3: Aerial picture of the flume. 40

Figure 3.4: View of the flume from the main channel: on the left, the side weir. 40

Figure 3.5: View of the flume: zoom on the side weir. 40

Figure 3.6: Tracers used in PTV technique: heavy (a) and light (b) beads. 42

Figure 3.7: CAM used in PTV technique from the ceiling. 43

Figure 3.8: UV lights used in PTV technique. 43

Figure 3.9: Plan view of the dimensionless coordinate system (format: x*, y*, z*). 48

Figure 3.10: Rating curve at downstream section of lateral channel. 49

Figure 3.11: Rating curve at downstream section of main channel for sluice gate at Y_g = 2 cm. 49

Figure 3.12: Flow regime at downstream section of main channel for sluice gate at Y_g = 2 cm. 50

Figure 3.13: Water surface profiles of series A with Y_g = 2 cm. 51

Figure 3.14: Water surface profiles of series A with Y_g = 3.4 cm. 52

Figure 3.15: Plan view of the flume: measurement cross sections for tests of series B. 53

Figure 3.16: Flow depth profile for test B10 (L18Q10.1Yg2.0). 53

Figure 3.17: Water surface profiles of series B: line plots. 54

Figure 3.18: Water surface at side weir site for test B11 (L23Q10.0Yg2.0). 54

Figure 3.19: Mean velocity along the flume for series B. 55
Figure 3.20: Flow velocity distribution for test B10 (L18Q10.1Yg2.0) at cross section CS1. 56
Figure 3.21: Flow velocity distribution for test B10 (L18Q10.1Yg2.0) at cross section CS3. 56
Figure 3.22: Flow velocity distribution for test B10 (L18Q10.1Yg2.0) at cross section CS4. 57
Figure 3.23: Streamlines of flow field at water surface for test B10 (L18Q10.1Yg2.0). 58
Figure 3.24: Contours of U_x at water surface for test B10 (L18Q10.1Yg2.0). 58
Figure 3.25: Contours of U_y at water surface for test B10 (L18Q10.1Yg2.0). 59
Figure 3.26: Contours of flow angles at water surface for test B10 (L18Q10.1Yg2.0). 59
Figure 3.27: Contours of U_y/U_{mean} vertical profiles for test B11 (L23Q10.0Yg2.0) at cross section x* = 0.383. 60
Figure 3.28: Water surface profiles of series C. 61
Figure 3.29: Mean velocity along the flume for series C. 61
Figure 3.30: Fr_x contours for test B11 (L23Q10.0Yg2.0). 63
Figure 3.31: Fr_y contours for test B11 (L23Q10.0Yg2.0). 63
Figure 3.32: Deflection of surface flow field through the side weir (red streamlines) and ongoing flow (green ones). 64
Figure 3.33: Image of heavy tracers and assumed dividing curve on the bottom. 64
Figure 3.34: 3D view of dividing surface detected from PTV images. 65
Figure 3.35: Separation zone at the side opposite to the side weir. 65
Figure 3.36: Helicoidal flow and reverse flow downstream the side weir. 66
Figure 3.37: Sketch of the flow field zones detected during the detailed test B10 (L18Q10.1Yg2.0). 67
Figure 3.38: Scheme for specific energy head computation. 67
Figure 3.39: Specific energy at up- and downstream sections. 68
Figure 3.40: Computational scheme for flow analysis. 69
Figure 3.41: Calibrated side weir coefficient as a function of Fr_u and comparison with other formulations. 70
Figure 3.42: Computational scheme for transversal flow velocity computation (cross section) 70
Figure 3.43: Longitudinal trend of flow velocity components for test B11 (L23Q10.0Yg2.0). 71
Figure 3.44: Comparison between up- and downstream U_x and U_y for all tests of series B. 72
Figure 3.45: Sketch of flow deflection at side weir site. 72
Figure 3.46: Longitudinal trend of flow angles for test B11 (L23Q10.0Yg2.0). 73
Figure 3.47: Comparison between up- and downstream flow angles for every test of series B. 73
Figure 3.48: Longitudinal trend of shear stress components for test B11 (L23Q10.0Yg2.0). 74
Figure 3.49: Up- and downstream shear stresses for tests of series B and mean shear stress at side weir. 75
Figure 3.50: Scheme for momentum balance computation. 76
Figure 3.51: Discharge ratio versus length ratio for series B. 78
Figure 3.52: Discharge ratio versus length ratio for series C. 78

Figure 3.53: Momentum ratio versus length ratio for series B. 79
Figure 3.54: Momentum ratio versus length ratio for series C. 79
Figure 3.55: Water depth ratio versus length ratio for series B. 80
Figure 3.56: Water depth ratio versus length ratio for series C. 80
Figure 3.57: Velocity ratio versus length ratio for series B. 81
Figure 3.58: Velocity ratio versus length ratio for series C. 81
Figure 3.59: Flow regime in the Froude graph for series B. 82
Figure 3.60: Flow regime in the Froude graph for series C. 82
Figure 3.61: Side weir aspect ratio versus length ratio for series B. 83
Figure 3.62: Side weir aspect ratio versus length ratio for series C. 83
Figure 4.1: Sketch of the experimental apparatus (plan view). 91
Figure 4.2: Cross section A-A' of the flume. 92
Figure 4.3: Aerial picture of the flume. 92
Figure 4.4: Downstream part of the flume: on the left, the sharp-crested weir, on the right, the sluice gate. 93
Figure 4.5: Drain system in the flume (a): toe drain detail (b), test for control seepage line (purple line, c)....93
Figure 4.6: Experimental apparatus with measurement devices (distorted scale). 95
Figure 4.7: Geotextile protection of the levee. 97
Figure 4.8: Coordinate system for the flume (plan view). 100
Figure 4.9: Coordinate system for the flume (section view A-A'). 100
Figure 4.10: Sharp-crested weir equation of lateral channel (calibration)....102
Figure 4.11: Definition of breach erosion lengths: a) before breaching; b) after breach inception. 104
Figure 4.12: Bed topography before breaching (test A1 - Q10.1Yg0.4S0.1%)....105
Figure 4.13: Longitudinal profiles of water level, levee crest and bed elevation before breaching (test A1 - Q10.1Yg0.4S0.1%)....105
Figure 4.14: Temporal development of water level at USs and river bed (test A1 - Q10.1Yg0.4S0.1%)....106
Figure 4.15: Temporal development of breach length (test A1 - Q10.1Yg0.4S0.1%). 106
Figure 4.16: High longitudinal velocity of the approaching flow (test A1 - Q10.1Yg0.4S0.1%). 107
Figure 4.17: Slowing down of flow downstream the breach (test A1 - Q10.1Yg0.4S0.1%). ..108
Figure 4.18: Significant flow deflection (U_x and U_y similar) at the breach site (test A1 - Q10.1Yg0.4S0.1%)....108
Figure 4.19: Separation zone at the side opposite to the breach (test A1 - Q10.1Yg0.4S0.1%)..... 109
Figure 4.20: Bed topography after breaching (test A3 - Q29.2Yg2.2S0.1%). 109
Figure 4.21: Longitudinal profiles of water surface, levee crest and river bed elevation after breaching (test A3 - Q29.2Yg2.2S0.1%). 110

Figure 4.22: Areal picture of the flume at the end of test A3 (Q29.2Yg2.2S0.1%). 110
Figure 4.23: Bed topography after breaching (test B6 - Q60.3Yg5.8S0.1%). 112
Figure 4.24: Temporal development of breach water discharge (test B10 - Q55.2Yg5.0S0.1%).. 112
Figure 4.25: Temporal development of breach length (test B10 - Q55.2Yg5.0S0.1%). 113
Figure 4.26: Bed topography after breaching (test C11 - Q7.2Yg0.0S0.1%): symmetrical breach. 114
Figure 4.27: Temporal development of breach length (test C11 - Q7.2Yg0.0S0.1%). 114
Figure 4.28: Temporal development of breach length (test C12 - Q45.3Yg4.0S0.1%). 115
Figure 4.29: Bed topography after breaching for the two breaches (test C12 - Q45.3Yg4.0S0.1%). 115
Figure 4.30: Definition of the bed variation parameter Δ_{max} 117
Figure 4.31: Computational scheme for flow analysis of movable bed tests 117
Figure 4.32: Q_{br} versus Q_u for each test at the final state. 118
Figure 4.33: Q_{br}/Q_u versus Fr_{pre} for each test. 119
Figure 4.34: Discharge ratio Q_{br}/Q_u of the tests B9 (Q45.1Yg4.0S0.1%) and C12 (Q45.3Yg4.0S0.1%). 119
Figure 4.35: Temporal development of dimensionless breach discharge and of breach length (test A3 - Q29.2Yg2.2S0.1%). 120
Figure 4.36: Side weir discharge over inflow discharge as a function of dimensionless side weir length for the fixed bed tests (B = 0.3 m, width of main channel in flume for fixed bed tests). 120
Figure 4.37: L_{br} versus Q_u at the end of each test. 121
Figure 4.38: L_{br} versus Q_{br} for each test. 121
Figure 4.39: Side weir relationship for the fixed bed tests. 122
Figure 4.40: Flow depth profiles for the fixed bed tests. 123
Figure 4.41: Flow velocity profiles for the fixed bed tests. 123
Figure 4.42: Water surface profiles before and after the breaching for test A4 (“Q40.4Yg3.4S0.1%”). 123
Figure 4.43: Components of flow velocity for test A3 (“Q29.2Yg2.2S0.1%”). 125
Figure 4.44: Sketch of the flow deflection at the breach site. 125
Figure 4.45: Deflection angles along the breach at the end of tests A3. 126
Figure 4.46: Scheme for specific energy head balance. 126
Figure 4.47: Specific energy head calculated at up- and downstream breach sections for the tests. 127
Figure 4.48: Q_{br} versus Δ_{max}/D_{50} for each test. 127
Figure 4.49: Temporal delay of river bed deformation for test B7 (“Q70.3Yg7.3S0.1%”). ... 128
Figure 4.50: Shear stress components along the breach at the end of test A3. 129
Figure 4.51: Shear stress at the side weir for the fixed bed tests. 130
Figure 4.52: Temporal development of breach erosion rate and of breach length (test A3). .. 131

Figure 4.53: Comparison between shear stress on side weir and breach erosion rate. 131
Figure 4.54: Upstream breach section (test A2 – "Q20.1Yg1.0S0.1%"). 132
Figure 4.55: Downstream breach section (test A2 – "Q20.1Yg1.0S0.1%").....132
Figure 4.56: Frontal view of the breach (test A2 – "Q20.1Yg1.0S0.1%", inflow from right side). 133
Figure 4.57: Mass failure at the downstream section of the breach.....133
Figure 4.58: Slopes of the breach sides. 134
Figure 5.1: Similarity between a levee breach and a side weir: (a) unmodified photo, (b) photo with weir shape superposed (modified from Saucier et al., 2009). 141
Figure 5.2: Side weir situation (plan view).....142
Figure 5.3: Side weir situation (longitudinal section A-A'). 142
Figure 5.4: Side weir situation (cross section B-B').....142
Figure 5.5: Water profiles in a channel along a side weir: (a) subcritical flow; (b) supercritical flow; (c) hydraulic jump; (d) E-Y diagram.....143
Figure 5.6: Overview of the hydraulic functioning of a side weir in case of subcritical flow: a) flow depth along the channel; b) Y-Q function; c) Y-E function. 145
Figure 5.7: Φ as a function of Fr: roots and minimum detection. 149
Figure 5.8: Side weir situation into "Froude graph": A) subcritical; B) supercritical; C) hydraulic jump. 150
Figure 5.9: Flow depth ratio r_Y contours in the Froude graph. 154
Figure 5.10: Discharge ratio r_Q contours in the Froude graph. 154
Figure 5.11: Length ratio r_L contours in the Froude graph. 155
Figure 5.12: Flow velocity r_U contours in the Froude graph. 156
Figure 5.13: Shear stress r_τ contours in the Froude graph. 156
Figure 5.14: Comparison between measured and predicted depth ratios for laboratory data...158
Figure 5.15: Comparison between measured and predicted discharge ratios for laboratory data... 158
Figure 5.16: Comparison between measured and predicted length ratios for laboratory data..159
Figure 5.17: Flow regimes during breach opening in the Froude graph with discharge ratio r_Q contours. 161
Figure 5.18: Flow regimes during breach opening in the Froude graph with length ratio r_L contours. 161
Figure 5.19: Map of levee breach of Ombrone river (Tuscany – Italy).....162
Figure 5.20: Front view of the breach of Ombrone river (Tuscany – Italy) in December 2009. 162
Figure 5.21: Side view of the breach of Ombrone river (Tuscany – Italy) in December 2009 163
Figure 5.22: Cross-section of the Ombrone river at the breach site (water at flood level before breaching). 163
Figure 5.23: Ombrone breach event in the Froude graph with length ratio r_L contours. 165

Figure 5.24: Ombrone breach event in the Froude graph with flow discharge ratio r_Q contours... 165

Figure 5.25: Ombrone breach event in the Froude graph with flow depth ratio r_Y contours... 166

Figure 5.26: Dimensionless ratios at the limit condition for the assumed Froude range (highlighted area). 168

Figure 5.27: Comparison between final breach length and river flood width for experimental and real events data. 169

Figure 5.28: Comparison between peak breach and river discharge for experimental and real events data. 170

Figure 6.1: Stage 0: river flow situation before breaching (section view). 176

Figure 6.2: Stage 0: river flow situation before breaching (frontal view). 176

Figure 6.3: Stage 1 of test A3 (Q29.2Yg2.2S0.1%) of movable bed experiments with breach location. 176

Figure 6.4: Stage 1 of breaching and river flow: overflow and local erosion of the levee (section view). 177

Figure 6.5: Stage 1 of breaching and river flow: overflow and local erosion of the levee (plan view). 177

Figure 6.6: Stage 2 of breaching and river flow: backward erosion of protected side (section view). 178

Figure 6.7: Breaching stage 2 during the movable bed experiments: almost symmetrical breach lengthening upstream (L_{brup}) and downstream (L_{brdw}). 178

Figure 6.8: Breaching stage 2 during the movable bed experiments: discontinuous mass failure. 179

Figure 6.9: Stage 2 of breaching and river flow: symmetrical breach lengthening (plan view). 179

Figure 6.10: Stage 3 of breaching and river flow: erosion of upstream side (section view). 181

Figure 6.11: Photo series of stage 3 of breaching experiment A3 at three different times since breach trigger ($t_0 = 0$ s): a) $t_1 = 82$s; b) $t_2 = t_1 + 31$s; c) $t_3 = t_2 + 36$s. 181

Figure 6.12: Sketch of stage 3 of breaching and river flow (time step t_1): breach development. 182

Figure 6.13: Sketch of stage 3 of breaching and river flow (time step t_2): mean flow velocity decreasing and breach development. 182

Figure 6.14: Sketch of stage 3 of breaching and river flow (time step t_3): 2D flow features at the breach location and breach development. 183

Figure 6.15: Evolution of breaching and river flow at different time steps of stage 3: a) water level decreasing and breach channel formation (t_1); b) water level decreasing and downstream breach development (t_2); c) water level decreasing, downstream breach development and river bed deformation (t_3). 184

Figure 6.16: Dune formation during stage 4 of breaching experiment B8. 185

Figure 6.17: Bed deformation at the end of breaching experiment B8. 186

Figure 6.18: Longitudinal section of stage 4 of breaching process: riverbed deformation. 186

Figure 6.19: Stage 4 of breaching process at different cross-sections: a) erosion of river bed and of river side of levee at upstream zone; b) breach channel, breach flow and slight

bed aggradation at the middle of the breach length; c) river bed aggradation at downstream zone. 187

Figure 6.20: Stage 4 of breaching process (plan view): shear stress and three-dimensional effects.....188

Figure 6.21: Qualitative trend of the breach features during the breaching process: a) Stage 1; b) Stage 2; c) Stage 3; d) Stage 4; e) Temporal trend of breach features. 189

Figure 6.22: Interpretation of the breaching process in the "*Froude graph*" with Q_{br}/Q_u contours. 190

List of Tables

Table 2.1: Factors influencing flow through a levee breach (modified from Saucier et al., 2009). 10
Table 3.1: Summary of conditions and measured data types for the performed test series. 46
Table 3.2: Summary of main variables investigated in tests of series B and C. 84
Table 4.1: Summary of conditions for the performed test series. 98
Table 4.2: Summary of the closure operations of the sluice gate. 111
Table 4.3: Values of the calibration parameter k for movable bed tests. 124
Table 4.4: Summary of main variables investigated in tests (part I). 136
Table 4.5: Summary of main variables investigated in tests (part II). 136
Table 5.1: r_L maximum values for different C_d methods. 153
Table 5.2: Main testing conditions of analysed laboratory data. 157
Table 5.3: Flow features of the real breach event of Ombrone river. 164
Table 5.4: Dimensionless numbers of the real breach event of Ombrone river. 164
Table 5.5: Comparison between measured and predicted ratios for the Ombrone breach event. 166
Table 5.6: Dimensionless ratios at the limit condition. 168

List of Symbols

Parameter	Description	Dimension
A	wet area of a cross section in the main channel	$[m^2]$
B	wet width of a cross section in the main channel	[m]
b_{br}	transversal width of the levee breach	[m]
C_d	discharge coefficient	[-]
C_{ds}	discharge coefficient of side weir	[-]
C_{dbr}	discharge coefficient of breach	[-]
C_h	Chézy coefficient	[-]
D_{50}	mean sediment size	[m]
D_{br}	breach depth	[m]
d_s	scour hole depth	[m]
E	specific energy head of the flow	[m]
e_{br}	vertical erosion rate of the breach	[m/s]
Fr	Froude number	[-]
H	energy head of the flow	[m]
h	water surface level	[m]
h_f	water surface level on the flood side	[m]
h_p	water surface level on the protected side (tailwater)	[m]
k_i	hydraulic conductivity	[m/s]
k_d	soil erodibility coefficient	$[m^3/(N \cdot s)]$
l_{br}	longitudinal erosion rate of the breach	[m/s]
L	length of the lateral outflow structure	[m]
L_{br}	breach length	[m]
L_s	side weir length (fixed bed tests)	[m]
M	momentum at a cross section	[N]
$1{:}m_f$	flood side slope (outer slope)	[-]
$1{:}m_p$	protected side slope (inner slope)	[-]
$1{:}m_{br}$	breach side slope	[-]
p_s	side weir height	[m]
Q	water discharge flowing through a cross section	$[m^3/s]$
q	water discharge per unit length at a cross section	$[m^2/s]$
Q_{br}	discharge flowing through the breach	$[m^3/s]$
Q_{seep}	seepage flow through the levee	$[m^3/s]$
Q_s	discharge flowing over the side weir (fixed bed tests)	$[m^3/s]$
R	hydraulic radius of the flow	[m]
Re	Reynolds number	[-]
S_0	bed slope	[-]
S_f	friction slope	[-]
t	temporal reference during an experimental test	[s]
t_d	time of breach development	[s]
t_i	time of breach initiation	[s]
t_{br}	total time of breaching process	[s]
$U_{mean}=U$	mean flow velocity at each cross-section	[m/s]
U_x	longitudinal component of local velocity	[m/s]
U_y	transversal component of local velocity	[m/s]
U_z	vertical component of local velocity	[m/s]

$\|U\|$	modulus of flow velocity	[m/s]
Y	flow depth at a point of a cross-section	[m]
Y_g	downstream sluice gate opening (experimental set-up)	[m]
Y_{mean}	mean flow depth of a cross-section	[m]
Z_b	elevation of the main channel bed	[m]
Z_{br}	elevation of breach channel	[m]
Z_l	elevation of the levee crest	[m]
Z_p	elevation of the ground at protected side	[m]
W_b	width of levee base	[m]
W_c	width of levee crest	[m]

Greek symbols:

α	Coriolis correction coefficient for kinetic energy	[-]
β	Boussinesq correction coefficient for momentum	[-]
Δ	river bed deformation between down- and upstream sections	[m]
Δ_{max}	maximum river bed deformation in main channel	[m]
θ	deflection angle	[°]
Π	hydraulic pressure on cross section	[N]
τ	shear stress	[N/m^2]
φ_f	flood side slope angle	[°]
φ_p	protected side slope angle	[°]
φ_{br}	breach slope angle	[°]

The subscripts associated to a variable are referred to:

br	breach
d	section downstream the breach site
lc	lateral channel (evacuation channel)
mc	main channel
post	situation after breaching in time (final configuration)
pre	situation before breaching in time
s	side weir (fixed bed tests)
u	section upstream the breach site
x	longitudinal direction
y	transversal direction

1 Introduction

1.1 Problem definition and motivations

Flooding is a natural hazard which probably has the highest occurrence in time and space across the world, causing every year a considerable amount of damages in terms of loss of life and property (Jonkman and Vrijling, 2008; EC, 2010; IFRC/RC, 2010).

Flood levees are among the most ancient and widely used defence structures against river flooding in the world. Levees are water barriers (earthen dikes or embankments) built on the banks of a river in order to prevent the river flow from flooding the lateral areas. Several most important European and Italian rivers are embanked. This is a structural system for flood defence aimed to reduce the areas that a river would naturally flood, so that extensive portions of alluvial plains become available for human activities. However, the construction of levees has two main consequences on the flood risk:

(i) it increases the flooding hazard by reducing the lateral flood storage and hence the river capability of lamination of the flood wave;

(ii) the amount of potential damages induced by flooding is dramatically increased in the flood prone areas mainly occupied by vulnerable elements (human lives, buildings, infrastructures, activities).

Moreover, it is commonly agreed that flood risk is rising worldwide because of climate changes (i.e. increase of flood hazard due to change in the frequency of high flows) and of the continuous increase in the expected damages due to the development of floodplain areas.

Therefore, although the probability of flooding may be lower because a levee exists, the consequences are much higher when the levee breaches.

Flooding from embanked rivers may occur when the structural defence fails in containing the water flow inside the river banks, so that flood water passes over the levee or through it, leading to a hole or breach in the structure.

Levee collapse may have disastrous consequences. Many countries in the world have experienced extensive and frequent losses of life and property over the last decades (Jonkman and Vrijling, 2008; Loat, 2009). The problem of river flooding is becoming increasingly more severe due to human intervention in the floodplain at an ever increasing scale.

Flood mapping is a methodology aimed to evaluate the flood extent and assess human activities at risk in the flood areas in order to take adequate and coordinated measures to reduce flood risk. Assessment of flood risk is therefore becoming a vital component of appropriate management strategies for protecting communities and reducing damages. Unfortunately, the present knowledge of the river levee vulnerability is rather poor. Nowadays, the assessment of flood risk considers only the overflowing of the river levees without collapse: given a probability of flood occurrence, the potential flooding scenario (flood hazard map) is simulated by analysing the amount of water overflowing levees and spreading it in the floodplain, while the flood risk map shows the potential adverse consequences to human activities associated with that flood event.

On the other hand, the analysis of possibility of levee failures is advisable (EXCIMAP, 2007) but usually it is not performed and finds consideration in a scanty number of studies, primarily in the form of scenarios at a local river reach scale (Vorogushyn, 2008). The levee breaching is not usually taken into account because of the complexity of the process, the

difficulty in assessing some key parameters, such as the final length of the breach, and the lack of adequate and reliable models to be implemented at a basin scale.

The current knowledge about the breaching process developed during the last decades is mainly focused on the erosion mechanisms which involve dam embankments and sea dikes. The river levee case is often analysed by means of models developed for the case of dam breaching, while specific tools are missing. Actually, the hydro-morphodynamic conditions prevailing on a river levee are completely different from the case of static water behind a dam. The river flow field governs the breaching process and the breach flow in turn induces changes in the river hydro-morphodynamics. This dynamics causes important modifications in the flow field and in the morphology of the river bed, which evolve together with the breaching process. Such an interaction between these two parts of the system "river-breach" is not completely understood at the current knowledge, and it is neglected by the available models, which therefore can address only partially the prediction of the breach features of a river levee during the breaching process until its finale stage.

The significance of such knowledge gap is even more evident if one considers that most of rivers are embanked with earthen levees for hundreds of kilometres and that the breaching is a frequent phenomenon during a flooding. It follows that there is an urgent need to better investigate this problem in order to take adequate measures to mitigate flood risk from rivers.

1.2 Objectives

The primary and overall objective is to improve the knowledge about the processes associated with the breaching of river levees and to investigate the physical conditions that determine a final configuration of the levee breach.

The research therefore attempts to be process-oriented and to focus on the development of a new approach for the understanding of the breach evolution in river levees by taking into account the interaction between breach development and river hydro-morphodynamics. The breaching process is investigated without strong assumptions about the physical mechanisms, by considering not just the processes affecting the river levee but also the hydro-morphodynamics of the river flow. A detailed study of the dynamic relationship between breach development and river hydro-morphodynamics is considered to be the key for advancing the knowledge about the behaviour of a levee affected by a breach during a flood event.

The proposed approach analyses the river-breach system by means of two series of experimental investigations and an analytical model of the river flow.

The final goal is to define a stage of equilibrium in the mechanisms that govern the physics of the breach and of the river flow.

1.3 Methodology

The research methodology adopted in this study is reflected by the working phases described in the following chapters of this report.

In Chapter 2, a thorough review of the current knowledge is performed about breaching of flood embankments whenever it is relevant for river levees. Available studies, knowledge, models and experiments about breaching are analysed and compared. The present research is planned on the basis of this review: the gaps in the current knowledge and modelling are identified in order to develop new approaches to the problem and, hence, to improve the present understanding associated with the entire breaching process of river levees.

In Chapter 3, experimental investigations conducted on side weir flows in a fixed bed laboratory flume (University of Florence) as well as the main results are addressed. The main objective of these experiments is to investigate the purely hydrodynamic processes of the flow in a channel when a lateral outflow takes place, as in case of a levee breach.

In Chapter 4, experimental investigations on the breaching process of a river levee conducted at a laboratory scale (University of Braunschweig) as well as the main results are reported. The main objective of these experiments is the collection of experimental data concerning the processes of breach formation and evolution due to an overtopping flow on an earthen river levee built in a flume with movable bed. The primary outcome of this working phase is the investigation of the evolution and equilibrium stage of the breaching process and the collection of a consistent and rare data-base of experimental tests regarding the breaching mechanisms as well as the hydro-morphodynamics of the river flow.

In Chapter 5, a simple analytical model is presented in order to analyse the hydrodynamics of the stream flow in a river when a lateral outflow takes place on one of its side. The model is based on the theory of side weir flow for subcritical steady flow and fixed bed conditions. An overall picture and understanding of the hydrodynamic processes are given and the model is applied to the results of the laboratory tests and to some real case data.

Finally, the results of the laboratory tests with a fixed bed in Chapter 3 and with a movable bed in Chapter 4 as well as by the analytical model in Chapter 5 are integrated into Chapter 6. As a result, an overall description and interpretation are provided of the hydro-morphodynamic processes taking place during a river levee breaching with a particular focus on the evolution of the river hydro-morphodynamics as the main relevant issue to advance the current knowledge on river levee breaching.

2 Levee breaching processes and modelling: state-of-the-art review and specification of objectives and methodology

"Failure" of a levee can be defined as the "Inability to achieve a defined performance threshold (response given loading)", as suggested by Gouldby and Samuels (2009, definition in the "Language of Risk" adopted in the frame of the EU-project FLOODsite).

In the context of breach modelling, levee failure is considered to be the situation where erosion or structural failure of the embankment cause flood water to pass over or through it in an increasingly uncontrolled manner.

Breach can occur anywhere in the structure used to retain water. The breaching process might relate to any stage of erosion or failure, i.e. from an initial critical seepage to the complete collapse of the structure. However, breach typically implies that failure has occurred leading to a hole or gap in the flood defence structure.

Numerous researchers have analysed the breaching problem and attempted to define distinct stages of the entire breach development. None of these definitions has been agreed upon for general use, perhaps due to confusion arising from the differences in the processes that occur through breaching of different types of material and structures (i.e. head cut or surface erosion processes as a function of soil type and state). Moreover, different processes take place according to which kind of dike is considered (sea dike, dam, river levee). The focus of the present work is on earthen river dike (that is a *levee*) and on the river flow processes that govern the breach evolution.

In the next Sections, the following aspects are investigated:

- Analysis of causes of breach initiation by specifying the hydraulic/morphological boundary conditions and the initial conditions (Section 2.1);
- Review of the parameters defining the breaching process (Section 2.2);
- Analysis of the breaching processes that may result in a levee failure (Section 2.3);
- Analysis of the hydrodynamic processes of a levee breach (Section 2.4);
- Review of the sediment transport models available for the breaching process (Section 2.5);
- Classification and discussion of available breaching models (Section 2.6).

This Chapter will critically review/analyse the current knowledge of the state-of-the-art in order to identify the gaps in understanding and modelling levee breaching processes. As a final result, the objectives and methodology of the present study are defined more precisely in Section 2.7.

2.1 Causes of breach initiation

Breach initiation and breach growth are associated with complex processes and interactions between water, soil and structure. Hence a large range of factors from different types will affect the rate and size of breach formation. Two primary factors are the type of structure and the type of hydraulic loading, but also the quality of the construction, the type and properties of the material used can all have a significant effect on both breach initiation and breach progression. These features are analysed in Section 2.1.1, while the most common

hydraulic flow conditions that can trigger a breaching process will be discussed in Section 2.1.2, namely overtopping and seepage flow.

2.1.1 Morphological and hydraulic boundary conditions

The breaching of a river levee is determined by two types of boundary conditions: morphological boundary conditions (structure) and hydraulic boundary conditions (river flow). The structure is essentially defined by geometrical and material parameters. The river state is represented primarily by the flood water level and its temporal duration.

There are two main aspects that particularly need to be considered when dealing with breach formation through structures.

First, the breach formation process is very complex and can thus be affected in diverse manners by different design parameters. Significant changes in the breaching process can simply result from the use of different *construction materials*: non cohesive fill, cohesive fill and rock fill materials lead to different erosion mechanisms (Morris, 2009b). The “ideal” material for levee construction is commonly considered a silty clay. Also the conditions of the dike materials are important: Hanson and Hunt (2007) highlighted the importance of both the soil compaction and the moisture content on the soil erodibility. Moreover, a surface protection layer can play a relevant role, since it can delay breach initiation by protecting against surface erosion, or if poorly maintained, can provide a focal point for initiating erosion. Specific studies about the role of grass cover during the breaching process of sea dikes can be found in D’Eliso (2007), Stanczak (2008) and Mous (2010). The breaching process, from breach initiation to the total collapse of the structure, might depend sequentially upon a number of different design features, making the prediction of the actual failure process extremely complex and difficult.

Second, the current ability to predict breach growth in terms of soil erosion is really limited to quite simple structures (e.g., homogeneous embankment covered by grass). Even the design of a simple flood embankment can differ significantly from country to country: flood embankment in the UK, Hungary or France are typically built from locally excavated soil, which ranges from clayey silts to sandy soils and, in some situations, a more cohesive, clayey core is included to limit seepage.

Figure 2.1 illustrates a typical geometry of a levee for primary flood protection used to channelize major river systems. The geometries of flood protection levees vary considerably, based on the level of intended protection and local experiences with successful levee construction. Usually, a river levee is about 3-6 m high and its crest is 3-4.5 m wide. The cross section has commonly a trapezoidal shape, with side slopes defined by 3-4 units of horizontal distance every 1 unit of vertical rise. A levee is typically constructed by compacted earth drawn from locally available sources. The central core is usually built of a clay or silty clay, which has a high degree of workability and a permeability that guarantees a good protection against seepage.

A levee provides a separation between the flood susceptible community on the “protected side” of the levee (the floodplain or polder) and the rising floodwaters on the “flood side” of the levee (the river). A breach in the levee will then provide a pathway between the risk-source and the risk-receptors (Figure 2.2), linking directly flood and protected side (Morris, 2009b).

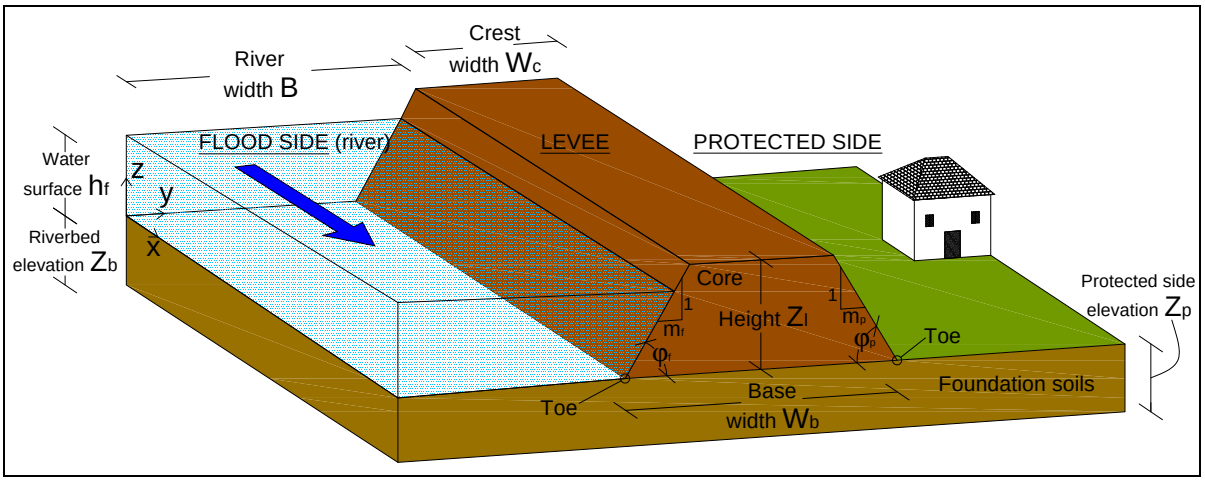

Figure 2.1: Definitions of terms associated with river levees.

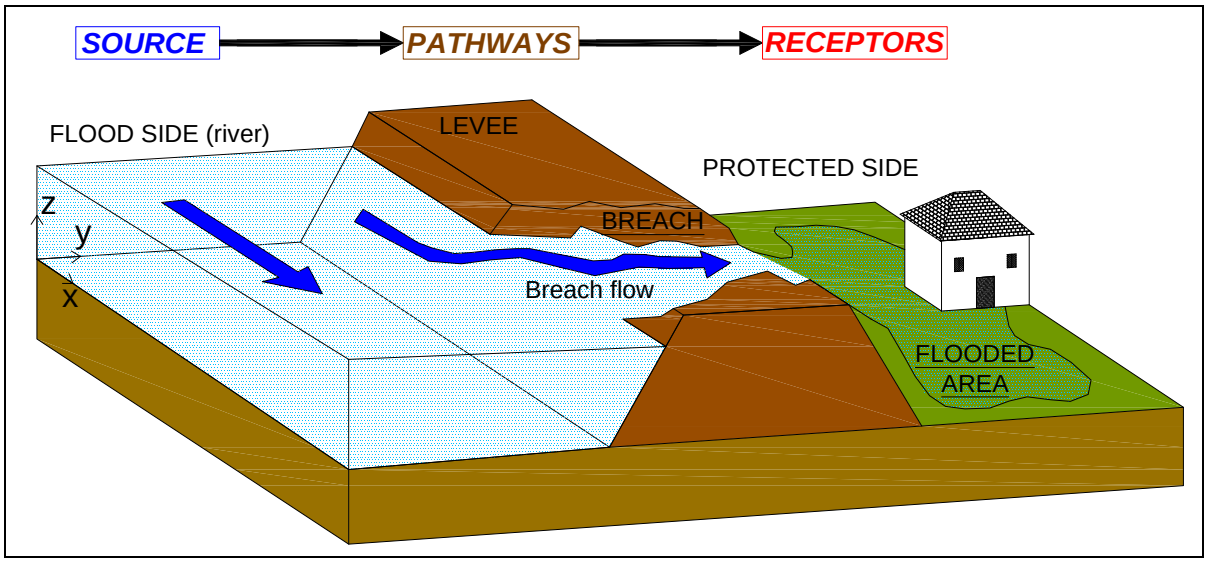

Figure 2.2: Levee breach as pathway between risk-source and risk-receptors.

The type of **hydraulic loading** acting on a levee significantly affects the way in which a breach might occur. A river levee might be subjected to prolonged wet or dry periods, and subsequently progressive or rapidly varying flood levels. The “flooding source” is in that case defined by the water levels on the flood side of the levee and by the volume of water available to flood the protected land (Saucier et al., 2009). When a flood source rises to overflow its banks (a “flood stage”), the flood side of the levee experiences a change in total stresses induced by the rising flood waters acting on the levee face. These stresses vary with time, according to the stage of the flooding source. Both the total volume of water available to flow through the breach and the rate at which the upstream water level drops as the breach grows will affect the nature of erosion within the breach and hence the rate and extent of the overall breach growth.

The hydraulic conditions will depend upon catchment size and type, river reach and scheme design (Morris, 2009b). Additional loads from a variety of sources can take place: for example the presence of a bend in the river reach modifies the flow distribution, inducing secondary flows normal to the channel centre line, which may lead to increased flow velocities adjacent to the bank of the channel so that toe of the bank is eroded and likelihood of levee failure is increased.

2.1.2 Initial conditions: overtopping and seepage flow

Several causes can start the breaching process of a levee: Figure 2.3 lists the more common failure modes.

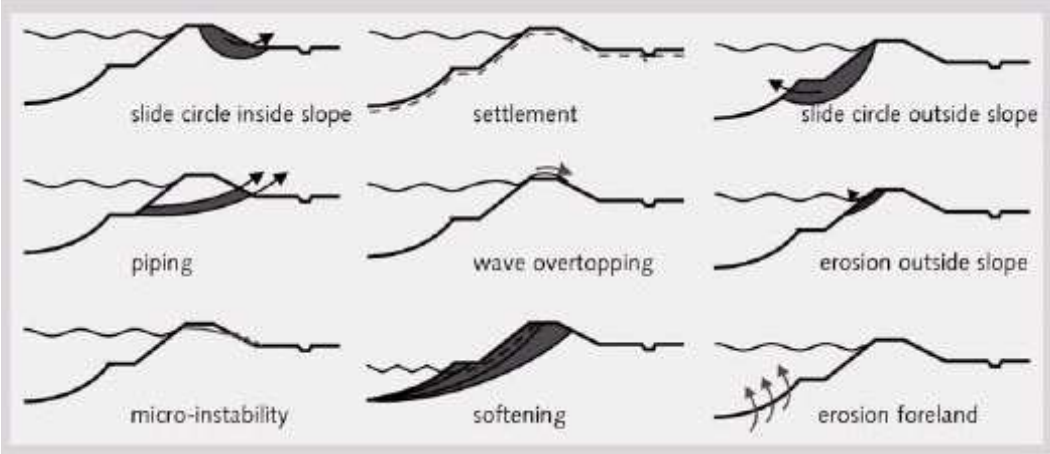

Figure 2.3: Common failure mechanisms of the breaching of a flood embankment (Morris et al., 2007).

Although all these mechanisms can contribute to breach a dike, the experience shows that some of them are predominant and more frequent than the others.

According to Foster et al. (2000), the major of dam failures are triggered by overtopping (48.4%) and piping (46.1%).

Nagy (2006) and Nagy and Tóth (2005) carried out a study in the EU-IMPACT Project about breaching events regarding river levees in Carpathian basins from 1802 up to 2004. From 506 analysed breach data, 87% are attributed to overtopping, piping and loss of levee slope stability, whose majority were due to overtopping (≈ 70%) which has reduced in favour of piping and slope instability over the last fifty years due to the continuous raising and reinforcement of the levees.

Horlacher et al. (2005) analysed 84 levee failures on the Elbe catchment in Saxony during the August 2002 flood: overtopping, piping as well as slope stability were the primary failure modes and overtopping had the main percentage.

In Sections 2.1.2.1 and 2.1.2.2 some characteristics of the two primary failure modes will be specified, namely overtopping and seepage flow. The detailed erosion processes will be discussed in Section 2.3.

2.1.2.1 Overtopping

Overtopping occurs when the water level in the river exceeds the crest of the levee and water spills over the levee. Because of the relatively steep landside slopes of the levees, the water moves rapidly down the landside and then erosion is initiated in locally weak spots where the flow tends to concentrate the erosive forces (Saucier et al., 2009).

2.1.2.2 Seepage

Seepage of water through and beneath a levee during times of flood is a natural phenomenon. Seepage becomes a matter of concern for the safety of a levee when piping or heaving occur, since they are related to erosion of soil particles from the internal core of the levee (piping) or from the foundation layer (heaving). The internal erosion damages the levee and/or its foundation resulting in settlements or collapses (Ozkan, 2003).

2.1.2.3 Effect of weak spots and other factors

Initiation of the breaching process by seepage or overtopping flow is not yet fully understood. Usually, a breach starts from a weak point in the levee and weak points can not be visible or clearly detectable. Specific factors may weaken the dike and thus contribute to trigger breaches, such as:

- *Surcharge loadings* on bank protection;
- *Vandalism* of the dike;
- *Presence of trees or shrubs* on a levee, which may affect the stability of the structure, although their potential impact is complex. The presence of root systems may increase the strength of the soil and hence increase soil stability, while the presence of shrubs and particularly trees may provide a surcharge loading to the system and hence reduce stability;
- *Burrowing animals* may precipitate a piping failure of a levee by means of their dens.

2.1.3 Implications for the present study

The process that results in a breach through a river levee is very complex because of manifold interactions between water, soil and structure. The process can be easily influenced by different design parameters: embankment type, design conditions, construction material and hydraulic loadings that control the breaching process. The final development of a breach will be the result of the boundary and initial conditions affecting the levee.

A model, that would aspire to analyse and reproduce the development of a breach, should take into account the actual morphological and hydraulic conditions of the levee in the most appropriate way as possible. Since the breaching process comprises a complex interaction between hydraulic, geotechnical, biological and structural processes, a combination of knowledge and skills cutting across these different disciplines is therefore required in order to develop reliable models for breach prediction.

2.2 Review of breaching parameters

The two primary tasks in the analysis of risk induced by levee breaching are the prediction of the outflow hydrograph and the routing of that hydrograph through the alluvial plains.

Predicting the outflow hydrograph can be further subdivided into predicting the breach characteristics (e.g. shape, depth, length, rate of breach formation) and routing the inflow through the breach. The routing tasks, through the breach and through the floodplains, are handled in most of the widely used computer models with various one-dimensional routing methods (Wahl, 1998). However, the breach models differ widely in their treatment of the breach simulation process. Many models do not directly simulate the breach formation itself; rather, the user determines the breach characteristics independently and provides that information as input to the routing model. The following defines the parameters concerning breach geometry and temporal development that have importance for handling the breach problem.

In general, the flow through a levee breach may be affected by more than a dozen of factors, as shown in Table 2.1 (Saucier et al., 2009). The large number of variables influencing the breach geometry illustrates the complexity of the breach development problem

and the unique nature of each breach. Each of the parameters identified as an influencing factor may, in turn, be affected by its own set of uniquely varying parameters.

In addition, the variables may affect each other, so that the final breach configuration is governed by the evolution of all the interdependent variables. Ongoing researches seek to clearly define the roles of these various parameters in determining the final breach, but these roles are poorly understood at present.

Table 2.1: Factors influencing flow through a levee breach (modified from Saucier et al., 2009).

FACTOR	INFLUENCE
Flood wave height	Greater flood height increases flow through breach. Greater velocities of flow associated with higher flood wave height contribute to greater rates of levee erosion
Flood duration	Longer flood wave increases flow through breach
Stream discharge	Greater stream discharge permits greater flow through breach
Elapsed time	Greater elapsed time (measured from breach initiation) permits greater flow through breach
Breach size	Longer breach permits greater flow through the breach
Sediment concentration	Greater sediment concentration in breach discharge is thought to decrease the rate at which the eroded levee materials may be transported, thereby decreasing flow through the breach (still poorly understood)
Slope of breach	Greater slopes through the breach increase flow through it
Levee geometry	Larger levee sections reduce the rate at which the breach grows, thereby reducing flow through the breach
Levee strength	Greater levee strength (e.g., presence of vegetation) reduces the rate of levee erosion, reducing breach flow
Tail water height	Greater tail water heights reduces flow through the breach
Floodplain area	Smaller floodplain areas are flooded more rapidly, so that breach development is reduced
Floodplain topography	Gently sloping floodplains cause the generation of tail water effects, thereby reducing the flow through the breach

2.2.1 Geometrical parameters

Levee breaches have a typical shape that has been noticed in several cases regardless the location (country, river) of the breach (Nagy, 2005). Figures 2.4 shows a real breach, while Figures 2.5, 2.6 and 2.7 depict a developed breach as sketch in plan, cross-section and frontal view.

Figure 2.4: Californian levee (from Nagy and Tóth, 2005).

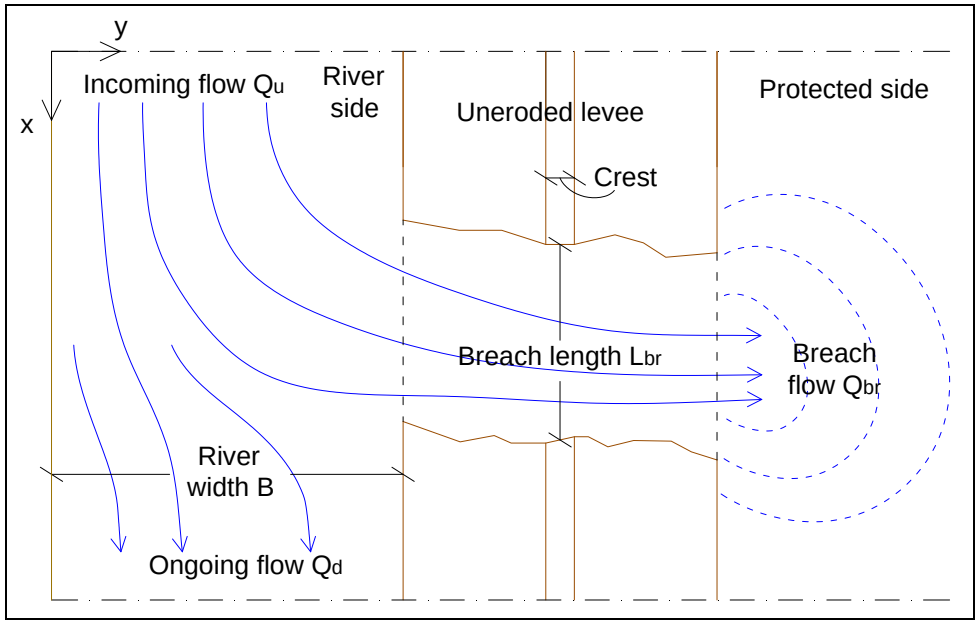

Figure 2.5: Plan view (plane xy) of a breach developed upon a river levee.

The remaining levee stubs are generally almost vertical. Their direction is either perpendicular to the longitudinal axis of the levee (x) or the opening narrows towards the protected side at a slight degree of inclination. The inclination of the plane of the levee stub is usually 0-25°.

The breach flow may dig a hole in the landside zone, called “scour pit”. Nevertheless, a small piece of earth (called “bar”) normally remains at the water side levee toe, which acts as a weir, thus reducing the height of overflow as the water falls over it (Figures 2.6).

A levee fails at a single point. Practical observations suggest that the vertical wall of earth that forms at the edge of a breach at the levee stub plays a key role in lengthening the breach.

The water flowing by the edge of the opening erodes the levee toe and the dike above it falls to form a vertical wall again. The greater the velocity of the flow, the faster the flowing water will wear the edge of the levee stub away and the faster process of repeated wall formation will be. If the material of the levee toe is such that even flows of lower velocity can disintegrate it, the breach in the failed dike will develop. Such soil types may include erosive soils, poorly compacted soils and disperse soils.

The breach discharge Q_{br} is driven by a change in total head (Δh) from the water surface on the flood side (h_f) to the water surface on the protected side (tail water height, h_p).

The breach discharge occurs through an area defined by the "breach length" $\mathbf{L_{br}}$ (a distance along the levee centre line) and the "breach depth" $\mathbf{D_{br}}$ (a depth at the apparent centre of the breach). The variable $\mathbf{b_{br}}$ indicates that portion of the levee cross-section which has been eroded by the breach, it is the "transversal width of the breach" and usually it equals the levee width. The erosion may extend below the levee section and into the foundation soils, as indicated by the scour depth $\mathbf{d_S}$. It is worth to note that the main dimension of the breach (L_{br}) is usually referred as *breach length* in the context of levee breaching (since it develops along the main direction of the river), while it is indicated as *breach width* dealing with dam breaches.

The Figures 2.6 and 2.7 depict the terms associated with levee breaches.

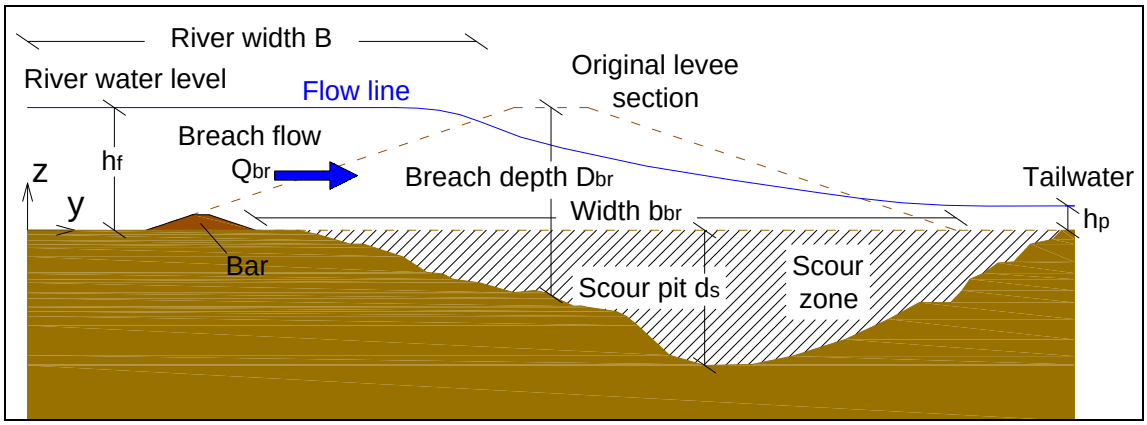

Figure 2.6: Definition of terms associated with levee breaches (section view yz).

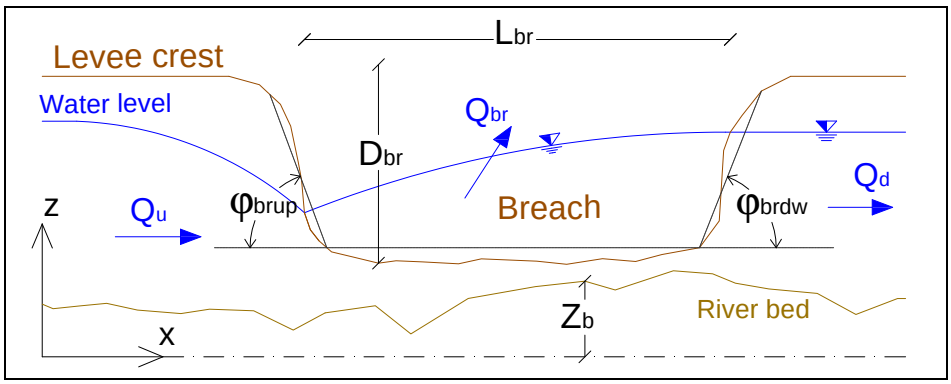

Figure 2.7: Definition of terms associated with levee breaches (frontal view xz).

The majority of the studies found that the fully developed breach assumed a trapezoidal shape, for which:

- The breach length L_{br} generally varies from 0.5 to 10 times the depth of the breach;
- The side slopes of the breach area φ_{brup} and φ_{brdw} typically vary from essentially vertical to 1V:1H (φ_{br} = 45°), with the most common slope corresponding to approximately 2V:1H ($\varphi_{br} \approx 60°$).

The breach length L_{br} is the most important geometrical parameter: during an event of levee breaching, assuming the source of flooding will continue indefinitely, shorter breach lengths would presumably prevent or minimize deeper inundation of the protected community and would permit the removal of floodwaters from the flooded community at the greatest possible rate.

Nagy (2006) defined the following factors that determine the breach length:

$$L_{br} = L_{br}\,(h_f, G, Riv, S, Q, Act, t) \tag{2.1}$$

Where
- h_f: head acting on the breach
- G: dimensions and geotechnical properties of the levee
- Riv: river flow conditions in the vicinity of the levee breach
- S: topographic conditions on the protected levee side
- Q: discharge of the river
- Act: flood emergency activity
- t: time

Regarding the hydraulic parameters, it is understood that the height of the overflowing water governs the breach outflow by means of the weir formula. Moreover, the boundary shear stress of the water over the breach sides is related to the height of overflow. The river discharge plays a major role, since higher discharge of a river will increase the breach discharge, the spill volume and the final breach length. Nagy and Tóth (2005) highlight that this relation between L_{br} and Q is quite evident for both small and large rivers.

In flood hazard assessment of river levees, several approaches were adopted to handle the breach morphology.

Rather often, the breach length L_{br} was considered based on scenarios, derived from past observations or from assumptions of physically plausible range. In several cases simple empirical models are used to estimate the breach growth, which were most of the time derived for dam breaches (MacDonald and Langridge-Monopolis,1984; Pugh, 1985; Von Thun and Gillette, 1990). One of the few contribution developed for the case of levee breach was developed by Verheij (2002) for compacted clay and sand levees.

Few authors tried to propose relations for estimating the maximum breach length L_{max}: MacDonald and Langridge-Monopoli (1984) and Von Thun and Gillette (1990) developed formulas on dam breaches, while Nagy (2006) proposed a formulation for Tisza River levees made by compacted clay. The maximum breach length of these formulas depends primarily on the water height in front of the levee h_w.

Other authors tried to correlate the final breach length with different parameters, as the dam erodibility and the *reservoir shape coefficient*, $V_w^{1/3}/h_w$, where V_w is the water volume retained by the dam (Froehlich, 2008; Xu and Zhang, 2009).

2.2.2 Temporal parameters

Levee breaching is a time-dependent process that develops according to two main phases:

- **Breach initiation time t_i**: the failure itself develops from the first indications of breach initiation to the time at which the breach is fully developed via direct connection with the flood source (Wahl, 1998);
- **Breach development time t_d**: the levee breach grows across its width and then expands along the levee alignment.

The total time of the breaching process is the sum: $t_{br} = t_i + t_d$.

To date, the majority of formulas employed to characterize breach timing have been developed from observations of dam failures (MacDonald and Langridge-Monopolis, 1984; Von Thun and Gillette, 1990; Froehlich, 2008) and they focus on the breach development time. Examples of empirical relationships for breach development time are given by Von Thun and Gillette (1990), Froehlich (2008), Xu and Zhang (2009).

The breach development time for dams is typically between 0.1 and 1.0 hour. The initiation of downstream erosion of embankment constructed of compacted clay may occur for 10 to 20 hours prior to breaching (Gilbert and Miller, 1989). The dam studies found that the rate of breach development for poorly compacted materials may be two or more times faster than well compacted materials.

The failure process is time-dependent because of a dynamic evolution of the breach. Since most breaches have been observed to erode both vertically down to the base and longitudinally, the temporal development of a breach is usually described by means of two parameters:

- The **vertical erosion rate $e_{br} = dD_{br}/dt$**, that describes the evolution of the deepening of the breach;
- The **longitudinal erosion rate $l_{br} = dL_{br}/dt$**, that describes the evolution of the lengthening of the breach.

Breach growth appears to be non-linear: the erosion rate depends on the erosion process and on the material type. The deepening and lengthening of a breach differ in case of overtopping or seepage flow and cohesive or non-cohesive materials.

The current knowledge of erosion rates is mainly focused on overtopping breaching, while few studies are available about progression of internal erosion and piping (Fell et al., 2003).

Typically, the detachment process of sediment is expressed by the excess shear stress equation (Hanson et al., 2001; Hanson and Hunt, 2007) written in the general formulation:

$$e_{br} = a \cdot k_d (\tau_b - \tau_{cr})^b, \quad \text{for } \tau_b > \tau_{cr} \tag{2.2}$$

in which:

e_{br}	erosion rate in volume per unit area per unit time [m/s]
k_d	detachment soil-dependent erodibility coefficient [$m^3/(N \cdot s)$]
τ_b	bed shear stress [N/m^2]
τ_{cr}	critical stress required to initiate detachment for the material [N/m^2]
a	coefficient [$N^{(1-b)} \cdot m^{2(b-1)}$]
b	dimensionless exponent [-]

The coefficient a gets the dimensions according to the value of the exponent b: a is dimensionless in the commonly used case of b = 1. Moreover, eq. 2.2 is defined for values of $\tau_b > \tau_{cr}$, while the erosion rate e_{br} is zero when the bed shear stress is less than the critical stress (i.e., when $\tau_b \leq \tau_{cr}$).

Some authors modelled the head cut migration as an important erosion phenomenon for cohesive material (Temple, 1992; Hanson et al., 2001) that was experimentally investigated by Hahn et al. (2000).

The longitudinal erosion rate is proposed to be related with the vertical rate for sand-dikes by Visser (1998) and for clay-dikes by Zhu (2006).

Experiments carried on by researchers like Britton (Britton et al., 2004) and Hanson (Hanson et al., 2003a and 2003b; Hanson et al., 2005) highlighted the influence of compaction moisture content over rates of lengthening: they observed that a 5% point change in water content could result in a 100-fold change in lengthening rate.

The rate of breach growth varies dramatically, according to the experiments of Hahn et al. (2000) as much as 60-fold, depending on the dike material ranging from sandy and silty to clayey soils.

In the large-scale embankment failure tests, accomplished in the IMPACT project (IMPACT, 2001), typical durations for development of the approximately 30 m long breaches range between 5-10 minutes for rock fill dams to 1 hour for clayey dams.

The reviewed studies indicate a strong variation of breach development rates, which makes the modelling of breach growth a highly complex task. There is lack of essential experience regarding how the length of a levee breach changes in time in the early stages of a developing failure. Only moderate progress has been achieved concerning sound simulation of breach development in fluvial levees over the past decades.

2.2.3 Breach initiation

Interaction between the structure and the water levels generates hydrodynamic and hydro-geotechnical processes and erosion mechanisms which may lead to the initiation of a breach. Possible causes of breach initiation are wave overtopping and seepage flow. Once initiated, breaching develops as a complex 3D morphological process that may lead to collapse of the levee and thus to flooding.

Little quantitative information is available about the breach initiation processes for overtopping or piping failure (Mohamed et al., 2002). Different parameters can significantly affect the timing and rate of breach initiation and growth, such as the presence of a protection layer (Stanczak, 2008).

Breach initiation is often neglected in the current breach models, assuming an initial breach location and weak spots in the levee in arbitrarily manner.

2.2.4 Breach location

The location of the failure is normally influenced by a combination of several causes or factors, although some of these may be dominant. The IMPACT project (2004) classified these factors as:

- *Internal factors*: concerning the geotechnical properties and state of the levee core
- *External factors*: concerning the surface of embankment
- *Environmental factors*: concerning the physical elements surrounding embankment
- *Human factors*: concerning human actions and events (e.g., lack of maintenance)

Besides this general list, there are also specific factors affecting the breach location. For instance, the presence of special stratification of the foundation soil (permeable layers, coarser

layers) can lead to hydraulic subsoil failure (Nagy and Tóth, 2005). Moreover, that kind of stratification is more likely to occur where the track of the levee intersects ancient river beds. This topic was also reported as possible reason of a recent breach event of Serchio River (Tuscany - Italy) in December 2009 (Bonanni et al., 2010).

As for breach initiation, also the location of the breach is not reproduced by the current breach models.

2.2.5 Implications for the present study

The accurate prediction of breach parameters is the key to make reliable estimates of peak outflow and resulting downstream inundation in close proximity to the levee.

The most used models for prediction of breach development follow an empirical approach.

The majority of the purely empirical equations used for estimating breaching parameters involve failures of embankment dams, while river earthen levees are expected to fail by different mechanisms. The main differences concern:

- The construction materials;
- The water volume available to the breach development;
- The flow hydrodynamics in river case compared with static conditions of dam reservoir;
- The erodibility of the substratum.

Most of the current predicting equations are not able to reproduce breaching characteristics in a river levee. This limits highly the development of integrated flood risk plans, which should include the breaching process in order to realistically evaluate the potential flood damages.

Specific tools to understand, analyse and predict the conditions of a levee breach in a river during a flood event are urgently needed, particularly concerning its geometrical and temporal parameters. Exemplary is the necessity of a better understanding of the factors and variables governing the breach lengthening and the breach discharge. The final breach length and discharge are among the most important parameter in assessing the consequences of a levee failure, but they are still characterized by significant uncertainties and knowledge gaps.

2.3 Breaching processes

As mentioned in Section 2.1, erosion and mass instability processes leading to breach differ by various factors, between which the most relevant are: the embankment conditions (materials), the hydraulic load and the erosion initial causes.

In the following, the details of the two primary erosion and breaching processes will be presented based on an extensive literature review, namely the external erosion induced by overtopping (Section 2.3.1) and the internal erosion induced by seepage (Section 2.3.2).

2.3.1 Breaching induced by overtopping

On the basis of the physical observations, several researchers (Visser, 1998; Hahn et al., 2000; Hanson et al, 2003a; Hanson et al, 2005; Zhu, 2006) developed a system to describe the stages of breach development associated with overtopping of embankments and subsequent erosion of the section (see Figure 2.8):

- Stage 1: downstream face is eroded until the protected side of the levee crown due to high shear stresses caused by high flow velocities (Figure 2.8b and c);
- Stage 2: erosion progresses toward the levee crest due to high flow velocities and momentum changes associated with slope transitions or water jets (Zhu, 2006) falling into the levee section over its crest. In this stage, factors as vegetation or soil treatments on the downstream face of the levee (D'Eliso, 2007; Mous, 2010), soil compaction, wetting front migration, and soil suction (Hanson et al., 2005; Hanson and Hunt, 2007) can play important roles (Figure 2.8d);
- Stage 3: levee crest is completely eroded so that the flood source is directly connected with the protected side (Figure 2.8e). The breaching process is then accelerated and the breach lengthens quite quickly. Moreover, particle erosion is supplemented by significant contributions from mass wasting processes. The nature of the temporal development of the breach length-to-depth ratio has not been clearly captured and described to date;
- Stage 4: levee section is completely eroded and breach length is increasing, while the deepening process may form the "scour pit" at the landside toe (Figure 2.8f). Sometimes, a small portion of the levee section may remain near the levee flood side toe as "bar" (Nagy, 2006). The lengthening dynamics involves mass-erosion mechanisms from the levee sections and their subsequent transportation through the breach (Hassan et al., 2004; Morris, 2009a; Morris, 2009c; Silva-Araya et al., 2010). The shape of the eroded levee section in stages 3 and 4 has led to the common characterization of the breach discharge in terms of weir equation, since the flow pattern resembles that of the flow over a compound, broad-crested weir (Saucier et al., 2009). The breach lengthens mainly in the downstream direction, with respect to the river flow direction, as shown by full-scale experiments in Chiyoda channel (Shimada and Yokoyama, 2011) and by small-scale experiments by Islam (2012). Stage 4 ends when the breach system achieves a final configuration of equilibrium, at which a quasi rest state is reached in the breach lengthening (Nagy and Tóth, 2005).

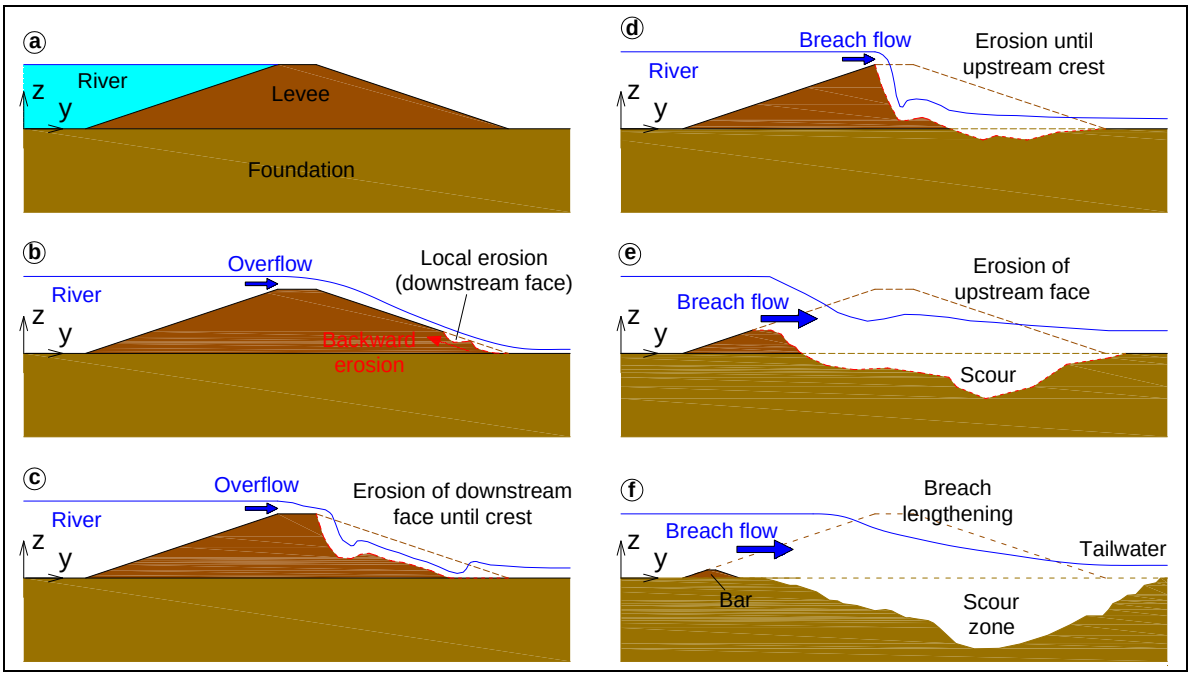

Figure 2.8: Stages of breach growth initiated by overtopping: a) initial levee; b) start of stage 1; c) end of stage 1; d) stage 2; e) stage 3; f) stage 4.

Breaching process by overtopping flow will significantly differ depending on the embankment materials (cohesive or non cohesive) and on other factors, as soil compaction conditions and moisture contents (Hanson and Hunt, 2007). Basically, the breaching mechanism concerns *progressive surface erosion* for non-cohesive materials or *head cutting* for cohesive materials (Morris, 2009b).

2.3.1.1 Breaching through non-cohesive material induced by overtopping

Specific features or processes may be identified for breaching of erodible (typically low cohesive as sand) embankment material (grain size greater than 60 μm).

In this case, initial surface erosion creates a gully, the slope of the gully steepens and it cuts back at a set angle towards the landward face of the embankment (Visser, 1998; Andrews et al., 1999; Coleman et al., 2002; Hassan et al., 2004). The angle that the eroding face might adopt can not be predicted to date. Figure 2.9 shows the non-cohesive breaching behaviour during the laboratory tests made by Hassan et al. (2004).

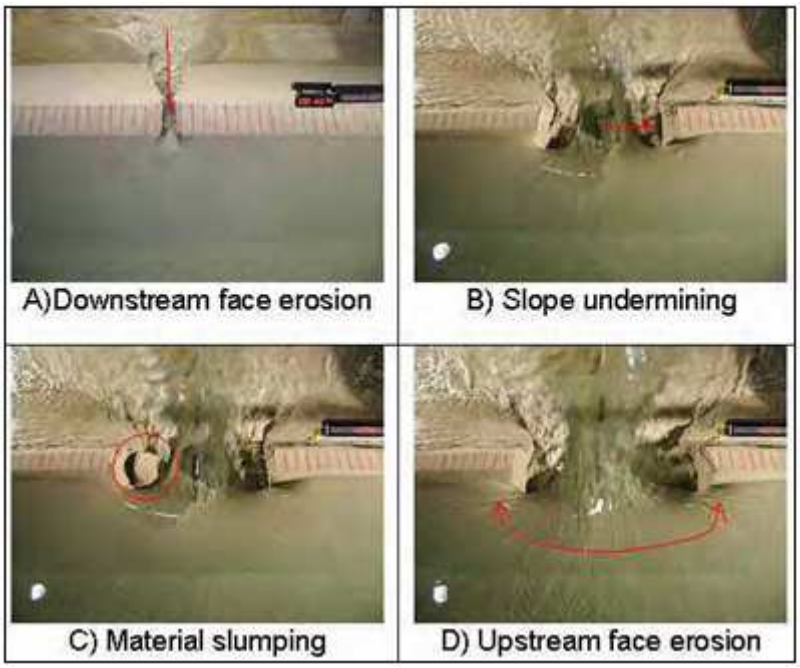

Figure 2.9: Breaching processes in laboratory test on homogeneous non-cohesive embankment (Hassan et al., 2004).

2.3.1.2 Breaching through cohesive material induced by overtopping

Erosion and breach growth in stronger, less erodible soils (typically, but not necessarily, cohesive, as clay) show different behaviour by the formation of head cuts (grain size smaller than 60 μm).

In this case, the initial overtopping flow results in sheet and rill erosion with one or more master rills developing into a series of cascading over falls that join into a large head cut (or step). The head cut moves upstream through the levee to form a breach (Hahn et al., 2000; Hassan et al., 2004; Hanson et al., 2005; Zhu, 2006). Figure 2.10 shows the cohesive breaching behaviour during the laboratory tests made by Hassan et al. (2004).

Various factors can influence the process, such as grading, compaction, water content and geometry (Hassan et al, 2004).

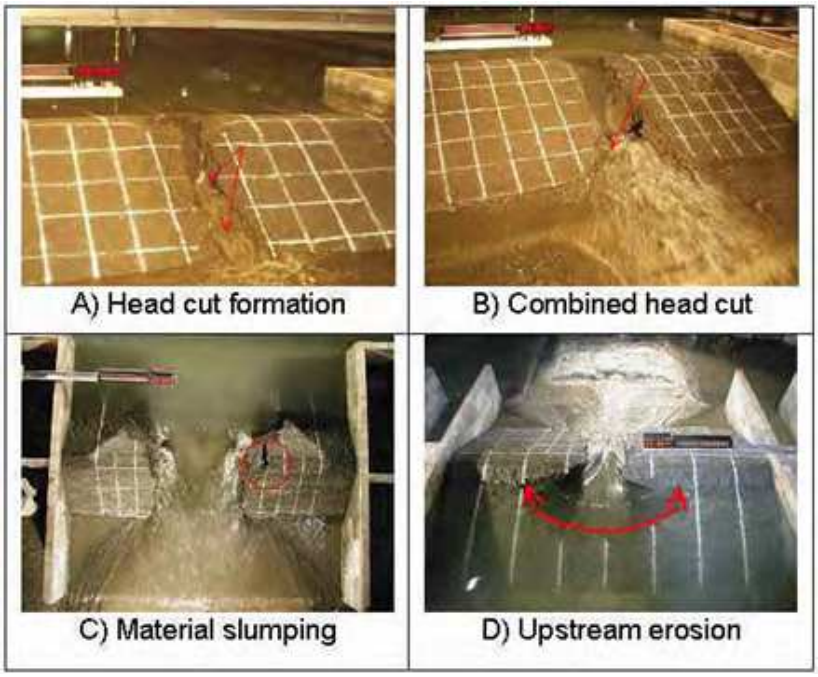

Figure 2.10: Breaching processes observed for cohesive material (Hassan et al., 2004).

2.3.2 Breaching induced by seepage

Whenever a levee is subjected to a differential hydrostatic head of water as a result of river stages higher than the surrounding land, seepage enters the pervious substratum through the bed of the river and through the riverside levee slope, and this creates an artesian head and hydraulic gradient in the sand stratum under or through the levee. This gradient causes a flow of seepage which can weaken the levee structure if the seepage flow reaches the protected side. In that case, the hydrostatic pressure can create piping of the landward slope or heaving in the pervious substratum landward which result in internal erosion and mass instabilities. Figure 2.11 provides a sketch.

The amount of seepage and hydrostatic pressure that may develop landward of a levee is related to the river stage, location of seepage entrance, thickness and permeability of the substratum and of the landside top stratum, underground storage, and geological features (Ozkan, 2003).

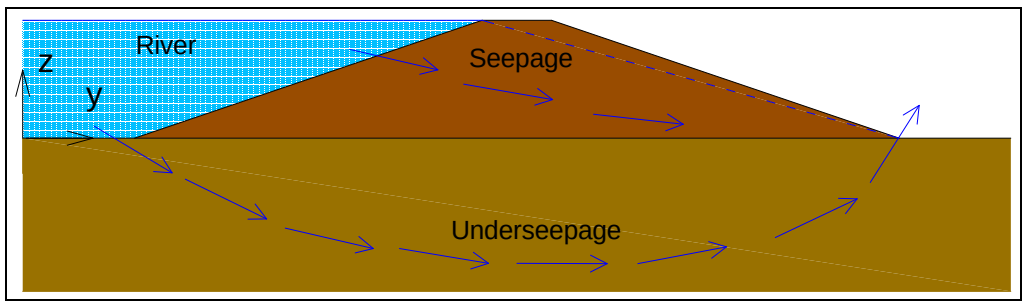

Figure 2.11: Schematic representation of seepage and underseepage flow.

The analysis of the seepage zone below hydraulic structures is described by groundwater flow field, and the critical conditions for the inception of the erosion processes is given in terms of critical idraulic gradient $i_c = h_{crit}/L_{seep}$, where L_{seep} is the seepage length. The heaving is analysed in terms of equilibrium of forces in the soil (Terzaghi, 1929), the piping is studied

in terms of global gradient (Bligh, 1927; Lane, 1935; Sherard et al., 1963; Van Zyl and Harr, 1981; Khilar et al., 1985).

Soil type, rate of head increase and the flow condition are the main factors for modes of seepage erosion failure.

The *soil type* controls whether heave is followed by a quick condition as in clean sand or whether heave leads to crack formation, concentrated flow and piping. Heave, leading to cracks, concentrated flow and piping, appears to be more common in granular soils with a large percentage of fines. Of course, the value of the permeability is critical for the piping process (Ojha et al., 2001).

A rapid *increase in head* may result in heave of the surface, leading to a quick condition (Van Zyl and Harr, 1981). This can be a typical failure condition on the downstream side of a water retention structure being filled rapidly.

Van Zyl and Harr (1981) also pointed out the importance of *flow conditions* in piping problems. According to the field observations, an unsaturated soil fails at lower gradients than the critical gradient of the soil. The first filling of a reservoir may induce this type of failure.

Cumulative effects of seepage under levees (such as forward erosion during flood and backward erosion after flood) can compromise levee safety (Ozkan, 2003).

As for breaching induced by overtopping, similar stages of breach evolution may also be identified in breaches initiated by under-seepage or through-seepage, as shown in Figure 2.12 (Foster et al., 2000; Mohamed et al., 2002; Fell et al., 2003 and 2005; Saucier et al., 2009):

- Stage 1: first observation of piping on the protected levee side until material starts being removed from the levee or foundation (Figure 2.12a);
- Stage 2: the erosion progresses toward the river side of the levee, pipe becomes directly connected with the flood source and soil over the pipe is vulnerable to collapse (Figure 2.12b);
- Stage 3: the soil over pipe collapses and levee section is effectively eroded down to the foundation. The flow through the breach is now unimpeded and it is able to increase the breach dimensions by a way similar to the previously described stages of overflow breaching (Figure 2.12c);
- Stage 4: the breach forms completely by lengthening phase, and vertical erosion can form the so called “scour pit”, until it reaches an equilibrium state (Nagy and Tóth, 2005) at its final configuration (Figure 2.12d).

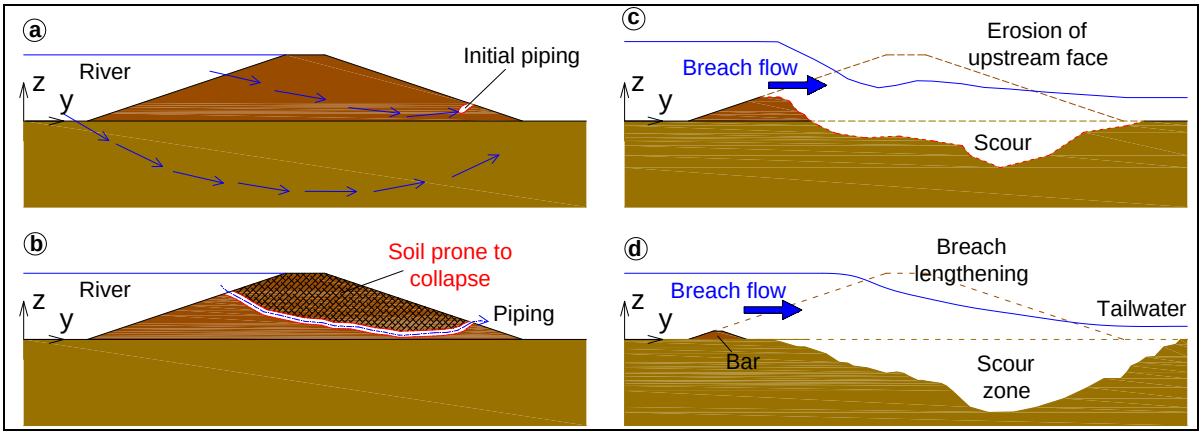

Figure 2.12: Stages of breach growth initiated by piping: a) stage 1; b) stage 2; c) stage 3; d) stage 4.

2.3.3 Implications for the present study

The major causes that initiate a breach in a river levee are overtopping and seepage. Overtopping occurs when the water level in the river exceeds the crest of the levee and water erodes the landside layer. Seepage occurs when water infiltrates into the levee until the landside and seeping water erodes the soil particles washing them away through a pipe. Each of these processes has specific mechanisms, influencing factors and evolution stages, but also some general characteristics, such as the two last stages which have similar features.

Analysis of breaching process by overtopping or seepage flow is a very difficult task involving the interaction between fluvial hydraulics, embankment stability and sediment transport.

The study of such a phenomenon should then comprise a multidisciplinary approach, to simulate the physical processes that cause the breach. Care should be taken in representing each stage of evolution: breach initiation, formation, progression and final stage of the breach.

The current knowledge about the initiation and development of a breach is not yet well-developed. It is limited to the general stages. In the last years, some researchers have attempted to investigate specific factors affecting the evolution of the breaching event, like the role of grass cover layer during the breaching initiation, the erodibility characteristics of the embankment soil, the flow conditions over or through the dike.

Although the main processes have already been analysed, the complexity of the problem and the variability of factors that can take place make the current knowledge quite lacking or limited to specific study-cases.

If recent analyses have been performed regarding the breach initiation and progress until the second stage, it is as well true that there are important gaps of knowledge about the third ad fourth stages of the process, which are the most important ones for the consequences of the breach event. The third stage concerns the direct connection of the breach with the flood source: a detailed analysis of which mechanisms take place from that time on both for the breach morphology (development of the breach length-to-depth ratio) and for the flood source dynamics is still missing. This maybe is not so evident for the case of dam breach, but it is particularly true for a river levee, where there is a more strong and complex interaction between the breach channel and the river flow field.

The fourth stage should describe how the breach progresses until its final configuration and it should analyse which conditions both in the breach channel and in the river occur at the achieving of the final equilibrium. Nowadays, the final configuration of equilibrium is mainly supposed, but it is scarcely analysed. Some contributions are given for the case of dam breach, while the breaching dynamics of a river levee and its evolution until an equilibrium stage is lacking. Moreover, no significant studies have been found about the analyses of an equilibrium that can develop without external constraints (as the flood wave attenuation, the tailwater raising, or unerodible sections of the levee).

Specific investigations should be carried out on the dominant processes during a breaching event in relation with the environmental and boundary conditions. That is particularly important when dealing with river levee, since it is the river itself (with its levels, velocities and morphology) that determines the conditions acting on the levee.

The link between levee and river has not been sufficiently addressed to date. The concepts, schemes and models developed do not consider any kind of interaction among the evolution of the breach and the watercourse behaviour, even if important amounts of water spills from the breach influencing the flow of the river itself. In fact, the current knowledge and analysis approach to the problem are usually limited to dam embankments.

A new study about river levee breaching should take into account the geotechnical processes of erosion and instability of the levee as well as the hydro-morphodynamic evolution in the river during the flood event. Deeply investigating this dynamic relationship may substantially advance the understanding of the behaviour of a river levee affected by a breach.

2.4 Hydrodynamic processes

As explained in Sections 2.1-2.2-2.3, the hydraulic loading and the river flow conditions in the vicinity of the breach are relevant during the formation and the final configuration of the breach itself. In order to study the system river-breach, it is then important to characterize the hydraulic behaviour of the stream through and along the levee breach.

The flow patterns through a breach are briefly described in Section 2.4.1, while the main focus of this Section is the characterization of the flow in the river when an outflow discharges laterally through a breach of one of its levee (Section 2.4.2).

2.4.1 Hydrodynamics of flow through the breach

When a levee is overtopped by the river flow and a breach develops according to the mechanisms described in Section 2.3, different flow regions develop. Several authors investigated the flow patterns over an overtopped embankment during stage 2 of the breaching process (Powledge et al., 1989; Fritz and Hager, 1998; Chinnarasri et al., 2003).

Chinnarasri et al. (2003) carried out experiments in a rectangular flume with a sand dike and observed flow regimes and dike damages due to overtopping flow. Four flow zones were noticed:

1. *Subcritical flow* upstream dike crest: small energy slope and flow velocities, Fr < 1;
2. *Critical flow* at dike crest: critical depth at the middle of the horizontal dike crest;
3. *Supercritical flow* on downstream side: steep slope of the dike surface, high flow velocities, Fr > 1;
4. *Subcritical flow* at the downstream dike toe: low hydraulic forces, small energy slope, small flow velocities. Supercritical water profile joins with the subcritical tailwater flow by means of a hydraulic jump, where the flow is turbulent and water and sediment are strongly mixed.

The flow over the dike is rapidly varied, usually described by the weir flow theory, with particular reference to broad-crested weirs (flow streamlines parallel to the crest, hydrostatic pressure distribution above the crest, critical flow depth on the weir crest).

The discharge equation for a broad-crested weir is derived considering the passage of the flow through the critical depth over the weir crest:

$$Q_w = C_d \cdot L_w \cdot H_w \cdot \sqrt{2gH_w} \tag{2.3}$$

With:
- Q_w flow discharge over the weir [m^3/s]
- L_w length of the weir [m]
- H_w total head over the weir [m]
- C_d discharge coefficient [-]

The dimensionless coefficient C_d has been found to be a function of weir geometry and flow conditions (Chanson, 2004). Dingman (2009) indicates that C_d ranges from 0.33 to 0.41.

2.4.2 Hydrodynamics of flow along the breach

The situation of river levee breach resembles the case of open channel flow with a side weir, in which the discharge decreases along the flow direction.

As observed by Saucier et al. (2009), the flow pattern through a levee during the breaching progress closely resembles that of the flow over a compound, broad-crested weir.

This is a typical case of spatially (gradually) varied flow, where flow depth varies gradually along the length of the channel because of water running out of the river (Chow, 1959).

The diminution of water causes disturbance in the energy and momentum content of the flow and, as a result, the hydraulic behaviour of the flow is complex.

As the discharge in the river decreases along the weir, the water depth varies depending on the flow regime in the channel: in subcritical flow the water depth increases in the flow direction, while supercritical flow will make water depth to decrease downstream (Chow, 1959; Montes, 1998; Borghei et al., 1999; May et al., 2003; Rosier, 2007). Subcritical situation is the most common one.

2.4.2.1 Side weir equation

The rate of change of the water depth along the weir can be predicted by applying the continuity condition coupled with the energy or momentum equation, under the main assumption of one-dimensional steady flow. Moreover, a classical weir equation is usually employed in order to describe the flow that spills over the side weir.

Many authors (Subramanya and Awasthy, 1972; Borghei et al., 1999; Muslu, 2001; Rosier et al., 2008) adopted the De Marchi hypothesis (1934) that considers the specific energy head of the flow to be approximately constant along the side weir. Such an assumption leads to a system of first order differential equations for the prediction of the flow features (flow depth and discharge) along the side weir, which has a discharge coefficient C_{ds} and the Coriolis coefficient α as parameters. De Marchi (1934) derived an analytical solution of the side weir problem.

Several studies about the discharge coefficient C_{ds} have been conducted in order to propose reliable formulations based on experimental tests (Subramanya et Awasthy, 1972; Ranga Raju et al., 1979; Hager, 1987; Singh et al., 1994; Jalili and Borghei, 1996; Borghei et al., 1999; Muslu, 2001).

The kinetic Coriolis coefficient α takes into account the non-uniformity of velocity distribution in the channel section, and it is likely greater than unity in case of side weir (El-Khashab et al., 1976; May et al., 2003).

The Boussinesq coefficient β (Chow, 1959) is the equivalent coefficient into the momentum formulation, where also the outflow angle θ plays an important role for the overflow phenomenon (Hager, 1987; Montes, 1998; Rosier et al., 2008).

2.4.2.2 Validity of De Marchi hypothesis

The De Marchi hypothesis of constancy of specific energy head along a side weir is often used.

Experimental confirmation of this assumption may be sought in several experimental works (El-Khashab and Smith, 1976; Ranga Raju et al., 1979; Montes, 1998; Borghei et al.,

1999). The hypothesis has been proved also for side weir flows acting on movable bed (Paris et al., 2012).

2.4.2.3 Complexity and non-uniformity of flow along the side weir

The presence of a side weir along one side of a river induces an asymmetry of the flow and endows it with a complex, three dimensional character in front of the weir (Montes, 1998). At the beginning of the weir, the outflow is drawn from the upper strata of the channel, while further down, the discharge is collected from the lower strata, with the streamlines following a spiraling trajectory. The flow along the opposite side of the channel is less strongly affected by the lateral outflow and continues within the onward channel (May et al., 2003).

Moreover, the flow direction over the side flow weir is no longer at normal angle to the weir plate, like in frontal weir, but it assumes variable angles θ, more acute at the beginning and closer to 90° at the end of the weir. In fact, the deflection angle depends upon the relative velocity of the flow approaching the weir: the higher this velocity, the more oblique the angle. Also, the angle will tend to vary along the length of the weir as the mean velocity of the flow remaining in the channel decreases in the downstream direction, at least in subcritical conditions (May et al., 2003).

Finally the water level in the main channel changes along the weir depending on the flow conditions in the channel, so that the head acting on the side weir varies with distance and causes a change in the rate of outflow per unit length of weir.

All these conditions endow the flow with a complex three-dimensional behaviour and with a non-uniform velocity distribution.

Helpful information concerning the flow pattern in side weir channels can be derived from studies concerning lateral intake structures and open-channel diversions or river bifurcations: in those situations, the transverse pressure gradient in the vicinity of the intake induces regions of mean flow velocity gradients, depth varying surfaces of flow division and separation, vortices, zones of flow reversal and local sediment deposition (Rosier, 2007). Hager and Volkert (1986) investigated flow conditions in distribution channels, which are open channels where steady, gradually varied flow occurs with decreasing discharge in the flow direction. Different flow zones along a lateral weir have been analysed by other researchers (Hager and Volkert, 1986; Neary et al., 1999; Hsu et al., 2002; Kamrath et al., 2006; Rosier, 2007).

2.4.2.4 Movable bed effects along the side weir

The presence of a movable bed in the main channel endows the system river-breach with one more degree of freedom. When a lateral outflow due to levee breach occurs, both the hydrodynamics and the bed morphology are subjected to changes. Rosier (2007) and Bechi (2008) studied the interaction between side weir overflow with bed morphology changes by means of numerical models and experimental investigations: they observed erosion (upstream) and deposition (downstream) mechanisms in the main channel along the side weir.

Faeh (2007) modelled numerically the breach erosion of a river embankment and he indicates the presence of bed morphology modification, due to a reduced transport capability in the river, that his model could not take into account.

An experience of laboratory investigation regarding the situation of levee breach in mobile-bed conditions was found in Fujita and Tamura (1987). The investigations were focused on analysing the lengthening process and the final topography of the breach in case of presence/absence of river flow. Most of the available space of the facility was dedicated to the

alluvial plain, in order to simulate the sand deposition and the scour hole formation due to the breach flow. Few information and focus were directed toward the river part. Similar experiments were performed by Islam et al. (1994) and analysed by Islam (2012).

2.4.3 Implications for the present study

The hydrodynamics of the flow around the breach is the driving action of the breaching process. The flow field in the vicinity of the breach is quite complex and two main sections can be detected, regarding the flow through the breach channel and the features of the flow in the river along the levee breach.

The flow through the breach has been analysed by several authors, while few ones have focussed on the river flow. More works about lateral outflows have been found dealing with side weirs.

A complete approach to the river levee breach problem, either in the direction of numerical modelling or for experimental investigations, should consider the river flow dynamics starting from the description of the physical mechanisms governing the outflow and the hydro-morphodynamics of the river flow. Knowledge given by other researches dealing with open-channel flows affected by lateral outflows are important to detect the features of the flow field and to assess a consistent tool for a realistic analysis.

Particularly, the complexity and non-uniformity of flow along the breach has to be considered, together with the three-dimensional features of the flow and their effects in terms of riverbed modifications. All these mechanisms have to be analysed with particular reference to the levee breach situation. To date, none of these phenomena are highlighted in the current breach modelling.

2.5 Sediment transport processes and models

The soil of the levee eroded by the flow action is washed away from the breach by the sediment transport capacity of the flow, as bed and suspended load.

This Section deals with sediment transport processes and models available in order to understand and simulate the morphodynamic processes in the breach channel.

The sediment transport processes associated with dike breaching are generally out of the applicability ranges of available sediment transport models, thus limiting their capability when applied in breach models. However, the simulation of such a process is important since the sediment transport capability of the flow in the breach governs the progress of erosion.

2.5.1 Sediment transport processes

The progress of erosion under breaching conditions is determined by the sediment transport capacity of the flow.

Sediment transport (also called *sediment load*) is defined as the mass-rate of material transport (weight per unit time; [F T^{-1}]) and it has two principal constituents:

- **Wash load**: very fine particles (clay or fine silt) transported in suspension by the water, which are not present in the channel bed;
- **Bed-material load**: material present in the channel bed and banks which is subject to entrainment, transport, and deposition, depending on hydraulic conditions. Bed-material load consists of two components (Bor, 2008):

- **Bed load**: transport of soil particles in the wave boundary layer in close contact with the bed through rolling (gravel-size particles) and sliding (sand particles). The bed load is determined in relation with the effective shear stress τ_b acting on the grain surface;
- **Suspended load**: transport in suspension without continuous contact with the bed. It is related to the total bed shear stress τ, as the sum of the skin friction (effective shear stress τ_b) and the bedform pressure friction (form-related shear stress τ_f).

The total sediment transport $\mathbf{q_s}$ is then obtained as the sum of the bed load ($\mathbf{q_{s,b}}$) and suspended load ($\mathbf{q_{s,s}}$) transport rates (Liu, 2001; Chanson, 2004).

The transport of material is governed by the balance between the total erosive force acting on a particle to the gravitational force resisting movement: the ratio between them is called *dimensionless shear stress* or *Shield's particle mobility parameter* $\boldsymbol{\theta_{sh}}$ (Shields, 1936). The critical value for motion inception $\boldsymbol{\theta_{sh}^*}$ is a function of the boundary Reynolds number (Dingman, 2009).

Dealing with a breach channel some important general aspects have to be taken into account:

- The bed load determines the bottom evolution, while the suspended load is responsible for the erosion of breach sides (Stanczak, 2008);
- The flow is unsteady, usually super-critical with Froude number Fr = 1÷5 and Shields parameter θ_{sh} = 0.3÷100;
- The slopes of the levee protected side φ_p and of the breach side φ_{br} are steep, with values of $\varphi_p \approx 30°$ and φ_{br} > internal friction (≈ 32°);
- The water properties, especially viscosity, are strongly influenced by the high sediment concentration resulting in viscosity larger than that of pure water;
- Non-equilibrium sediment transport conditions prevail (Visser, 1998).

Under such severe conditions, the flow dynamics is so extreme that little is known about the response of the sediments. Anyway, these aspects characterize the sediment transport in a breach channel and have to be considered when applying any sediment transport equation.

2.5.2 Sediment transport models

The simulation of the erosion and the transport of sediment through the breach can include both equilibrium sediment transport equations (such as Yang, Bagnold-Visser and Smart) and erosion equations (such as Hanson, in Hanson et al., 2005).

Sediment transport equations are typically based upon steady state equilibrium conditions and are designed for use in establishing long term sediment behaviour. This is not consistent with the conditions found during breach initiation and growth. Even for breach initiation, where flow is relatively small and erosion less aggressive, the physical length of erosion is typically small (i.e. the levee crest) and hence insufficient to allow equilibrium sediment conditions to develop.

The selection of a sediment transport equation to be used in any mobile bed problem is difficult and is typically based on professional judgement, previous experience, or even personal preference. When considering the breaching process, the problem becomes even more difficult. Most existing sediment transport equations were derived for steady state

subcritical flow conditions, equilibrium sediment transport, specific types of sediment, and for a certain range of sediment diameters.

These conditions are likely to be violated during the breaching process since conditions are typically unsteady, supercritical flow, and with a wide variety of soil types used for levee construction.

Research in the area of the unsteady non-uniform sediment transport is still in its early stages and more work is required in order to achieve reliable results that could be used for simulation of problems such as breach formation. Some researches deal with dam-break induced geomorphic flows and morphology modifications in the downstream valley (Paquier, 2002; Zech et al., 2004), while an experimental study was found regarding the material sedimentation over the floodplain due to a river levee breach (Islam et al., 1994).

However, in the absence of any other method to predict the sediment transport, careful selection from the existing sediment transport formulas might be undertaken. The following might be taken into consideration when selecting these formulas:

- Their applicability to flow on steep slopes and for supercritical flow;
- Their derivation (are they based on dam breach experimental data?).

A list of equilibrium sediment transport equations can be found in Visser (1995 and 1998) and Bor (2008). The equations can be classified according to:

- The reproduced sediment transport type: bed, suspended or total load;
- The equation structure: critical discharge, shear stress, regression analysis, steady equilibrium, stream power or energy approach;
- The applicability range: sediment properties (as size, specific gravity), channel geometry (slope), flow field (mean velocity, Froude number, Shields number).

The review of the sediment transport formulas and the comparison with experimental results made by Visser (1995), confirm that none of the present equations have been set-up for and tested to the extreme hydraulic conditions acting during a breaching process. The validity ranges of the formulas (when it is known) are well exceeded in breach tests, especially regarding the mobility parameter θ_{sh}, the slope angles φ and the depth-averaged concentration. Generally speaking, most of the tested sediment transport formulas predict transport rates much larger than the experimental rates. Moreover these conclusions hold for the first stages of the breach erosion process, when the flow is supercritical, while more investigations have to be studied for the last stages, really important in determining the final dimensions of the breach.

The alternative to the sediment transport equations, is to use an **equation based upon rate of soil erosion**, which would appear to be more consistent with the observed physical processes. These empirical equations predict the rate of detachment of material per unit time depending upon an erodibility coefficient, a critical shear stress (both are properties of the soil), and the effective shear stress (property of the flow), as already discussed in Section 2.2 (equation 2.2).

The use of such an erosion equation has two big advantages: firstly, the equation reflects a dynamic erosion process and is not based upon steady state equilibrium conditions which clearly do not apply; secondly, the erodibility parameter, k_d, can be used to reflect variations in erosion as a function of soil state which has been identified as an important issue for breach modelling.

The drawback to using an equation based upon an erodibility coefficient, such as k_d, is the need to define a value for that parameter and for the two coefficients (a and b). To date this has been undertaken through laboratory or field testing (Hanson et al., 2005) but there are a number of different methods by which this might be done and results are not yet consistent between approaches (Regazzoni et al., 2008, Wahl et al., 2008b).

The principal approaches to measure, calculate or estimate the soil erodibility are:

- Database of soils, with measures of erodibility for an increasing number of soil types and states;
- Closer analysis and comparison of erosion test equipment (such as the JET and HET tests);
- Guidance on parameters to measure 'in the field' for accurate assessment of erodibility.

Simple guidance on the likely range of erodibility for a given soil and state are available, but they need to be refined in order to enhance breach modelling accuracy. Nevertheless, it should be recognized that the accuracy of breach prediction offered by this approach (predictive breach modelling based upon erosion equations) is far more accurate than application of simplistic peak discharge equations and offers a better long term solution for model development than use of traditional sediment equations (Morris, 2009c).

2.5.3 Implications for the present study

The morphological evolution of the breach channel is ruled by the erosion and sediment transport capacity of the flow. A sediment transport model for cohesive and non-cohesive materials in the context of the both discrete and continuous erosion is then required in order to describe the sediment transport processes associated with the breaching of river levees.

A number of sediment transport models are available but none of them is capable to describe properly the process that occurs during levee breaching, as they are based on assumptions which are not strictly valid under breaching conditions:

- The available models are derived for steady subcritical flows, equilibrium sediment transport and mild slopes, while during levee breaching the flow is generally supercritical, non-equilibrium transport conditions prevail, and the slopes are relatively steep;
- The bed transport is described with the median grain size, i.e. single grain size, then most of existing multiple-grain size functions cannot properly reproduce bed gradation and the extensions of single-grain size functions to multiple-grain size functions may produce unreliable results.

Nowadays there are no sediment transport models that can be directly incorporated in the prospective breaching model. A new breach model must include a set of sediment transport models to be selected depending on the specific situation.

2.6 Available breach models

Several breach models were developed over the last decades in the attempt of reproducing realistically the breaching process and hence the breach outflow hydrograph.

Modelling the breaching process means simulating the evolution of the breach and hence the temporal trend of the flow outing from the broken levee. The outflow hydrograph is

related to the breaching process, so that different temporal stages are defined as for the levee erosion process (see Section 2.3):

- The initial stage concerns a starting seepage through or flow over the embankment, whose current modelling ability is limited and really uncertain because of the uncertainty about the breach initiation process and its time development;
- During the development stage, the outflow discharge increases until reaching the peak value $Q_{br,max}$, whose behaviour depends on the deepening of the breach channel and successive longitudinal erosion;
- The final stage shows the decreasing of the breach discharge depending on the available flood water (the flood hydrograph in the river), the levee design and condition, the breach sizes and the rapid repair works.

A recent breaching model review is found in the IMPACT and FLOODSite Projects (particularly Morris, 2009b and 2009c).

The current ability in modelling the peak discharge is moderate (± 30%), while it is still poor in predicting the growth rate and the ultimate breach dimensions.

2.6.1 Classification of available breach models

Breach models are typically described as one of the following main kinds of models:

- Purely empirical models;
- Semi-physically based, analytical and parametric models;
- Physically based models.

2.6.1.1 Purely empirical models (Morris, 2009b and 2009c)

Purely empirical models are usually based upon data collected from a series of documented breach events and which are not necessarily or explicitly physically based. Breach parameters (e.g., peak discharge, breach length, etc.) are estimated from predictor equations, derived as best fit to the available data. The primary advantage of these equations is their simplicity and the small amount of required input parameters as compared to more complicated methods. In such a way, they can provide some useful insights into levee breach geometries and the associated time to develop the breach.

However, this simplicity also represents one of their main weaknesses, as the prediction may be associated with considerable uncertainty. An additional limitation is that in general only integral quantities are predicted by the equations, thus ignoring the temporal development of the variables.

Wahl (1998 and 2004) proposes a review of the predicting breach parameters (e.g., breach geometry, time of breach formation, peak of breach hydrograph) for earth dams, while only few empirical equations were found for the case of river levee breaching (Nagy, 2006). Empirical equations developed for dam breaches implicitly consider the fact that the dam retains a finite volume of water which is exhausted during flow through the breach (flux boundary condition for the solution of the boundary value problem of breach growth).

This approach conflicts with the conditions present during major flood events in rivers. During these events, the volume of water available to flow through the breach may be essentially unbounded (at least for major floods). In this case, the breach geometry and breach development time may indeed be considered as independent variables. Solution of the

boundary value problem for levee breaches relies upon entirely different boundary conditions, so that the particular solution for a levee breach should not be expected to be the same as that one obtained for a dam breach.

Furthermore, the empirical equations developed from dam breach observations typically limit the progression of erosion so that breach does not proceed into the foundation soils beneath the dam. In the case of major levee failures, scour of the foundation soils may give a significant contribution to increase the area through which water may flow into the floodplain.

The application of empirical equations to a given breach may be inappropriate if the characteristics of the breach (e.g., the material of the levee) and the mechanisms of its development do not conform to those for which the empirical equations were developed.

For these reasons, a strong motivation exists to understand the basic properties influencing breach growth and the specific mechanisms governing breach erosion and growth. One or more of these mechanisms may be at work at any given time, and a breach model would ideally uncover which mechanisms dominate each stage of breach development and identify bifurcation points at which the relative influences of various mechanisms are changed. This sophisticated characterization of the breach size and development represents the goal of breach growth models (Wahl et al., 2008a).

2.6.1.2 Semi-physically based, analytical and parametric models

The large range of uncertainty associated with the non-physically based methods on one hand and the complexity of the physically based methods on the other hand, prompted researchers to develop models based on an improved understanding of the physical processes involved, but with simplified assumptions to model the failure of dikes. The purpose of these models is to improve the prediction capability by adding some of the mechanisms involved in the entire breaching process without complicating excessively the computation procedure. The breach growth is often simulated by using a greatly simplified set of physical rules in combination with certain empirical observations. This approach is employed in the simulations developed from BREACH, BEED, and DEICH_P models (Saucier et al., 2009).

The following assumptions are usually made in such models:

- A weir equation can adequately represent the flow over the embankment;
- Critical flow conditions exists on the embankment crest;
- An initial breach is typically selected before the time dependent breach growth process starts.

Based mainly on the above assumptions, a model can be developed to simulate breach growth as a time-dependent process and compute breach hydrograph by using the principles of hydraulics.

Typically, like described in Saucier et al. (2009), the modelled mechanisms are:

- Assumed an initial breach, the hydraulic conditions in the vicinity of the breach are commonly defined to fit the assumptions of a broad-crested weir equation;
- The rate at which the levee is removed, and also the rate at which the breach grows, is governed by the rate at which soil is sheared away from the exposed surface of the levee or by the rate at which the flow through the breach is able to transport materials away from the breach;
- The average flow velocity through the breach is used to estimate the rate of mobilising shear stresses acting on the exposed levee surfaces;

- The erosion rate of the flow through the breach is estimated from an equation employing the "excess shear stress rate" ($\tau_b - \tau_{cr}$);
- Several breach models (e.g. BREACH model) supplement the volumetric erosion rate through investigating mass wasting mechanisms such as the collapse of the side walls of the breach, by means of geotechnical considerations;
- The volumetric transport rate of the water flowing through the breach is also considered, and it may be calculated from a conventional sediment transport equation;
- The rate at which material is removed from the levee section is taken as the larger of the values of the volumetric erosion rate and the volumetric transport rate;
- Several alternative empirical geometric constraints on the breach geometry (e.g., the breach length is maintained proportional to the breach depth) are also commonly assumed.

Some typical models describing the evolution of the dam breach channel are given by, for instance, Macchione and Rino (1999) and Covelli (2006), while few studies are given for the specific case of river levees (Fujita and Tamura, 1987).

This type of breach models is widely used in practice, as they give some account of the physical mechanisms governing breach growth while retaining computational simplicity by empirically-justified constraints.

In spite of the simplicity of these methods, they often require the model user to provide an erosion rate for the breach growth or the final dimensions of the breach shape and time of failure of the embankment. The model simply predicts a growth pattern to fit these parameters and hence produces a flood hydrograph. However, these parameters cannot be easily identified and they can differ significantly from one case to another. Hence, whilst these models appear to provide a more accurate prediction of the flood hydrograph, as compared to empirical equations, they simply reflect the data provided by the user and hence can also include a large degree of uncertainty within these data.

2.6.1.3 Physically based models

Physically based numerical models simulate the failure of embankments based on the observed processes, such as the flow regimes, erosion and instability processes. Principles of hydraulics, sediment transport, and soil mechanics are used (e.g., NWS-BREACH).

Assuming the flow field through the breach may be adequately characterized at a particular instant during the levee breach development, a physically based model considers where the levee is being eroded by the fluid flow, by comparing estimates of the mobilising shear stress rate imposed by the flow to erosion rates of the soil obtained from laboratory testing performed at various mobilising stress rates. This comparison may be done at every point along the levee and local ground surface at the instant in time for which the flow conditions have been characterized.

Based upon the field of local erosion rates, the volume of soil eroded during a small increment of time may then be calculated, so that the entire topography of the ground surface is altered. The revised ground surface is then fed back into a redefined hydrodynamic model to update estimates of the fluid flow field.

Physically based models can be further subdivided into empirical and theoretical models, based upon the degree of use of empirical relationships within the model versus theoretical processes. For example, SIMBA model (Hanson et al., 2005; Temple et al., 2005) predicts the

growth and progression of head cut advance through cohesive material, the stages of breach formation, flood hydrograph and breach dimensions. The model is based around the use of an erodibility coefficient for the embankment soil, whose value is determined experimentally.

Other models (as FIREBIRD and HR BREACH) use theoretical relationships to simulate the physical processes. However, there is always a degree of empirical relationships embedded within the models, as modelling "factors" or coefficients (e.g. weir discharge coefficient).

In the last decades many models have been developed to simulate the failure of embankments. From the models review proposed by Morris (2009b), it results that only Fujita and Tamura (1987) performed numerical simulation in the context of river levees.

Faeh (2007) modelled numerically the breach erosion of a river levee without taking into account the sediment transport in the river.

A recent model (RIC-Nays) was developed as a two-dimensional numerical model for flood flow and morphology and it was applied to simulate the breaching of an earthen levee (Islam and Tsujimoto, 2011 and 2012). Islam (2012) applied this model to experimental investigations of river levee breaches performed by Islam et al. (1994) and Zenno et al. (2011) used it in order to simulate the full-scale experiments in Chiyoda channel.

Like the others approaches, physically based numerical models have advantages and weaknesses.

The advantages of using physically based models may be summarised as follows:

- The breach growth processes are simulated by modelling observed physical processes, generally incorporating aspects of hydraulics, sediment transport, soil mechanics and structural behaviour;
- A real estimate of the outflow hydrograph and breach growth process is predicted, without (in more recent models) predefining or constraining the predicted growth process;
- Uncertainties within individual processes or parameters may be included within the model.

The limitations of physically based models may be summarised as follows:

- Computer codes are required;
- Model runtimes can become quite long as the simulation of processes becomes more complex and not justified when limited data are available for model calibration;
- Current computing power means that 1D/pseudo2D models incorporating hydraulics, sediments, soil mechanics and structural stability are feasible; 2D/pseudo3D models incorporating all of these elements are being considered and developed, but are not yet practical in terms of model run time or validated in terms of improved performance (relative to the faster 1D models).

2.6.2 Limitations and uncertainties of available breach models

To date most of breach modelling has focussed upon the development of a generic breach model that can be applied to any situation. In recent years there has been recognition of fundamental differences in processes as a result of morphological and hydraulic boundary conditions.

For instance, it is recognized that there are substantially different hydraulic load conditions between coastal, fluvial and reservoir embankments and these may alter the way in which breach initiates and grows. A breach growth through a river flood levee will be affected by the flow field and the hydro-morphodynamic evolution in the river channel, which defines boundary conditions completely different from the dam breach case, where approach flow conditions are static. Hence, there is a need to investigate different hydraulic load conditions that embankments may be exposed to and identify how breach initiation and growth processes are affected by these variations.

In general, most of the available numerical dam breach models rely on bed-load type erosion formulas that imply assumptions of gradually varied flow and relatively large flow depth in comparison to the size of roughness elements. These formulations may be appropriate for some stages of the breaching process, but are not consistent with the mechanisms of much of the breaching processes as observed in the field and laboratory tests.

Analysis of field and laboratory tests confirms the dependence of breach growth processes on the soil properties and hence on their erodibility. This suggests that breach models should utilize erosion equations rather than sediment transport equations. A majority of (fluvial and dam) modellers to date have used sediment equations and attempted to maintain sediment continuity through the model.

Use of erosion equations includes the representation of soil properties by an erodibility coefficient and hence allows for simulation of the same soils with varying erodibility arising from different soil states. Such an approach is not possible by using sediment transport equations. Accepting a rate of erosion calculation, rather than conservation of sediment mass, also allows for the soil wasting processes referred above.

Further limitations of the existing breach models may be summarised as follows:

- The simulation of breach location and initiation is usually assumed as an initial arbitrary breach;
- Infiltration processes are scarcely considered in the available models (some examples have been found in D'Eliso, 2007 and Stanczak, 2008), although seepage influences erosion and induces mass instability;
- Discrete erosion is another gap in modelling, as being solved with continuous averaged models;
- Embankment base erosion is usually neglected, although is important in determining the final breach dimensions;
- Backwater effects are neglected or simplified, but the shape of the outflow hydrograph is strongly affected by the water level growth in the inundated area;
- Laboratory and field tests on real river flood embankments are not available and hence validation data sets are limited.

2.6.3 Implications for the present study

Modelling the entire breaching process of a flood levee means simulating the breach growth at each stage of the process and the consequent outflow discharge hydrograph. This means also predicting breach initiation and location physically derived from the prevailing initial and boundary conditions.

At present, several breach models exist with different grades of approximation-sophistication and thus with different capabilities to reproduce the actual physical mechanisms and the entire breaching process. Usually three types of models are distinguished:

- Purely empirical models;
- Semi-physically based, analytical and parametric models;
- Physically based models.

Even the most advanced physical based models neglect some important aspects of the breaching process and anyone deals with the specific case of flood river levee without introducing strong approximations. The available models usually applied to the levee case focus on a breaching process which is governed by a static volume of water stored upstream the levee, while when a breach develops in a levee, a complex flow field takes place and there is a mutual relationship between breach evolution and river hydro-morphodynamics. As a matter of fact, the river flow dynamics and morphology influence the breach evolution.

An advance in the research field of river levee breaching is then possible only if this complex dynamics of the river is taken into account and coupled with the breaching process.

Investigating such an interaction can be achieved only through a process-oriented approach (both by means of analytical/numerical models and of experimental investigations), which analyses the involved phenomena without strong assumptions about the physics of the problem and which considers not just the processes affecting the levee but also the dynamics of the flow and the evolution of the bed in the river.

2.7 Specification of objectives and methodology

A thorough review of the state-of-the-art about breaching of embankments has provided an analysis of available studies, knowledge, models and experiments of river levees. Particularly, the existing kinds of breach models have been compared highlighting both performances and weaknesses. An important conclusion is that most of the current knowledge is based on the specific case of dam breach, which can not apply totally to the case of river levee breaching that is expected to have important differences regarding the involved physical processes.

The present research has been planned on the basis of this review, in the sense that the gaps into the existing knowledge and modelling were identified in order to develop new approaches to the problem and, hence, to improve the present understanding associated with the entire breaching process of river levees.

The following objectives and methodology were derived for the present study.

2.7.1 Objectives

The process that leads a flood river levee to breach by overtopping or seepage flow is very complex because it involves mutually dependent interactions between fluvial hydraulics, embankment stability and sediment transport and it is still scarcely understood.

The most used models for the prediction of breach development follow an empirical approach, in which the predicting equations are not able to reproduce the breaching characteristics in a river levee, since they are essentially developed for dam embankments, whose conditions (static water basin) greatly differ from those prevailing in river levees (dynamic flow field).

Hence, the main goal of this research is the development of a new approach for the understanding of the breach evolution in river levees, which should be possibly process-oriented. The proposed approach will investigate the breaching process without strong assumptions about the physical mechanisms, and it will consider both the erosion of the levee and the hydro-morphodynamics of the river flow.

A detailed study of the dynamic relationship between breach development and river hydro-morphodynamics may substantially advance the knowledge about the behaviour of a levee affected by a breach during a flood event and it will provide useful insights on the involved phenomena: the understanding of such processes will help to develop future breaching models for the specific case of river levee.

2.7.2 Methodology and procedure

The research develops according to a new approach, in which the breaching process is split up two main phases:

- A “transitory” phase, which takes into account the first three stages of the general breaching process (see Section 2.3) in which the breach forms and develops according to the interaction between hydraulic conditions in the river and the geotechnical characteristics of the levee material;
- A “regime” phase, in which the breach reaches its final dimensions (related to the fourth stage of the general breaching process) and a steady equilibrium is supposed to be achieved as asymptotic trend of the breach and river hydro-morphodynamic variables.

Both the phases involve an interaction between breach development and river flow. Particularly, the main focus is on the hydro-morphodynamics of the stream flow, since the river determines the conditions acting on the breached levee.

The study is conducted according to three different steps, which focused on and analysed the river hydro-morphodynamics as governing mechanism during the breaching process:

1) Fixed bed hydrodynamic investigations

The first step is to perform a series of experimental investigations regarding lateral outflows in order to understand the hydrodynamics of the process.

An experimental work is conducted on side weir flows in a fixed bed water-recirculating flume with rectangular cross section.

The main objective of the experiments is to investigate the hydraulic regime of a channel when a lateral outflow takes place on one side of the channel in steady conditions, with a subcritical flow as initial regime. A side weir represents a breach that has gained its final configuration and which is then under stationary conditions.

The rectangular side weir had zero height crest and different values of the length: the final aim is to simulate the flow outing from a river when a breach occurs on one of its levee and various lengths of the breach are investigated.

The main result of such experimental activity is to highlight the purely hydrodynamic processes which take place inside a channel during a lateral outflow without considering the mobility of the materials.

2) Movable bed morphodynamic investigations

The second step is to perform a series of experimental investigations regarding a levee breaching process at a laboratory scale.
The main objective of these experiments is the collection of experimental data concerning the processes of breach formation and evolution due to an overtopping flow on an earthen river levee built in a flume with movable bed.
In order to analyse both the breach evolution and the river morphodynamics, a movable bed flume filled with sand was used with a sandy model of the levee as a lateral boundary. Steady flow conditions were set during the tests. In such a way, the "transitory" phase of breach evolution was monitored until an equilibrium of breach and/or hydraulic variables was assumed to be achieved at the "regime" phase.
The primary outcome of this step is to collect a consistent (and usually not available) data-base of experimental tests in which the breaching process of a river levee is investigated together with the hydro-morphodynamics of the river flow.

3) Analytical flow modelling

During the third step, the hydrodynamics of the stream flow is analysed by means of a 1D analytical model that is able to reproduce the main features of the flow field in the river channel when a lateral outflow takes place on one of its side.
The flow in the river is analysed with reference to the theory of the side weir flow in the most common case of subcritical regime. The stream flow is analysed for a steady flow and a fixed bed (non-erodible) geometry, i.e. for a given configuration of the levee breach.
The primary outcome of this step is to get an overview of the river response to the outflow in terms of flow depth, flow velocity and discharge. The "regime" phase is investigated within this step by considering the governing equations of conservation of mass and energy of a one-dimensional flow. An overall picture and understanding of hydrodynamic processes are given. The model is applied to the results of the experimental tests and to some real case data.

The descriptions given by these three tools are integrated each other, in order to give an overall explanation of which processes take place during a river levee breaching with a particular focus on the river part, which is the main governing action.

3 Fixed bed laboratory investigations

The laboratory investigations on fixed bed conditions have been carried out at the Environmental and Civil Engineering Laboratory of Florence during May-November 2011 and were supervised by Prof. E. Paris.

The main objective of these experiments was to investigate the hydraulic regime of a channel with a fixed bed in subcritical regime, when a lateral outflow takes place on one side of the channel, as in case of levee breach in a river. When a breach occurs in a river levee, a lateral flow discharges out of the river: this situation resembles the overflow through a side weir (Kamrath et al., 2006; Saucier et al., 2009; Oertel et al., 2011) and the levee breach can be then considered as a side weir. The hydraulic variables were observed in different scenarios: a side weir was placed on one side of the channel with the height crest at bottom level of the main channel (zero height crest) and several values of the length. The crest height was set to zero in order to simulate a breach configuration where the entire levee section is eroded vertically until the river bed and the breach has achieved different lengths.

The main result of such experimental activity is to highlight the purely hydrodynamic processes which take place in the main channel during a lateral outflow without considering the mobility of the materials: the bed layer of the channel was not erodible as well as the lateral weir that simulates the levee breach. Hence, the side weir is aimed to represent a breach that has gained its final configuration and which is under stationary conditions: steady flow conditions during a breaching process are referred to the last stage of the process, in which the breach is assumed to do not lengthen more and the outflow discharge to get a constant value.

3.1 Experimental set-up

3.1.1 Experimental facilities

The experimental investigations were carried out in a 5 m long, 0.435 m wide and 0.3 m deep glass-walled water-recirculating tilting flume with rectangular cross section. Figures 3.1-3.2 show the plan and cross view of the apparatus and some pictures are given in Figures 3.3-3.5.

The flume was subdivided longitudinally into two separated channels by a vertical 0.3 m high glass wall. The main channel represented the actual testing facility where the incoming liquid discharge was put in. It was 0.3 m wide and 0.16 m deep, since its bottom was raised by a new plexiglass layer. The second channel, 0.125 m wide and 0.3 m deep, constituted a lateral channel which allowed to evacuate the diverted discharge. At about 2 m from the flume entrance section on the left side, a 0.16 m deep window was inserted on the vertical separation wall, which could reach a length of about 0.5 m: it worked as side weir in order to spill the lateral outflow. The main and the lateral channels were separated each other by the glass wall and the lateral channel upstream end was closed toward the inflow basin, so that water could flow in the lateral channel only through the side weir.

The bottom of the lateral channel was lower than the main channel in order to avoid backwater effects from the outflow toward the main flow.

At the downstream end of the main channel a sluice gate was set to control the downstream boundary condition, while the lateral channel ended over the storage basin.

A fixed roughness composed by granular gravel with a D_{50} = 6.8 mm was stuck down to the bottom of the main channel in order to provide a realistic resistance to the flow: the Chézy coefficient resulted in the order of $C_h \approx 10$. The gravel was coloured with black spray in the central region, where the side weir is placed, in order to get more evident images during the cam acquisitions.

The flume had an inclination $S_0 \approx 0.1\%$, that was checked by simulating the data collected during the first tests with the hydraulic numerical model Hec-Ras.

The recirculating water discharge was regulated by a valve and measured by means of an electromagnetic flow-meter (IDM).

The carriage moving along the flume was used for measurement of water surface and flow velocity as described in Section 3.1.2.

The goal of the experimental activity was not to scale a singular case of study, but it was to investigate a process without reproducing a real prototype. Nevertheless, it is important to check the main properties of the physical model in order to verify that a realistic process is reproduced. Fluvial hydraulic systems are mainly governed by gravity action, so that the Froude number gets high importance. According to the typical values of the variables recorded during a test with the median length of the side weir (L_s = 23 cm, see Table 3.2 for numerical values), it is calculated Fr ≈ 0.57, which is a realistic value for a real river in subcritical flood regime. The Reynolds number is evaluated in the order of $Re \approx 3 \cdot 10^4$, which, for a relative roughness ε_r of about 10^{-1}, is referred to a fully turbulent flow that is consistent with conditions found in real rivers. Moreover, a possible order of magnitude for the length scale of the investigated phenomena can be $\lambda_L = 1:10^2$, which would give the following values of the variables referred to a river prototype:

- River width = 30 m;
- Side weir length = 23 m;
- Flow velocity = 4.8 m/s;
- Flow discharge = 1000 m^3/s.

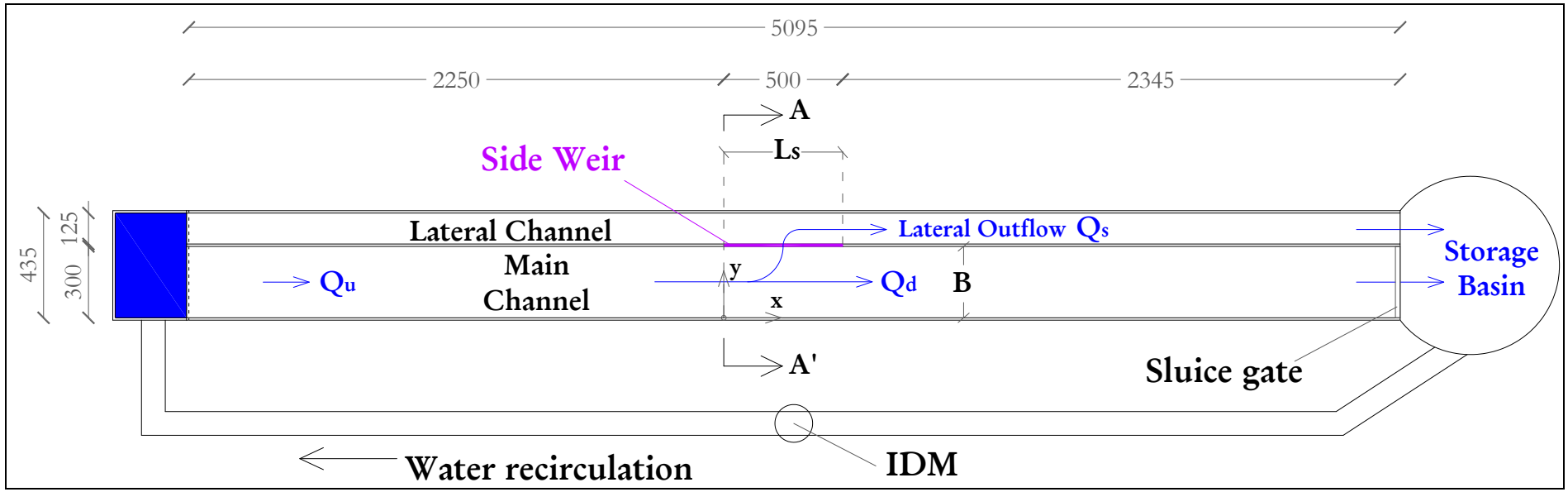

Figure 3.1: Sketch of the experimental apparatus (plan view: the dimensions are in mm).

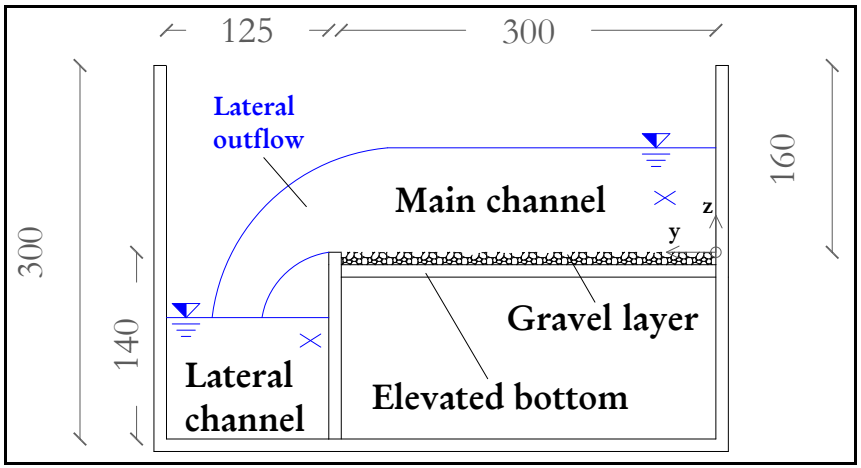

Figure 3.2: Cross section A-A' of the flume (the dimensions are in mm).

Figure 3.3: Aerial picture of the flume.

Figure 3.4: View of the flume from the main channel: on the left, the side weir.

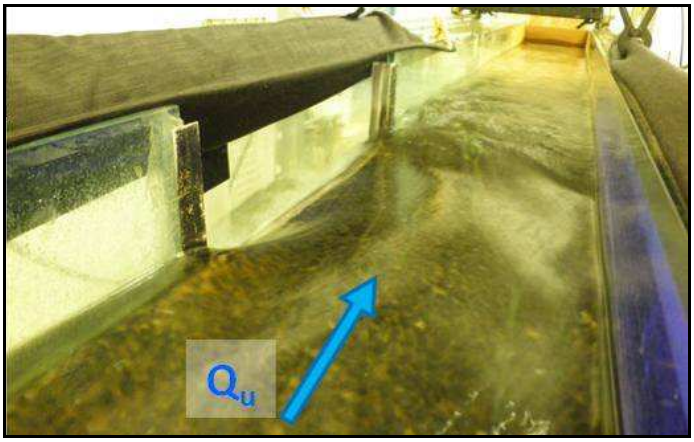

Figure 3.5: View of the flume: zoom on the side weir.

3.1.2 Measuring techniques and observations

Within this Section the instruments used to measure the variables during the experimental tests are described into different paragraphs. Basically, the hydrodynamics of the flow was observed by means of measures of water levels, flow discharge values, vertical profiles of velocity and superficial flow field.

3.1.2.1 Water surface profile

The water level was recorded by means of ultrasonic sensors (USs) Honeywell series 943-F4V-2D-1C0-330E. All the sensors recorded the water level with a frequency of 4 Hz and a maximum error of ± 1 mm. Water level data were elaborated as average values over a time window of 60 seconds. All the gauges were fixed to the flume structure or to the carriage by means of metal frames and they recorded the distance between the probe and the water surface. The recorded levels were then transformed into a distance referred to the bottom of the main or of the lateral channel, depending on where the measure was taken.

The fixed USs working in the main channel were used to measure the water depth at some sections along the central alignment, while the sensor attached to the carriage was moved along and crosswise the flume to record the water surface profile. Finally, the water level recorded by the US in the lateral channel was used to gain the outflow discharge, as explained in the next Section.

The data recorded by the ultrasonic sensors were saved and managed into a PC by means of the software LabView.

3.1.2.2 Flow discharge

The inflow discharge (Q_u) was delivered from a basin by the use of a recirculation system where a pump fed one pipe controlled by an electromagnetic flow meter (IDM). A steady flow rate could therefore be easily set and maintained accurately throughout the duration of each test.

The lateral outflow discharge (Q_s) was determined by using the water level measured by an ultrasonic gauge: Q_s was calculated by means of the rating curve of the lateral channel previously calibrated. As a further control, the discharge flowing in the main channel downstream the side weir Q_d was also calculated by using the rating curve at the last downstream US in the main channel.

The inflow discharge was acquired into the PC by means of LabView software.

3.1.2.3 Velocity profiles

Vertical velocity profiles were measured by means of an acoustic doppler profiler DOP1000.

The profiler gave a 1D-velocity profile along the flow depth where it was submerged. The probe had an emitting frequency of 2 MHz and each 1D-profile was the result of 600 acquisitions with a spatial resolution of one point every 0.7 mm of distance along the beam alignment. Velocity profiles were elaborated as average values over a time interval of about 60 seconds for each profile acquisition. The profiler was tilted with an angle of 70° with respect to the flow direction in order to catch properly the velocity profile and to be not too far from the vertical axis: the sample volume length in the flow direction depended on the flow depth and it was less than 7 cm. The probe was set on an iron frame fixed to the carriage

and it was necessary to submerge it enough to avoid air entrainment: therefore, the first acquisition channel was about 15 mm below the water surface.

Velocity profiles were acquired both in the streamwise and crosswise directions, as explained in Section 3.3 at the description of each test series.

3.1.2.4 Particle Tracking Velocimetry – PTV

Surface flow field was acquired through a Particle Tracking Velocimetry technique. Streamlines were recorded by means of tracers floating in the flow and video-cam hung on the ceiling (see Figures 3.6-3.7). The tracers were luminous beads lighted by two Wood's UV lights placed at the plexiglass vertical walls of the channel (see Figure 3.8): the tracers became fluorescent when lighted by the UV lights acting on dark background so that their passage was recorded by a PixelFly VGA cam with an acquisition frequency of 19.2 frames per second. Some black sheets were used to cover the metal frame of the flume in order to reduce the noise on the images. Moreover, the gravel layer at the bottom of the flume was coloured with a black paint spray.

Even if it was not possible to use this PTV technique at other flow depths, a qualitative visualization of the flow in the lower, near bed, layer was also performed with heavier tracers.

Tracers were trapped at the end of the flume by means of a net placed over the storage basin.

The procedure used to perform the PTV acquisition as well as the data elaboration methods are explained in Sections 3.2 and 3.3.

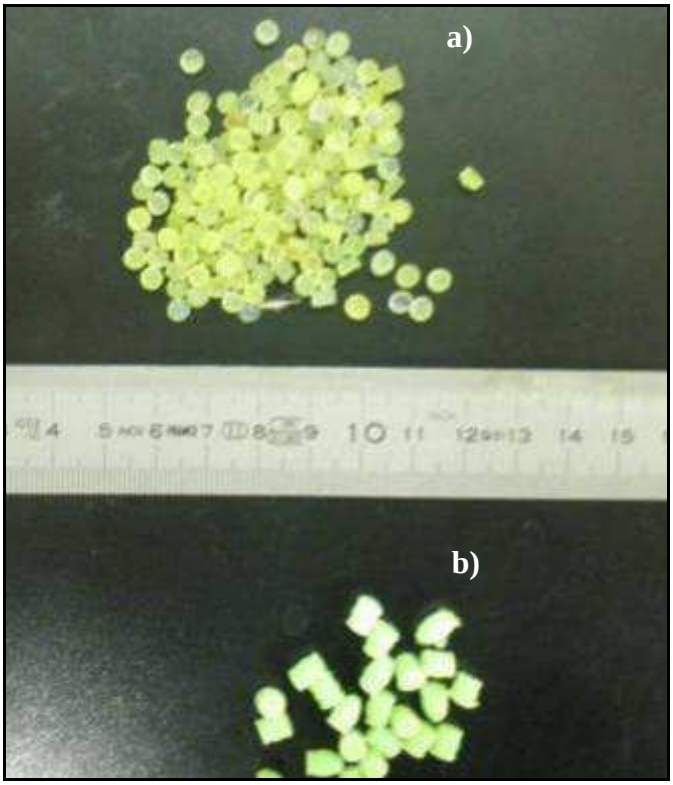

Figure 3.6: Tracers used in PTV technique: heavy (a) and light (b) beads.

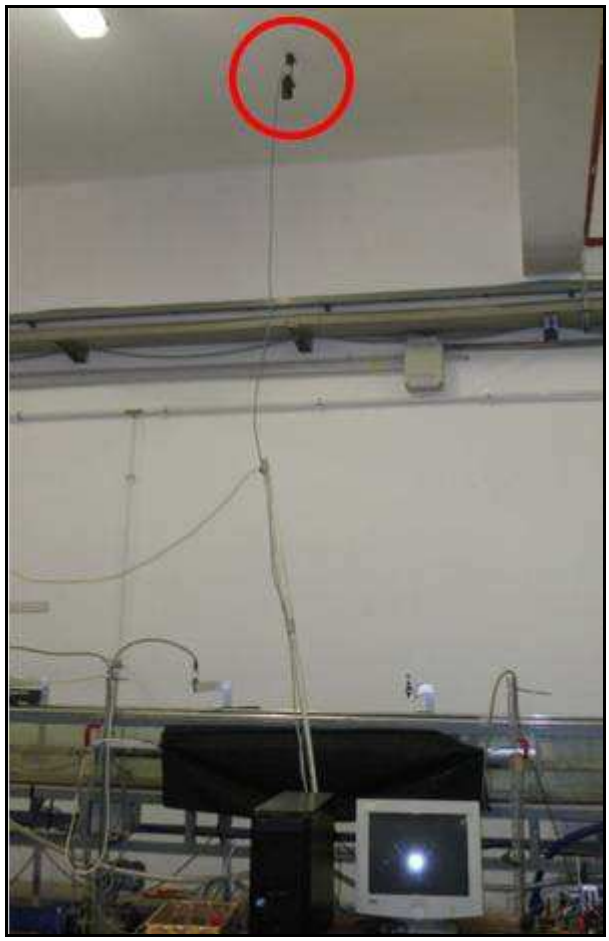

Figure 3.7: CAM used in PTV technique from the ceiling.

Figure 3.8: UV lights used in PTV technique.

3.1.2.5 Experimental errors

The ultrasonic sensors acquired data with a precision of ± 1 mm. This means that the percentage experimental error ranges between a maximum value, where the minimum flow depth is measured, and a minimum value, where the maximum flow depth is gained. Therefore, a maximum error of ± 3.3% can be predicted when the flow depth is measured at the side weir alignment, while a minimum error of ± 0.8% is foreseen regarding the downstream flow depth.

The error over flow depth also gives an error on the calculation of the flow discharge through the use of the rating curves at the downstream section of the main and lateral channel. An error of ± 1 mm on the measure of the flow depth in the main channel results in an error less than ± 1% over the computed downstream discharges. By the same way, an error of ± 1 mm on the measure of the flow depth at the ultrasonic gauge in the lateral channel results in a maximum error of ± 4.4% over the outflow discharge computed by means of the rating curve of the lateral channel.

3.2 Testing programme and test procedure

In order to analyse the influence of the breach configuration on the river flow, the side weir length L_s was chosen as main test parameter. The lateral window in the model set-up was set to different lengths by means of regulating plexiglass wall so that the upstream section remained fixed while the downstream varied from on test to another, whereas the height of the side weir was always at the level of the main channel bottom (i.e. zero height crest, as depicted in Figure 3.2 of Section 3.1.1), since a breach usually erodes vertically until or under the levee toe. This choice was made in an attempt to simulate the lengthening process in the more realistic way (lengthening mainly downstream, as mobile bed experiments will show).

A constant value of the inflow discharge Q_u was chosen and kept in steady condition throughout the duration of the test.

The opening height of the downstream sluice gate Y_g is a very important task, since it controlled the downstream boundary condition which has great influence on physical processes in subcritical flow. This condition was chosen in order to have subcritical flow along the channel or at least for the part downstream the breach, since this is the most common hydraulic situation found in real cases during flood events of embanked rivers. The flow conditions at the downstream sluice gate were checked by coupling measures of flow rate and water depth at a section close to the gate: these data are presented in Section 3.3.

3.2.1 Test series

Three main series of tests were performed, whose conditions are summarized in Table 3.1.

The code of each test is composed by a string of characters which identifies the main features of the test, as explained by the following sketch.

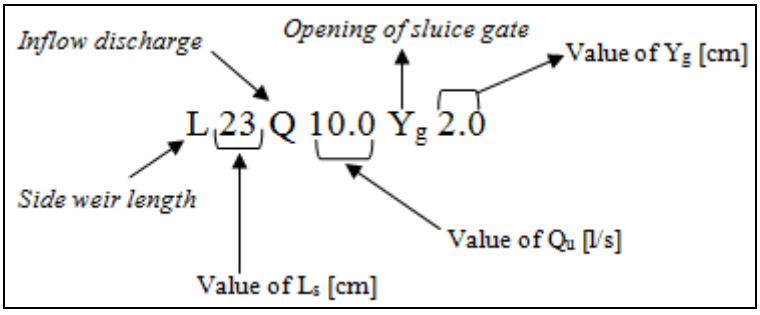

Tests of series A concern conditions without lateral outflow: the side weir was closed and different inflow discharge and downstream boundary conditions were imposed. The aim of these tests was to collect data to check the rating curves and to provide a reference case that could be compared with the next lateral outflow series. Water surface was measured as longitudinal profile along the flume.

The largest number of tests was performed for series B: an inflow discharge Q_u = 10 l/s and a downstream sluice gate opening Y_g = 2.0 cm were set and ten different lengths L_s of the side weir were imposed, ranging from 3 to 47 cm every 5 cm. This sluice gate opening was set in order to have subcritical flow, as it will be shown in Section 3.3.2. Among series B, three side weir lengths were analysed by investigating the flow field and the velocity profiles in a more detailed way. Particularly, velocity profiles in longitudinal direction were investigated for every test, while velocity profiles also in transversal direction were measured for the detailed tests only (tests B7, B11 and B16). Moreover, a detailed survey of the water level surface was collected at the side weir site for these three tests, whereas, during the other ones, water surface profile was acquired only at the central alignment of the main channel. Anyway, water levels, velocity profiles streamwise and flow field were recorded for every test of series B.

Series C is the last series of data, for which the downstream boundary condition was changed to Y_g = 3.4 cm in order to investigate the influence of a different downstream condition on the lateral outflow, while the inflow discharge kept the steady value Q_u = 10 l/s. Only longitudinal water surface profiles were acquired for this series of tests, while no direct velocity measurement was taken.

Table 3.1: Summary of conditions and measured data types for the performed test series.

Series	Test	Run Code	Side weir length L_s [cm]	Side weir height p_s [cm]	Inflow discharge Q_u [l/s]	Sluice gate opening Y_g [cm]	Water surface measurement			Vertical velocity profiles		PTV
							Point measurement	Longitudinal profile	Side weir site survey	Longitudinal	Transversal	
A	1	L00Q3.00Yg2.0	0	0	3.0	2.0	No	Yes	No	No	No	No
	2	L00Q4.50Yg2.0	0	0	4.5	2.0	No	Yes	No	No	No	No
	3	L00Q6.50Yg2.0	0	0	6.5	2.0	No	Yes	No	No	No	No
	4	L00Q6.50Yg3.4	0	0	6.5	3.4	No	Yes	No	No	No	No
	5	L00Q8.00Yg3.4	0	0	8.0	3.4	No	Yes	No	No	No	No
	6	L00Q10.0Yg3.4	0	0	10.0	3.4	No	Yes	No	No	No	No
B	7	L03Q9.52Yg2.0	3	0	9.5	2.0	Yes	Yes	Yes	Yes	Yes	Yes
	8	L08Q10.1Yg2.0	8	0	10.1	2.0	Yes	Yes	No	Yes	No	Yes
	9	L13Q10.0Yg2.0	13	0	10.0	2.0	Yes	Yes	No	Yes	No	Yes
	10	L18Q10.1Yg2.0	18	0	10.1	2.0	Yes	Yes	No	Yes	No	Yes
	11	L23Q10.0Yg2.0	23	0	10.0	2.0	Yes	Yes	Yes	Yes	Yes	Yes
	12	L28Q10.1Yg2.0	28	0	10.1	2.0	Yes	Yes	No	Yes	No	Yes
	13	L33Q10.1Yg2.0	33	0	10.1	2.0	Yes	Yes	No	Yes	No	Yes
	14	L38Q10.1Yg2.0	38	0	10.1	2.0	Yes	Yes	No	Yes	No	Yes
	15	L43Q10.1Yg2.0	43	0	10.1	2.0	Yes	Yes	No	Yes	No	Yes
	16	L47Q10.1Yg2.0	47	0	10.1	2.0	Yes	Yes	Yes	Yes	Yes	Yes
C	17	L03Q9.70Yg3.4	3	0	9.7	3.4	No	Yes	No	No	No	No
	18	L08Q10.0Yg3.4	8	0	10.0	3.4	No	Yes	No	No	No	No
	19	L13Q10.1Yg3.4	13	0	10.1	3.4	No	Yes	No	No	No	No
	20	L18Q10.0Yg3.4	18	0	10.0	3.4	No	Yes	No	No	No	No
	21	L23Q10.0Yg3.4	23	0	10.0	3.4	No	Yes	No	No	No	No
	22	L28Q10.0Yg3.4	28	0	10.0	3.4	No	Yes	No	No	No	No
	23	L33Q10.0Yg3.4	33	0	10.0	3.4	No	Yes	No	No	No	No
	24	L38Q10.0Yg3.4	38	0	10.0	3.4	No	Yes	No	No	No	No
	25	L43Q10.0Yg3.4	43	0	10.0	3.4	No	Yes	No	No	No	No
	26	L47Q10.0Yg3.4	47	0	10.0	3.4	No	Yes	No	No	No	No

3.2.2 Test procedure

Each test was performed following a specified procedure for the data collection according to each series. Anyway, some features were common for each test.

Before starting a test, every device was checked and placed in the right location.

The downstream sluice gate was set to the predefined height and the side weir was opened until the tested length. Then the pump was switched on and the inflow discharge was regulated by means of the valve up to the design value. The physical model took about 15 min to achieve stationary conditions. Steady flow conditions were checked by acquiring water surface levels and inflow discharge values. Measurement operations started after about 30 min from the beginning of the test and they needed different time slots according to the chosen measurements.

Point measures of the water surface in fixed cross sections were taken during a single acquisition of 60 s. Longitudinal water surface profile was recorded by means of an ultrasonic sensor fixed to the carriage at the centreline of the main channel width. Detailed water surface around the side weir was acquired by moving the US on the carriage in the transversal direction and by driving the carriage along the flume. The spatial area investigated by such a detailed survey was chosen with reference to the side weir length L_s: a distance of L_s upstream the side weir and $2 \cdot L_s$ downstream it was investigated by several longitudinal strips each one having a spatial resolution of one point every $L_s/10$ in front of the weir.

Velocity profiles were acquired by setting the velocity profiler on the carriage at the designed position (in the spatial reference of the flume) and direction (x or y). The profiler was submerged of some mm in order to avoid air bubbles entrance and the depth had to be set for each different cross section. The submergence depth was measured manually each time. Velocity profile measurements were taken at fixed sections and/or at some sections where it seemed important to catch the flow features (as for the three detailed tests of series B). Regarding the detailed tests, the sections investigated were located in function of the side weir length L_s at various distances: L_s upstream from the beginning of the weir, at the upstream, middle and downstream sections of the side weir, L_s and $2 \cdot L_s$ downstream from the end of the side weir. At each of these sections, the operator had to perform a sufficient number of longitudinal velocity profiles in order to describe the flow field, while a predefined number of 72 velocity profiles were acquired in the transversal direction.

Surface flow field was recorded by means of PTV technique: light tracers were put one by one in the flume upstream at different transversal positions of the cross section to get the streamlines of the flow over the entire width of the main channel. Heavier tracers were put all in a one in the flume and the overall behaviour of the flow in the lower strata was highlighted.

3.3 Measured data and experimental results

Within this Section, the main features of data collected during experimental investigations are presented. Detailed results regarding each experimental test are presented into an internal report (Michelazzo, 2013).

Before describing the results of each test, it is necessary to define the spatial reference that is used for the following elaborations. The variables used to describe the physical model, measured during the tests or calculated in the post-processing, are listed into the previously defined list of symbols.

3.3.1 Spatial reference system

The spatial reference used to locate the measurement in the flume is a 3D Cartesian coordinate system in which:

- The origin is located on the bottom of the main channel, at the beginning of the side weir and at the right side (opposite to the side weir);
- The x-axis is fixed to the glass wall, directed downstream as the flow direction;
- The y-axis is the cross section axis, directed toward the side of the main channel where the side weir is located;
- The z-axis is the vertical axis, directed toward the top.

Figures 3.1-3.2 show the coordinate system used during the experimental investigations.

During the next elaboration of the data, a dimensionless coordinate system is sometimes used, in which:

- The dimensionless x-axis is $x^* = x/B$;
- The dimensionless y-axis is $y^* = y/B$;
- The dimensionless z-axis is $z^* = z/Y_{mean}$, where Y_{mean} = mean flow depth in the cross section.

Regarding the dimensionless system, the side weir is defined between the coordinates (0, 1, 0) and (L_s/B, 1, 0) as depicted in Figure 3.9.

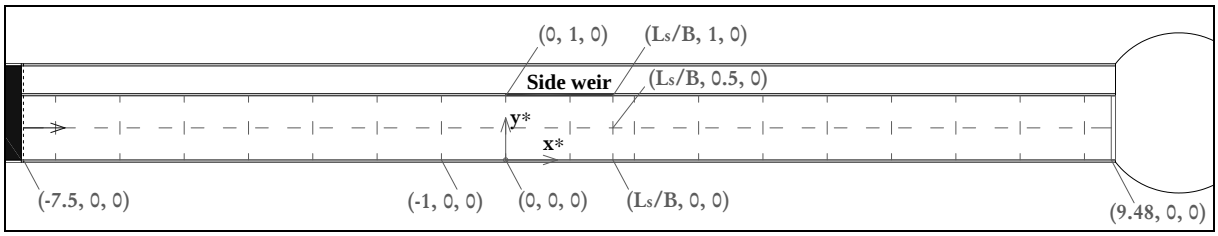

Figure 3.9: Plan view of the dimensionless coordinate system (format: x*, y*, z*).

3.3.2 Measured data post-processing

Post-processing of collected data was necessary to create a consistent data base which was used to analyse the investigated phenomena.

Experimental data were collected during a limited time window, since the inflow was steady and time invariant conditions were assumed for the flow field. A time interval of 60 seconds was considered long enough to make the mean flow field constant in time at every cross section.

Water level data were collected by means of the ultrasonic sensors which recorded the water surface at fixed cross sections and along the flume by means of a sensor set on the carriage. Since they were calibrated with the zero level set at the bottom of the channel, the water levels recorded by the probes were directly converted in flow depths. Regarding the detailed water depth survey performed at the side weir site for some tests, a spatial interpolation was made in order to fit the real water surface with a cell size of 1 mm.

Inflow rate was acquired by the IDM installed at the inflow pipe. Inflow discharge values were recorded by the operator as visual recording and by the PC acquisition system in order to check that the recirculated discharge was constant in time.

The lateral outflow through the side weir was calculated from the water depth recorded by an US installed in the lateral channel 0.695 m far from the flume outlet and by the use of the channel rating curve. The lateral channel downstream section ended directly over the water basin with an ogee-shaped bottom. Several measures of inflow discharge and flow depth at the US were taken in order to calibrate the rating curve of the lateral channel at the US section. The side weir was opened while the downstream sluice gate was closed in order to divert all the inflow discharge toward the lateral channel through the side weir. Figure 3.10 plots the measured data and the regression law which allowed to know the spill discharge. It was then possible to calculate the downstream discharge as in equation 3.1:

$$Q_d = Q_u - Q_s \tag{3.1}$$

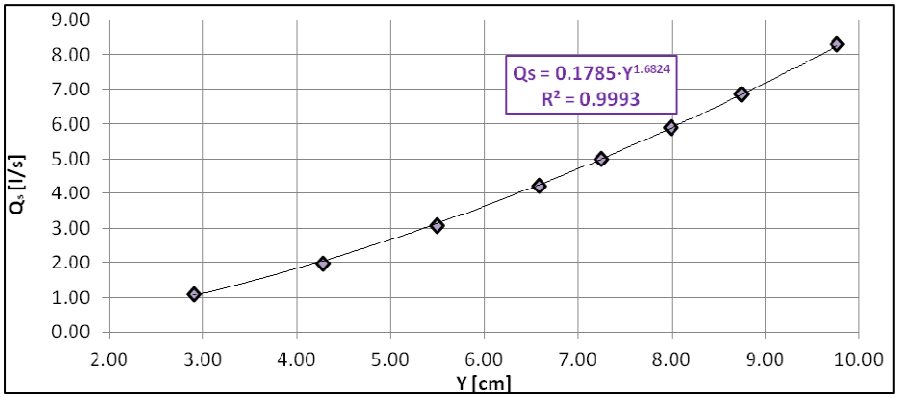

Figure 3.10: Rating curve at downstream section of lateral channel.

The water depth-flow rate relationship was analysed for the downstream part of the main channel as well in order to have another equation for calculating Q_d and, consequently, Q_s. An ultrasonic gauge 0.695 m far from the flume outlet was set in the main channel and coupled measures of water depth and flow discharge were taken. Side weir was closed at this stage and sluice gate was raised at an opening of Y_g = 2.0 cm. These data were useful to analyse the flow regime at the downstream part in comparison with an uniform flow condition and to check the discharge flowing downstream in the main channel. The resulting rating curve is plotted in Figure 3.11, where the regression law is split up three different reaches: the presence of the sluice gate gives this inconstant behaviour which is also compared with the uniform flow condition. Figure 3.12 shows that the downstream condition imposed to the system results in a flow which was always subcritical. This analysis was performed only for the Y_g = 2.0 cm configuration, which was the main one investigated.

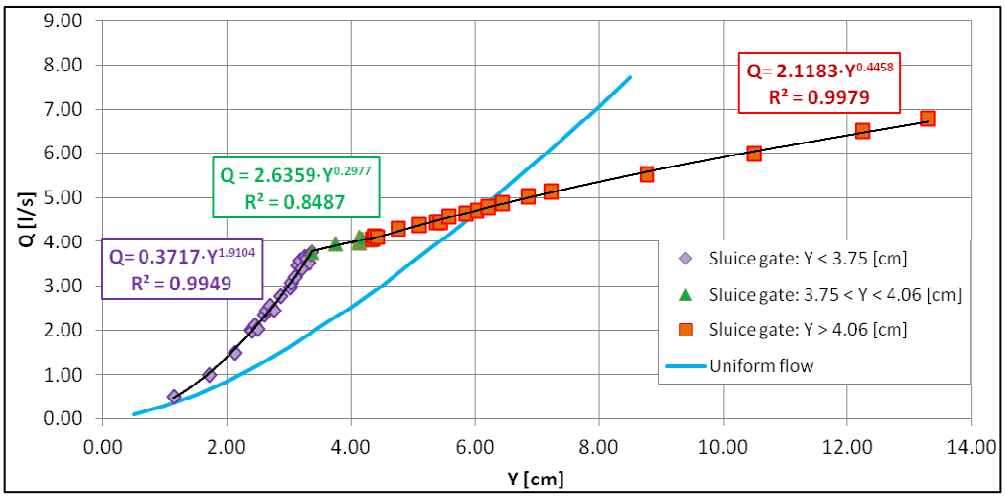

Figure 3.11: Rating curve at downstream section of main channel for sluice gate at Y_g = 2 cm.

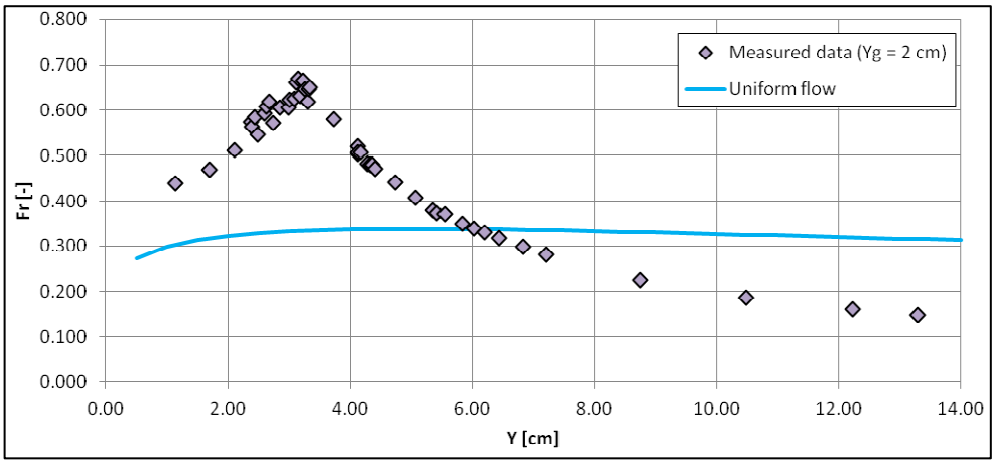

Figure 3.12: Flow regime at downstream section of main channel for sluice gate at Y_g = 2 cm.

Flow velocity was analysed by means of three different methods.

Mean flow velocity on the cross sections was calculated by means of discharge and water depth measures. Since inflow discharge was known and lateral outflow was calculated, the discharge in the main channel upstream and downstream the side weir could be used, while along the side weir it was not possible to measure it. The water depth measured at the central alignment of the main channel was assumed to be the mean water level in that cross section. The mean flow velocity at an x-section was then given by:

$$U_{mean}(x) = \frac{Q(x)}{B \cdot Y_{|y^*=0.5}(x)} \tag{3.2}$$

Local velocity of the flow field was acquired by means of DOP1000. It gave the velocity profile along the flow depth U(z) in the direction of the beam. The profiler was oriented toward the main flow direction (x-axis) and, for the three detailed tests, toward the transversal direction (y-axis) too. Velocity was assumed to be positive in the main direction of the flow (as the positive x-axis) and toward the side weir (as the positive y-axis). The probe was inclined of 20° on the vertical axis in both cases and it was necessary to submerge it under water: the first acquisition channel was then at about 15 mm from the water surface. Each acquisition counted for 600 velocity profiles (with one acquisition channel every 0.7 mm of depth) and it took about 60 seconds. Parameters as amplification level of the signal, maximum detectable distance, maximum velocity were set before each acquisition. The raw data had to be elaborated: the time average velocity profile was taken over the 60 seconds and the velocity profile was completed for the first 15 mm above the probe (i.e., the part of the profile close to the water surface) with a constant velocity value equal to the first recorded channel. The lower part of the profile was cut at the level of the corresponding water depth measured by the US, and, consequently, the conventional lower limit of the velocity profile at the flume bottom was detected.

The velocity profiles along the longitudinal axis were referred to the vertical axis in each section $U_x(z)$, while the transversal profiles data $U_y(z)$ were combined in order to be assigned to the correct position in the cross section, since each transversal profile had its axis in the plane of the transversal section. Moreover, transversal profiles, which partially overlapped each other, were compared each other and they were made consistent by means of filtering operations.

Velocity data were then interpolated in order to obtain a continuous spatial distribution of the velocity field $U_x(z)$ and $U_y(z)$ on the cross section. Border values were assigned at the

limits of the cross section: zero velocity values at the bottom and at the glass walls and maximum velocity at the vertical surface corresponding to the side weir.

Surface flow field was completed by using the PTV technique on the water surface acquired around the side weir site by means of PTV technique.

Singular luminous tracers position along the water surface was detected by means of a system of Wood lights and a CAM which recorded images with a frequency of 19.2 frames per second. Raw data were elaborated one image after the other by a Matlab routine which: smoothed the images and subtracted the background off, identified the tracers as white blobs on dark background, located the blobs in the spatial reference, linked particle locations from different images to form trajectories. Specific filters were created in order to reduce background light noise and to avoid wrong links between streamlines of different tracers. The streamlines of the superficial flow field were then analysed and elaborations, as 2D velocity vectors computation, were performed.

Heavier tracers were employed to visualize the near bed flow pattern. It was not possible to perform a detailed streamline analysis in this case because of the interaction between the particles and the bottom. Anyway, a qualitative visualization of the flow patterns in the lower strata of the flow was achieved.

3.3.3 Experimental results for each test series

In the following Section some of the more relevant results are shown, whereas all details are given in an internal report (Michelazzo, 2013).

3.3.3.1 Series A data

The tests of series A were performed without lateral outflow: the side weir was kept closed and different inflow discharges and downstream boundary conditions were set (see Table 3.1). Water surface profile Y(x) was recorded along the centreline of the main channel. Figures 3.13-3.14 plot the flow depth longitudinal profiles. This series represents preliminary tests to be used as reference case.

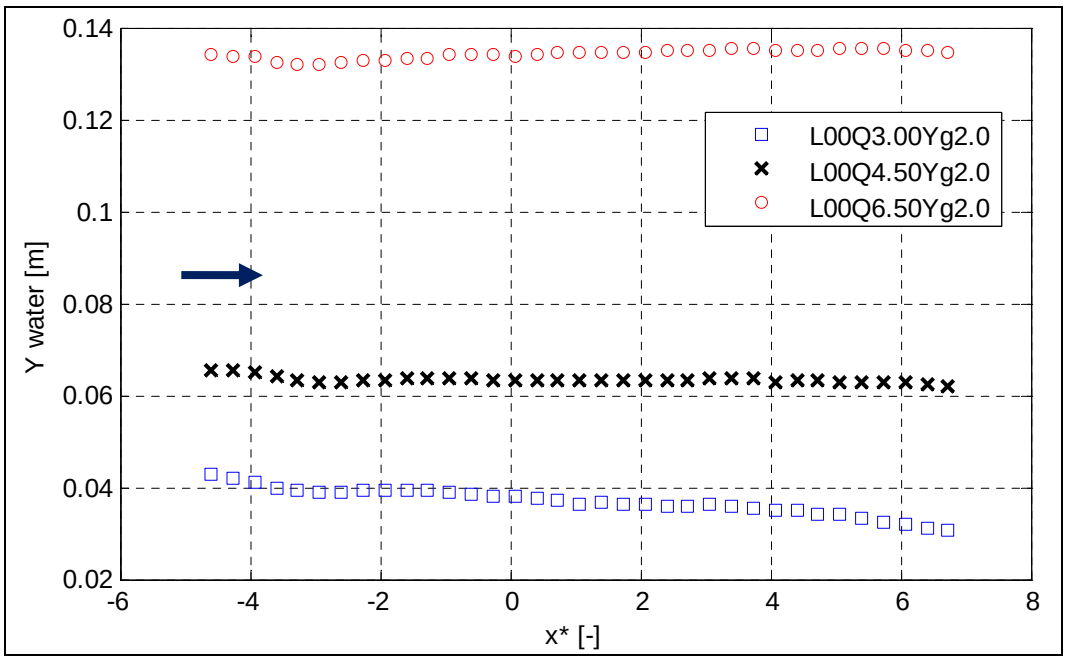

Figure 3.13: Water surface profiles of series A with Y_g = 2 cm.

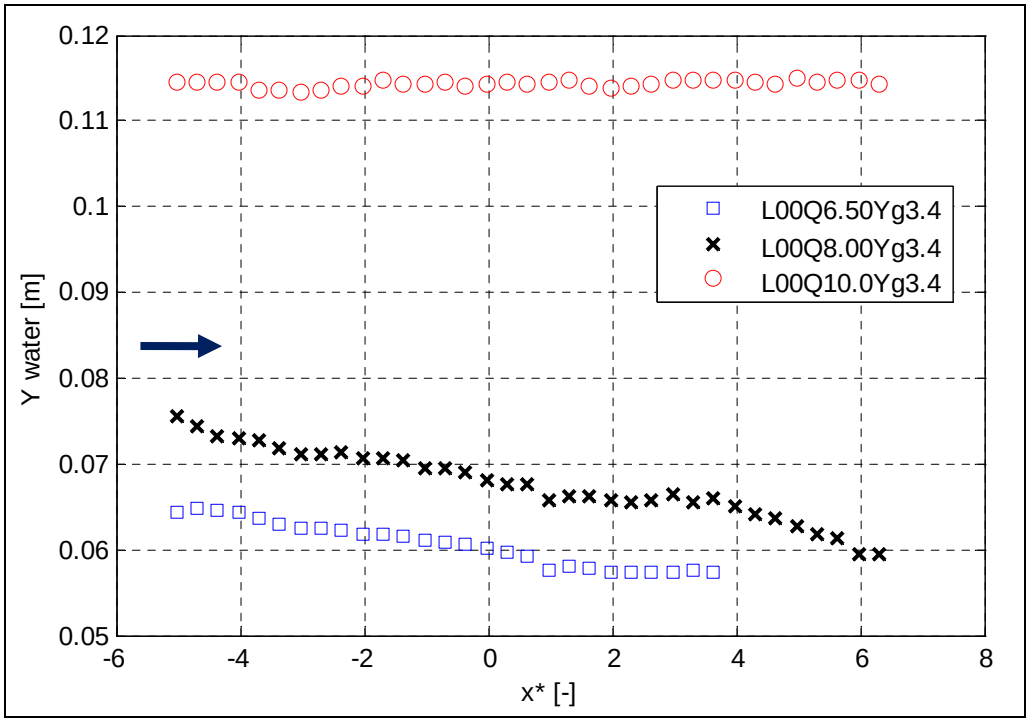

Figure 3.14: Water surface profiles of series A with Y_g = 3.4 cm.

3.3.3.2 Series B data

Tests of series B were performed with the side weir opened at different lengths and the same setting of inflow discharge (Q_u = 10 l/s) and downstream boundary condition (where the sluice gate was kept raised at an height of 2 cm).

Series B is made of two different kinds of tests: the “standard” ones and the “detailed” ones.

Regarding the “standard” tests, four ultrasonic sensors were placed in fixed positions along the central alignment of the main channel: two of those were set upstream the side weir, while two other downstream it. The fifth sensor was located in the lateral channel at the downstream end. The recorded level was referred to the bottom of the main channel for US1, US2, US3, US4 and of the lateral channel for US5. Vertical profiles of longitudinal component of velocity were taken at six cross sections (CS): all these sections were in fixed positions during all the tests, aside from the forth one which was set at the downstream section of the side weir (that changed for each test). Six velocity profiles were recorded for each cross section at regular transverse distances: they are marked as bold lines in the following 3D plots. Water depth at sections 3 and 4 was measured by visual survey and by an hydrometric rod.

The location of the measurement cross sections for velocity profiles is explained in Figure 3.15.

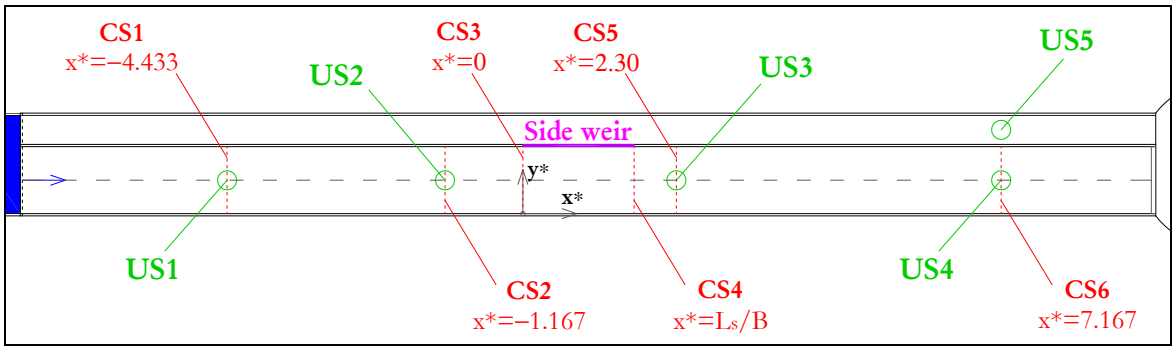

Figure 3.15: Plan view of the flume: measurement cross sections for tests of series B.

Water profile all along the flume was measured by means of an US attached to the carriage and set at the centreline of the main channel.

The PTV technique allowed to visualize and process the streamlines of the flow field at the water surface, whereas only visual analysis was possible for the lowest strata. In the Figures showing the PTV analysis, the side weir is depicted as coloured horizontal line starting at (x* = 0, y* = 1).

Three “detailed” tests (B7, B11 and B16) of series B were investigated more deeply in terms of velocity profiles and water depths. Transversal component of velocity profiles was taken and the longitudinal profiles were recorded in specific locations for each test. Moreover, a detailed water depth survey was conducted close to the side weir site.

The main hydrodynamic features of the system are here described, whereas the detailed results for each test are reported in Michelazzo (2013).

The flow depth profile of one exemplary test is plotted in Figure 3.16: the flow field was accelerated toward the side weir site. It is a typical drawdown subcritical profile with flow depth decreasing downstream as the flow is accelerating. Once the upstream end of the side weir is reached, the water depth generally tended to increase downstream in subcritical conditions. In the downstream zone, the hydrodynamics was governed by the downstream sluice gate.

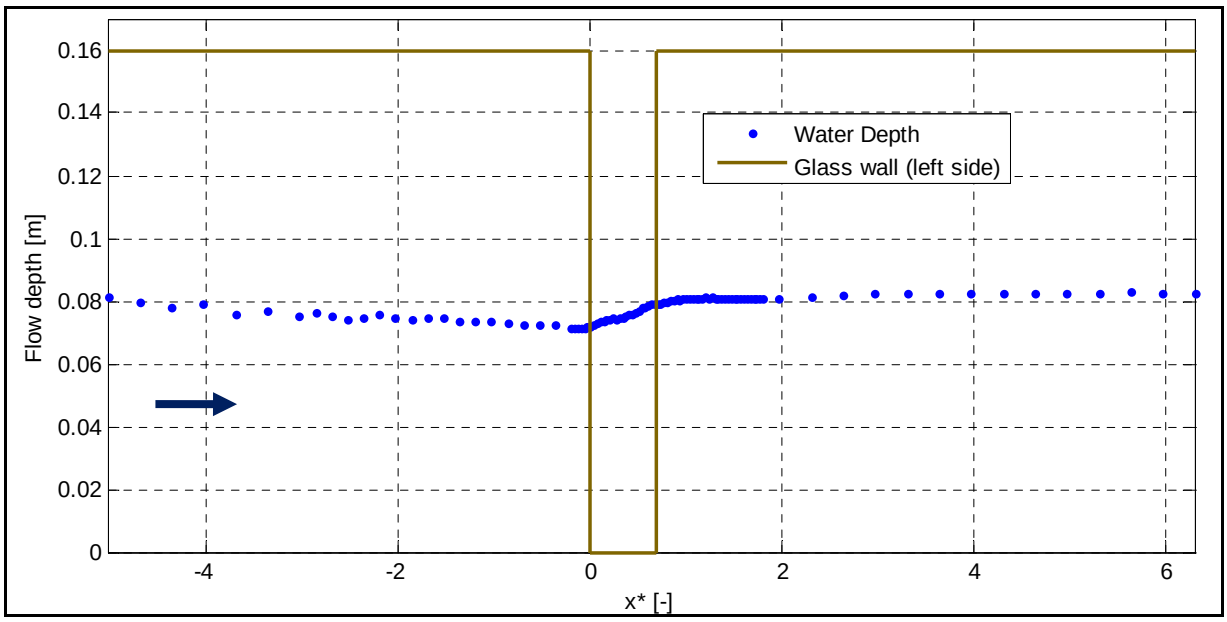

Figure 3.16: Flow depth profile for test B10 (L18Q10.1Yg2.0).

In order to provide a comparison, the longitudinal water surface profiles of tests of series B are all plotted in Figure 3.17. The water profiles are plotted as lines for a better view.

It can be noticed that the upstream water profile decreased more for greater values of the side weir length, because a greater lateral outflow discharges out. The upstream water profile was always above the calculated critical depth Y_{cr}, which means that the approaching flow was subcritical. Anyway, the flow depth along the side weir was not always increasing: a first decreasing part was observed for the tests having the longest side weirs and this may indicate that a first supercritical zone occurred for those tests.

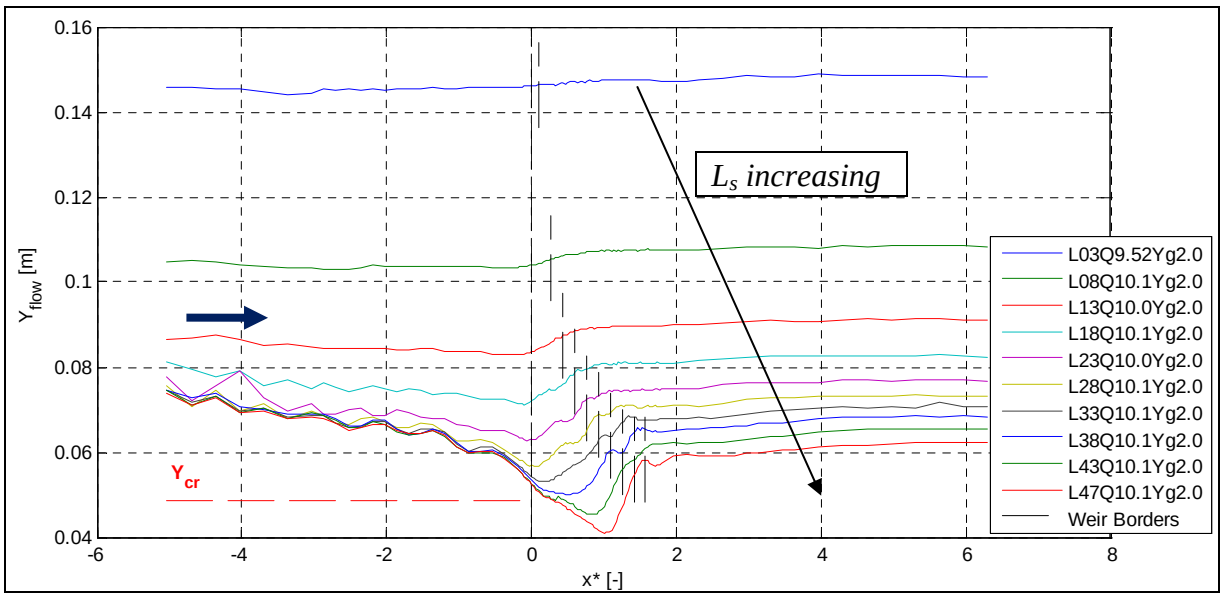

Figure 3.17: Water surface profiles of series B: line plots.

The drop of the water depth was more evident in the proximity to the side weir, as detailed survey of water surface showed for the “detailed tests” (see Figure 3.18).

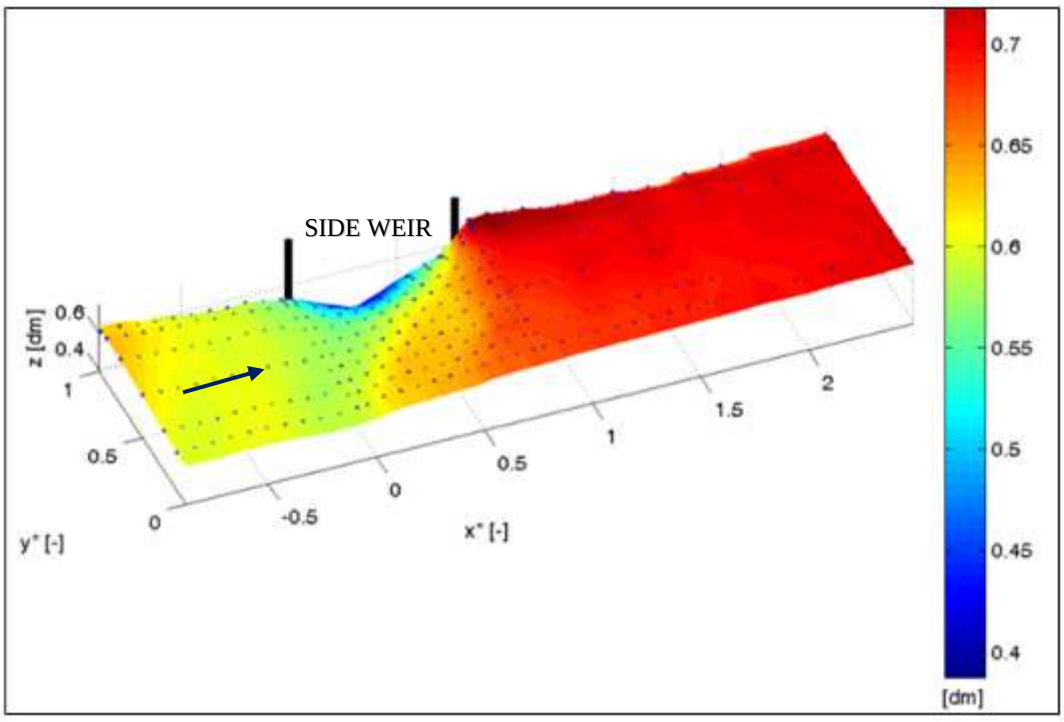

Figure 3.18: Water surface at side weir site for test B11 (L23Q10.0Yg2.0).

The mean flow velocity in the main channel increases going toward the upstream end of the side weir and then the flow slows down toward the downstream end because the discharge decreases and the flow depth increases (see Figure 3.19). The side weir zone is not covered by data because no direct measurements of flow discharge were available within that part.

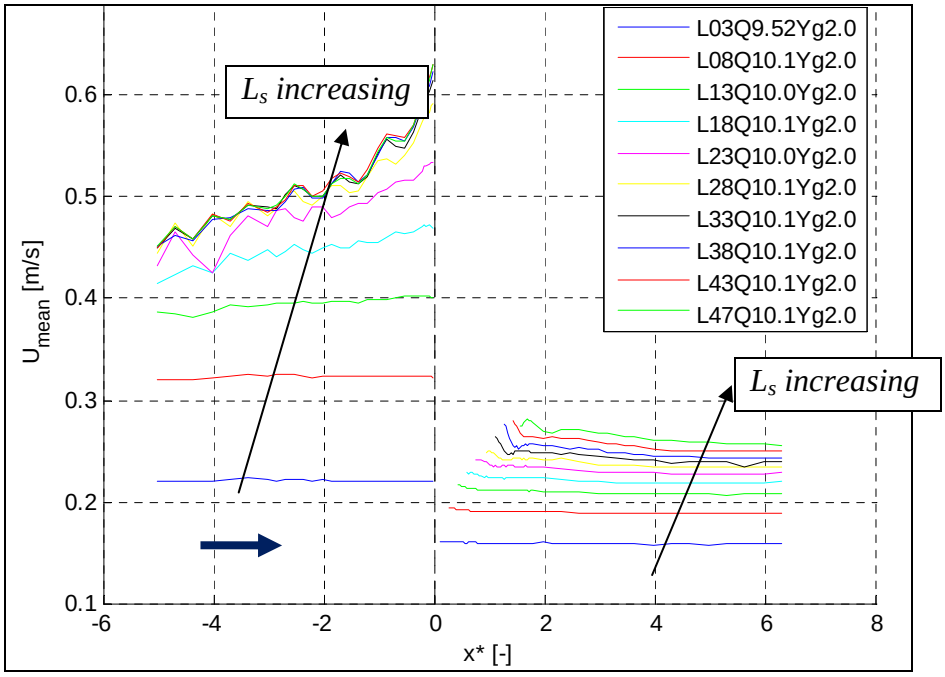

Figure 3.19: Mean velocity along the flume for series B.

The flow field was moreover investigated by means of longitudinal and transversal velocity profiles and the PTV technique.

The longitudinal velocity profiles show the influence of the side weir on the velocity distribution, which is distorted and deflected toward the weir itself. The longitudinal velocity distribution is almost uniform in the up- and downstream zone of the flume (see Figure 3.20), while it gets a non-uniform shape at the side weir site (see Figures 3.21-3.22). In the following Figures (3.20-3.22), the flow velocity is normalized by the mean flow velocity at each cross-section.

Particularly, the velocity distribution is more influenced in the zone closer to the side weir: it is accelerated at the cross section CS3 (at the beginning of the lateral weir), whereas at the cross section CS4 (at the end of the lateral weir) it is accelerated in the left and central part and it is decelerated in the lower strata, where a reverse flow likely occurs and the flow is again attracted through the side weir.

All these data showed that the flow gets three-dimensional features when an important lateral outflow takes place: several three-dimensional zones were detected by means of the velocity profiles and the PTV technique and they are described in Section 3.5.

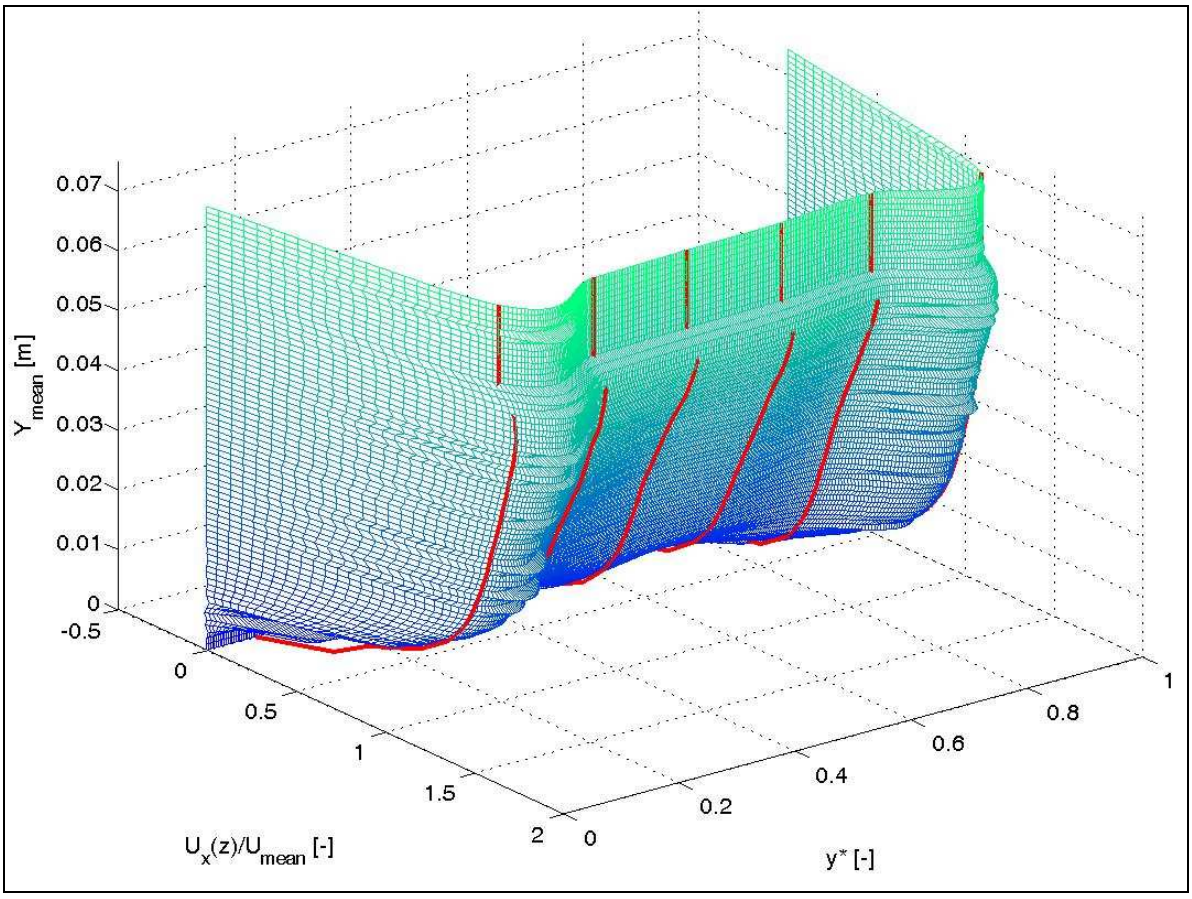

Figure 3.20: Flow velocity distribution for test B10 (L18Q10.1Yg2.0) at cross section CS1.

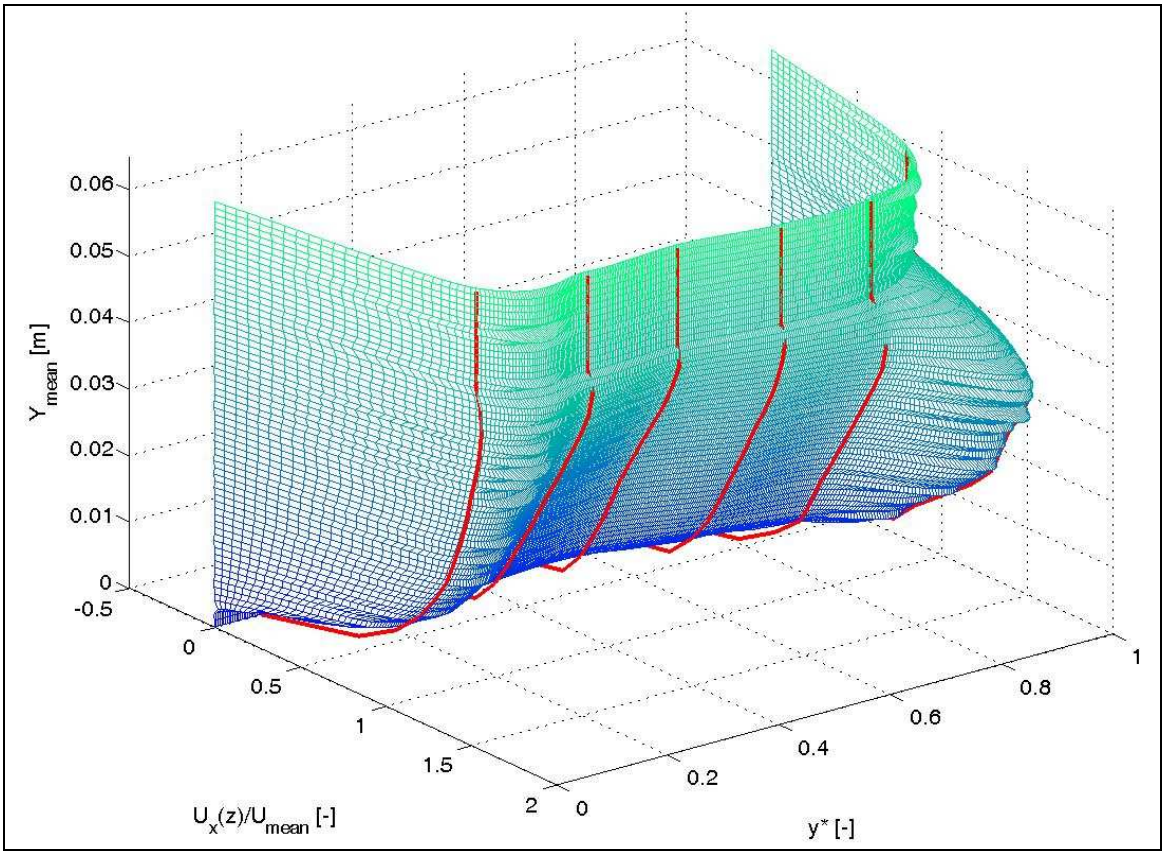

Figure 3.21: Flow velocity distribution for test B10 (L18Q10.1Yg2.0) at cross section CS3.

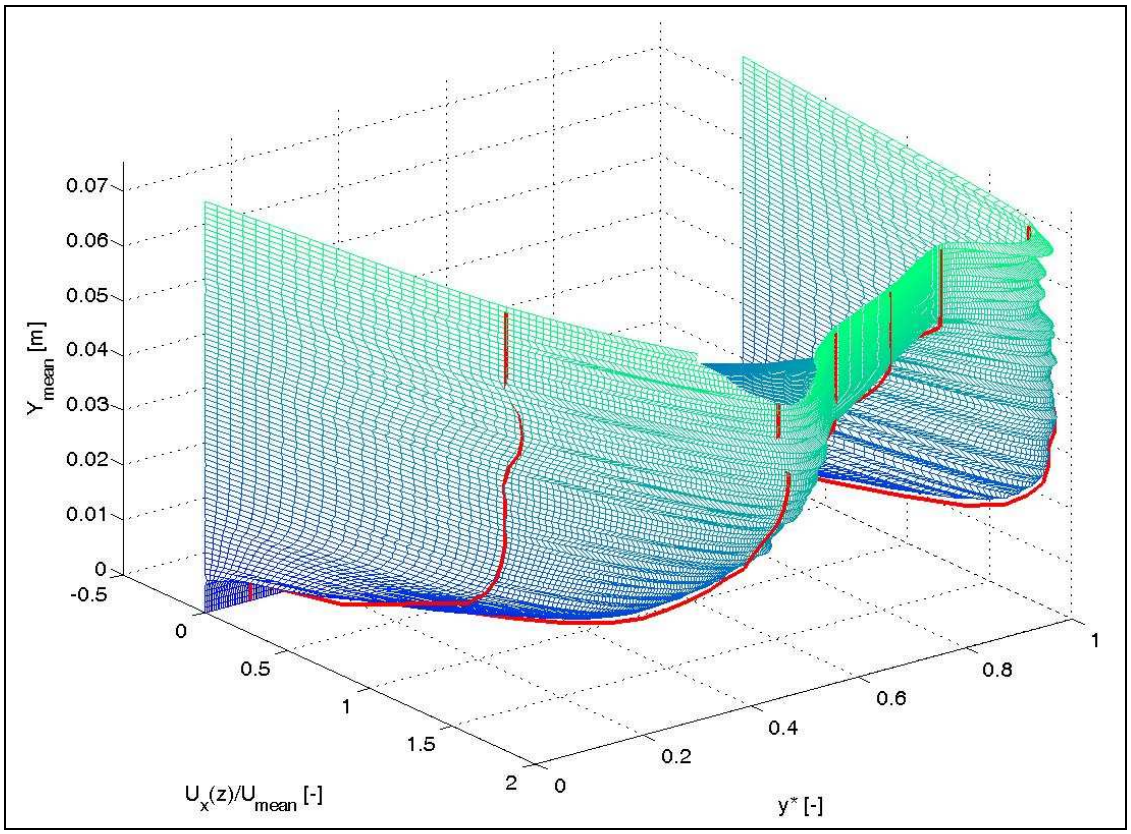

Figure 3.22: Flow velocity distribution for test B10 (L18Q10.1Yg2.0) at cross section CS4.

The PTV analysis shows clearly how the surface streamlines are deflected toward the side weir (see Figure 3.23) and the different behaviour of the two components of the flow velocity: the longitudinal velocity U_x decreases along the side weir (Figure 3.24), as it was already found by means of the analysis of the flow depth and velocity profiles, while the transversal velocity U_y increases downstream in front of the weir (Figure 3.25). U_y seems to get a maximum value around the downstream corner of the weir, where also the flow angles θ are greater (Figure 3.26). The flow angle θ is called "deflection angle" and it is defined as:

$$\theta = \tan^{-1}\left(\frac{U_y}{U_x}\right) \tag{3.3}$$

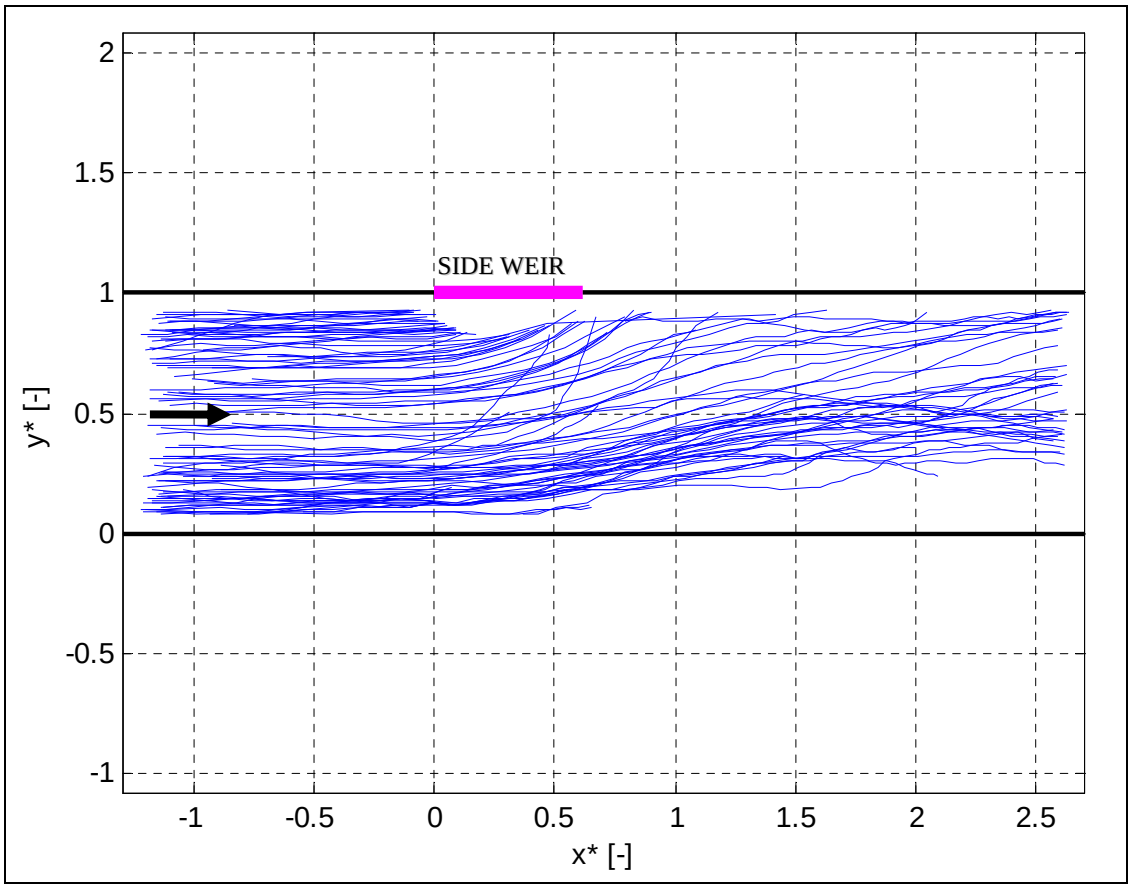

Figure 3.23: Streamlines of flow field at water surface for test B10 (L18Q10.1Yg2.0).

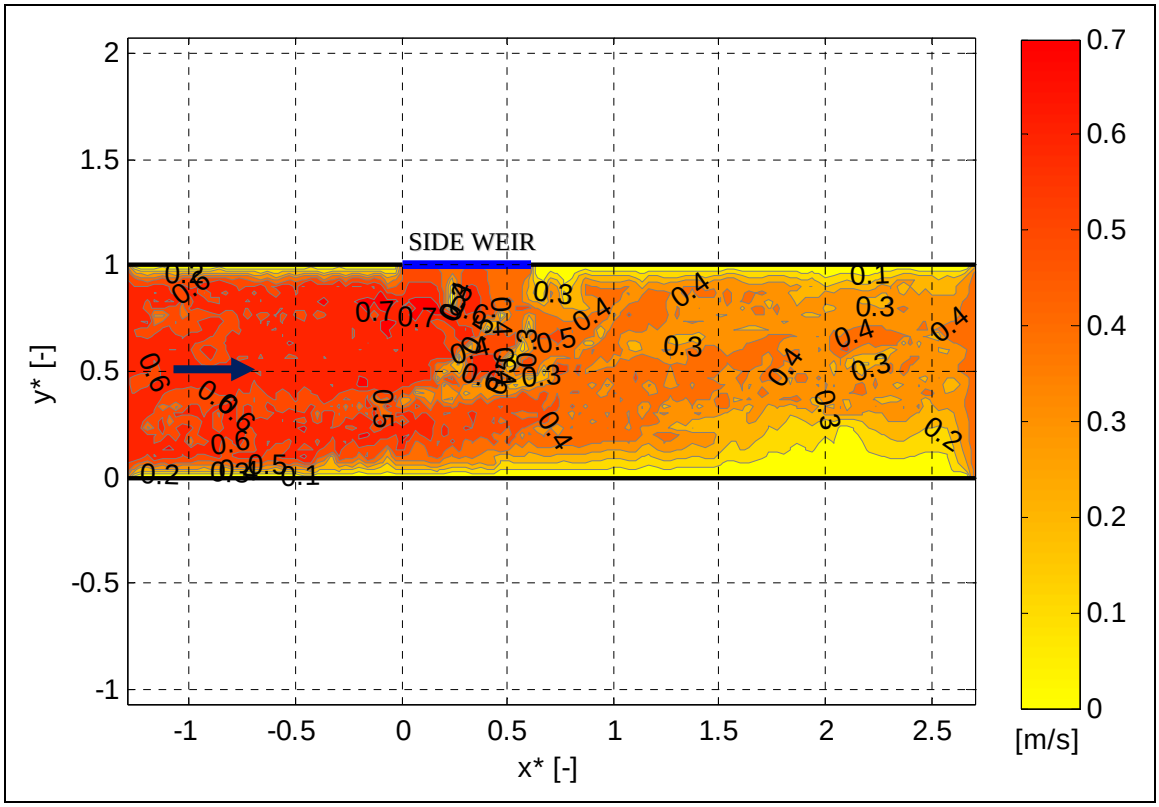

Figure 3.24: Contours of U_x at water surface for test B10 (L18Q10.1Yg2.0).

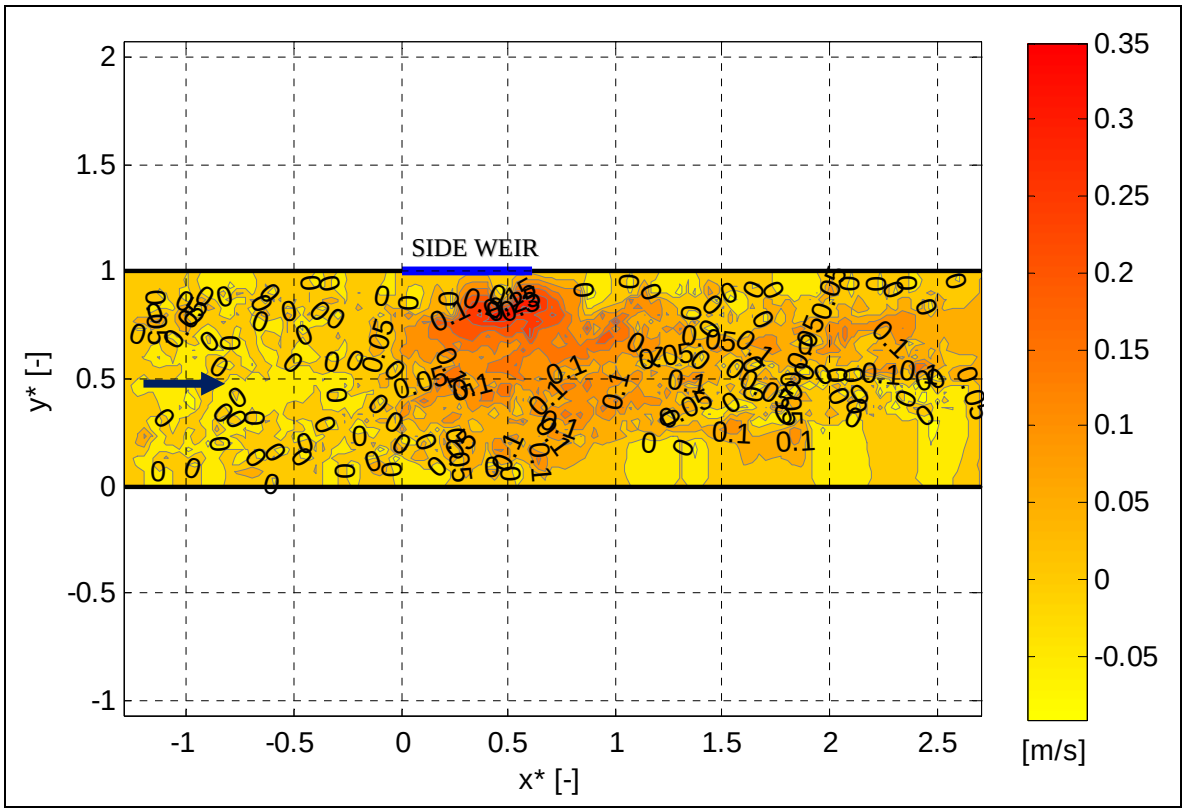

Figure 3.25: Contours of U_y at water surface for test B10 (L18Q10.1Yg2.0).

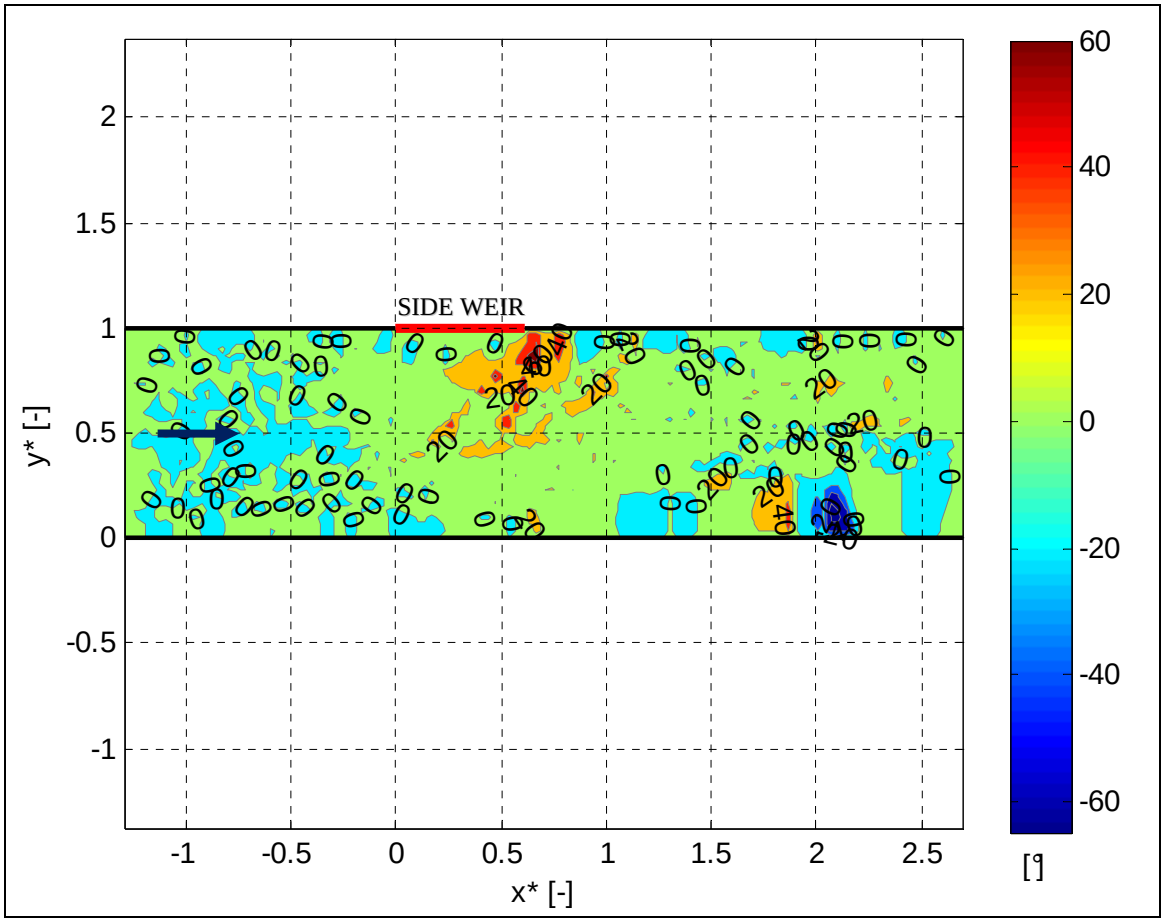

Figure 3.26: Contours of flow angles at water surface for test B10 (L18Q10.1Yg2.0).

The contours of velocity, derived from the transversal velocity profiles, show the acceleration of the flow field in the transverse direction (Figure 3.27).

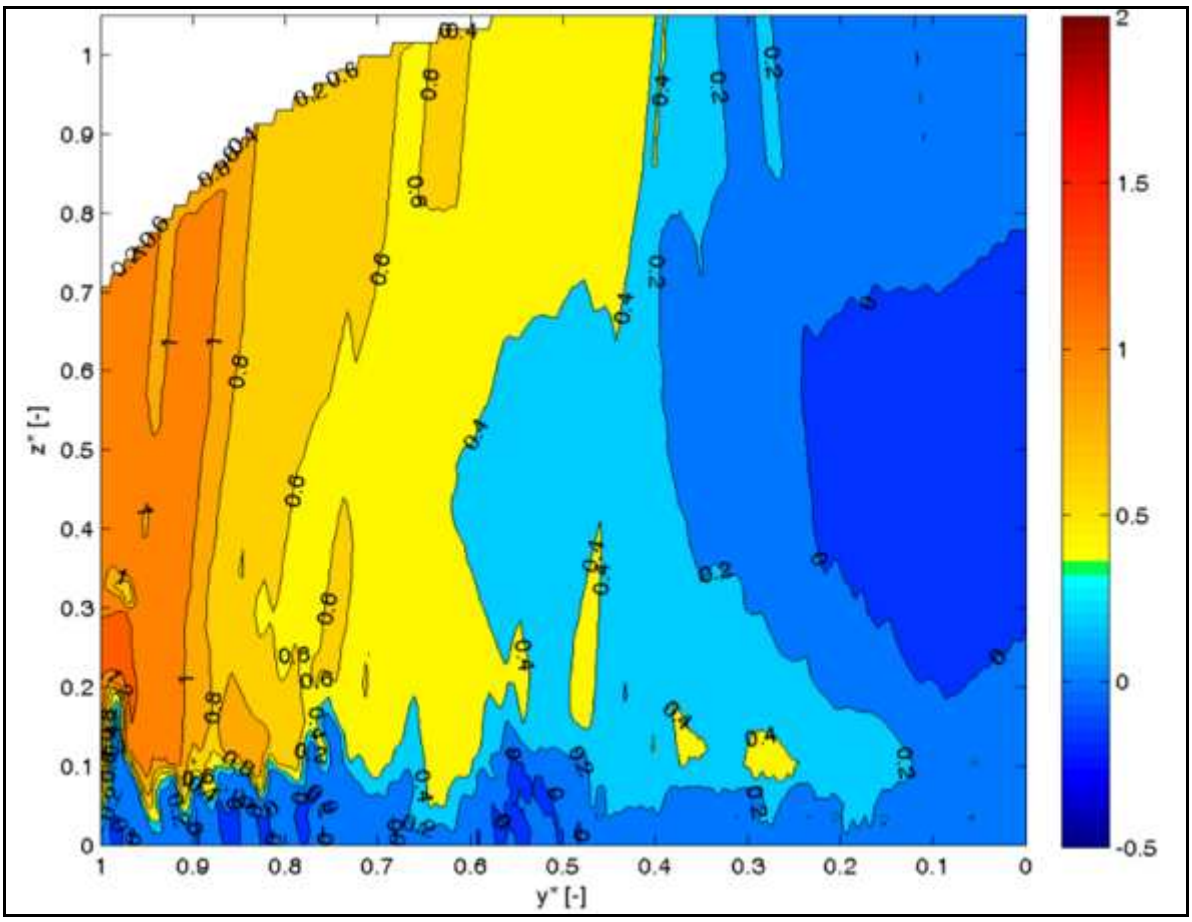

Figure 3.27: Contours of U_y/U_{mean} vertical profiles for test B11 (L23Q10.0Yg2.0) at cross section x* = 0.383.

3.3.3.3 Series C data

Tests of series C were performed to check the influence of the downstream boundary condition on the behaviour of the physical system. The sluice gate was set to a level of Y_g = 3.4 cm, in order to get an initial water depth close to that one of the uniform flow. The inflow discharge was maintained equal to 10 l/s and the ten different lengths of the side weir were tested again. The water depth profile along the centreline of the main channel was acquired and plotted in Figures 3.28: the general behaviour of the flow depth profile is similar to that one of series B which was discussed in the previous Section.

The mean velocity was calculated along the upstream and downstream part of the channel, and the profile along the flume is plotted in Figure 3.29. As it was already observed for series B, the mean flow velocity increases approaching to the weir, and then the flow slows down because a part of the discharge spills through the lateral weir.

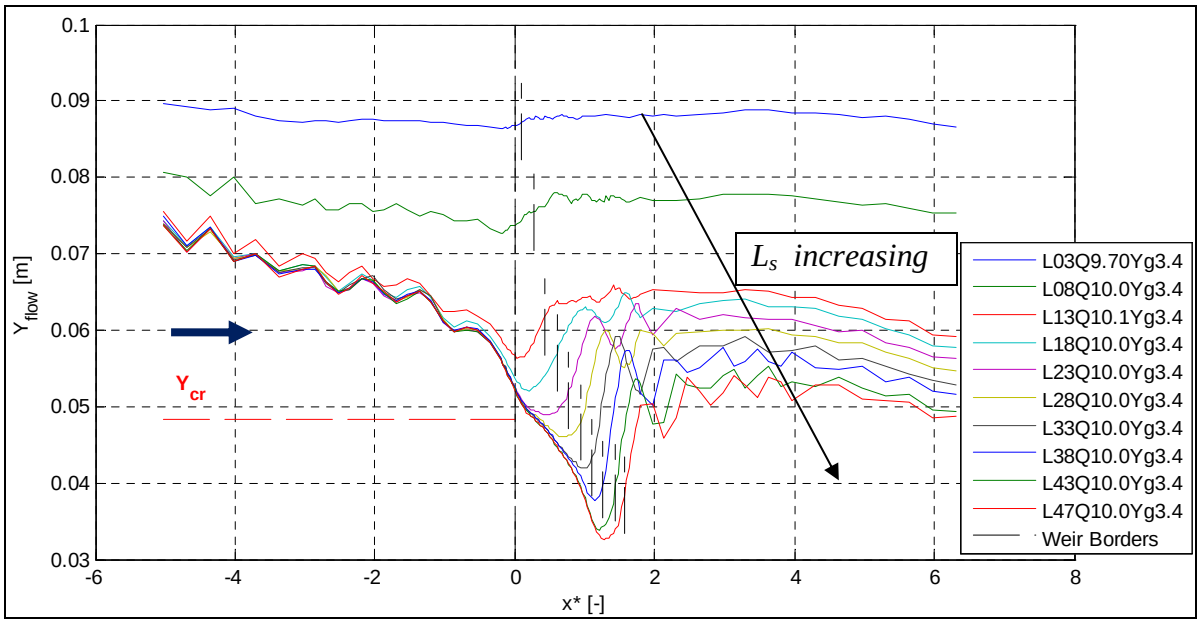

Figure 3.28: Water surface profiles of series C.

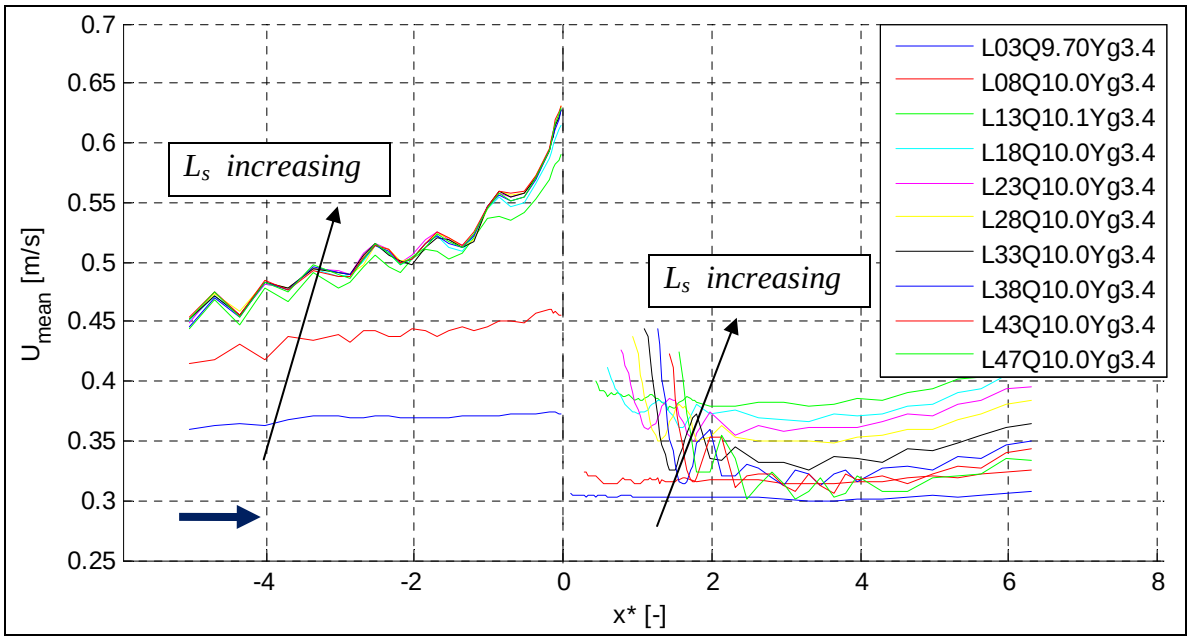

Figure 3.29: Mean velocity along the flume for series C.

3.4 Data analysis with a focus on process understanding

Data presented in Section 3.3 were analysed and elaborated in order to understand the hydrodynamics of the process. Flow regime and hydrodynamic mechanisms, which take place in the main channel as consequence of the lateral outflow, were the main focus of this investigation.

The observed phenomena were quite complex because they had three-dimensional features which took place in different zones of the channel. Tests of series B, particularly the detailed ones, provided a good basis to detect these phenomena. The analysis of data presented in Section 3.3 highlights some flow field features which were common to all tests and that will be described as referred to three different areas of the main channel: the zone upstream the side weir, the part along the side weir and the zone downstream it. Generally speaking, the longer was the side weir, the more evident the influence on the flow field was.

3.4.1 Analysis of the flow hydrodynamics

The main hydrodynamic features of the flow were described in Section 3.3.3.2 regarding data of series B. The hydrodynamics of the main flow is here analysed further.

As a general behaviour, the flow was in a quite uniform regime upstream the side weir, where the velocity distribution on the cross section resembled the theoretical logarithmic form typical of uniform turbulent flow, except for some disturbances to the flow that were likely related to the inflow of the flume (see the “flow velocity distribution” Figures presented into the internal report in Michelazzo, 2013). The flow showed an accelerated profile while moving towards the side weir site: it was a drawdown subcritical profile with depth decreasing downstream. The decreasing of water depth was related to the acceleration of the flow in the longitudinal direction which became stronger while going closer to the weir. The increase of the flow velocity concerned that part of the flow which was closer to the lateral weir (i.e., on the left side): positive values of $3 \cdot U_{mean}$ were found both for U_x and U_y at the weir site. Anyway, the overall effect on the entire cross section was to increase the mean velocity U_{mean} while approaching to the weir site (see previous Figures 3.19 and 3.29). The upstream water profile drew down more for bigger values of the side weir length, because of a greater lateral outflow discharge (see Figures 3.17 and 3.28): the water depth at the beginning of the side weir ($x^* = 0$) decreased and it almost equalled the critical depth.

The water depth profile along the side weir length got two different behaviours depending on the test. Water profile increased along all the side weir length up to the downstream section for tests with small length L_s, while, when the side weir was longer, the depth profile decreased along the first part of the weir and then it raised up to the downstream depth. The former behaviour is typical of a flow that remains subcritical, whereas, in the latter case, the lateral outflow was so strong that the flow profile decreased as in a supercritical regime and then it joined the downstream depth. Since the downstream boundary condition provided a subcritical flow, a hydraulic jump should have occurred within the weir length or somewhere downstream if the flow was supercritical along the side weir. The hydraulic jump was not so evident during the experimental tests, maybe because it occurred as an undular or weak jump.

The hydraulic regime of the flow is visualized in Figures 3.30 and 3.31, in which the Froude number is computed on the basis of the detailed flow depth survey and the surface flow field analysis (with the PTV technique). The Froude number is computed with reference to the longitudinal and the transversal component of the flow, i.e.:

$$Fr_x = \frac{U_x}{\sqrt{g \cdot Y}} \qquad \text{and} \qquad Fr_y = \frac{U_y}{\sqrt{g \cdot Y}}$$

Figure 3.30 highlights the acceleration of the flow along the first part of side weir. The maximum of Fr_x is obtained close to the weir with values around the supercritical regime, while in the downstream part the flow is subcritical again. It is interesting to observe that the ongoing flow after the weir is still concentrated toward the left side where the weir is placed. Figure 3.31 shows that the transverse component of the flow gets important values close to the downstream zone of the side weir and the Fr_y obtains relatively high values.

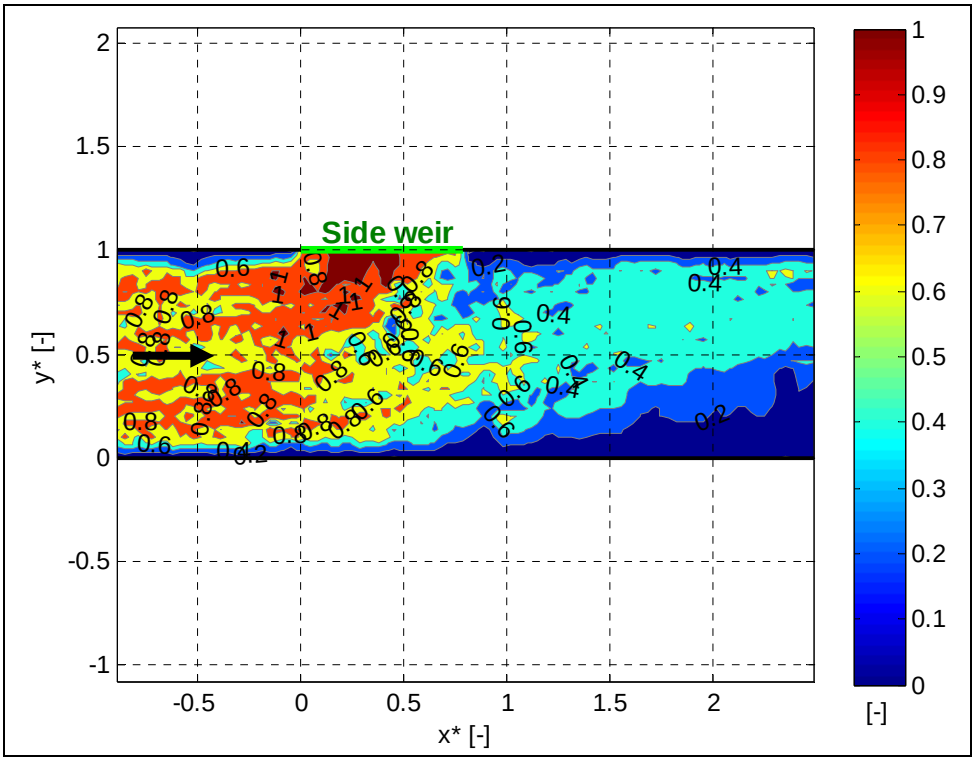

Figure 3.30: Fr_x contours for test B11 (L23Q10.0Yg2.0).

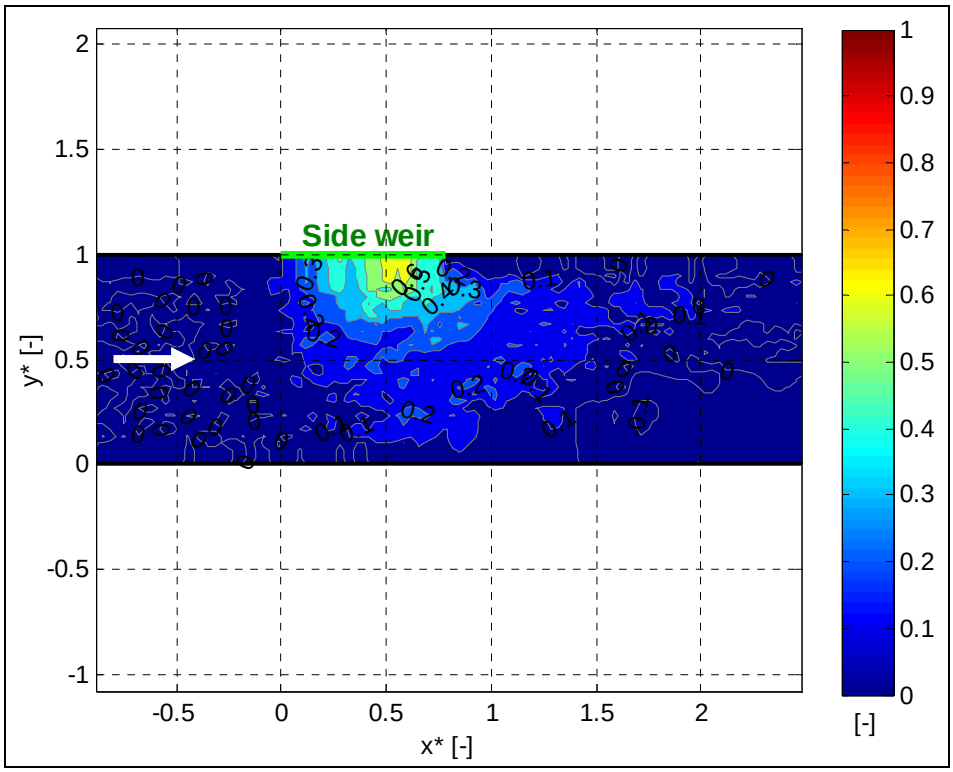

Figure 3.31: Fr_y contours for test B11 (L23Q10.0Yg2.0).

3.4.2 Analysis of the three-dimensional zones

The flow in the main channel got important three-dimensional effects induced by the lateral outflow. The flow discharge was partially withdrawn laterally through the weir, while the remaining part routed downstream. The PTV technique was useful to describe the surface flow field. Figure 3.32 shows the streamlines of one test. The flow is divided into two different parts: the red coloured streamlines detect the flow withdrawn through the weir, while the green ones show the remaining part in the channel. As an overall effect, the entire surface flow field was deflected toward the side weir.

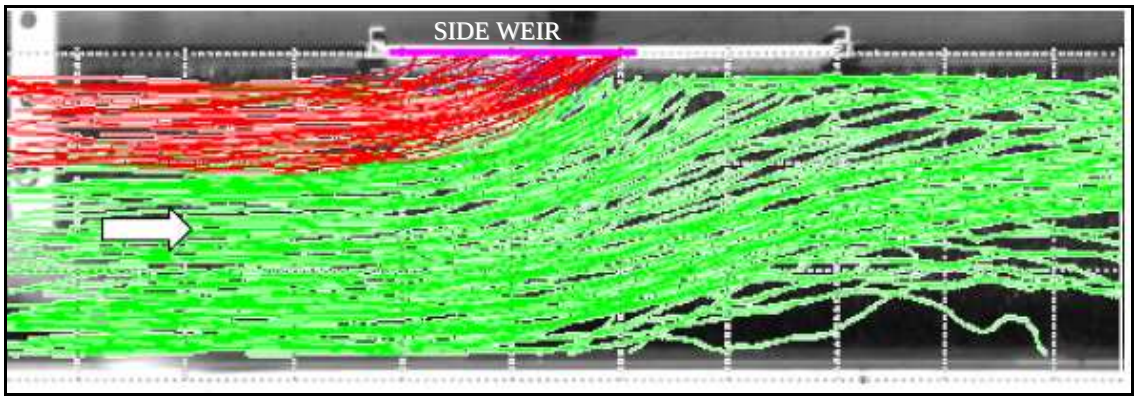

Figure 3.32: Deflection of surface flow field through the side weir (red streamlines) and ongoing flow (green ones).

This dividing zone developed in the vertical z-direction as a *dividing stream surface* and its lower border was detected by analysing the heavier tracers images (see Figure 3.33).

Figure 3.33: Image of heavy tracers and assumed dividing curve on the bottom.

The dividing surface got a larger distance from the weir on the bottom of the main channel than at the water surface, and this is confirmed by Neary et al. (1993 and 1999).

The presence of larger portions of the dividing surface on the bottom means that a lateral weir of zero height attracts lower strata stronger than upper ones.

The dividing surface was detected for one detailed test from the superficial and channel bottom tracers analysis and it is depicted in Figure 3.34.

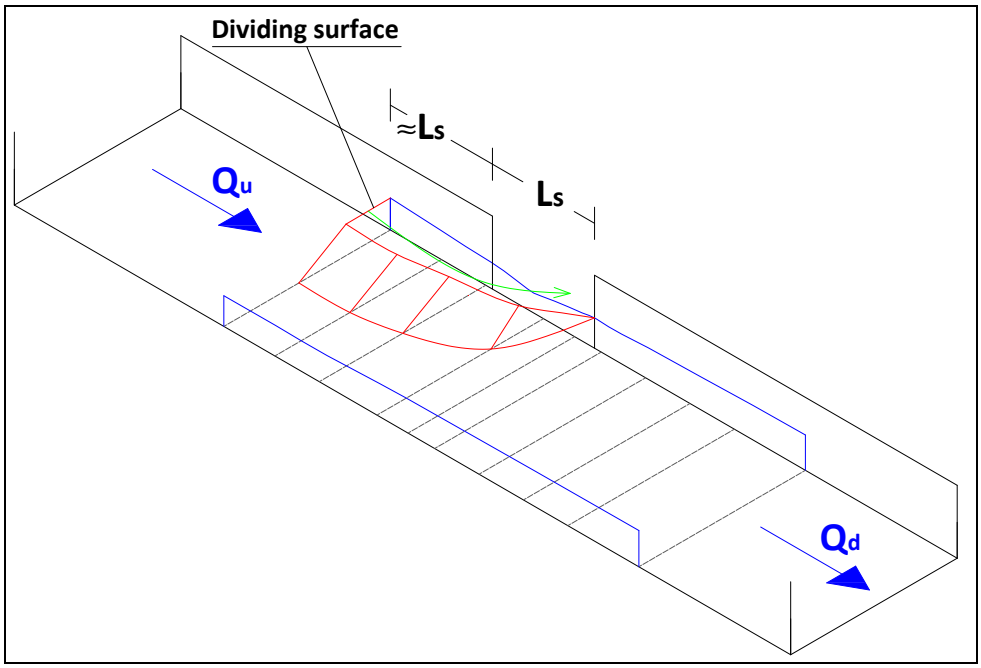

Figure 3.34: 3D view of dividing surface detected from PTV images.

Another feature of the deflection effect was that the streamlines turned toward the side weir with increasing flow angles: the highest deflection angles θ were found closer to the downstream section of the side weir (Figure 3.26).

Streamline analysis shows another interesting phenomenon. A “dead water” zone (“B” zone) was detected at the right side, opposite to the side weir. This zone was particularly evident for the tests with long weirs: tracers recirculated clockwise inside this *separation zone* which seemed to be induced by a longitudinal pressure gradient due to the slowing down of the flow. The size of this zone was processed from the analysis of velocity profiles and superficial streamlines: it started at about the middle length of the side weir and it developed quite far downstream (see Figure 3.35). It is likely that the presence and extension of this zone depends on the main channel aspect ratio (Y/B) and that it tends to vanish for very small values of Y/B.

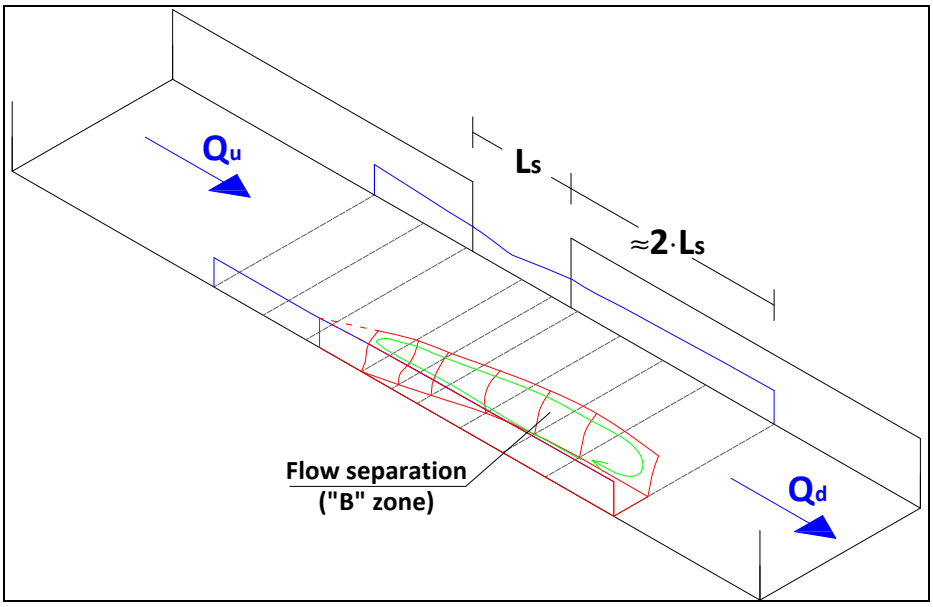

Figure 3.35: Separation zone at the side opposite to the side weir.

Another three-dimensional effect occurred at the downstream zone of the main channel: an *helicoidal flow* developed at the downstream end of the side weir close to its side. Contours of U_y in the cross section plane downstream the side weir showed that the helicoidal flow had counter-clockwise direction, with upper strata oriented toward the weir side and the lower ones toward the opposite side. The overlapping between this transversal rotating motion and the longitudinal flow created the helicoidal motion which developed quite far downstream: the secondary motion was absorbed in the main flow at a distance of about $2 \cdot L_s$ from the lateral weir. The helicoidal flow had quite high strength, since the U_x and U_y reached positive values of $4 \cdot U_{mean}$.

The reason of this motion has to be searched at the downstream corner of the weir, where the dividing streamline meets a singular point and there is a local flow stagnation. This creates a downflow motion and the vortex is turned into the helicoidal motion by means of the main flow, as in case of flow around bridge piers. Moreover, the near bed part of the flow was withdrawn by the side weir backward: negative values of $U_x \approx -[0.5 \div 1] \cdot U_{mean}$ were observed in the first sections downstream the side weir, and this indicates the presence of a localized reverse flow, also observed by Emiroglu et al. (2011). The water depth of the downstream part was quite uniform, whereas the velocity distribution needed a certain distance from the weir in order to return to a more regular profile. Figure 3.36 depicts a reconstruction of this secondary flow.

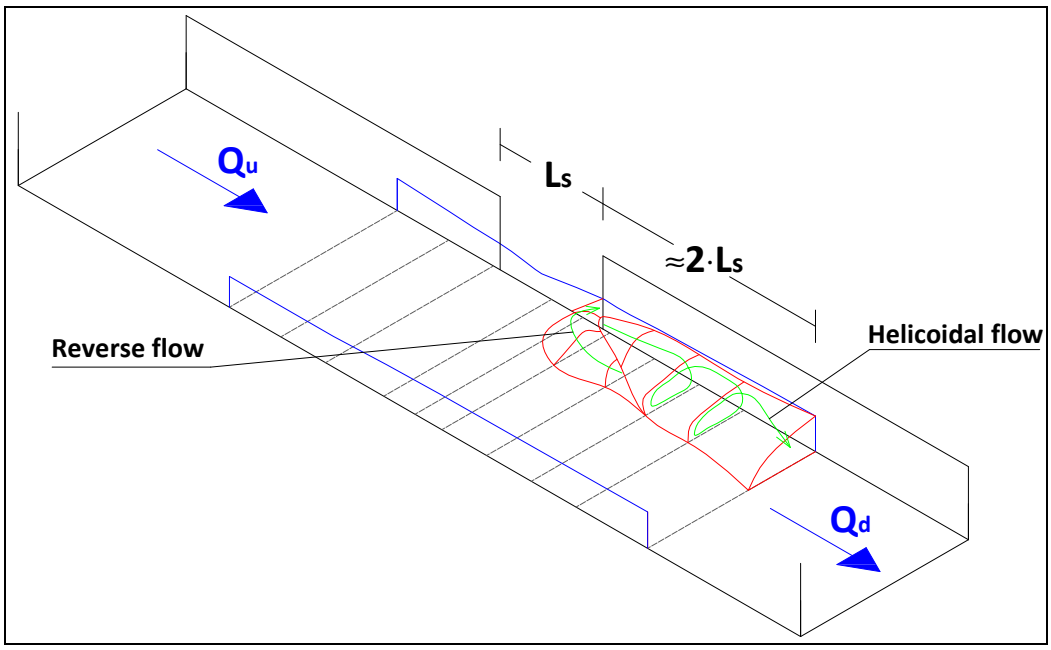

Figure 3.36: Helicoidal flow and reverse flow downstream the side weir.

The resulting flow field was highly complex and all these three-dimensional effects are summarized in Figure 3.37.

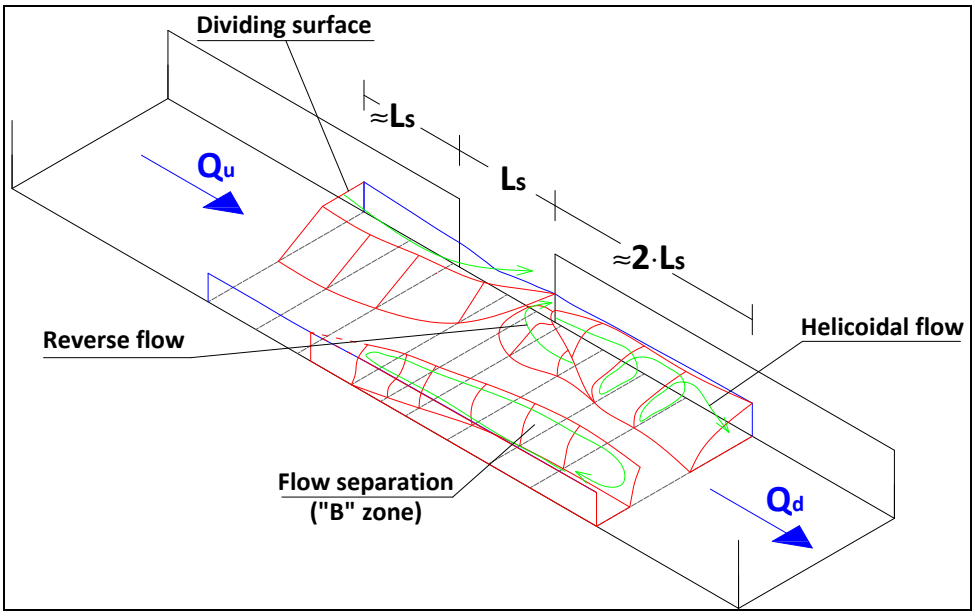

Figure 3.37: Sketch of the flow field zones detected during the detailed test B10 (L18Q10.1Yg2.0).

3.4.3 Analysis of the De Marchi hypothesis

The De Marchi hypothesis is usually applied when dealing with lateral outflow through side weirs in subcritical flow regimes. This assumption states that, along a side weir, the specific energy head of the main flow maintains a constant value. It is interesting to verify if this hypothesis applies for the cases investigated of side weir with zero height crest.

The specific energy head is computed at the up- and downstream sections (Figure 3.38) as:

$$E = Y + \frac{\alpha U^2}{2g}$$

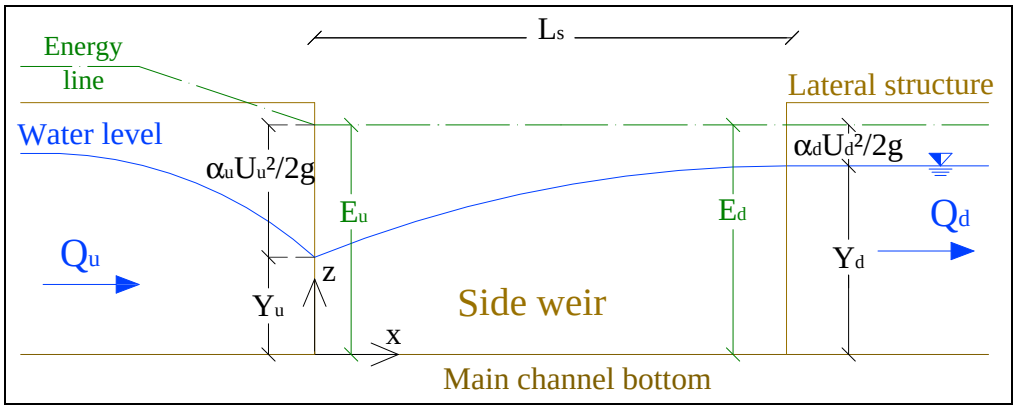

Figure 3.38: Scheme for specific energy head computation.

The Coriolis coefficient α is calculated from the detailed data about flow velocity distribution in the longitudinal direction, by means of a discretization of the cross section as a grid composed by i,j rectangular cells:

$$\alpha = \frac{\int_A u^3 dA}{U_{mean}^3 \cdot A} = \frac{\sum_{i,j} u_{i,j}^3 \cdot A_{i,j}}{U_{mean}^3 \cdot \sum_{i,j} A_{i,j}} \qquad (3.4)$$

Where $u_{i,j}$ is the longitudinal velocity component referred to the element area $A_{i,j}$ that discretizes the total wet area A of the cross section.

Data reported in Table 3.2 show that the Coriolis coefficient gets values in the range [1.3÷2.3] at the downstream section because of the influence of the lateral outflow on the main flow, whose effects were also described in terms of three-dimensional zones in the Section 3.4.2.

According to the experimental work of El-Khashab and Smith (1976) and to the indications of May et al. (2003), the Coriolis coefficient at the beginning of the weir is quite small compared to the one calculated in Table 3.2. As a matter of fact, the flow feature along the upstream section should change a little for various side weir lengths, since the inflow is always the same and the flow depth profile tends to the critical depth as limit value (see Figure 3.17). Therefore, it was chosen to take α_u constant and equal to 1.15. On the other hand, the downstream Coriolis coefficient is highly affected by the non-uniform velocity distribution induced by the side weir, and the downstream flow conditions change for different weir lengths because of greater lateral outflows. As a matter of fact, α_d was taken as computed in Table 3.2. The specific energy head values are plotted in Figure 3.39 (the tests are identified by "L##", that means "Weir length L_s = ## cm"), where the De Marchi hypothesis seems to be confirmed for the first seven tests within an error of ± 10%: the three tests with longest weirs do not verify the hypothesis. The flow regime regarding those tests was not entirely subcritical. As a consequence, the constancy of the specific energy is violated since the supercritical flow causes energy losses along the first part of the weir that are not negligible.

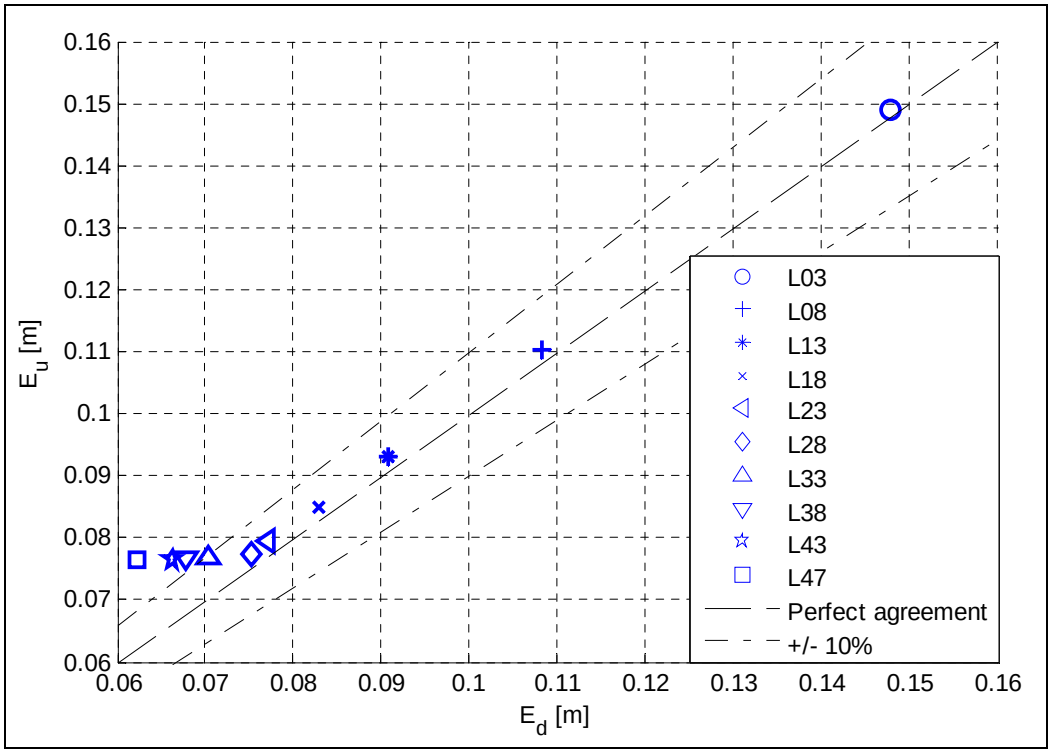

Figure 3.39: Specific energy at up- and downstream sections.

3.4.4 Computational analysis of the flow along the side weir

3.4.4.1 Computational scheme

A computational analysis of the collected data was performed in order to get information about the flow features along the side weir, which is the main focus of the present work. Particularly, the flow depth profile was discretized into N spatial intervals Δx, each one being equal to the minimum between 1 cm and $L_s/10$. The water surface level **h** was calculated at the middle point of each Δx and it was considered to be constant on its Δx interval.

Figure 3.40 depicts the computational scheme that is used in the following elaborations.

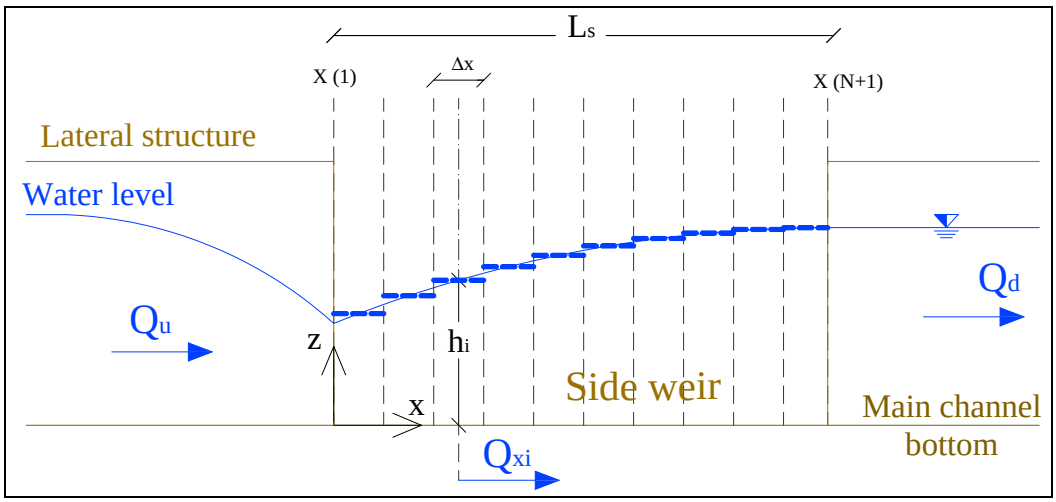

Figure 3.40: Computational scheme for flow analysis.

The lateral outflow was calculated according the side weir equation (3.5), which needed a calibration to fit the final measured lateral outflow:

$$Q_{s,calc} = \int_0^{L_s} C_{ds} \cdot \sqrt{2g \cdot \left(h(x) - p_s(x)\right)^3} \cdot dx \qquad (3.5)$$

With
C_{ds}: side weir discharge coefficient [-]
h: water level acting on the weir [m]
p_s: crest of the side weir, equal to zero [m].

It was chosen to calibrate the discharge coefficient to fit the measured side flow discharge Q_s. The calibrated discharge coefficient is then given by:

$$C_{ds} = \frac{Q_s}{\sum_{i=1}^{N} \Delta x \cdot \sqrt{2 \cdot g \cdot h_i^{\,3}}}$$

The calibrated C_{ds} is plotted versus the Froude number calculated at the upstream section of the weir (Fr_u) in the Figure 3.41: it results that the discharge coefficient for the lateral weir decreases with the upstream Froude number, and this is consistent with the relationships proposed by other authors. This analysis was performed for the tests of series B, which was the series with more detailed data according to the employed techniques of measurement.

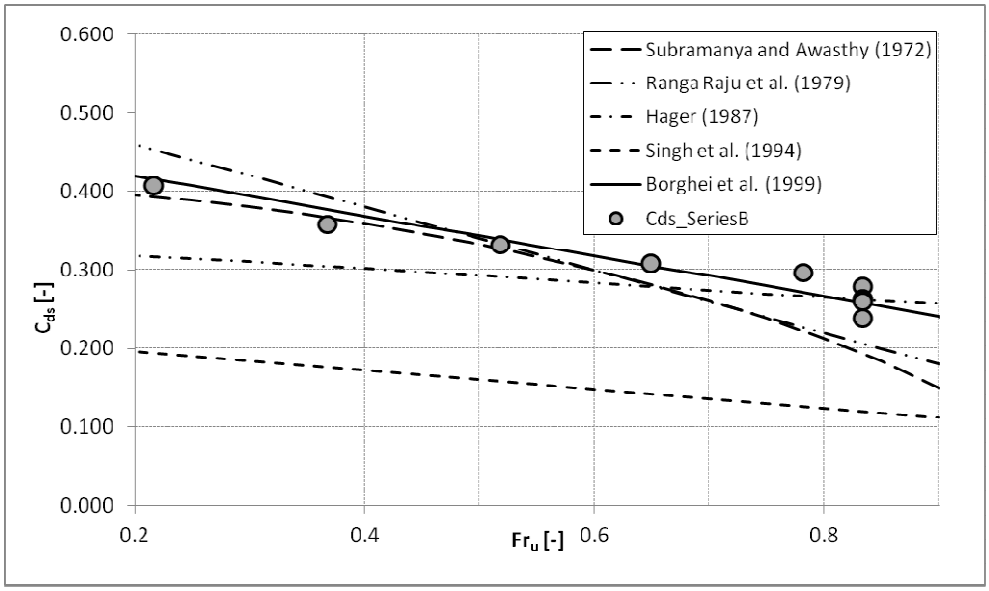

Figure 3.41: Calibrated side weir coefficient as a function of Fr_u and comparison with other formulations.

3.4.4.2 Flow velocity

Once the discharge coefficient was calibrated, the flow discharge was calculated in the main channel along the flume for each i-position, since the flow outing from the side weir is given by the calibrated side weir law. The longitudinal and transversal components of the flow in the main channel are then calculated, from the continuity principle applied in x and y directions, according to the equations (3.6). Note that the longitudinal velocity is assumed equal to the mean velocity on the cross-section. A further transversal component of the flow velocity is calculated in equations (3.6) as referred to the weir crest U_{ys}, by the use of the flow depth Y_s recorded at the weir crest from the detailed water surface survey (see Figure 3.18 and Figure 3.42):

$$\begin{cases} U_{xi} = \dfrac{Q_{xi}}{A_i} = \dfrac{Q_u - \sum_{j=1}^{i} Q_{s,j}}{A_i} \\ U_{yi} = \dfrac{Q_{s,i}}{Y_i \cdot \Delta x} \\ U_{ysi} = \dfrac{Q_{s,i}}{Y_{si} \cdot \Delta x} \end{cases} \tag{3.6}$$

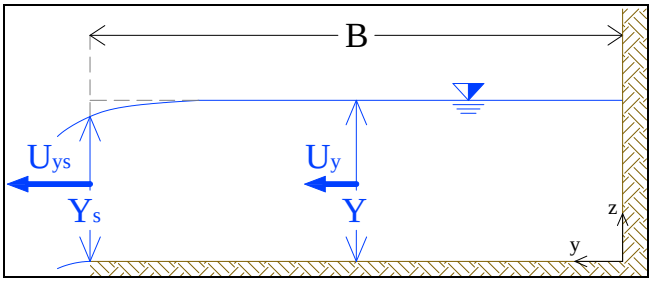

Figure 3.42: Computational scheme for transversal flow velocity computation (cross section).

The flow field at the weir site is affected by the lateral outflow and it gets important 2D features, which make the transversal velocity U_y to get values in the order of the main flow velocity U_x. Figure 3.43 shows the trend of the velocity components along the weir for the detailed test B11. The longitudinal component of velocity U_x decreases along the weir of about 50% due to the lateral outflow, while the transversal component increase is more evident when U_y is calculated on the weir crest. As a matter of fact, U_y is mainly given by the square root of the flow depth, which varies more along the weir crest than at the middle of the main channel. Moreover, the flow depth at the weir crest is lower than at middle axis of the channel (Y_s/Y ranges between 0.64 and 0.9 along the weir for test B11) and this makes the transversal velocity to increase from the main channel toward the side weir.

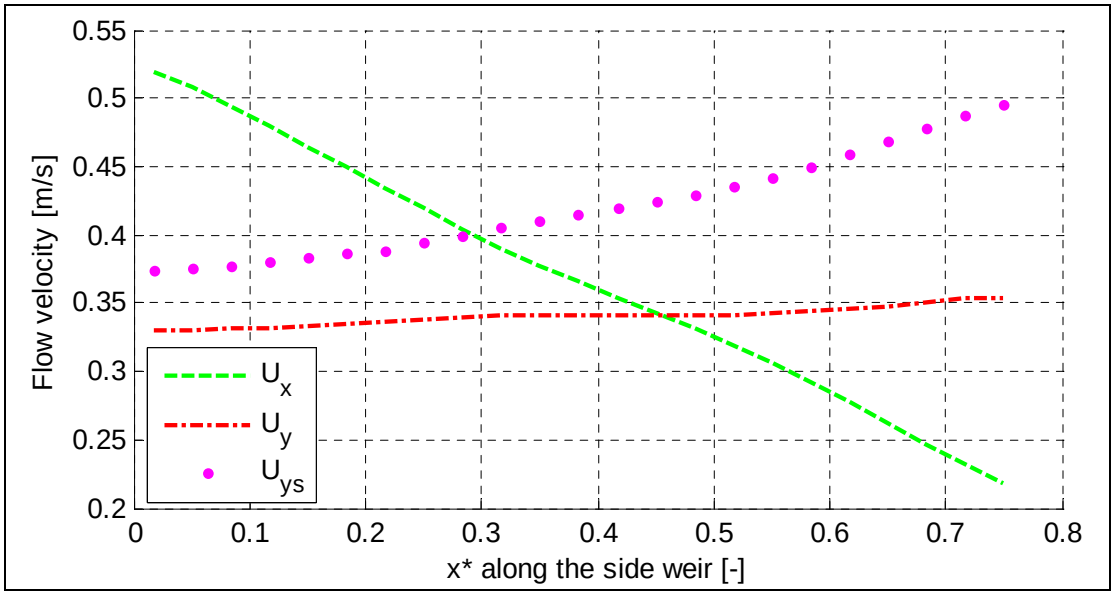

Figure 3.43: Longitudinal trend of flow velocity components for test B11 (L23Q10.0Yg2.0).

The overall effect of the lateral outflow, for increasing side weir length, on the flow velocity is analysed in terms of flow velocities calculated at the up- and downstream sections of the side weir: U_u is the velocity calculated at the upstream section and U_d is calculated at the downstream one. The longitudinal velocity is always reduced along the weir, while the transversal velocity (at middle of main channel) slightly increases downstream (see Figure 3.44). As general trend, the longer is the side weir the greater is the velocity U_x, since the flow is more attracted by the weir, and the lower is the velocity U_y, since the water depth in front of the side weir decreases.

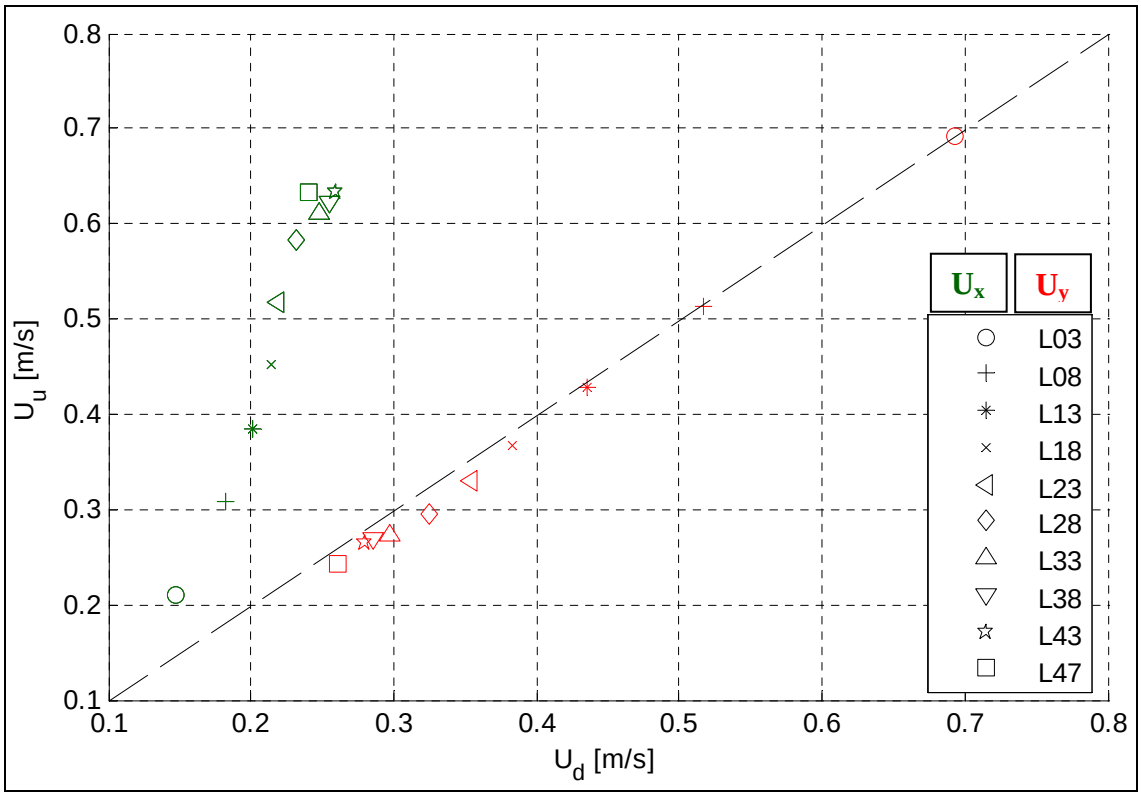

Figure 3.44: Comparison between up- and downstream U_x and U_y for all tests of series B.

3.4.4.3 Deflection angle

The angle of the flow is calculated by means of the previous analysis as referred to the main channel centreline θ_0 and to the side weir crest θ_s (Figure 3.45 and equations 3.7):

$$\begin{cases} \theta_0 = \tan^{-1}\left(\dfrac{U_y}{U_x}\right) \\ \theta_s = \tan^{-1}\left(\dfrac{U_{ys}}{U_x}\right) \end{cases} \tag{3.7}$$

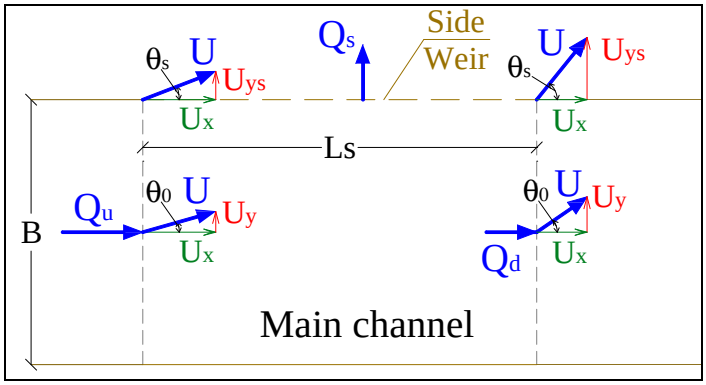

Figure 3.45: Sketch of flow deflection at side weir site.

Since the longitudinal velocity decreases along the weir while the transversal component tends to increase, the resulting flow angle θ increases along the lateral outflow (Figure 3.46). The angles calculated at the weir crest are greater than the ones at the middle of the channel

because of the greater value of the transversal velocity: this effect is consistent with the physics of the flow which turns toward the side weir.

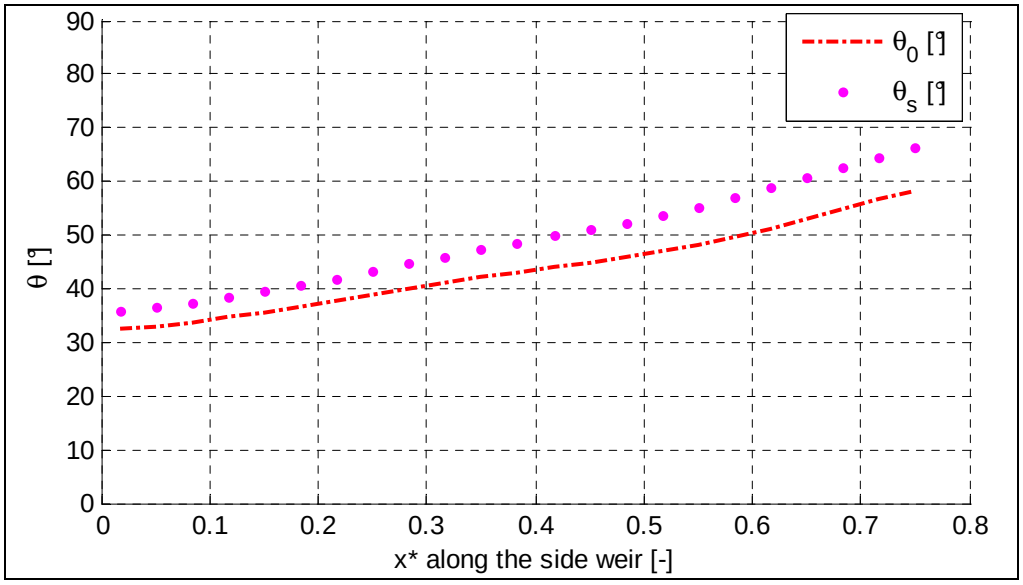

Figure 3.46: Longitudinal trend of flow angles for test B11 (L23Q10.0Yg2.0).

The overall effect of the lateral outflow, for increasing side weir length, on the flow angles is analysed in terms of angles calculated at the up- and downstream sections of the side weir.

Figure 3.47 shows that the downstream flow angle is always greater than the upstream one. Moreover, as the side weir lengthens, the flow angles tend to reduce their values: this effect is due to the acceleration of the flow in the longitudinal direction for longer weirs and to the reduction of the transversal velocity because of the lowering of the water level in front of the weir.

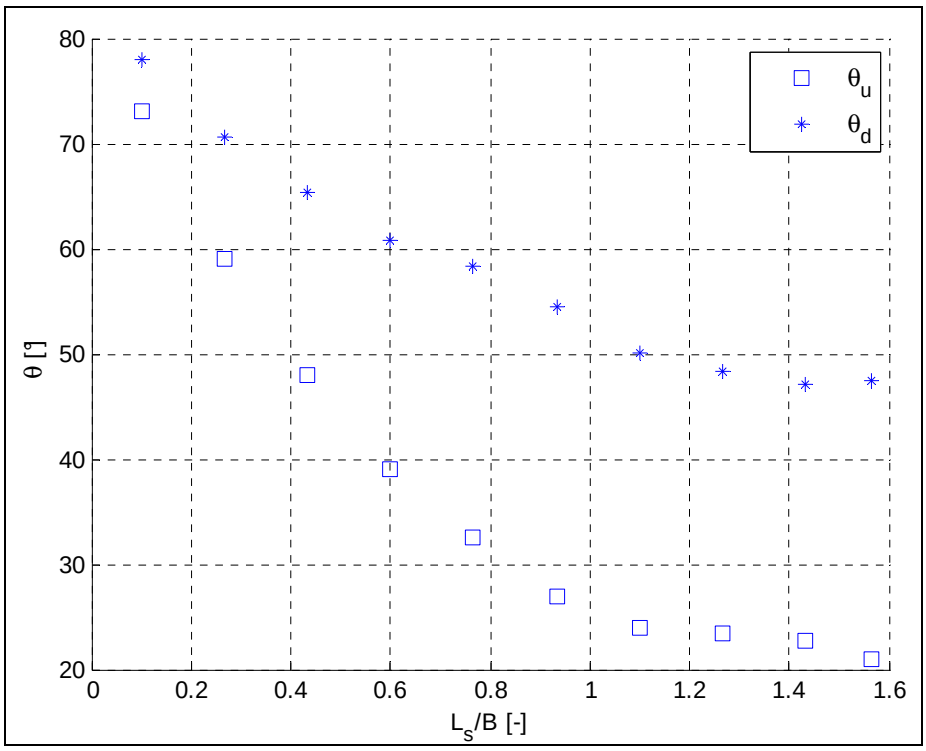

Figure 3.47: Comparison between up- and downstream flow angles for every test of series B.

3.4.4.4 Shear stress

The computation of the velocity components allows to calculate the trend of the shear stress. The shear stress τ is computed with reference to the two components of the main flow:

$$\tau = \begin{cases} \tau_x = \dfrac{\rho}{C_h^{\,2}} \cdot |U| \cdot U_x \\ \tau_y = \dfrac{\rho}{C_h^{\,2}} \cdot |U| \cdot U_y \end{cases} \tag{3.8}$$

With:

ρ	density of the water [kg/m^3]
$\lvert U\rvert = \sqrt{U_x^{\,2} + U_y^{\,2}}$	modulus of flow velocity [m/s]
$C_h = 5.75 \cdot \log_{10}\left(\dfrac{12 \cdot R}{2.5 \cdot D_{50}}\right)$	Chézy coefficient [-]
R	hydraulic radius [m]
D_{50}	mean sediment size for roughness computation [m]

The modulus of the shear stress is given by:

$$|\tau| = \rho \cdot \frac{|U|^2}{C_h^{\,2}} \tag{3.9}$$

The trend of τ along the weir is plotted for one test in Figure 3.48: the shear stress highly decreases along the weir because of the slowing down of the flow. The shear stress reduction is in the order of more than 50% and it is mainly due to the lowering of the longitudinal component τ_x, while the transversal component τ_y gets a more slight trend.

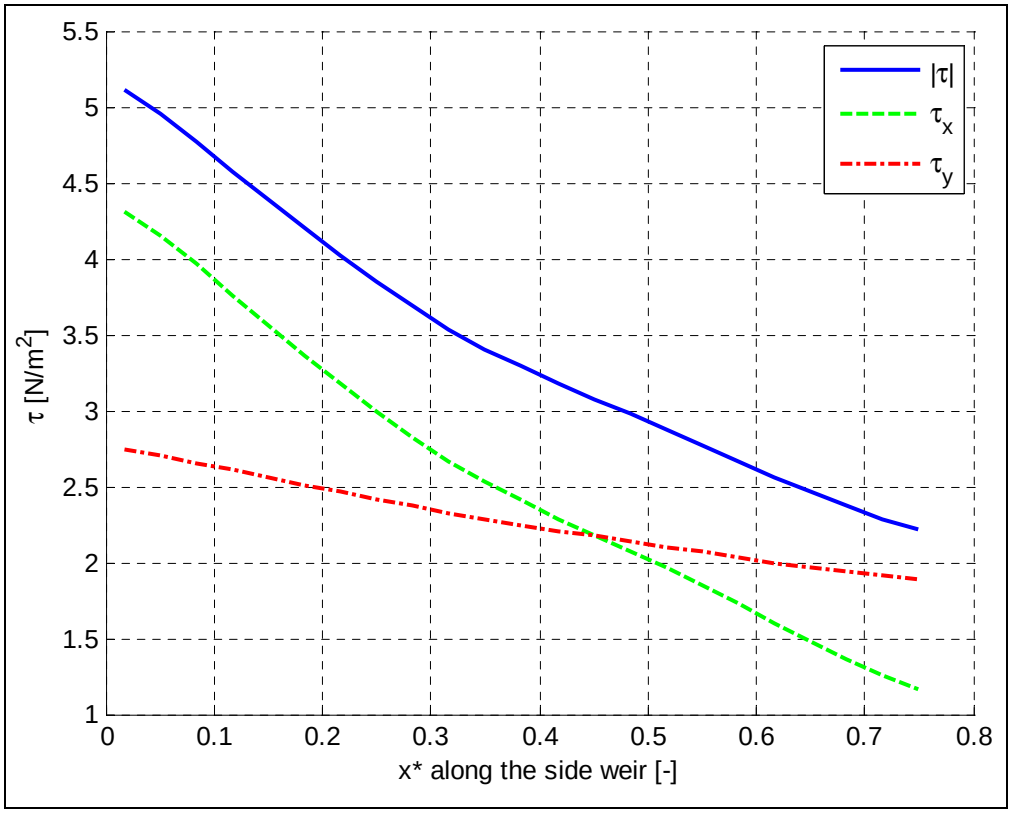

Figure 3.48: Longitudinal trend of shear stress components for test B11 (L23Q10.0Yg2.0).

The influence of the side weir length on the shear stress is evaluated by calculating the modulus at the up- and downstream sections for the ten tests of the series B. Figure 3.49 shows that the shear stress $|\tau|_u$ tends to increase, due to the acceleration of the flow caused by longer weirs, while the downstream shear stress $|\tau|_d$ decreases and it is always lower than the upstream one. Moreover, a mean shear stress acting on the side weir $\tau_{s,mean}$ in the outflow direction was calculated, as in equation 3.10:

$$\tau_{s,mean} = \rho \cdot \frac{\overline{U}_s^{\,2}}{C_h^{\,2}} = \frac{\rho}{C_h^{\,2}} \cdot \left(\frac{Q_s}{L_s \cdot \overline{Y}_s} \right)^2 \tag{3.10}$$

Where $\overline{Y}_s$ is the mean flow depth in front of the side weir at centreline of the main channel.

It is interesting to note that the mean shear stress acting on the weir section decreases of one order of magnitude for longer side weirs and it tends to an asymptotic low value: this effect is mainly due to the lowering of the water head in front of the weir.

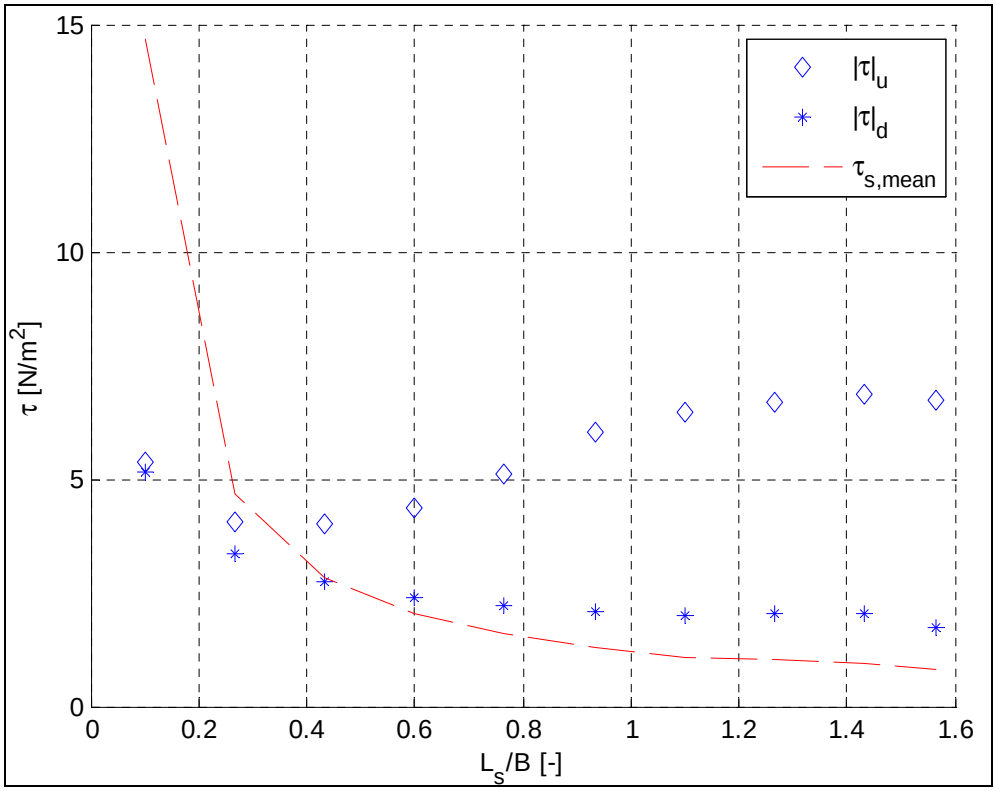

Figure 3.49: Up- and downstream shear stresses for tests of series B and mean shear stress at side weir.

3.4.5 Characteristic parameters of the main flow

The main features of the flow regime described in Sections 3.4.1-3.4.4 are summarized by means of characteristic parameters.

In particular, dimensionless parameters are useful to analyse the system regardless the dimensions of the model and to search for the existence of a general validity into the investigated phenomena.

The following dimensionless parameters are investigated:

- $r_L = L_s/B$ length ratio
- $r_M = M_{sx}/PPM_{ux}$ momentum ratio (with M_{sx} = longitudinal component of momentum of the lateral outflow and PPM_{ux} = sum of hydraulic pressure Π and the momentum M at the upstream section, which are described in the equation 3.11)
- $r_U = U_d/U_u$ velocity ratio
- $r_Q = Q_s/Q_u$ discharge ratio
- $r_Y = Y_d/Y_u$ water depth ratio
- $r_{Ys} = \overline{Y_s}/L_s$ side weir aspect ratio (with $\overline{Y_s}$ = mean water depth along the weir)

The momentum ratio r_M was derived by imposing the momentum balance in the main channel for the side weir length, as it is sketched in Figure 3.50. The longitudinal component of momentum of the lateral outflow M_{sx} is computed as difference between the pressure-plus-momentum (PPM = Π + M) at the upstream and at the downstream sections, and by neglecting the shear stress along the weir length:

$$M_{sx} = (\Pi_u + M_u) - (\Pi_d + M_d) \tag{3.11}$$

Where: $\Pi = \frac{1}{2} \cdot \gamma \cdot B \cdot Y^2$ is the hydraulic pressure on a cross section [N]

$M = \beta \cdot \rho \cdot Q \cdot U$ is the momentum at a cross section [N]

The Boussinesq coefficients β were computed from the data of vertical velocity profiles according to a discretization of the cross-section as a grid composed by i,j rectangular cells:

$$\beta = \frac{\int_A u^2 dA}{U_{mean}^2 \cdot A} = \frac{\sum_{i,j} u_{i,j}^2 \cdot A_{i,j}}{U_{mean}^2 \cdot \sum_{i,j} A_{i,j}}$$

The Boussinesq coefficients resulted in a range of [1.10÷1.48] at the downstream section (see Table 3.2), which confirmed the non-uniform characteristic induced by the lateral outflow on the flow regime. These coefficients were neglected for series C, since no velocity profile was recorded for those data.

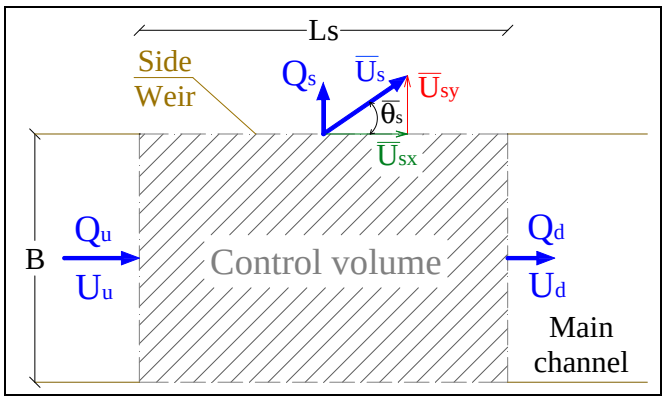

Figure 3.50: Scheme for momentum balance computation.

The mean water depth along the weir $\overline{Y}_s$ was computed from data of water profiles at the centreline and it was used to calculate the ratio r_{Ys}.

The following graphs show the relationship between the dimensionless parameters previously described: data plotted refer to each of the ten tests for both series B and C.

The analyses of the plots show that the intensity of the lateral outflow grows, as the L_s/B ratio increases: spill discharge and outing momentum increase and they seem to tend to an upper limit (see Figures 3.51-3.52-3.53-3.54). Both the maximum r_Q and r_M are reached for the longest L_s and they are in the order of 50%-60%. Moreover, tests of series B reached higher outflow discharges but smaller outflow momentum compared with series C, because of the different downstream condition provided by the sluice gate: a slower flow regime imposed at downstream by a more closed sluice gate produces a higher pressure Π_d, which causes more flow to out through the side weir Q_s but also a minor outing momentum M_{sx}.

The water depth ratio follows an increasing trend for the first tests (short lengths L_s) and then it decreases for the other ones (long lengths L_s). This is due to the fact that the upstream depth decreases until the critical depth, while the downstream flow depth decreases continuously as the downstream discharge is decreased. The first behaviour is typical of subcritical flows, while the second one is typical of supercritical flows and the limit between the two regimes was dependent on the downstream boundary condition (see Figures 3.55-3.56). This change of the flow regime was assumed at the test with $L_s/B = 0.93$ for the series B and at the test with $L_s/B = 0.43$ for series C: the limit is referred to a lower side weir length for tests of series C because their downstream boundary condition had a more opened sluice gate ($Y_g = 3.4$ cm) which provided a flow regime with higher Froude numbers, with respect to the series B data whose sluice gate was more closed ($Y_g = 2.0$ cm) so that the downstream flow had a more evident backwater profile.

A similar trend is noticed for the flow velocity ratio: it decreases until the flow is certainly subcritical and then it tends to increase, and the downstream velocity is always smaller than the upstream one (see Figures 3.57-3.58). Here again the limit is different according to the boundary condition imposed at the downstream end of the flume. The last two tests of series B and C show a velocity ratio smaller than the previous ones: this effect depends on the combination between the increase of the spill discharge and the decrease of the downstream flow depth when the side weir is lengthened. Moreover, some flow disturbances are possibly given by the more opened sluice gate.

The flow features at the up- and downstream sections are expressed in the plan of upstream and downstream Froude numbers (Figures 3.59 and 3.60), which indicate that, as the side weir lengthens, the flow regime tends to become supercritical upstream, while it remains subcritical downstream. The downstream Froude number increases as well, even if less than the upstream one: this is an effect of the downstream boundary condition in the flume which does not allow an uniform rating curve at the downstream (see Figure 3.12), that would provide an almost constant Froude number as in case of real rivers.

Figures 3.61 and 3.62 describe the conditions prevailing on the side weir in terms of aspect ratio, which dramatically decreases with the weir length and it tends to a lower limit, which is similar for the tests of both series B and C.

Numerical values of the main variables recorded and computed during the experimental tests of series B and C are summarized in Table 3.2.

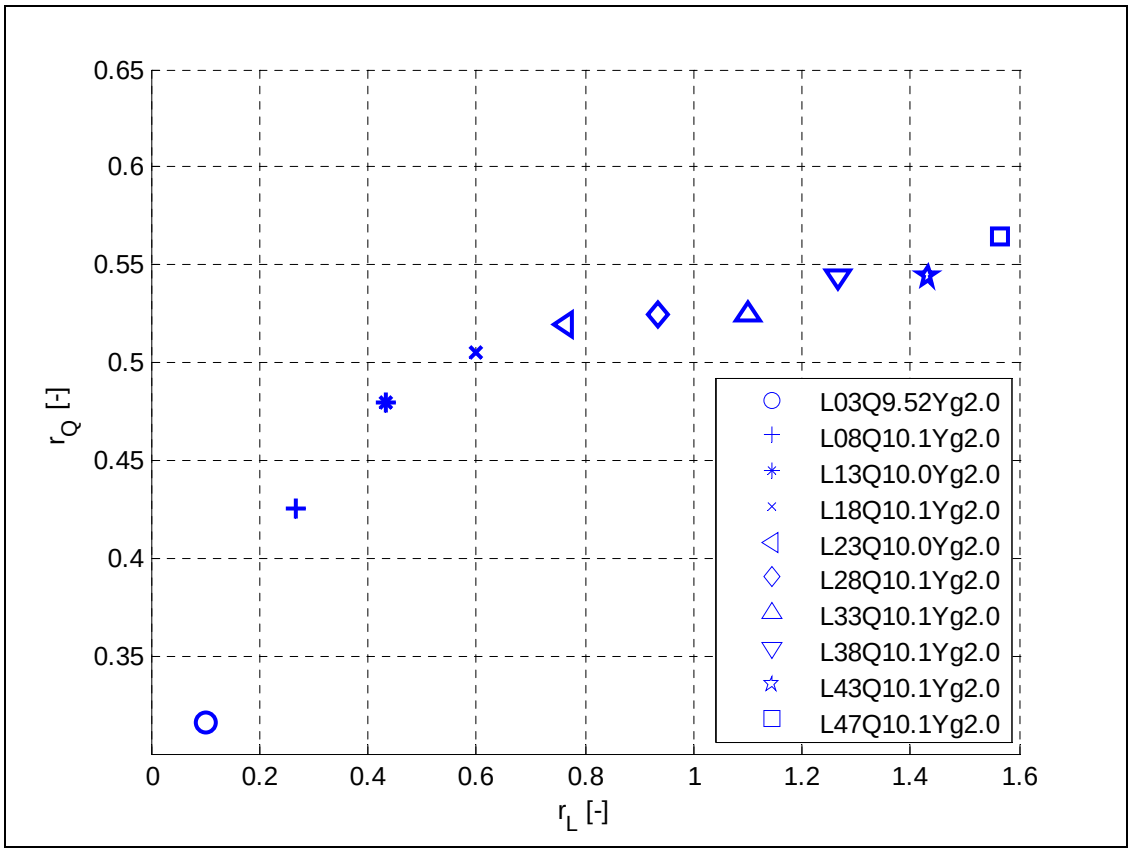

Figure 3.51: Discharge ratio versus length ratio for series B.

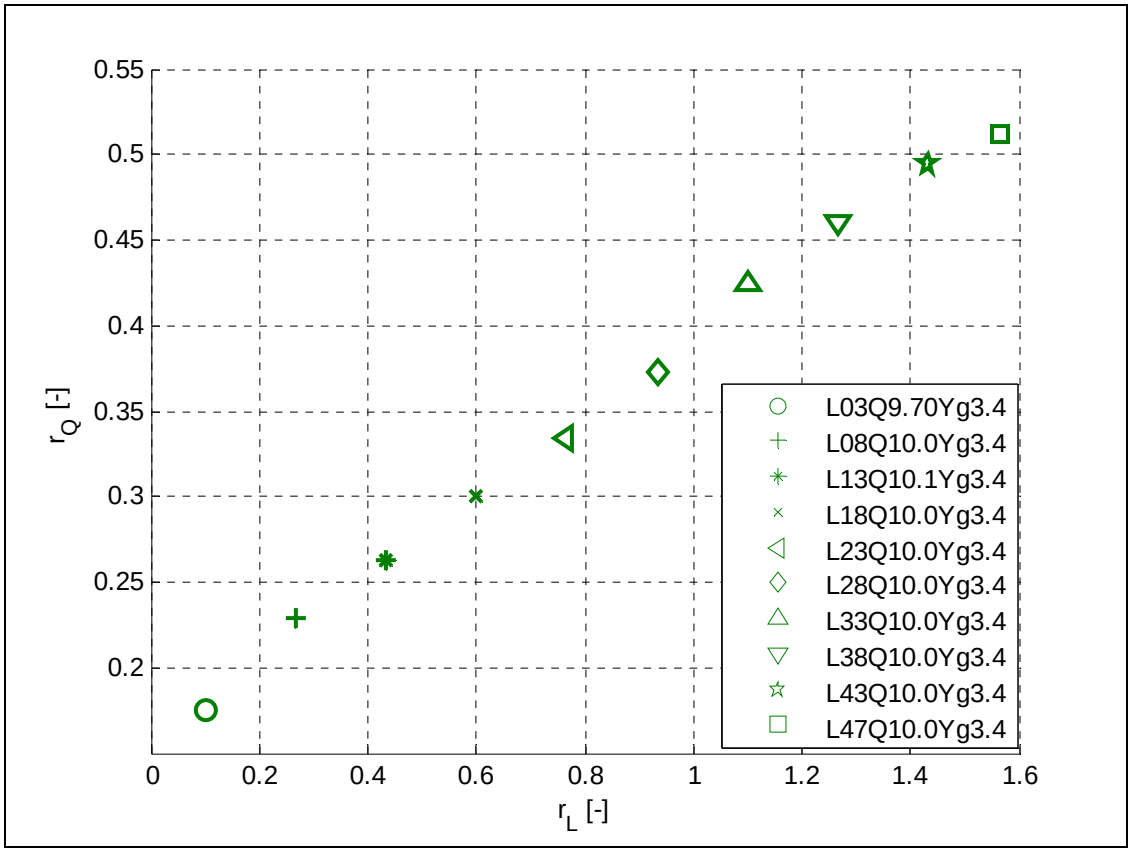

Figure 3.52: Discharge ratio versus length ratio for series C.

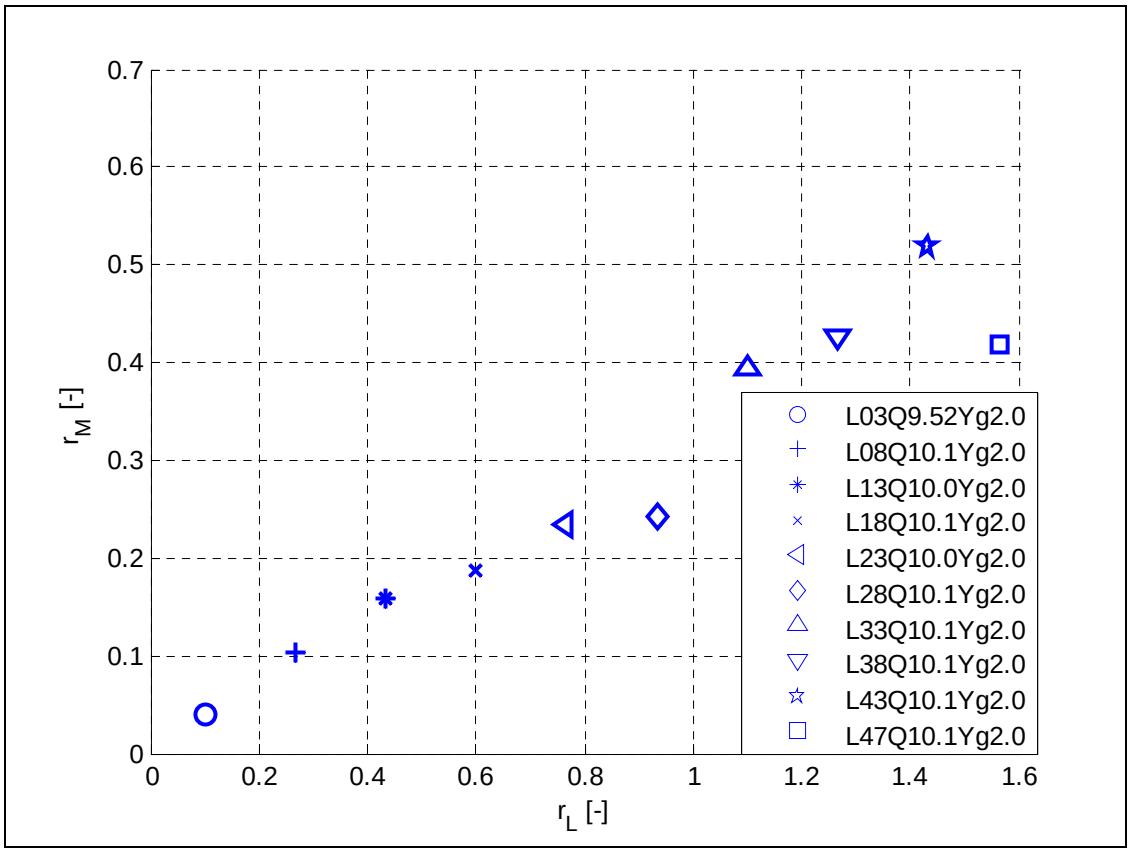

Figure 3.53: Momentum ratio versus length ratio for series B.

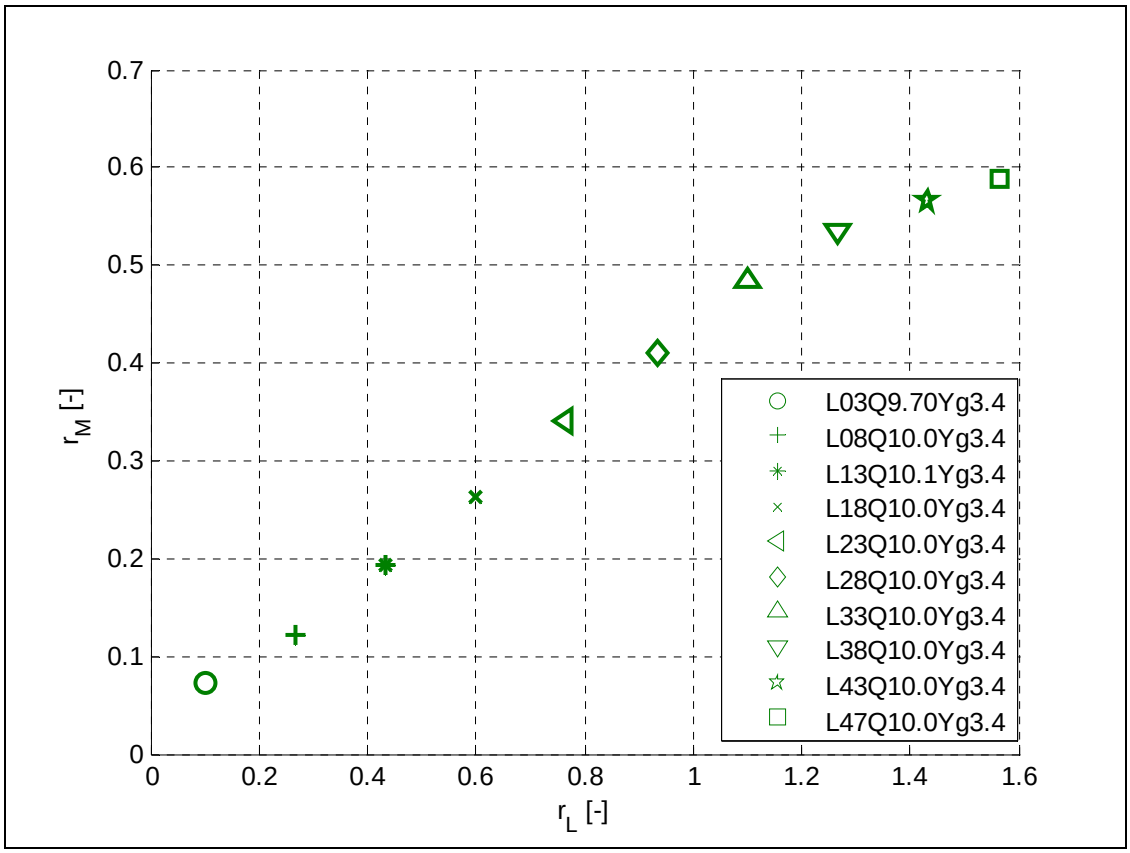

Figure 3.54: Momentum ratio versus length ratio for series C.

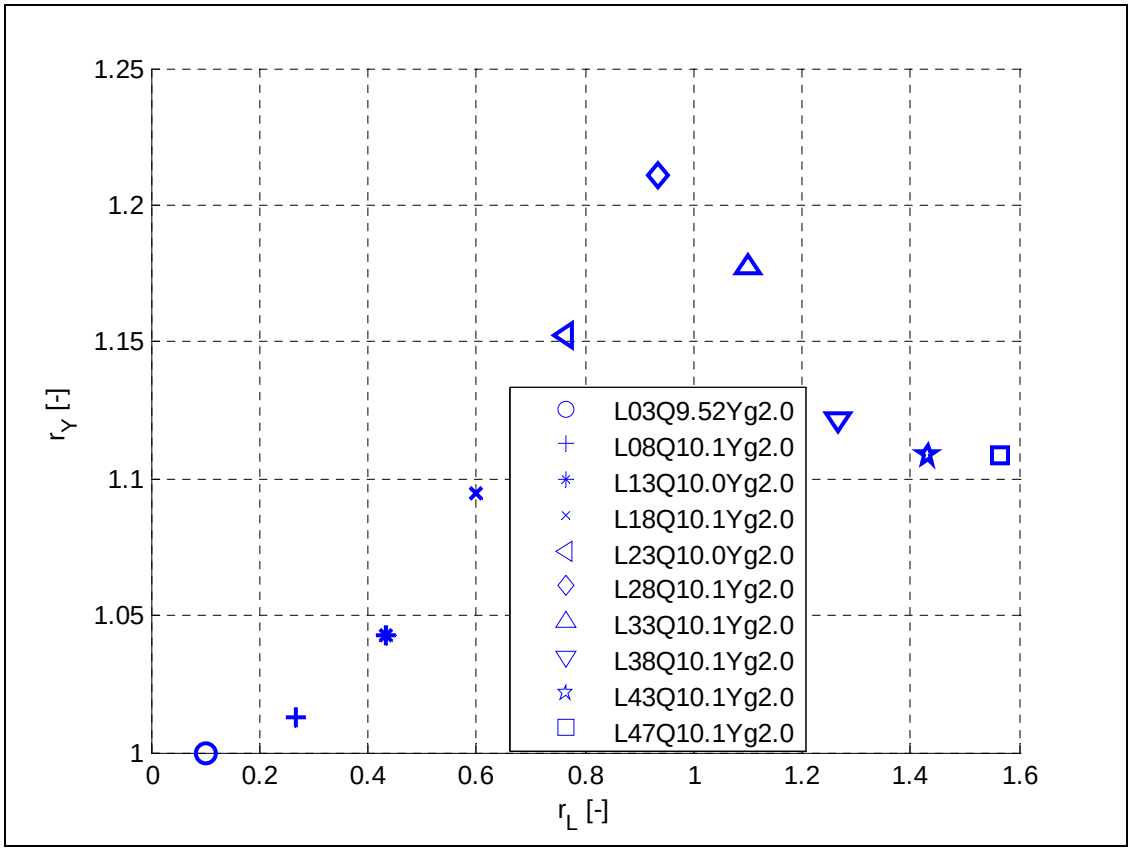

Figure 3.55: Water depth ratio versus length ratio for series B.

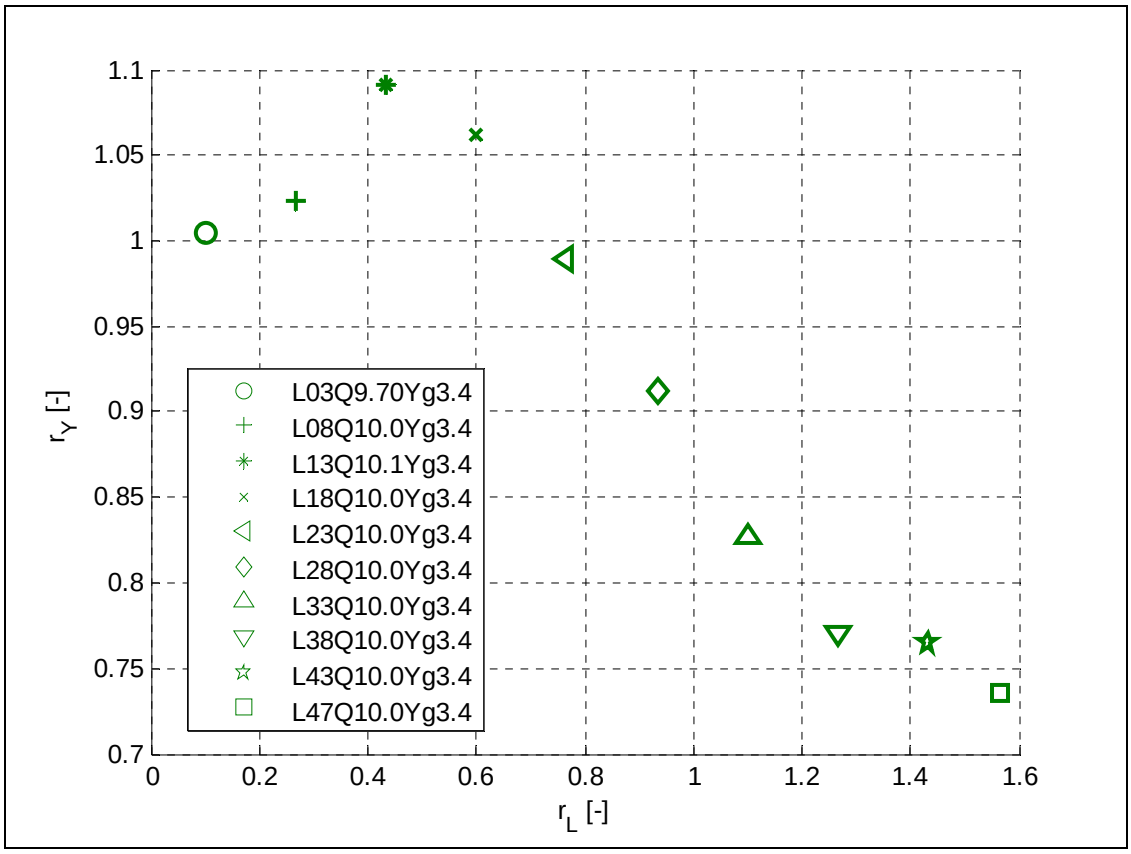

Figure 3.56: Water depth ratio versus length ratio for series C.

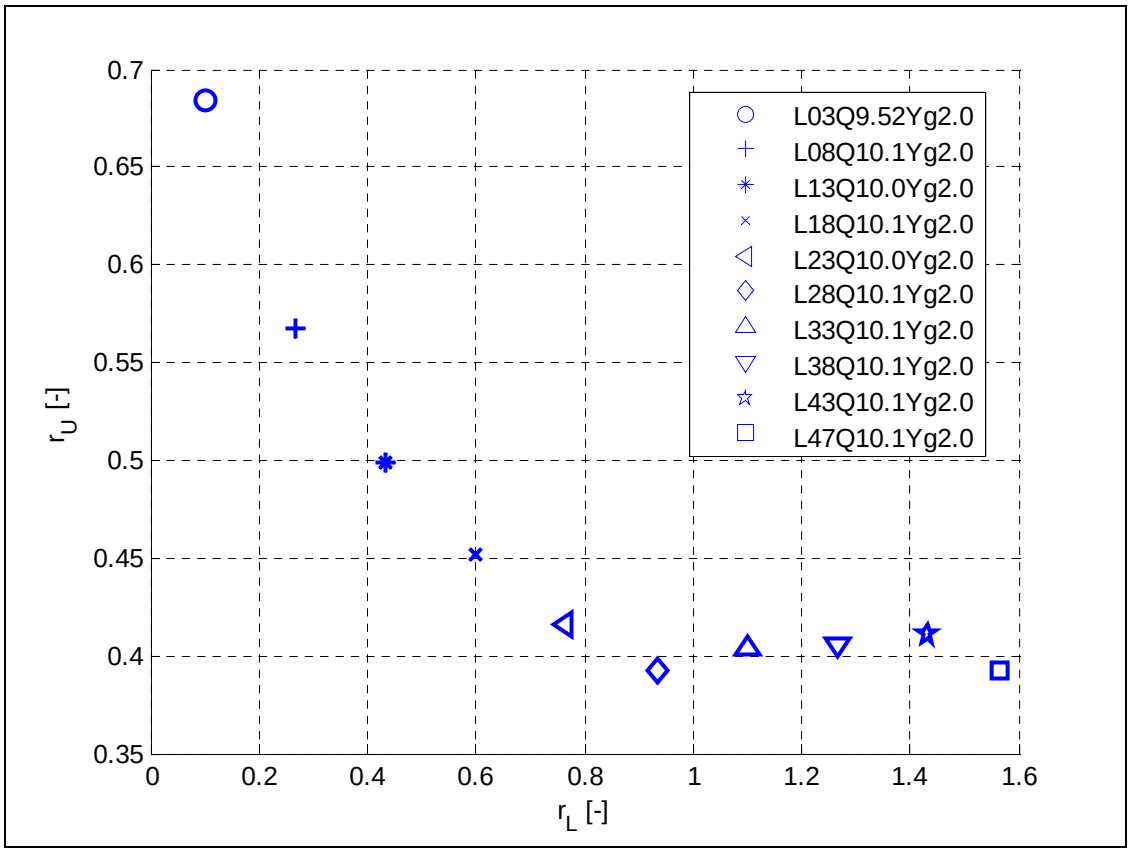

Figure 3.57: Velocity ratio versus length ratio for series B.

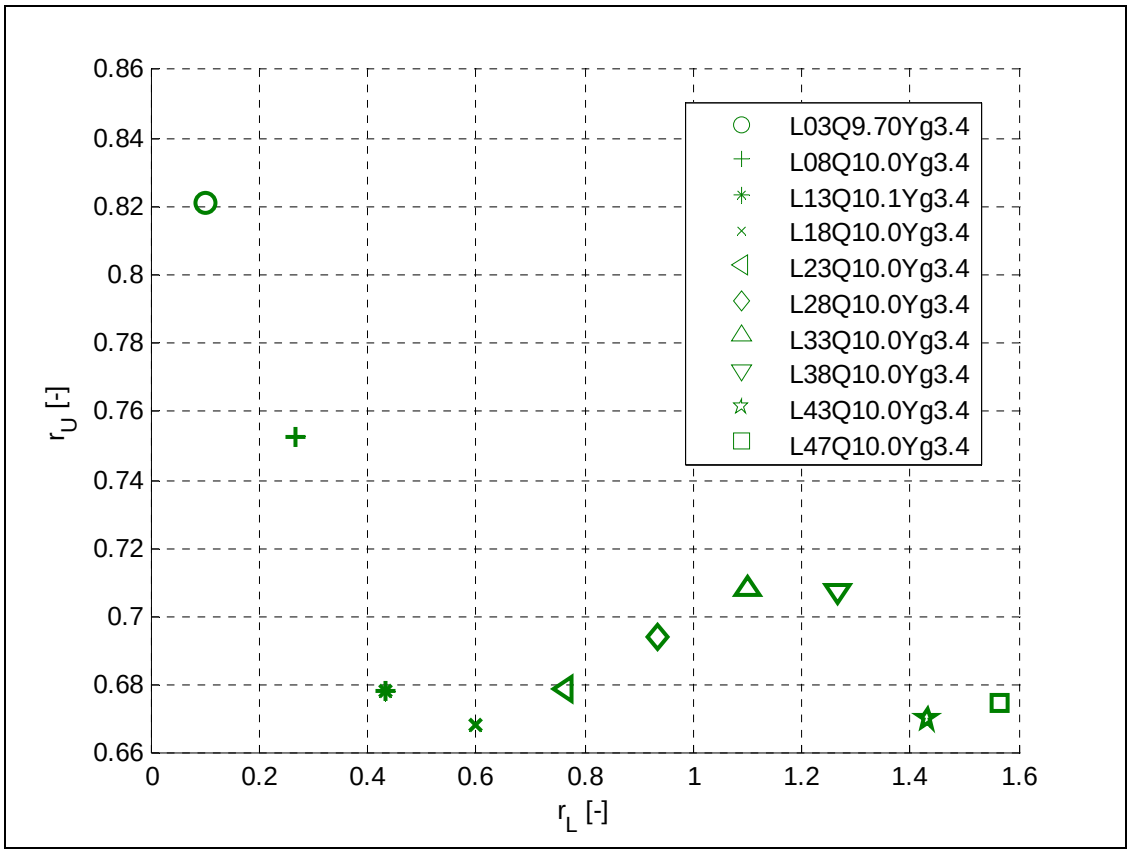

Figure 3.58: Velocity ratio versus length ratio for series C.

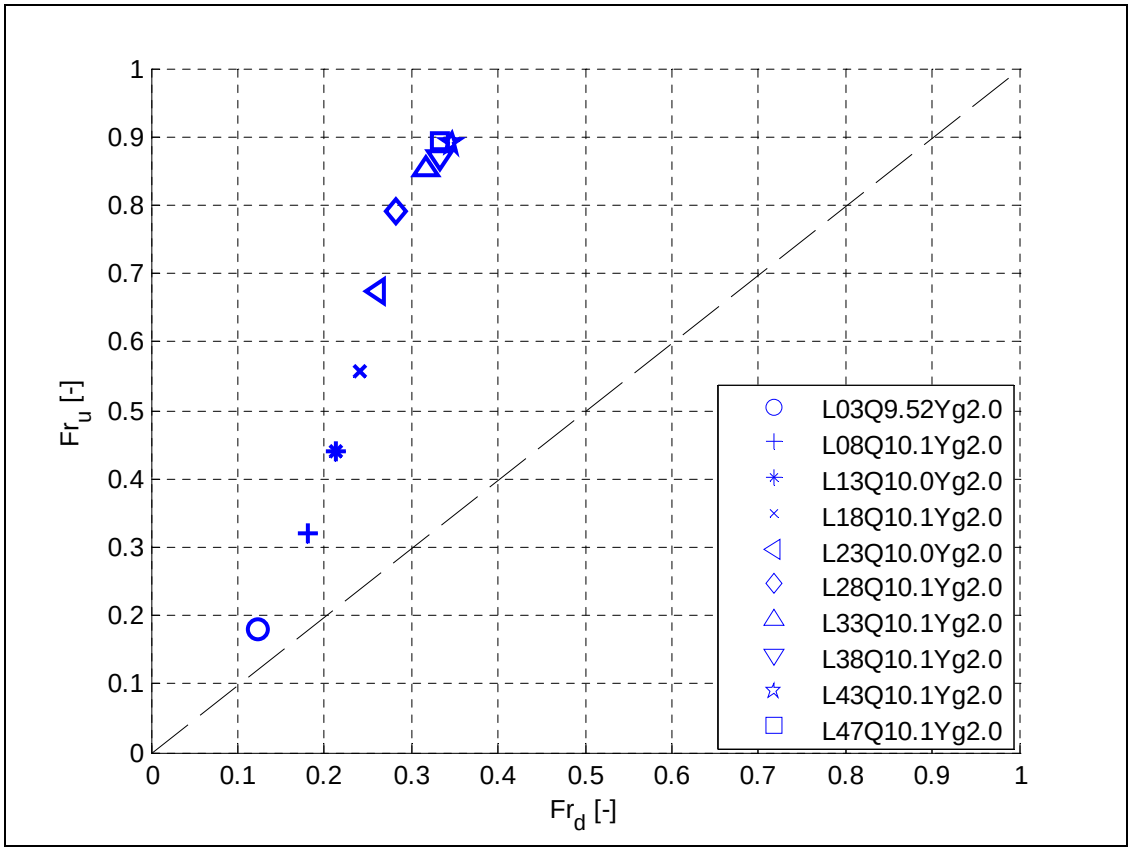

Figure 3.59: Flow regime in the Froude graph for series B.

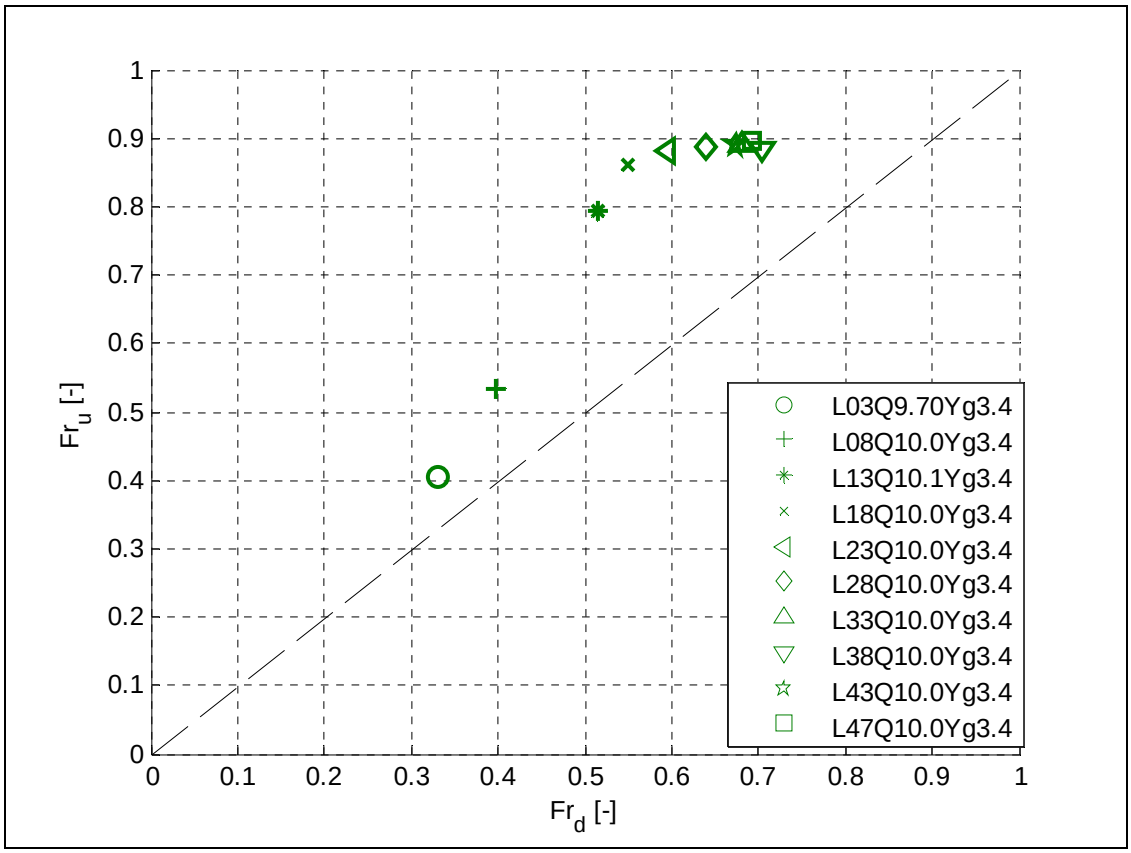

Figure 3.60: Flow regime in the Froude graph for series C.

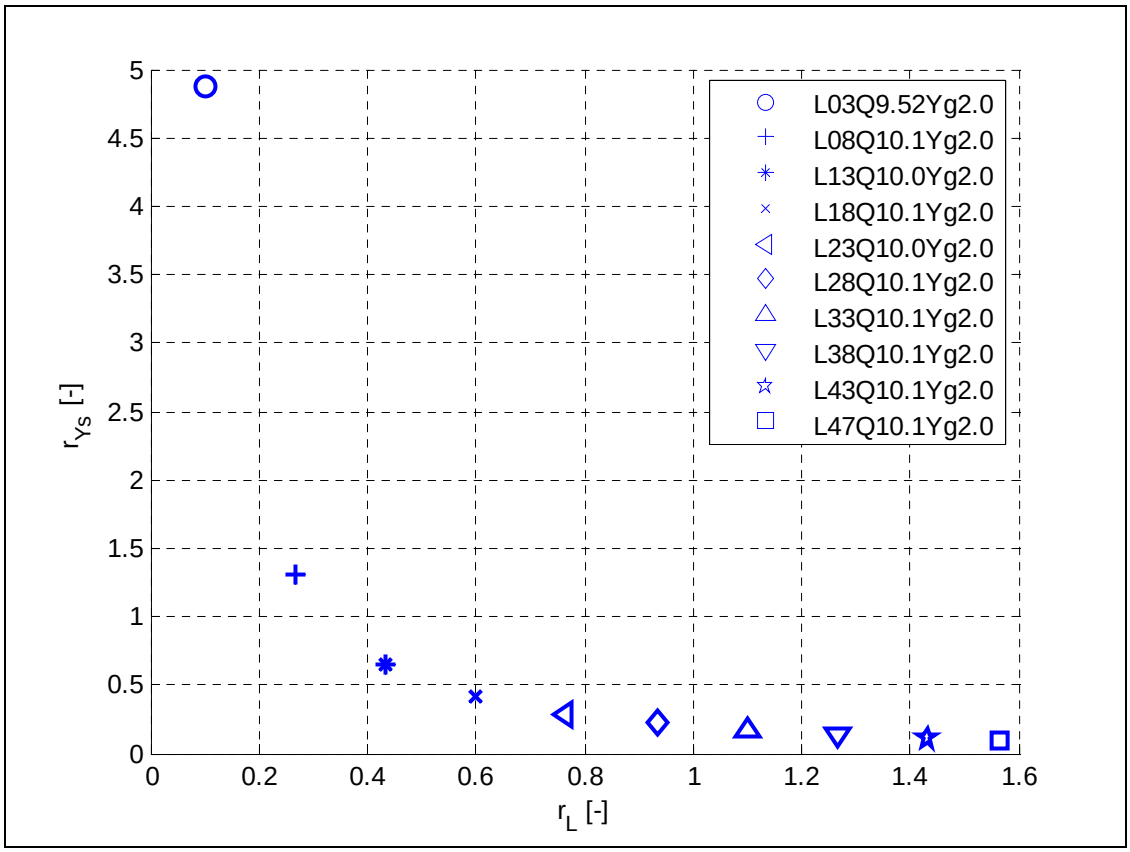

Figure 3.61: Side weir aspect ratio versus length ratio for series B.

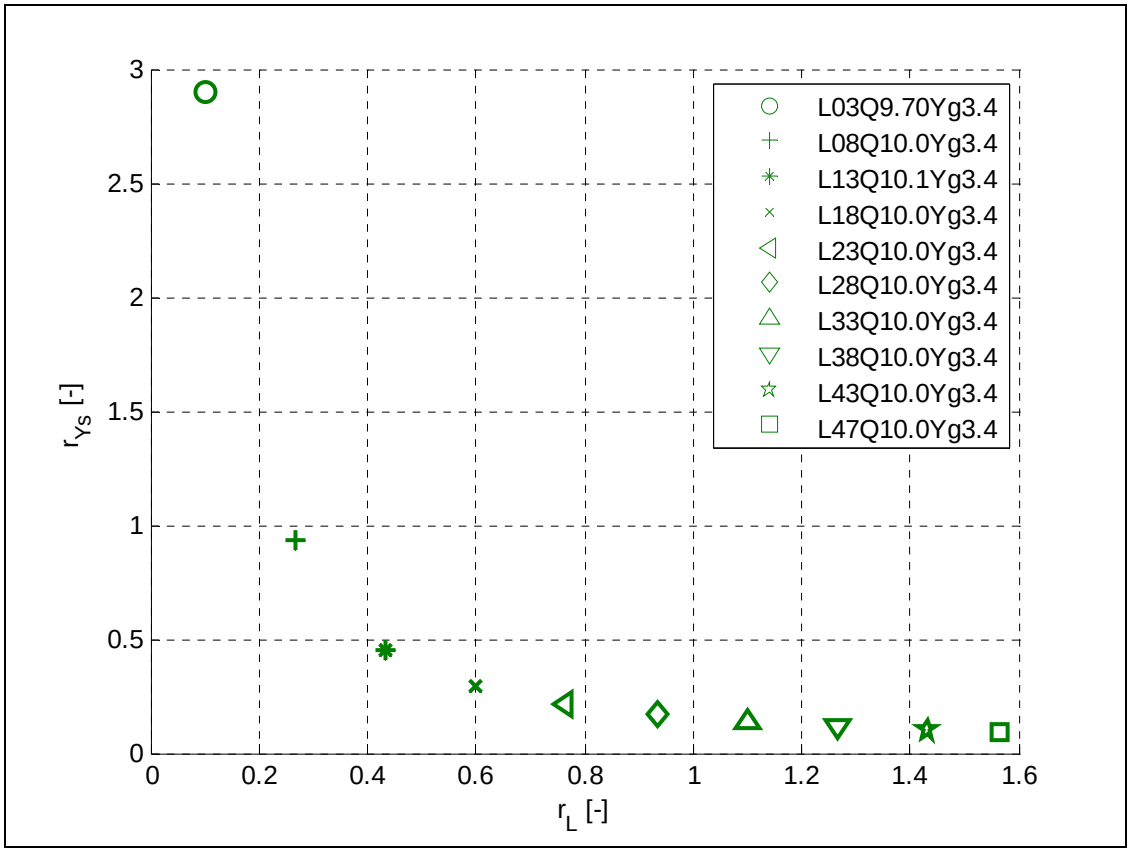

Figure 3.62: Side weir aspect ratio versus length ratio for series C.

Table 3.2: Summary of main variables investigated in tests of series B and C.

Series	Test	Run Code	Inflow discharge	Outflow discharge	Side weir discharge	Side weir		Upstream section				Downstream section			
						Mean flow depth	Mean shear stress	Flow depth	Mean velocity	Alpha	Beta	Flow depth	Mean velocity	Alpha	Beta
			Q_u [m^3/s]	Q_d [m^3/s]	Q_s [m^3/s]	$\overline{Y}_s$ [m]	$\tau_{s,mean}$ [N/m^2]	Y_u [m]	U_u [m/s]	α_u [-]	β_u [-]	Y_d [m]	U_d [m/s]	α_d [-]	β_d [-]
B	7	L03Q9.52Yg2.0	0.0095	0.0065	0.0030	0.146	14.67	0.146	0.217	1.64	1.21	0.146	0.148	1.51	1.21
	8	L08Q10.1Yg2.0	0.0101	0.0058	0.0043	0.105	4.66	0.104	0.323	1.52	1.17	0.106	0.183	1.64	1.26
	9	L13Q10.0Yg2.0	0.0100	0.0052	0.0048	0.085	2.82	0.084	0.398	1.41	1.15	0.087	0.198	1.67	1.26
	10	L18Q10.1Yg2.0	0.0101	0.0050	0.0051	0.075	2.02	0.072	0.467	1.32	1.13	0.079	0.212	1.83	1.31
	11	L23Q10.0Yg2.0	0.0100	0.0047	0.0052	0.067	1.59	0.063	0.530	1.38	1.15	0.072	0.216	1.90	1.32
	12	L28Q10.1Yg2.0	0.0101	0.0048	0.0053	0.062	1.31	0.057	0.592	1.28	1.11	0.069	0.232	2.34	1.48
	13	L33Q10.1Yg2.0	0.0101	0.0047	0.0053	0.057	1.09	0.054	0.621	1.91	1.32	0.064	0.246	2.02	1.37
	14	L38Q10.1Yg2.0	0.0101	0.0046	0.0055	0.054	1.03	0.053	0.629	1.73	1.26	0.060	0.255	2.31	1.46
	15	L43Q10.1Yg2.0	0.0101	0.0045	0.0055	0.050	0.95	0.053	0.640	2.52	1.54	0.058	0.257	2.28	1.46
	16	L47Q10.1Yg2.0	0.0101	0.0044	0.0057	0.048	0.81	0.052	0.642	1.06	1.02	0.058	0.252	1.26	1.10
C	17	L03Q9.70Yg3.4	0.0097	0.0080	0.0017	0.087	14.06	0.087	0.372	-	-	0.087	0.306	-	-
	18	L08Q10.0Yg3.4	0.0100	0.0077	0.0023	0.075	3.85	0.074	0.455	-	-	0.075	0.342	-	-
	19	L13Q10.1Yg3.4	0.0101	0.0074	0.0026	0.058	2.01	0.057	0.590	-	-	0.062	0.400	-	-
	20	L18Q10.0Yg3.4	0.0100	0.0070	0.0030	0.054	1.56	0.054	0.615	-	-	0.057	0.411	-	-
	21	L23Q10.0Yg3.4	0.0100	0.0067	0.0033	0.050	1.30	0.053	0.628	-	-	0.052	0.426	-	-
	22	L28Q10.0Yg3.4	0.0100	0.0063	0.0037	0.048	1.17	0.053	0.631	-	-	0.048	0.438	-	-
	23	L33Q10.0Yg3.4	0.0100	0.0058	0.0043	0.046	1.23	0.052	0.627	-	-	0.043	0.444	-	-
	24	L38Q10.0Yg3.4	0.0100	0.0054	0.0046	0.045	1.13	0.053	0.628	-	-	0.041	0.444	-	-
	25	L43Q10.0Yg3.4	0.0100	0.0051	0.0050	0.043	1.16	0.052	0.631	-	-	0.040	0.423	-	-
	26	L47Q10.0Yg3.4	0.0100	0.0049	0.0051	0.042	1.06	0.052	0.629	-	-	0.038	0.424	-	-

3.5 Summary and concluding remarks

An experimental work has been conducted on side weir flow in a fixed bed water-recirculating tilting flume with rectangular cross section.

The main objective of the experiments was to investigate the hydraulic regime of a channel when a lateral outflow takes place on one side of the channel in steady conditions, with a subcritical flow as initial regime. The rectangular side weir had zero height crest and different values of the length: the final aim is to simulate the flow outing from a river when a breach occurs on one of its levee and it achieves various final lengths. The flume was tilted by a constant slope of about 0.1% and a fixed roughness composed by granular gravel with a D_{50} = 6.8 mm was stuck down to its bottom, in order to provide a realistic resistance to the flow. Side outflow was collected by a lateral channel, whose set-up did not allow backwater effects from the outflow toward the main flow.

The main result of such experimental activity was to highlight the purely hydrodynamic processes which take place in the main channel during a lateral outflow without considering the mobility of the materials: the bed layer of the channel was not erodible as well as the lateral weir.

The hydrodynamics of the flow was observed by means of measures of water levels at predefined locations, flow discharge values (inflow, lateral outflow and downstream flow), vertical profiles of velocity (in the longitudinal and, for three detailed tests, in the transversal direction) and superficial flow field (by means of PTV techniques).

Six preliminary tests (series A) were conducted without lateral outflow, in order to check the system functioning and set-up, to collect data for verification of the rating curve of the main channel and to provide a reference case for the next tests.

Ten different tests were performed in series B, according to the imposed side weir length, which ranged from $L_s/B = 0.1$ to $L_s/B = 1.57$. The tests were conducted with a constant value of the inflow discharge (Q_u = 10 l/s) and a predefined set-up of the downstream sluice gate (Y_g = 2.0 cm), in order to have an initial subcritical flow regime.

Further ten tests (series C), regarding the same ten side weir lengths, were performed by modifying the height of the sluice gate at the end of the flume, in order to analyse the influence of the downstream boundary condition on the system: in particular, the sluice gate was set to a greater height (Y_g = 3.4 cm) which anyway provided subcritical flow as initial condition. The testing conditions and measure data types are reported in Table 3.1.

The test procedure required to achieve a stationary state and then to perform the measurement operations. The physical model took a quite short time to achieve steady conditions in the order of 15 minutes: this means that the response of the main flow to the lateral outflow in terms of hydrodynamic variables is very fast, at least in fixed bed conditions.

Data highlight how the side weir influences the flow field in the main channel. For increasing side weir length, the outflow discharge increases and, consequently, the upstream flow is more deflected by the side weir so that the upstream velocity increases and water level is decreased. The flow depth profile is drawn down toward the side weir since the entire flow is accelerated and this behaviour is intensified for longer side weirs, when the flow depth at the beginning of the weir was approaching the critical depth. The flow depth along the side weir was usually increasing because of the subcritical feature of the flow, whereas a first decreasing part was observed for the tests having the longest side weirs, which indicates that a first supercritical zone likely occurred in those tests.

The upstream water profile was always greater than the calculated critical depth, which means that the approaching flow was subcritical. The ongoing flow was subcritical as well, since the hydrodynamics of the downstream zone was governed by the downstream sluice gate.

The threshold between the subcritical and the supercritical behaviour was different according to the downstream boundary condition and a very exact limit was not detected. Anyway, it was defined in function of the following features of the side weir:

- $L_s/B_{th} = 1.1$ and $Q_s/Q_{u,th} = 0.52$, for downstream sluice gate at $Y_g = 2.0$ cm
- $L_s/B_{th} = 0.6$ and $Q_s/Q_{u,th} = 0.30$, for downstream sluice gate at $Y_g = 3.4$ cm

Even if an indication of the regime threshold is given, it is not possible to conclude about the exact conditions at which supercritical flow zone occurs, also because an evident hydraulic jump was not localized. Therefore, further tests are recommended in order to better specify the threshold between the subcritical and the supercritical regime of the flow along the side weir and in order to define the existence, the location and the type of the hydraulic jump. This may have important implications on the investigated phenomena, since a supercritical flow along the weir spills out less discharge than a subcritical flow, due to the decreasing flow depth. The knowledge about the existence conditions of the subcritical and the supercritical flow along the side weir would therefore help in analysing the flow field in further details and in defining the characteristics that a prospective ideal model should have in order to reproduce the observed phenomena. Moreover, such an analysis would define more precisely the applicability field of simple models, i.e. models based on the widely-used assumption by De Marchi, which is limited to subcritical flows.

Additional tests would be useful to further investigate the influence of the downstream boundary condition on the flow regime, which is a very important topic, since the downstream condition highly affects the lateral outflow. Moreover, a way to set a predefined uniform rating curve as downstream boundary condition should be achieved, which is not straightforward since the flow discharge at the downstream section changes depending on the lateral outflow. The used set-up did not allow such uniform rating curve to take place, which, anyway, is a realistic condition occurring in real rivers.

The longitudinal velocity profiles show the influence of the side weir on the velocity distribution, which is distorted and deflected toward the weir itself. Flow velocity increases upstream the side weir up to values of $3 \cdot U_{mean}$. Data showed that the flow gets three-dimensional features when an important lateral outflow takes place.

The analysis of the surface flow field around the side weir showed that the side weir deflects the streamlines toward itself with increasing flow angles going closer to the downstream section of the weir. Moreover different zones of the flow field were detected, such as a *diving surface* along the weir, a *separation zone* at the side opposite to the weir, an *helicoidal flow* and a *reverse flow* downstream the weir. The *dividing surface* was induced by the flow attraction through the lateral weir and it got a larger distance from the weir on the bottom of the main channel than at the water surface. The *separation zone* seemed to be induced by a longitudinal pressure gradient due to the slowing down of the flow. The *helicoidal flow* arose at the downstream corner of the weir, at a singular point of local flow stagnation. The proposed interpretation is that the local flow stagnation creates a downflow motion, which is turned into the helicoidal motion by means of the main flow, as in case of flow around bridge piers. Finally, a *reverse flow* occurred at the near bed part of the channel, which was due to a backward withdraw of the side weir at the downstream corner. These three-dimensional effects developed for a size of L_s upstream and $2 \cdot L_s$ downstream and the resulting flow field was quite complex. Simple 1D models can not take into account such

phenomena, but they can only consider the influence of this complexity on the velocity distribution by means of Coriolis and Boussinesq correction coefficients. Anyway, only a complete three-dimensional model can aim to reproduce such phenomena (Neary et al., 1999). The collected data about vertical velocity profiles in longitudinal and transversal direction and about the superficial flow field are extremely important data necessary to calibrate an ideal numerical model.

The De Marchi hypothesis of constant specific energy head along the side weir was analysed for the tests of series B. The specific energy head computation assumed a constant upstream Coriolis coefficient $\alpha_u = 1.15$, whereas the downstream Coriolis coefficient was calculated from the recorded velocity distribution (see Table 3.2). The De Marchi assumption was verified for tests having $L_s/B \leq 1.1$ and $Q_s/Q_u = 0.52$, within an error of $\pm$ 10%, and this is useful to define the limitation and the applicability of models based on the assumption of constant specific energy head.

A computational analysis of the collected data was performed in order to get the longitudinal trend of some variables, as the longitudinal and transversal flow velocity, the deflection angle and the shear stress. The methodology was based on discretizing the recorded flow depth profile into a predefined number of spatial intervals, in which the flow outing through the side weir was calculated by means of the side weir law (eq. 3.5) with the discharge coefficient calibrated on the measured side flow discharge. The flow rate in the main channel along the weir was then calculated, as well as the transversal and the mean longitudinal velocity according to continuity principles (eq. 3.6). The outflow angles were computed as in equation 3.7, on the basis of the velocity components. Finally, the shear stress was calculated as longitudinal and transversal components along the weir (eq. 3.8) and as mean value acting on the side weir. This analysis provided the following main outcomes:

- The calibrated discharge coefficient decreases as the side weir lengthens and it is a function of the upstream Froude number (in agreement with other authors);
- The longitudinal velocity U_x decreases along the weir of about 50% due to the lateral outflow;
- The transversal velocity U_y increases along the weir;
- The transversal velocity increasing is more evident at the weir crest, where the flow depth is lower than at middle axis of the channel;
- The flow angle θ increases along the lateral outflow and the longitudinal variation is more evident for longer weirs;
- The flow angle θ decreases its value for longer weirs;
- The shear stress reduction along the weir is in the order of more than 50% and it is mainly due to the lowering of its longitudinal component;
- The mean shear stress acting on the weir section decreases of one order of magnitude for longer side weirs and it tends to an asymptotic low value.

All these considerations give an overview of how the main physical variables change along the lateral weir and for increasing lateral outflow: since they consider variables averaged on the cross-section, they should be reproduced even in 1D numerical models.

Finally, the main features of the flow regime were described in terms of dimensionless parameters, which gave an essential overview of the physical variables of the system in terms of: flow discharges, momentum, flow velocities and flow depths. The velocity and the water depth ratios (r_U and r_Y) were defined as ratio between the related flow features at the

downstream and at the upstream sections. The outflow and the momentum ratios (r_Q and r_M) were defined as proportion of the related flow features at the side weir and at the upstream section. The length and side weir aspect ratios (r_L and r_{Ys}) took into account the features of the side weir and the principal geometric dimension of the main channel.

The discharge ratio $\mathbf{r_Q}$ summarizes the influence of the side weir in terms of water mass balance and it is the most important parameter, since the first effect of a side weir is to remove part of the water from the main channel. The momentum ratio $\mathbf{r_M}$ considers how much momentum is affected by the lateral outflow and it was derived by imposing the momentum balance in the main channel along the side weir length. The influence of the side weir on the main flow is furthermore described in terms of variation of flow depth and velocity values at the down- and upstream sections. In particular, the flow depth ratio $\mathbf{r_Y}$ gives an immediate indication of the flow depth feature along the weir. A further description of the flow along the side weir is given in terms of mean flow depth $\mathbf{r_{Ys}}$ and the dimensionless parameters are analysed with reference to the dimensionless length $\mathbf{r_L}$, which considers the relative geometric importance of the lateral weir compared with the main channel. Moreover, the flow features are described in terms of up- and downstream Froude numbers, that is the main parameter when dealing with open channel flows. It results that:

- Both the maximum r_Q and r_M are reached for the longest weir and they are in the order of 50%-60%, which seems to be around an upper limit;
- The r_Y and the r_U change their trend because of the change in the flow regime (likely from subcritical to supercritical);
- The upstream Fr increases with the side weir length because of the acceleration of the flow;
- The downstream Fr increases with the side weir length because of an effect of the downstream sluice gate, which does not guarantee an uniform rating curve;
- The r_{Ys} dramatically decreases with the weir length and it tends to a lower limit.

Future research is recommended in order to extend the collected data and to investigate other configurations, such as: longer side weirs, higher weir crests, different downstream conditions, further main channel characteristics (inflow, cross section dimensions, bed roughness).

4 Movable bed laboratory investigations

The laboratory investigations regarding movable bed conditions have been carried out at the laboratory of the Leichtweiß-Institute for Hydraulic Engineering and Water Resources of Braunschweig (LWI) during January-June 2012 and have been fully supported by the department of Hydromechanics and Coastal Engineering of LWI. The experiments were supervised by Prof. H. Oumeraci. A complete report about the experimental results is given in Michelazzo and Oumeraci (2013).

The main objective of these experiments was the collection of experimental data concerning the processes of breach formation and evolution due to an overtopping flow on an earthen river levee built in a flume with movable bed. Unlike most of experimental works concerning dam breaches, the present work was aimed to reproduce the situation of a river levee, in which the levee model is located longitudinally in the flume.

This Chapter addresses the description and the analysis of the breaching processes (formation and evolution) together with the river flow dynamics (evolution of flow hydrodynamics and bed morphodynamics) until an equilibrium of the system river-breach was assumed to be gained.

In order to analyse both the breach evolution and the river morphodynamics, a movable bed flume filled with sand was used with a sandy model of the levee as a lateral boundary. Steady inflow conditions were set during the tests. In such a way, the transitory phase of breach evolution was monitored until an equilibrium of breach and hydraulic variables was assumed to be achieved.

The present analyses are supplemented by other experimental investigations, that were made in fixed bed conditions and whose description is given in Chapter 3.

4.1 Experimental set-up

4.1.1 Experimental facilities

The experimental investigations were carried out in a 30 m long, 2 m wide and 0.8 m deep water-recirculating tilting flume with rectangular cross section. Figures 4.1-4.2 show the plan and cross view of the apparatus and some pictures are given in Figures 4.3-4.4.

The flume was subdivided longitudinally for a length of about 22.5 m into two separated channels by concrete blocks 0.35 m high. The main channel represented the actual testing facility where the incoming liquid discharge was put in. The bottom of the main channel was filled with bricks and sand bags and, above them, a sand layer 0.15 m deep was set as river bed. The levee model was set longitudinally on the right side of the main channel for a central testing reach 15 m long: it had a trapezoidal shape, 0.25 m high, 0.1 m wide at the crest with a slope of the sides of 1V:2H. The levee model was made by the same kind of sand used for the river bed, which was a medium sand with a D_{50} = 0.84 mm. A waterproof plywood structure was placed at the up and downstream parts of the flume, in order to provide fixed and stable conditions for the inlet and the outlet of the water: these structures were aligned with the levee model and they had the same geometry so that water flow did not meet changes of cross section along the flume. The wet cross section in the main channel had a maximum depth of 0.25 m and a maximum top width of 1.1 m.

A system of toe drains was set under the protected side of the levee model in order to control the seepage line and to prevent piping phenomena and breach self-triggering. The drain was made by geotextile bag filled with gravel. The levee was constructed by placing sand in layers of about 5 cm of height which were sprayed with water and hand compacted. The design shape of the levee was achieved by means of wooden templates attached to a carriage. The levee model was stable since the slope angle was less than the repose angle of the sand (33°). The river bed had the same kind of sand which was initially smoothed as flat bed and the initial flow conditions were under the critical condition for sediment movement.

The flume had an inclination $S_0 = 0.1\%$, set by means of the flume electronic control system. The sediment recirculation system was not activated.

A sluice gate was set at the downstream section of the main channel: it was used to regulate the downstream boundary condition. The downstream part of the flume, next to the plywood structure and before the sluice gate, had only bricks on its bottom but no sand, in order to make the sluice gate work above a fixed surface. At the end of the lateral channel, a sharp-crested weir 0.15 m high was fixed to stop the sand eroded through the breach and to provide a way to measure the water discharge flowing in the lateral channel.

The main and the lateral channels were isolated each other by the separation wall and the lateral channel upstream end was closed toward the inflow, so that water could flow in the lateral channel only through the breach. A small amount of water discharge could flow through the drains.

The bottom of the lateral channel was lower than the main channel in order to avoid backwater effects from the outflow toward the main flow.

Two carriages were moved along the flume for measurement of water surface and flow velocity as described in Section 4.1.2. The flap gate at the end of the flume was set almost at zero level only in order to stop the sand flux, and not as downstream boundary condition.

The goal of the experimental activity was to investigate a process, without reproducing a real prototype. Nevertheless, it is important to check that the main properties of the physical model are consistent with a real process. According to the typical values recorded during the tests (Table 4.3), the Froude number Fr gained in the main channel before the breaching is $Fr_{pre} = [0.02 \div 0.23]$, which actually is not very high for a river flood. Anyway, the flow accelerated after the breach trigger and the Fr increased up to $Fr_{br} = [0.1 \div 0.7]$, which is a more realistic range for a real river in subcritical flood regime. The Reynolds number is evaluated in the order of $Re \approx 10^5$, which, for a relative roughness $\varepsilon_r \approx 10^{-2}$, is referred to a fully turbulent flow that is consistent with conditions found in real rivers. During the experimental test, the flow acceleration induced by the breach flow allowed sediment particles to be moved as bed load and dunes appeared. The breaching process was let to develop for a time ranging from one hour until four hours (for test A3). Finally, the aspect ratio of the main channel during the breaching ($Y/B \approx 1/10$) is quite realistic. Moreover, a possible order of magnitude for the length scale of the investigated phenomena can be $\lambda_L = 1{:}5{\cdot}10$, which would give the following values of the variables (for test A3) referred to a river prototype:

- River width = 55 m;
- Flow discharge = 516 m^3/s;
- Breach length = 73 m;
- Breach discharge = 242 m^3/s.

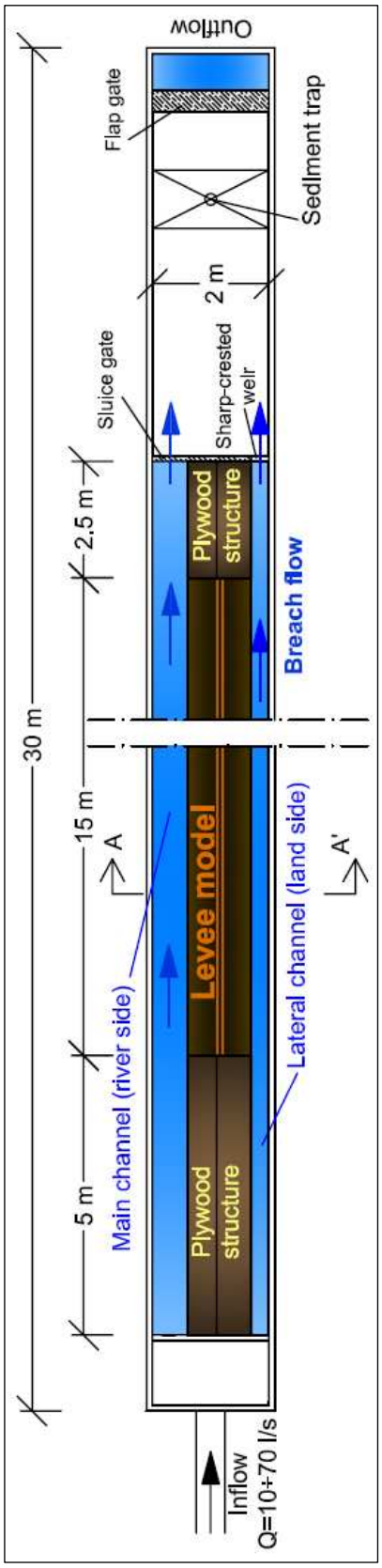

Figure 4.1: Sketch of the experimental apparatus (plan view).

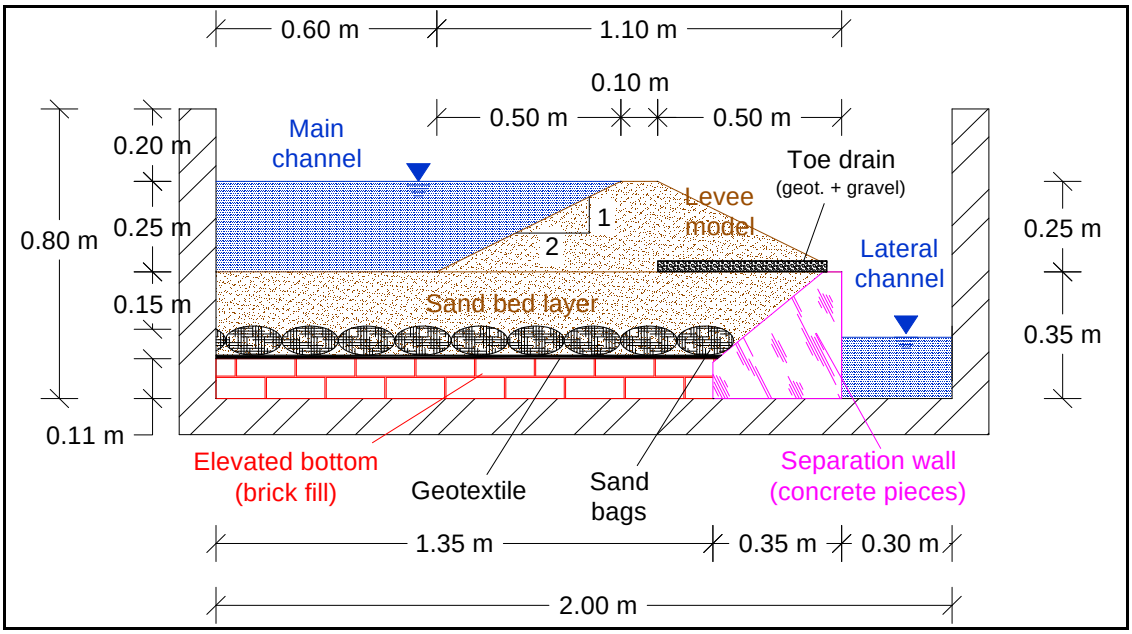

Figure 4.2: Cross section A-A' of the flume.

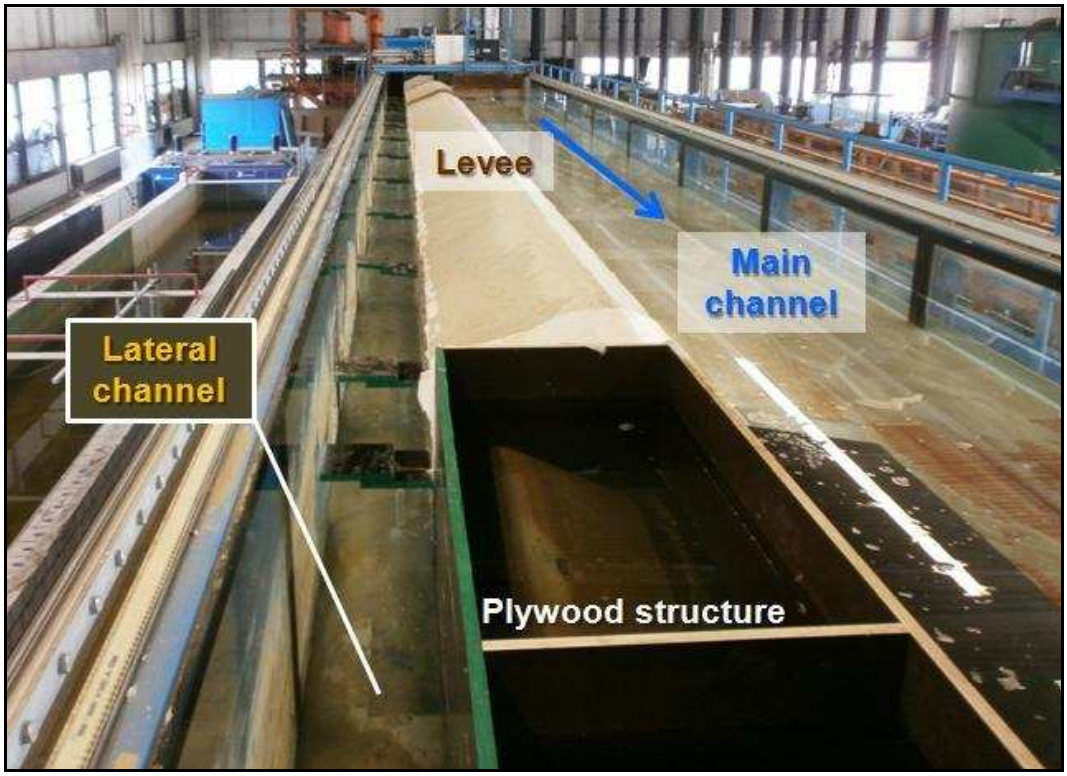

Figure 4.3: Aerial picture of the flume.

Figure 4.4: Downstream part of the flume: on the left, the sharp-crested weir, on the right, the sluice gate.

Figure 4.5: Drain system in the flume (a): toe drain detail (b), test for control seepage line (purple line, c).

4.1.2 Measuring techniques and observations

Within this Section the instruments used to measure the variables during the experimental tests are described into different paragraphs. Basically, the hydrodynamics of the flow was observed by means of measures of water levels, flow discharge values and point velocity values, the morphodynamics of river bed was acquired by bed profiler and the breach evolution was monitored by means of two cams.

4.1.2.1 Water surface profile

The water level was recorded by means of three ultrasonic sensors (USs).

The first sensor (US0 in Figure 4.6) was attached to the movable carriage and it was used to record the water surface profile along the flume and the levee crest profile as well. Since the sensor was able to detect a wide range, its accuracy was in the order of ± 13 mm.

The other two sensors were Honeywell series 943-F4V-2D-1C0-330E, which recorded the water level with a maximum error of ± 1 mm. These gauges were fixed to the flume structure at the downstream part 0.7 m far from the end section and at middle of the main and lateral channels (US1 and US2 in Figure 4.6) and they recorded the distance between the probe and the water surface. The recorded levels were then transformed into a distance referred to the bottom of the main or of the lateral channel, depending on where the measure was taken.

Data were recorded by the ultrasonic sensors with a frequency of 10 Hz and they were saved and managed into a PC by means of the software L~Davis.

4.1.2.2 Flow discharge

The inflow discharge Q_u was delivered from a tank by the use of a recirculation system where the inflow pipe was controlled by an electromagnetic flow meter (IDM). A steady flow rate could therefore be easily set and maintained accurately throughout the duration of each test.

The lateral breach discharge Q_{br} was determined by using the water level measured by ultrasonic gauge US2 and its relationship with the flow rate given by the sharp-crested weir working: this relationship was previously calibrated in a smaller channel which had the same geometry and the same weir of the lateral channel. The discharge flowing in the main channel downstream the breach Q_d was calculated by using the rating curve of US1 controlled by the sluice gate or as difference $Q_u – Q_{br}$.

4.1.2.3 Velocity components

The 3D components of the flow velocity were measured from time to time in various positions during the tests by means of an acoustic doppler profiler ADV-Nortek. The velocity range and the submergence of the probe were changed from measure to measure in order to search for the best setting in term of Signal-to-Noise Ratio and Correlation values. The probe had a sampling rate of 10 Hz.

4.1.2.4 Bed topography

The river bed was surveyed at the beginning and at the end of each test, at the assumed equilibrium stage. Three ultrasonic sensors “SONOMETER 05” working under water were used, which were fixed to the movable carriage. These sensors acquired with a frequency of 10 Hz a sampling point of diameter size of 2 cm. The maximum detectable range was 200 mm and the resolution was of ± 2 mm. The bed profiler probes were calibrated and their zero level was referred at the flat bed elevation in the main channel. The sensors were equally spaced from each other of 5 cm in order to cover the width of the river bed (0.6 m) for all the testing reach length with 12 strips of acquisition. The carriage was automatically moved by setting the starting point and the desired velocity (30 mm/s), which provided a spatial resolution of one point of acquisition every 3 mm in the longitudinal direction. Topography data were acquired in L~Davis software.

4.1.2.5 Breach development

The breach in the levee model was initiated, as described in Section 4.2.2, by cutting a little groove into the levee crest with a wood stick. The evolution of the breaching process was recorded by two cams both on the river side, one looking downstream and the other one upstream. Two meter sticks were placed on the crest of the levee in order to evaluate the erosion rate of the breach. No devices, but only visual observation, were employed to monitor the breach deepening.

4.1.2.6 Video techniques and other instrumentation

Two high definition cams were fixed to the flume frame to monitor the breach development: they provided two different points of view by focusing on the upstream and downstream section of the breach. The breach site was lighted to better focus the breach features. The breaching process was recorded until a test was ended.

Two different PCs were used to store data: one collected all data coming in L~Davis software, the other one was employed only as an acquisition system of the ADV. Two carriages were moving along the flume: the upstream one accommodated the US0 and the bed profiler and it was controlled by an electronic system through which the position of the carriage was known and was acquired to refer the position of the devices above it. The second carriage had the ADV on it and it was manually managed.

The valve of the inflow and the flap gate were set by a remote control.

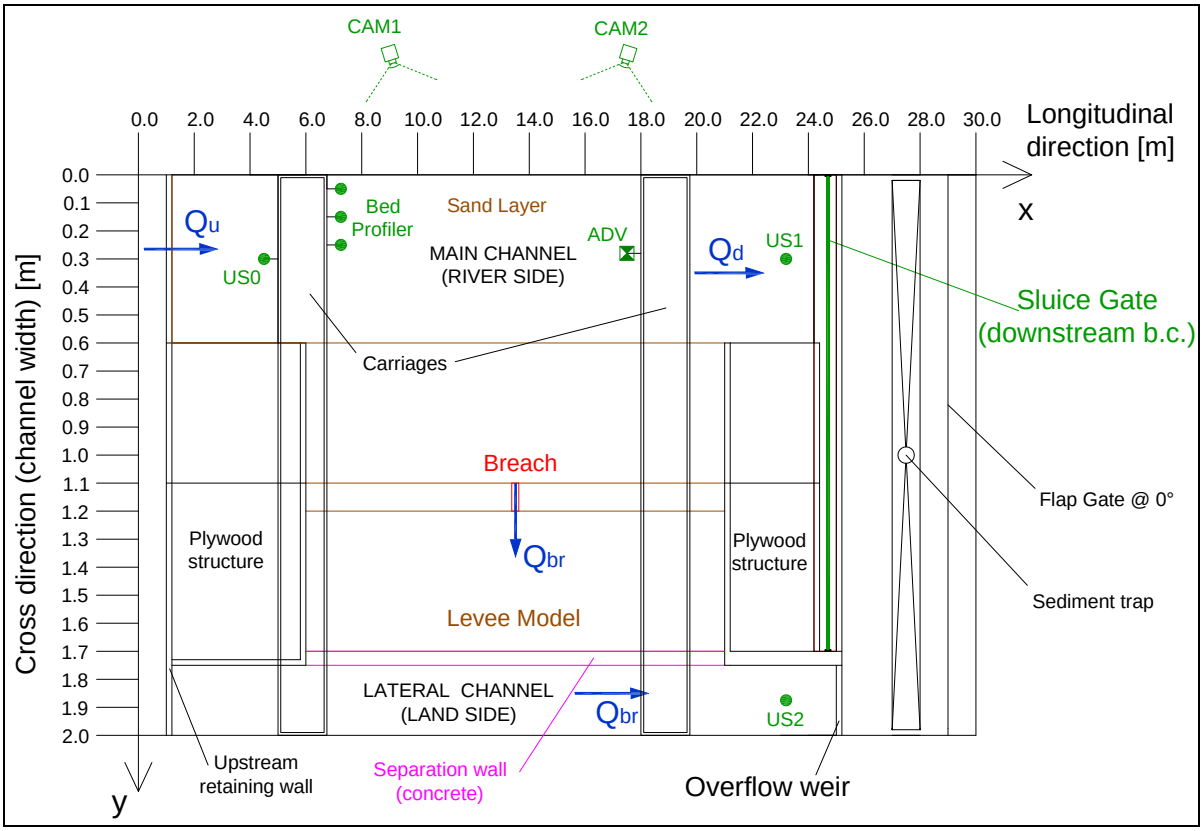

Figure 4.6: Experimental apparatus with measurement devices (distorted scale).

4.1.2.7 Experimental errors

The ultrasonic sensors acquired data with a precision of ± 1 mm.

The error over the flow depth measurement gives an error on the calculation of the flow discharge through the use of the rating curves at the downstream section of the main channel and at the lateral channel. An error of ± 1 mm on the measure of the flow depth at the downstream section results in an error of ± 4-5% over the computed downstream discharges.

By the same way, an error of ± 1 mm on the measure of the flow depth at the ultrasonic gauge in the lateral channel results in a maximum error of ± 5% over the outflow discharge computed by means of the weir equation.

Higher errors affected the water surface measurements through the sensor US0, which had an accuracy of around ± 1 cm: since the water depth in the main channel decreased during the breaching of the levee until around 10-15 cm, the error of US0 was in the order of ± 10%.

Finally, the bed profiler had a precision of ± 2 mm, which was equivalent to ± 1% of the measurement range (200 mm). The meters on levee crest, used to evaluate the lengthening rate, had marks every 2.5 cm, which therefore was the precision of such analysis.

4.2 Testing programme and test procedure

Breach evolution, river flow and river bed modification were analysed during various tests in which the inflow condition was changed. Different values of inflow discharge Q_u were tested (Q_u = 10÷70 l/s), while the flume slope, and consequently the initial river bed slope, was maintained constant and equal to 0.1%. The downstream boundary condition, given by the sluice gate configuration, was changed for each discharge so that the main channel water level before breaching was always around the levee crest, i.e. the sluice gate opening was adjusted to obtain a water depth of about 0.25 m all along the flume. Evolution process and final length of the breach, as well as river bed morphology and flow hydrodynamics, were investigated. The chosen value of Q_u was kept in steady condition throughout the duration of the test. Levee model geometry and sand material were not changed.

The initial flow field was always in subcritical regime: different initial Froude numbers were achieved for the tested inflow discharges.

4.2.1 Test series

Three main series of tests were performed.

The code of each test is composed by a string of characters which identifies the main features of the test, as explained by the following sketch.

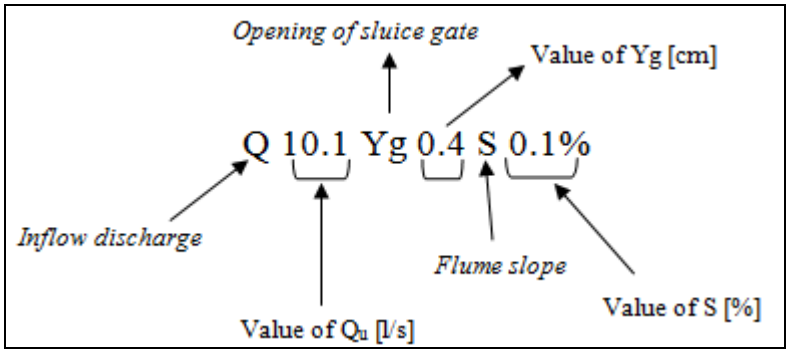

Tests of series A concerned conditions with the standard configuration of the levee, as explained in Section 4.1.1.

Tests of series B were performed on a partially modified set-up: the levee model upstream the breach site was covered by a geotextile in order to protect it against the flow erosion induced by the flow acceleration due to the breaching process (see Figure 4.7). This configuration allowed to test higher inflow discharges avoiding the erosion of the levee in the upstream zone (see results of tests of series A). Moreover, tests B7, B8, B9 and B10 were ended by progressively closing the downstream sluice gate to test the influence of the downstream condition on the breach dynamics.

Finally, two borderline cases were tested in series C: the case of dam breach with an almost static water level behind the levee and the case of multiple breaches during the same test. During the dam breach test it was necessary to maintain a small inflow discharge almost equal to the infiltration rate through the levee in order to have a steady water level in the main channel before starting the breaching. This is the reason why the inflow discharge was not zero even if the downstream sluice gate was completely closed. Actually, a very small river flow took place and water condition was not completely static in the main channel.

Several measurements were taken during each test: details about the measurement procedure are given in Section 4.2.2. Longitudinal profile of water surface, 3D point flow velocity and bed topography were recorded before and after the breach event. Water surface level and flow velocity were acquired in fixed points during the breach development, which was monitored by means of video recording.

A summary of the experimental conditions is given in Table 4.1.

Figure 4.7: Geotextile protection of the levee.

Table 4.1: Summary of conditions for the performed test series.

Series	Test	Run Code	Inflow discharge Q_u [l/s]	Sluice gate opening Y_g [cm]	Flume Slope S_0 [%]	Initial flow velocity U_{mean} [m/s] *	Initial Froude number Fr_{pre} [-] *	Sluice gate closing?	Upstream geotext. protection?	Notes
A	1	Q10.1Yg0.4S0.1%	10.1	0.4	0.1	0.035	0.022	No	No	
	2	Q20.1Yg1.0S0.1%	20.1	1.0	0.1	0.084	0.054	No	No	
	3	Q29.2Yg2.2S0.1%	29.2	2.2	0.1	0.145	0.098	No	No	
	4	Q40.4Yg3.4S0.1%	40.4	3.4	0.1	0.186	0.120	No	No	
	5	Q49.0Yg4.5S0.1%	49.0	4.5	0.1	0.239	0.158	No	No	
B	6	Q60.3Yg5.8S0.1%	60.3	5.8	0.1	0.270	0.172	No	Yes	
	7	Q70.3Yg7.3S0.1%	70.3	7.3	0.1	0.346	0.228	Yes	Yes	Sluice gate progressively closed
	8	Q35.3Yg2.7S0.1%	35.3	2.7	0.1	0.152	0.097	Yes	Yes	
	9	Q45.1Yg4.0S0.1%	45.1	4.0	0.1	0.204	0.131	Yes	Yes	
	10	Q55.2Yg5.0S0.1%	55.2	5.0	0.1	0.241	0.153	Yes	Yes	
C	11	Q7.2Yg0.0S0.1%	7.2	0.0	0.1	0.022	0.014	No	No	Dam breach
	12	Q45.3Yg4.0S0.1%	45.3	4.0	0.1	0.207	0.133	No	Yes	Multiple breaches

* Fr_{pre} and U_{mean} are calculated as average value over the length of the flume (since the flow discharge changes a little because of seepage)

4.2.2 Test procedure

Tests were performed following a general specified procedure for the data collection. Of course, each test had its own features which required the operator to make particular choices every time (for instance, the location of flow velocity measurement had to be chosen each time).

The tests developed according to three main phases:

(i) Steady flow before breaching;

(ii) Breach formation and evolution;

(iii) Final equilibrium of the system river-breach.

Before starting a test, every device was checked and placed in the right location.

The downstream sluice gate was initially closed and the flume was filled up with water at low flow rate (about 1-2 l/s) in order to provide a gradual saturation of the sand and to avoid erosion from the main channel bed or from the levee slope. Due to the infiltration inside the levee and through the drains, the inflow had to be gradually increased up to 6.5-7 l/s to fill the main channel until the water depth was around the levee crest in steady conditions: the infiltration rate was therefore equal to the inflow value. Then the downstream sluice gate was opened and the inflow discharge was increased until the design inflow was achieved and the water surface was around the levee crest in stationary regime all along the flume.

After temporal steady flow conditions were achieved, the water surface profile at centre line of main channel width, flow velocity and bed topography were measured.

Afterwards, a breach was initiated by cutting a rectangular groove (2 cm wide, 1 cm deep) on the levee crest at a central section of the model (called "*Breach Trigger Location*" – **BTL**): breach started by overflow of water at the *inception time* $\mathbf{t_0}$ and its formation and evolution were monitored during time by means of cam recording, while water surface level and flow velocity measurements were acquired in fixed points. When erosion of levee due to the breach reached the bottom of the main channel, the local toe drains that remained uncovered were removed in order to allow more vertical erosion. However, the separation wall provided a vertical constraint to the deepening of the breach which will be discussed in Section 4.4. This phase went on until an equilibrium in the breach lengthening and in the flow hydrodynamics was seemingly achieved, even if it was not always so evident. The water surface profile and the levee crest longitudinal profile were acquired before ending this phase.

During the last phase the inflow discharge was decreased until low values which did modify breach geometry no more, while the flume was filled up with water by raising up the flap gate. This operation was needed to acquire the bottom morphology of the main channel by bed profiler. The survey of a part of the breach area beside the main channel was also performed.

4.3 Measured data and experimental results

Data collected during experimental investigations are presented within this Section.

Before describing the results of each test, it is necessary to define the spatial reference that is used for the following elaborations. The variables used to describe the physical model, measured during the tests or calculated in the post-processing, are listed into the list of symbols.

4.3.1 Spatial reference system

The spatial reference used to locate the measurement in the flume is a 3D Cartesian coordinate system in which:

- The origin is located on the initial bottom of the main channel, next to the beginning of the breach groove and on the left side (opposite to the levee);
- The x-axis is fixed to the glass wall, directed streamwise;
- The y-axis is the transversal axis, directed toward the levee model;
- The z-axis is the vertical axis, directed toward the top.

Figures 4.8-4.9 show the coordinate system used during the experimental investigations.

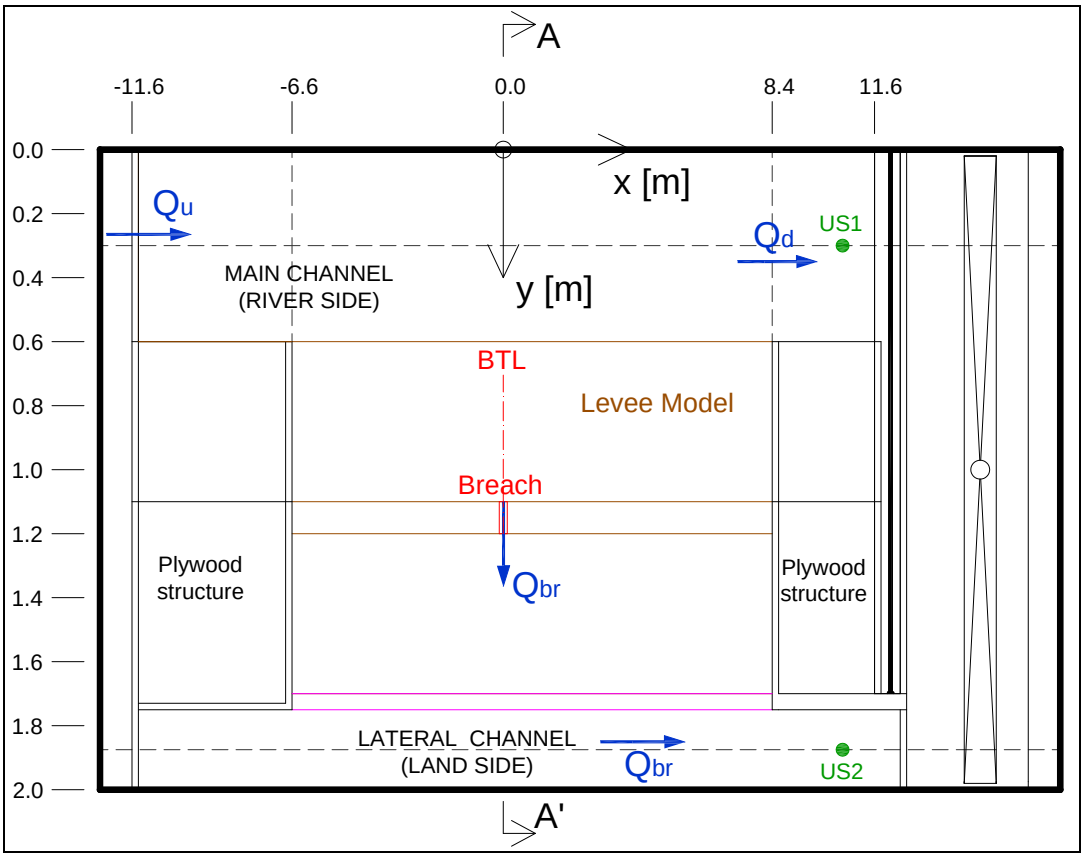

Figure 4.8: Coordinate system for the flume (plan view).

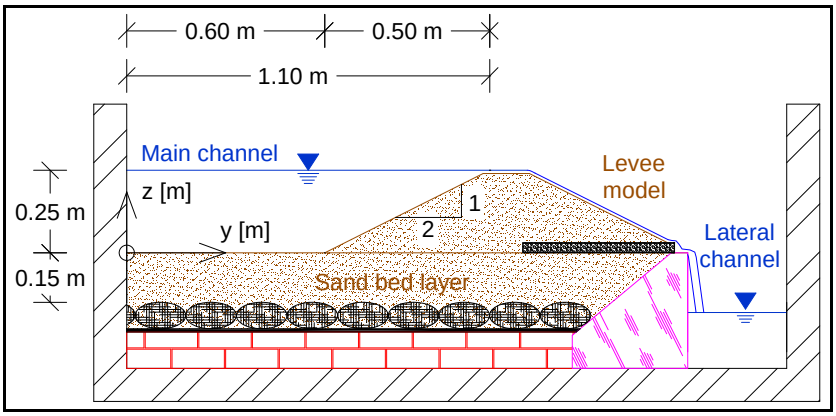

Figure 4.9: Coordinate system for the flume (section view A-A').

4.3.2 Measured data post-processing

Post-processing of collected data was necessary to create a consistent data base which was used to analyse the investigated phenomena.

Experimental data were collected by different ways during the three phases of the tests.

The flow during the first “before breaching” phase was steady and no or slight modifications occurred to the morpho- and hydrodynamic variables. Bed profile and water surface were recorded and point measurements of water level and velocity were acquired during a sufficient long time slot (about 10 min) and then elaborated as average values.

Since the US sensors were calibrated with the zero level referred to the bottom of the channel, the water levels recorded by the probes were directly converted in flow depths if no erosion or accumulation took place, as in case of US1 and US2.

The measurements along the flume (such as water surface and bed profiles) were referred to the Cartesian system by means of a sensor fixed to the movable carriage, which gave its x-position along the flume.

The “breach formation and evolution” phase was more complicated, since the variables changed in time due to the breach dynamics even if the inflow was maintained constant. Ultrasonic sensors 1 and 2 monitored continuously the water level, while the collection of ADV data was difficult because water level as well as bed morphology changed in time quite quickly. Moreover, one must consider that US0 recorded water surface usually in the upstream part of the flume, where erosion and accumulation of sand occurred and this did not allow to directly calculate the water depth.

The collection of the water surface profile (all along the flume at the centreline of the main channel) was furthermore complicated because of oscillation of water surface, as detailed results in the complete report show (Michelazzo and Oumeraci, 2013).

The breach evolution was recorded by means of two cams: video analysis allowed to elaborate the erosion rate of the breach by referring the breach length to the meter sticks on the levee crest.

Finally, bed topography was acquired after having stopped the inflow and filled up the flume in order to “freeze” the achieved configuration of the bed. During this filling phase, some features of the breach cross section (both the upstream and the downstream) changed because of further mass slumps: however, this affected only the morphology close to those sections.

Inflow rate was acquired by the IDM installed at the inflow pipe and it was checked to remain constant during each test.

Lateral outflow through the breach was calculated from the water depth recorded by US2 installed in the lateral channel by the use of the weir equation, which was calibrated in a smaller channel having the same geometry of the lateral channel. The calibration was made by taking several measures of inflow discharge and flow depth and the derived weir equation is shown in Figure 4.10.

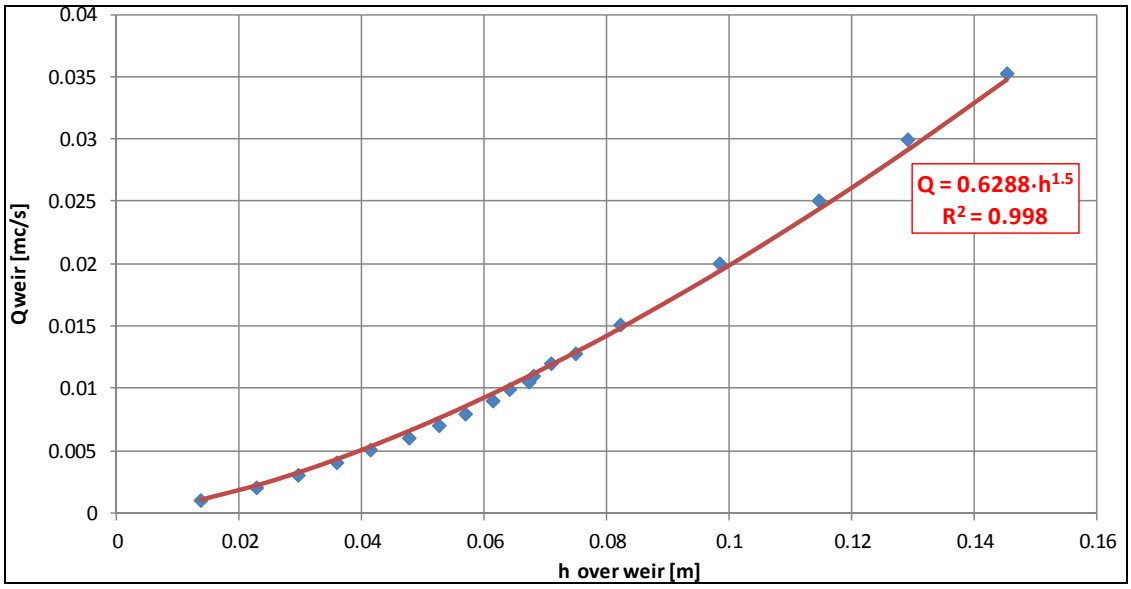

Figure 4.10: Sharp-crested weir equation of lateral channel (calibration).

The relationship of Figure 4.10 is valid in case of steady flow, that was achieved at the end of the tests. During the breach evolution, the lateral channel got water from the main channel and also the sand eroded: this dynamics made water level not to grow uniformly and unsteady phenomena occurred into the lateral channel which brought oscillations of the water surface and errors in the calculation of the water discharge flowing in the lateral channel.

Another way to monitor the breach outflow during the second phase was to calculate it as a difference between the inflow Q_u, the downstream discharge Q_d and the seepage flow Q_{seep}:

$$Q_{br} = Q_u - Q_d - Q_{seep} \tag{4.1}$$

A rating curve was needed in order to calculate the downstream flow rate Q_d from the US1, which recorded water depth Y_d at the sluice gate: this was not easy, since the sluice gate equation was not separately calibrated and its opening changed from test to test. Anyway, an analytical rating curve was developed by using the governing equation for a free flowing sluice gate. The discharge coefficient was calibrated for each opening of the sluice gate by using the flow rate and the flow depth recorded at the downstream cross section during the first steady flow phase (before breaching). Flow rate at the downstream cross section was derived by subtracting the seepage flow rate (≈ 7 l/s) from the incoming discharge.

The sluice gate equation used in the calculation of downstream flow rate was therefore:

$$Q_d(t) = C_d(Y_g) \cdot (0.6 + Y_g) \cdot Y_g \cdot \sqrt{2 \cdot g \cdot Y_d(t)}, \quad \text{if } Y_d(t) > Y_g \tag{4.2}$$

with g: gravity = 9.81 m/s^2
C_d: discharge coefficient calibrated for each test as previously explained [-]

Equation 4.2 is valid until flow depth is affected by the gate itself: when water depth decreases under the sluice gate, the relationship Q-Y is no more valid. Since the elevated main channel bed ends at the sluice gate section, a free overfall develops over a positive step when water surface decreases under the gate. In such a situation, flow crosses the downstream section with the critical depth and this relationship can therefore be used as rating curve:

$$Q_d(t) = \sqrt{g \cdot \frac{A^3(Y_d)}{B(Y_d)}}, \quad \text{if } Y_d(t) < Y_g \tag{4.3}$$

The seepage flow rate (i.e. infiltration discharge) was evaluated during the breach development by means of the simplified analytical method of Pavlovsky (1931). The hydraulic conductivity k_i was calibrated by considering that the seepage flow through all the levee model (15 m long) is equal to the inflow during the first phase of the tests, when the water surface is maintained at the levee crest in steady conditions. k_i resulted in: $k_i = 7 \cdot 10^{-3}$ m/s. Note that the calibrated k_i took into account implicitly the effect of the drain system, which increases seepage flow, and thus k_i value resulted higher than standard values. Since water depth decreased in time and varied in length during the breach development, seepage flow during time was calculated by assuming a constant water depth acting on the levee equal to the mean of two point measurements: the downstream flow depth (given by US1 at the downstream section) and the upstream water surface level (given by US0 which was maintained at a fixed upstream section chosen before each test), which were the only two water surface measurements acquired continuously in time. Moreover, seepage flow was calculated only for the length of the not breached levee, which was known by the video analysis of the breaching process.

The temporal development of the variables during the second phase was acquired and synchronized with the video-cam recording. Therefore, breach events were located in time and analysed together with the hydraulic variables development. Evolution in time of the measured variables was elaborated as running average.

The flow velocity averaged over the cross section was calculated by means of measured discharge and water depth. Water depth measurement was not easy to be determined because of deformation of bed channel. The mean flow velocity at an x-section was then given by:

$$U_{mean}(x) = \frac{Q(x)}{A(Y(x))} \tag{4.4}$$

3D local flow velocity was acquired by means of the ADV, which gave the velocity component of a point sampling volume located under the submerged probe. The correct procedure to collect ADV data requires to select the velocity range and the position of the probe under water. The “Signal-to-Noise Ratio” (SNR) and the correlation values were useful parameters to check the quality of data and to delete those having low quality. This operation was made inside the post-processing phase. One problem occurring with ADV was that its distance from the bed surface changed during the evolution phase, so that only a part of data could be accepted during this phase. The selected ADV data were elaborated as average value over the time period of acquisition, except from the first acquisition during the breach triggering of each test, which is elaborated only with a running averaging in order to show the variation of flow velocity during the first time slot after the breach trigger. The x-y location of the probe was acquired manually, while the depth of the sampling volume was set around middle of the water depth in that point, in order to have significant values of velocity. The velocity data were used to analyse the flow field.

Bed topography data were collected along the 15 m testing reach and 12 strips in order to cover the main channel bed width (0.6 m). Bed elevation of the breach channel was also acquired for a part of it (from y = 0.6 m to y = 1.1 m). Acquired data were despiked and elaborated as running average. A digital elevation model was then created by means of analytical interpolation of the collected data on a grid of size 0.01 m. The river side slope of the levee out of the breach borders was not acquired by sensors but its contours were numerically reproduced from the theoretical shape designed for the levee.

4.3.3 Experimental results for each test series

Some of the more relevant results are shown in this Section, whereas all details are given in the complete report (Michelazzo and Oumeraci, 2013).

4.3.3.1 Series A data

Tests of series A were performed with the standard setting of the levee model set-up.

Five different inflow discharges were tested, ranging from 10 to 50 l/s every 10 l/s.

Some general remarks are given in order to understand the plots. Regarding the digital elevation model of the river bed and the breach, the contours show the elevation in [mm] over the zero reference, which is the plane bed of the main channel. Flow goes in from left side (as the arrow) and the red dashed line BTL points to the section (x=0) where the breach was triggered.

Longitudinal profiles of bed elevation and of water surface were taken along the centreline of the main channel (y = 0.3 m) by the bed profiler and the US0 sensor, which was also used to take the levee crest profile (at y = 1.15 m). Note that the graphs of the variables in the spatial domain are plotted in distorted scale regarding y- or z-axis with respect to x-axis.

Temporal development of water surface levels was taken at a fixed location: US1 and US2 remained fixed for every test, while US0 position was set in the upstream part of the flume chosen before each test. Bed evolution was recorded in one fixed position in the upstream part by means of bed profiler until water surface elevation made it possible. Timing of breach triggering is marked as dash-dot black line (time t_0 in Table 4.5) and timing of drain removals as dashed black lines in all plots regarding the temporal developments during phase 2.

The breach development was recorded from the increasing of the breach length both in the up- and downstream directions, whose definition is explained by the following Figure 4.11.

The flow velocity was recorded by ADV in different positions during the second phase: the ADV position is marked as red point in the plots.

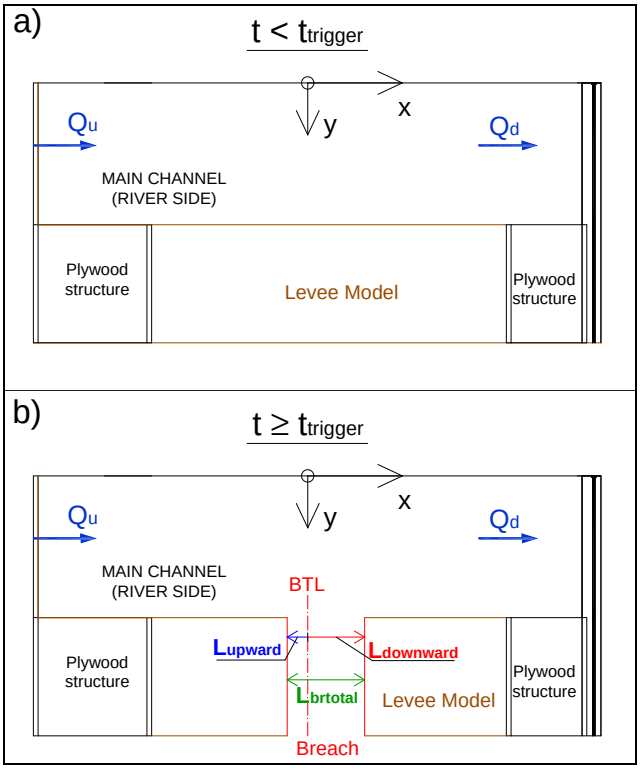

Figure 4.11: Definition of breach erosion lengths: a) before breaching; b) after breach inception.

During the first phase of tests, steady flow was always achieved: flow depth was almost at levee crest and no sediment transport occurred in the main channel, which, therefore, maintained its initial flat bed configuration before breaching (see Figure 4.12). Moreover, water depth was always larger than critical depth, and this provided a subcritical flow as initial condition (Figure 4.13). Actually, the water depth slightly increased downstream due to the seepage lateral flow which endowed the river flow with spatially gradually varied features: the flow depth increases in a subcritical regime if a lateral outflow takes place.

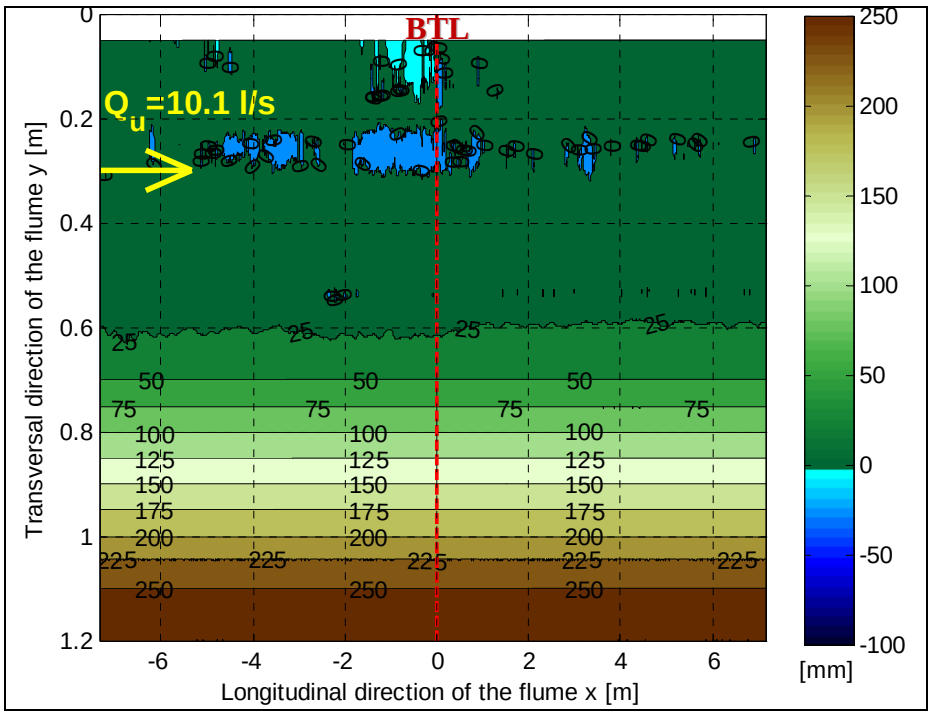

Figure 4.12: Bed topography before breaching (test A1 - Q10.1Yg0.4S0.1%).

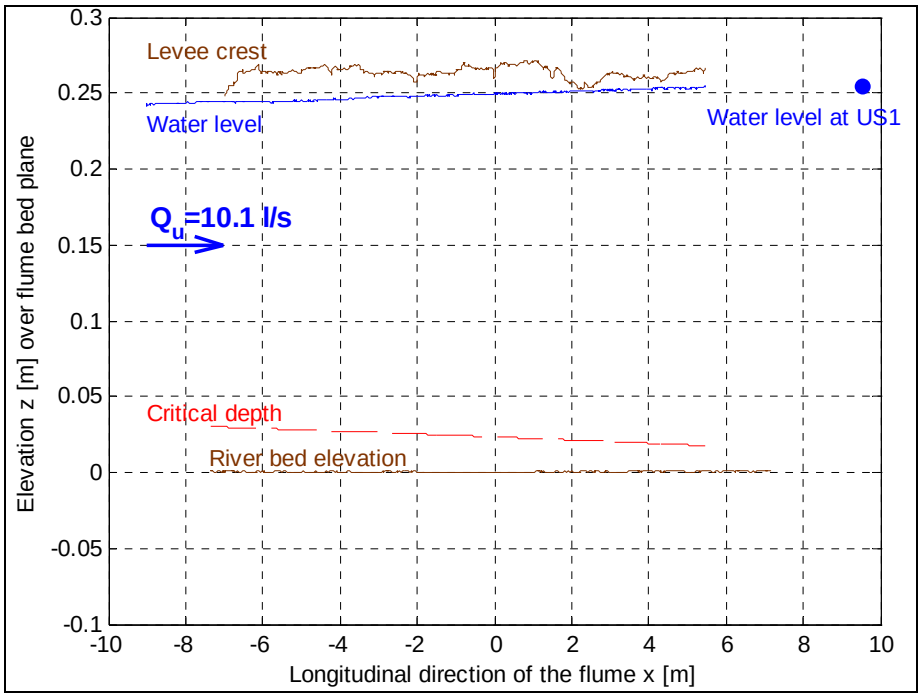

Figure 4.13: Longitudinal profiles of water level, levee crest and bed elevation before breaching (test A1 - Q10.1Yg0.4S0.1%).

A breach was triggered during the second phase and the temporal evolution of the river hydrodynamic variables together with the breach lengthening were monitored. As a general behaviour, water levels recorded by the three sensors (USs, as depicted in Figure 4.6) developed quite quickly toward an almost steady state (Figure 4.14): water level in the upstream part of the main channel (US0) decreased because of the draw effect by the breach, downstream water depth (US1) decreased because of discharge was diminished by the breach flow and water level in lateral channel (US2) increased due to the breach flow.

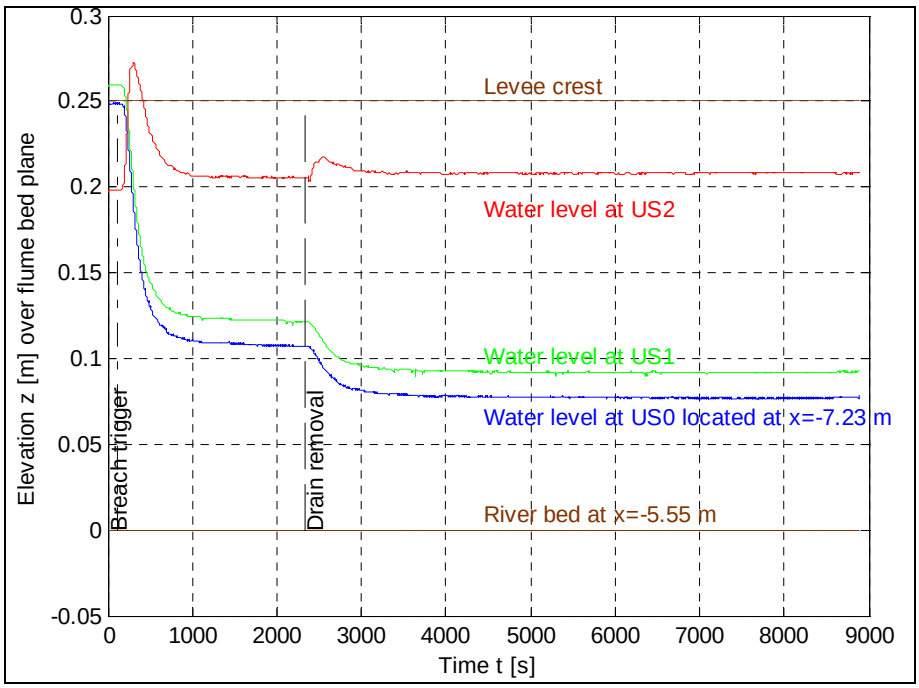

Figure 4.14: Temporal development of water level at USs and river bed (test A1 - Q10.1Yg0.4S0.1%).

Breach development was fast during the first 5-10 minutes after breach inception, then it slowed down but, unlike water depths, it did not reach a stable length most of tests. Unlike dam breach scenarios, the breach mainly lengthens in the downstream direction (Figure 4.15).

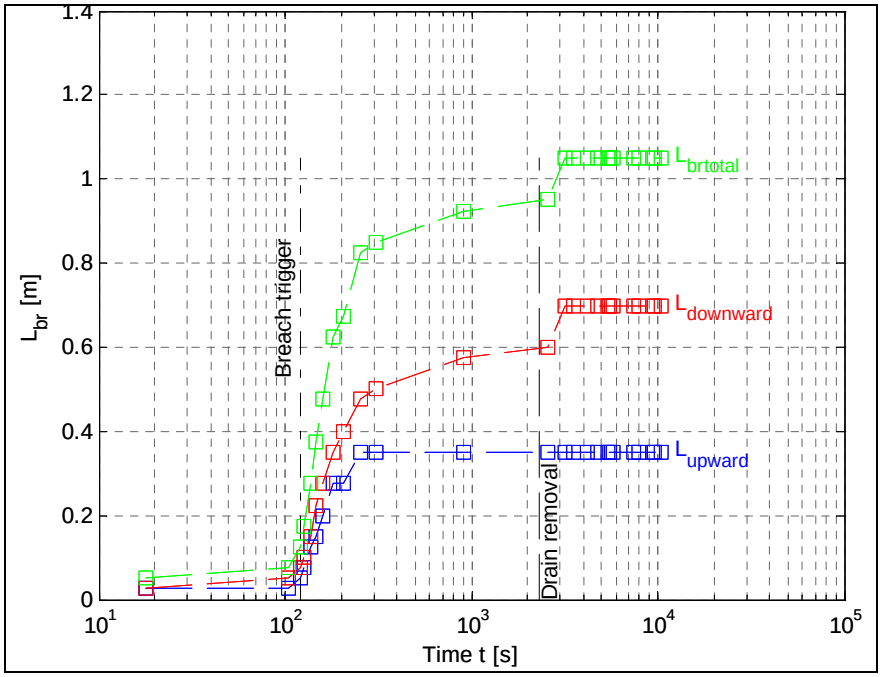

Figure 4.15: Temporal development of breach length (test A1 - Q10.1Yg0.4S0.1%).

The resulting velocity field was quite complex, as expected from the fixed bed experimental investigations (see Chapter 3), and only few times it was possible to catch the flow field features by means of point ADV measurements. Velocity recordings during test A1 were those having the best quality and they can be used to state some considerations on the flow field.

The three components of flow velocity vector are plotted in the following Figures (4.16-4.17-4.18-4.19), together with the location of the measurement in the xy plane, the value of the deflection angle θ and the velocity vector plotted with a length proportional to the velocity module $|U| = (U_x^2+U_y^2)^{0.5}$, with U_z assumed to be negligible.

Velocity plots of test A1 show how flow velocity U_x is higher upstream of the breach and then decreases downstream (Figures 4.16-4.17). Moreover, U_y got significant values close to the breach site, while it was almost zero out of the breach domain (Figure 4.18). Finally, the presence of a flow separation zone on the side opposite to the breach is revealed by velocity values decreasing until almost zero: this zone was classified as “B zone” in the fixed bed investigations (see Figure 4.19), but it had a less evident extension and strength in the movable bed tests, likely because of a lower aspect ratio (Y/B) of the main channel flow. For further details, see Michelazzo and Oumeraci (2013).

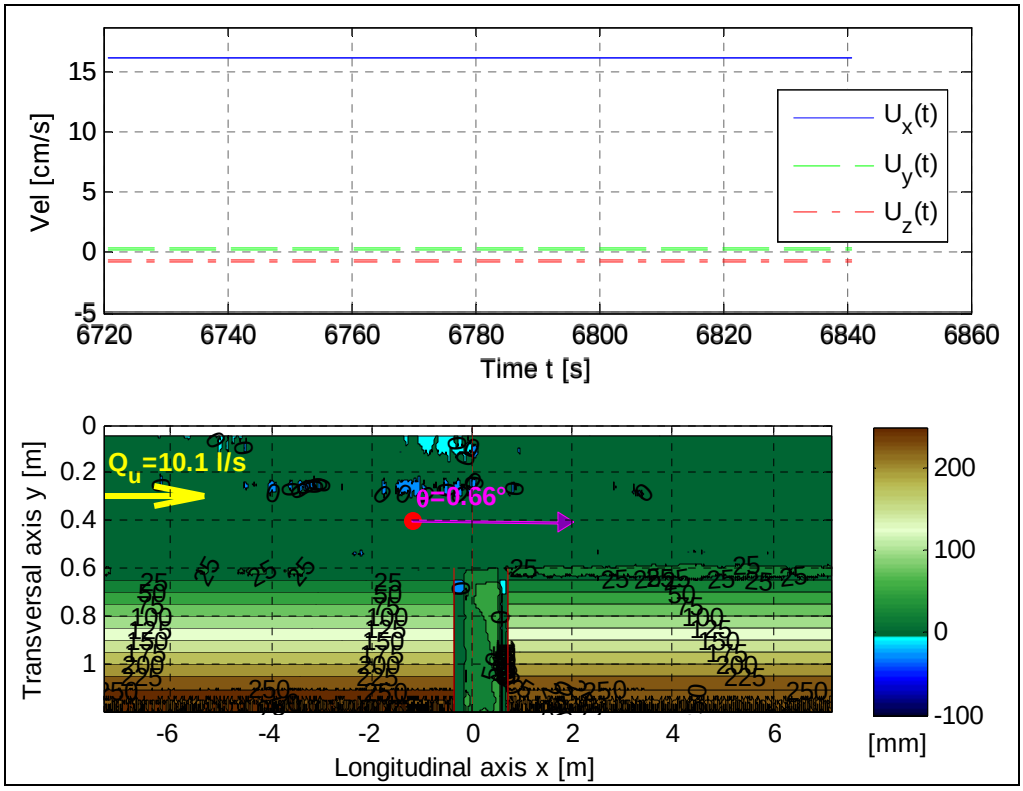

Figure 4.16: High longitudinal velocity of the approaching flow (test A1 - Q10.1Yg0.4S0.1%).

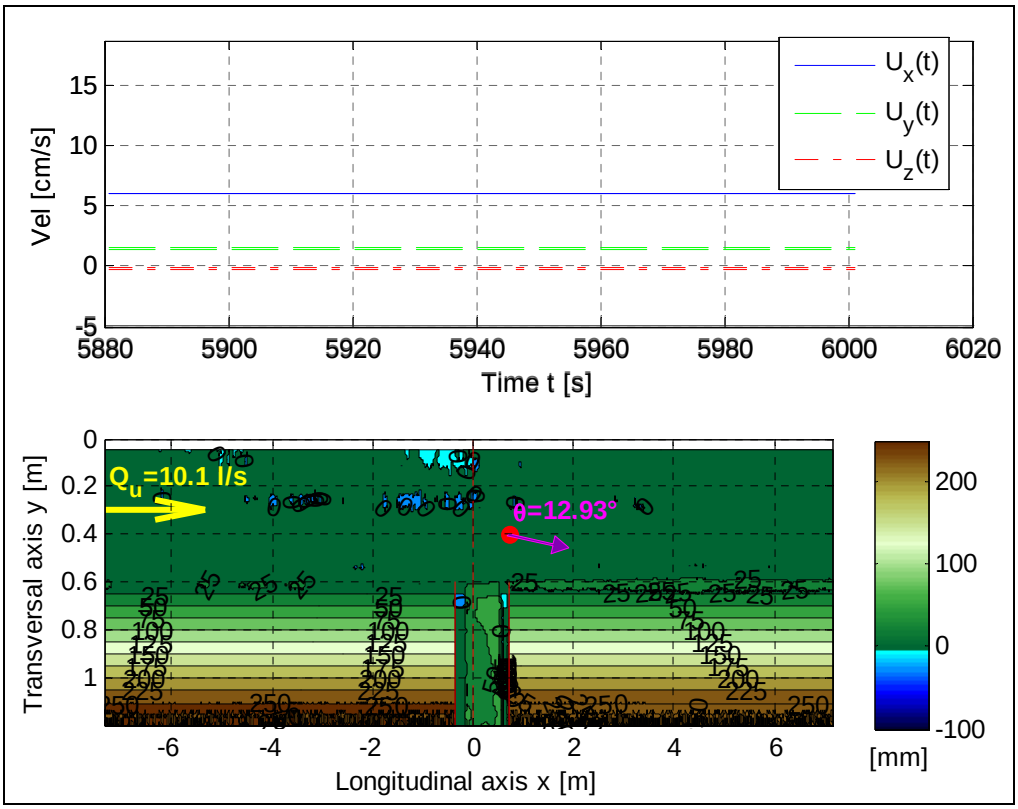

Figure 4.17: Slowing down of flow downstream the breach (test A1 - Q10.1Yg0.4S0.1%).

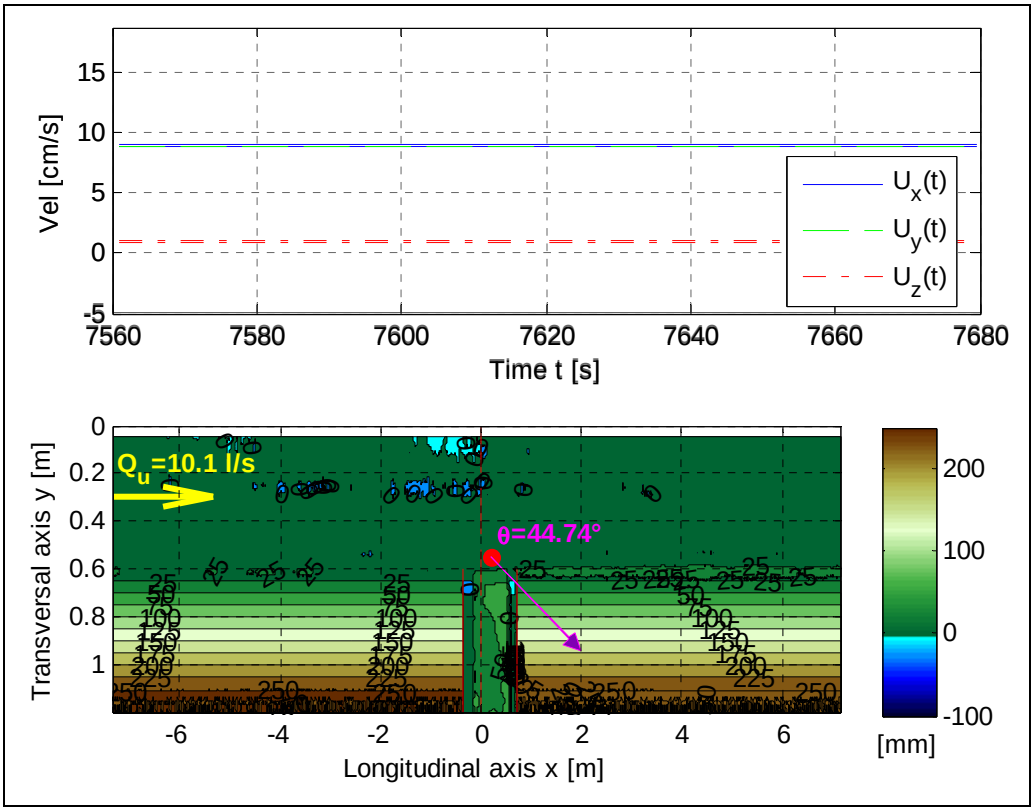

Figure 4.18: Significant flow deflection (U_x and U_y similar) at the breach site (test A1 - Q10.1Yg0.4S0.1%).

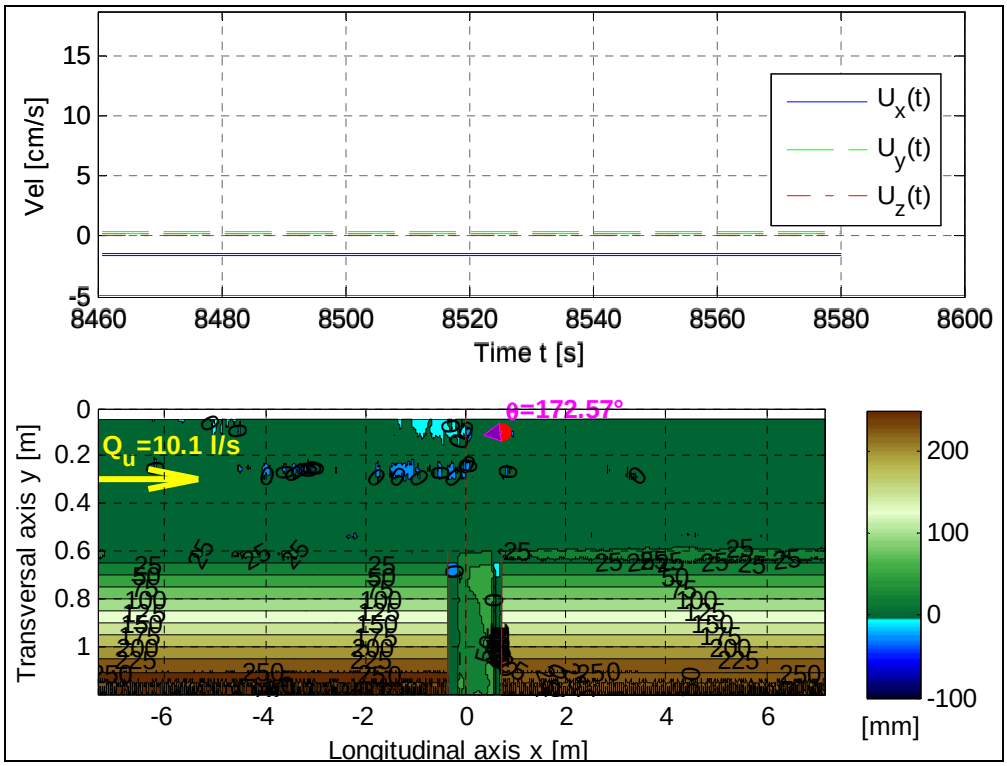

Figure 4.19: Separation zone at the side opposite to the breach (test A1 - Q10.1Yg0.4S0.1%).

The final phase of tests showed the final water surface profile and the deformation of river bed due to the breaching. It is evident how most of topographic deformations occurred in the upstream part as erosion phenomena, while sedimentation took place at the downstream part of the breach. A slight bed deformation was recorded in the remaining downstream part of the flume (Figures 4.20 and 4.21). River bed deformations occurred not only as general erosion/sedimentation phenomena but sediment transport caused the presence of bed forms (ripples and dunes).

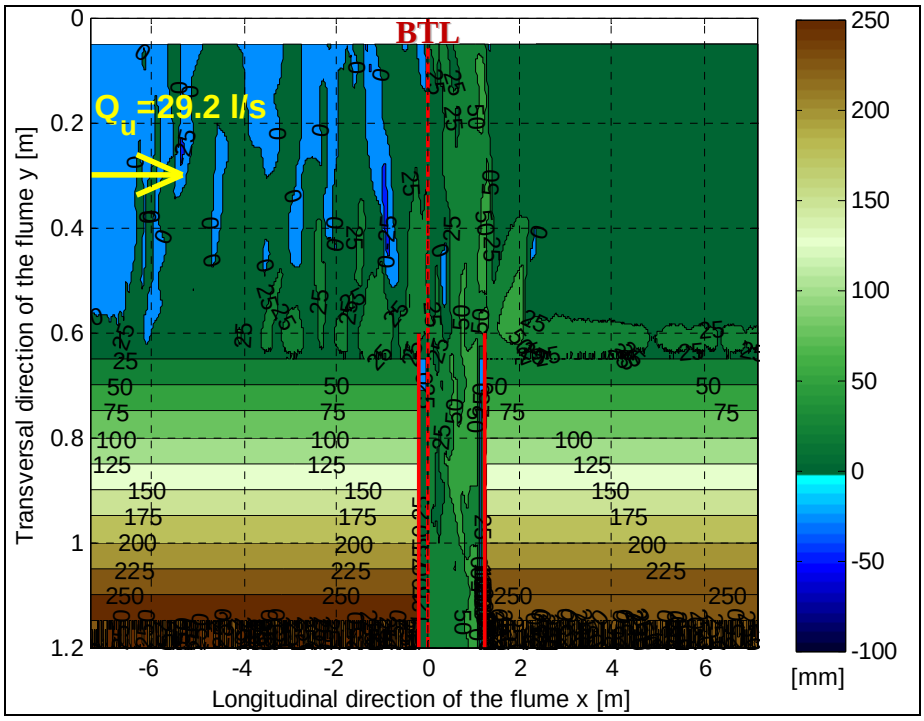

Figure 4.20: Bed topography after breaching (test A3 - Q29.2Yg2.2S0.1%).

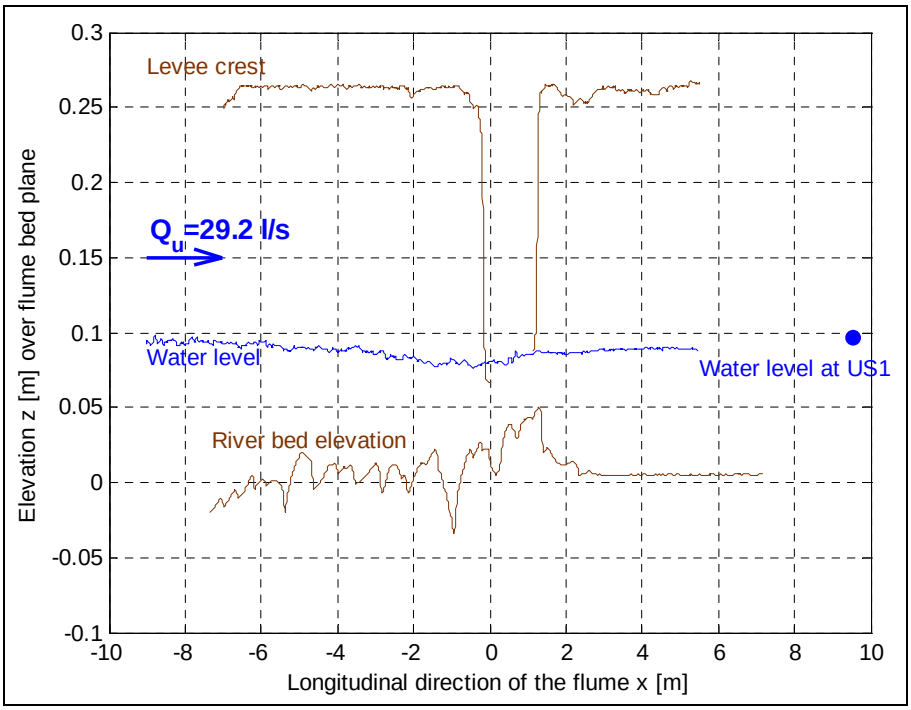

Figure 4.21: Longitudinal profiles of water surface, levee crest and river bed elevation after breaching (test A3 - Q29.2Yg2.2S0.1%).

The acceleration of flow in the upstream part of the flume caused erosion of the river side levee slope, which was not measured but only observed. In Figure 4.22 an areal picture at the end of test "Q29.2Yg2.2S0.1%" was taken looking upstream: one can notice the breach on the left, the strong river bed deformation upstream and at the breach site (dunes) and the erosion of the upstream part of the river side levee model.

Figure 4.22: Areal picture of the flume at the end of test A3 (Q29.2Yg2.2S0.1%).

4.3.3.2 Series B data

Tests of series B were performed on the partially modified levee set-up, which had the river side slope upstream the breach site protected against flow erosion.

General remarks made for series A are also valid in this case.

The longitudinal x-section until which the levee was covered by the geotextile layer is depicted as white dashed line in the bed topography plots.

At the end of tests B7, B8, B9 and B10 the downstream sluice gate was progressively closed in order to test the effect of the downstream boundary condition on the breach development: the timing of these closures is marked as purple dashed lines in the time development plots and the sluice gate was always closed by half of its previous opening. The last closure operation is referred to the completely closed gate for tests B8, B9, B10. Table 4.2 reports the timing of the closure events and the related opening of the sluice gate.

Table 4.2: Summary of the closure operations of the sluice gate.

Series	**Test**	**Sluice gate opening Y_g [cm]**	**Time t_{slgt} [s]**
B	7	7.3	0
		3.6	1320
	8	2.7	0
		1.3	7680
		0.6	8880
		0.0	9480
	9	4.0	0
		2.0	5340
		1.1	6540
		0.6	7440
		0.0	8040
	10	5.0	0
		2.5	2040
		1.3	2640
		0.6	3240
		0.0	3840

Comments regarding the general behaviour of the river-breach system are common with the series A tests and will not be repeated. The protection given by the geotextile to the upstream levee made more clear the general erosion of the river bed in the upstream part: river flow could convey sediment material only from the river bed, while sediment material from levee slope was protected and it did not feed the sediment transport in the main channel. Figure 4.23 well-illustrates this effect.

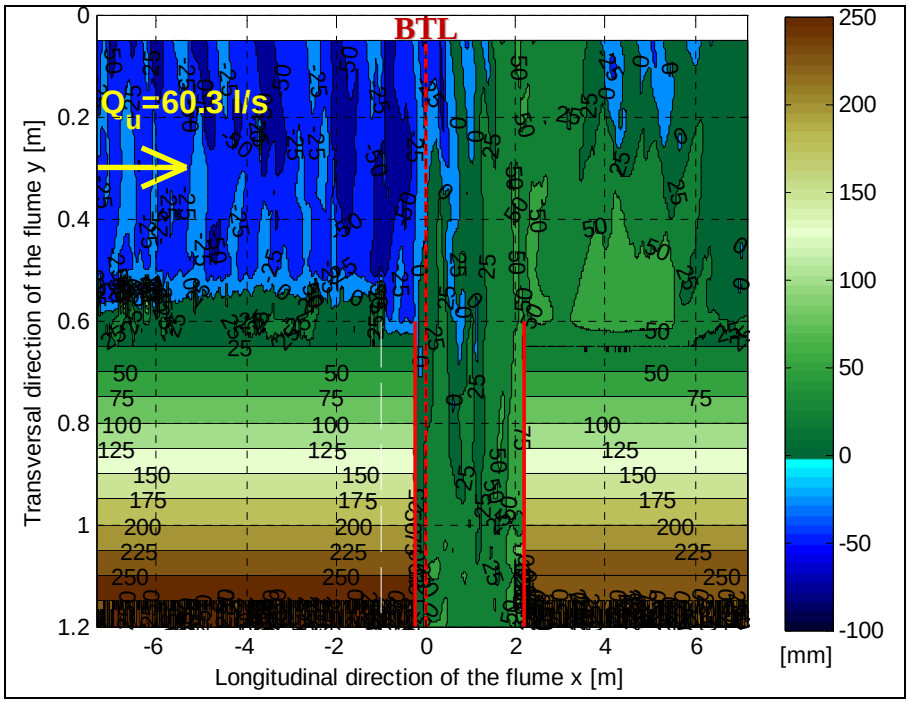

Figure 4.23: Bed topography after breaching (test B6 - Q60.3Yg5.8S0.1%).

The consequence of closing the sluice gate was to raise up the downstream water level and to cause more flow through the breach (Figure 4.24). This change of the hydrodynamic variables caused further breach lengthening (Figure 4.25).

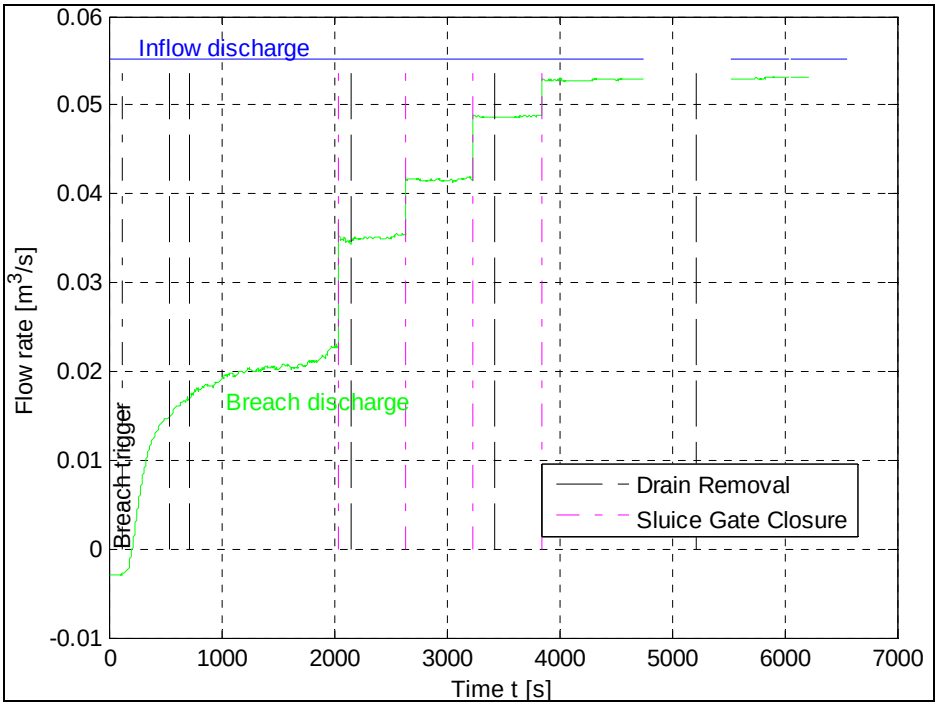

Figure 4.24: Temporal development of breach water discharge (test B10 - Q55.2Yg5.0S0.1%).

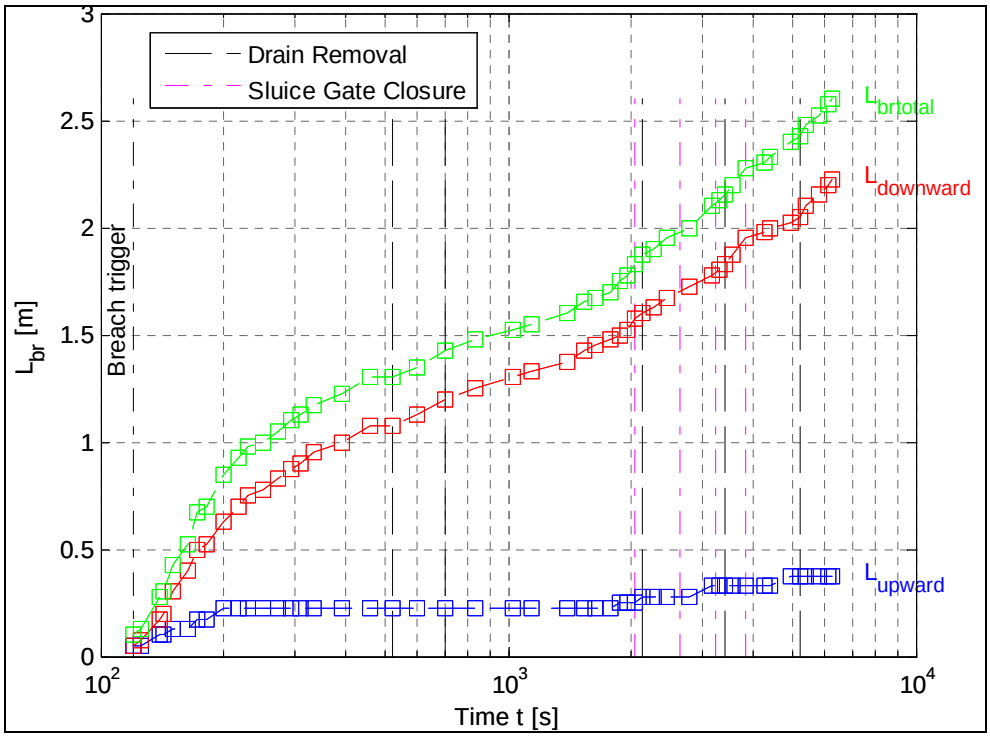

Figure 4.25: Temporal development of breach length (test B10 - Q55.2Yg5.0S0.1%).

4.3.3.3 Series C data

Tests of series C were performed at the end of the experimental investigations as limit cases. During test C11, the downstream sluice gate was maintained closed. A slight water inflow in the main channel was necessary to maintain a constant water level prevailing on the levee, because of the seepage flow through the levee. As a result, water prevailing on the levee was not completely in static condition, and flow had small velocity which decreased downstream, because of the seepage, until zero value close to the sluice gate.

The main result of this test is to observe how a dam breach develops symmetrically, with respect to the trigger initial section (BTL), both in the up- and downstream direction (see Figures 4.26-4.27). A slight prevalence of breach development in the downstream direction was anyway observed and this was explained by the presence of a little inflow Q_u.

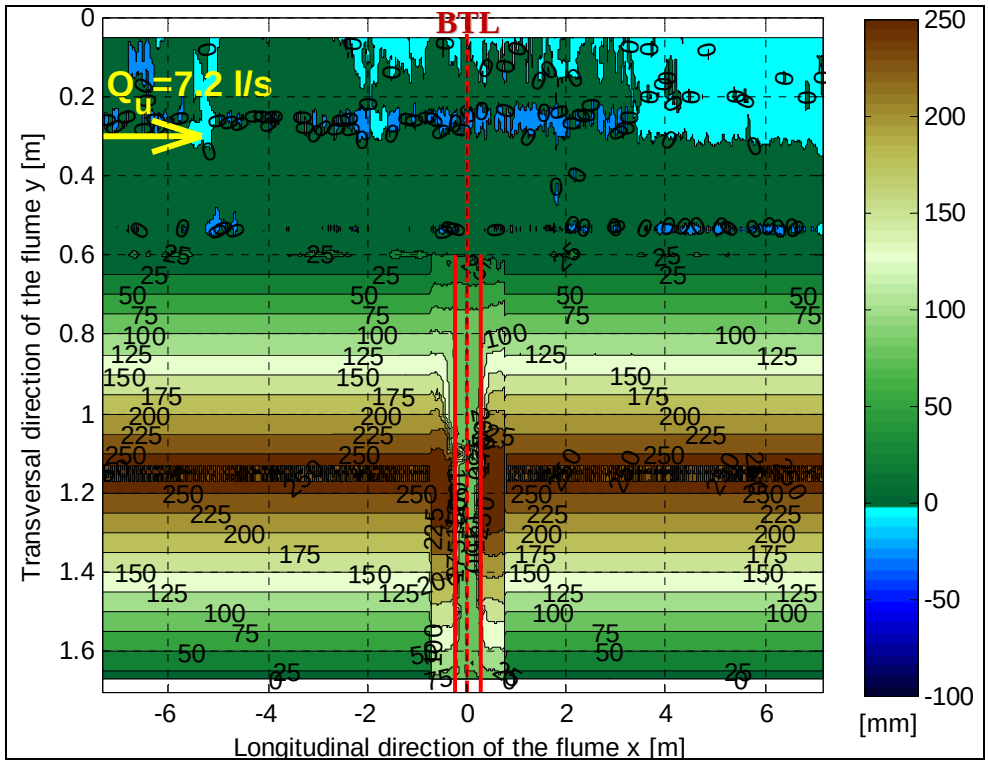

Figure 4.26: Bed topography after breaching (test C11 - Q7.2Yg0.0S0.1%): symmetrical breach.

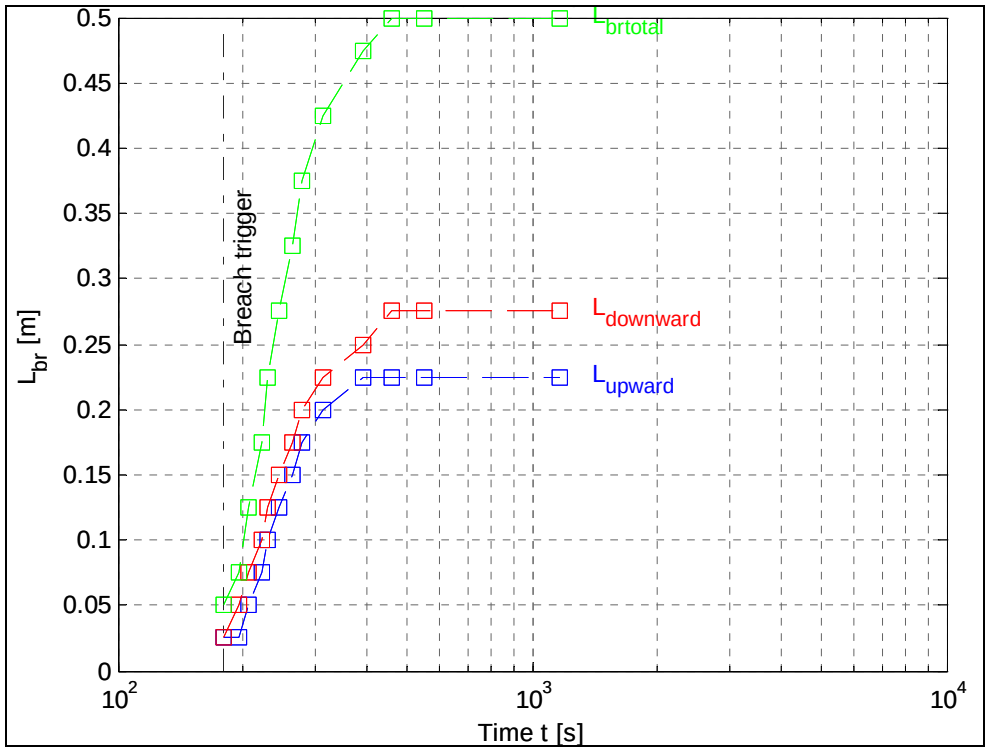

Figure 4.27: Temporal development of breach length (test C11 - Q7.2Yg0.0S0.1%).

Test C12 was performed with two simultaneous breaches: two notches were dug on the levee crest at two different sections and the development of both the two breaches was recorded. Breach number 1 is referred to the upstream breach, breach number 2 to the downstream one. Drains removal timing is marked as dashed lines (for the breach N°1) and dash-dot lines (for the breach N°2).

The downstream breach developed faster than the upstream one and it initially grew until a greater length. Then, probably also because of a drain removal, lengthening of breach N°1 started again.

At the end of the test, the two breaches had almost the same length (see Figures 4.28-4.29).

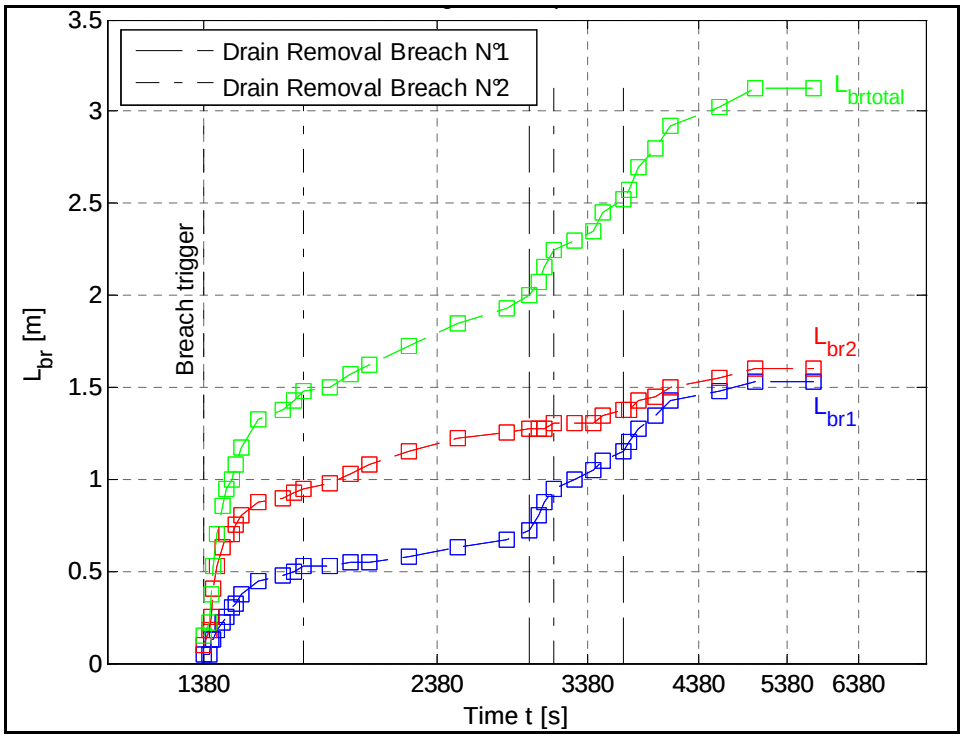

Figure 4.28: Temporal development of breach length (test C12 - Q45.3Yg4.0S0.1%).

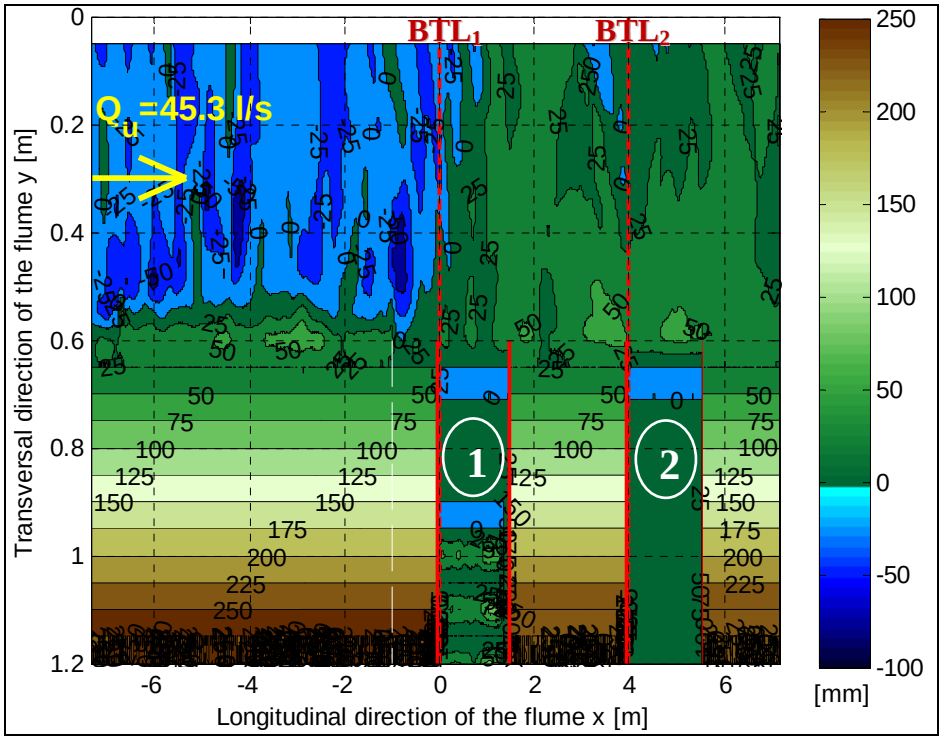

Figure 4.29: Bed topography after breaching for the two breaches (test C12 - Q45.3Yg4.0S0.1%).

4.4 Data analysis with a focus on process understanding

Data presented in Section 4.3 were analysed and elaborated in order to understand the behaviour of the physical system. Breach development, river hydro-morphodynamic mechanisms and their mutual influence are the main focus of this investigation. Some analyses are supplemented by the key results of the fixed bed experiments (Chapter 3): since the fixed bed tests were conducted regarding ten different side weir lengths and the same boundary conditions (i.e. the inflow discharge and the downstream sluice gate opening were set equal for all the ten tests), they are here used to discuss the behaviour of the hydrodynamics of the flow during the breach lengthening of each movable bed test. In other words, it is assumed that the ten fixed bed tests can represent a sequence of steady states of each movable bed test during its development and that the fixed bed results may provide some insights about the hydrodynamics of the movable bed experiments.

Some experimental data are reported for every test in Tables 4.4-4.5. These data are then plotted in Figures in order to get some insights of the investigated phenomenon. If not differently specified, the variables are referred to the final phase of each test (end of third phase). When some variables were measured immediately after the downstream sluice gate closure, they are marked with "*slgt*".

Sometimes the variables are expressed as dimensionless groups, by means of three basic independent parameters: Q_u, D_{50} and ρ, where D_{50} is the mean grain size diameter and ρ water density. Wetted width of main channel before breaching B_{mc} = 1.1 m is also used to normalize the variables.

In the following plots, notation "*standard set-up*" refers to those tests in which the levee model was not covered by geotextile, "*modified set-up*" refers to tests in which the upstream levee was protected by a geotextile, while "*after slgt cl*" indicates those values of the variables which have been recorded after the downstream sluice gate was completely closed. A possible interpolation curve is also plotted in order to highlight the relationship between the variables.

A measure of the river bed modification was taken into account by means of the characteristic parameter $\boldsymbol{\Delta_{max}}$, which was calculated as the vertical distance between the maximum and the minimum elevation of the bed at the centreline of the main channel (at the transversal coordinate y = 0.3 m) in the vicinity of the breach (see Figure 4.30): the reach considered for such analysis measured one breach length upstream the triggering section and two breach lengths downstream the trigger, since this was the spatial range in which the effects of the breach on the river hydrodynamics were evident according to the fixed bed experiments. As a matter of fact, the maximum aggradation of river bed occurred close to the downstream section of the breach while all the upstream zone of the flume was involved by a general erosion.

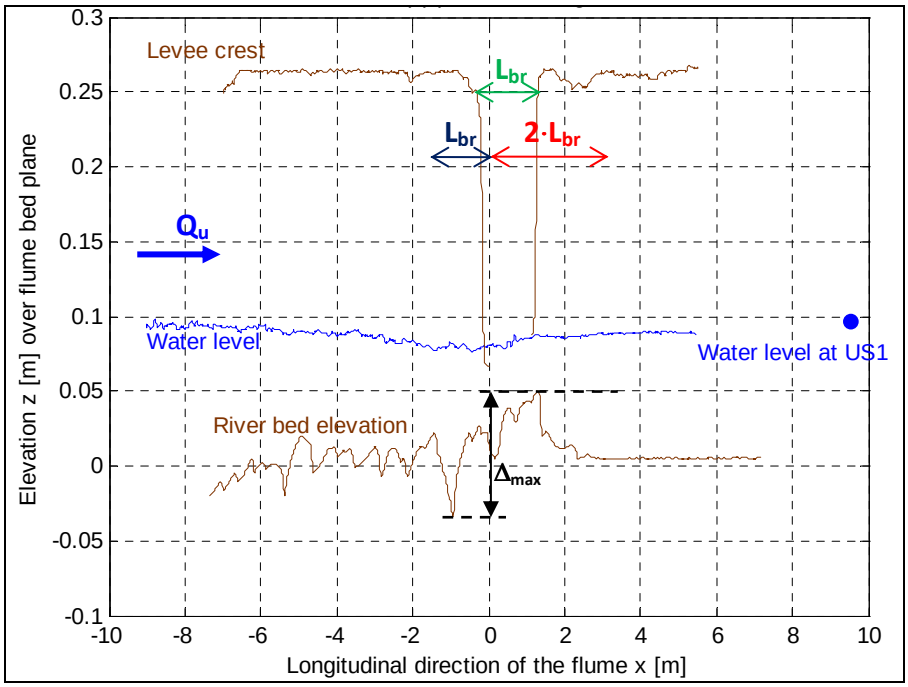

Figure 4.30: Definition of the bed variation parameter Δ_{max}.

A further schematization of data was used in order to elaborate them according to the same criteria. River bed, water level and breach depth were sketched as linear trends along the breach. Water level and river bed were simplified as linear vectors whose start and end values were taken as mean of the points within a strip of 3 cm centred on the initial and final points of the breach, respectively. Breach depth was elaborated as constant elevation equal to the average value along the breach channel. The vertical distance in river bed, between down- and upstream section, is defined as the parameter **Δ**. The points delimiting the breach length were detected where water level intersected the levee. Water level and river bed were referred to a transversal coordinate y=0.3 m (middle of the main channel), while the breach depth signal was taken inside the breach channel at y=1 m: these references were considered to be representative of the morphology, which of course changed along the transversal direction, but it also maintained similar features.

These operations allowed to filter data from irregularities and to make the computational results more clear. Figure 4.31 depicts vectors of water level, river bed and breach depth as coloured bold dashed lines. The spatial discretization used is also depicted.

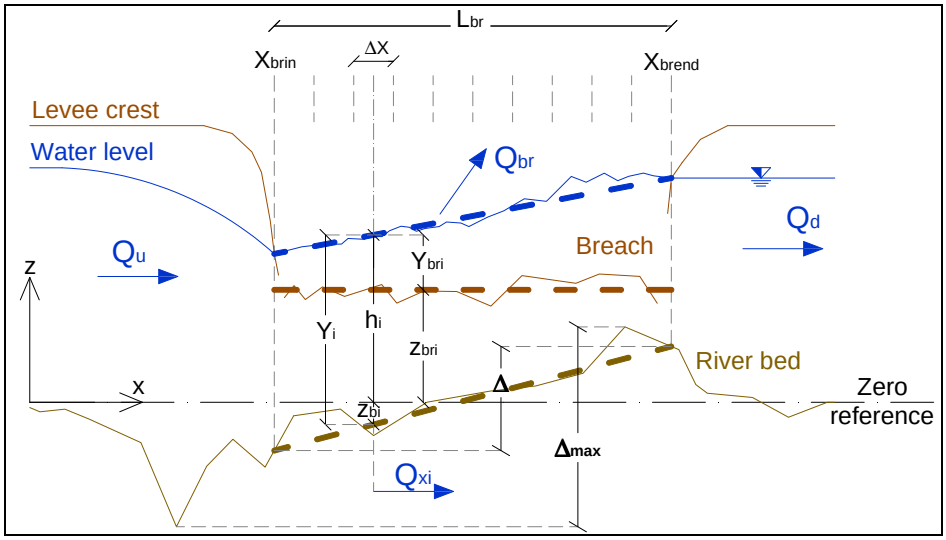

Figure 4.31: Computational scheme for flow analysis of movable bed tests.

4.4.1 Analysis of breach discharge

The plot between the breach discharge at the end of the tests and the incoming discharge in Figure 4.32 shows that a strong linear relationship exists: this is clear since the inflow discharge is the hydraulic loading acting on the breach.

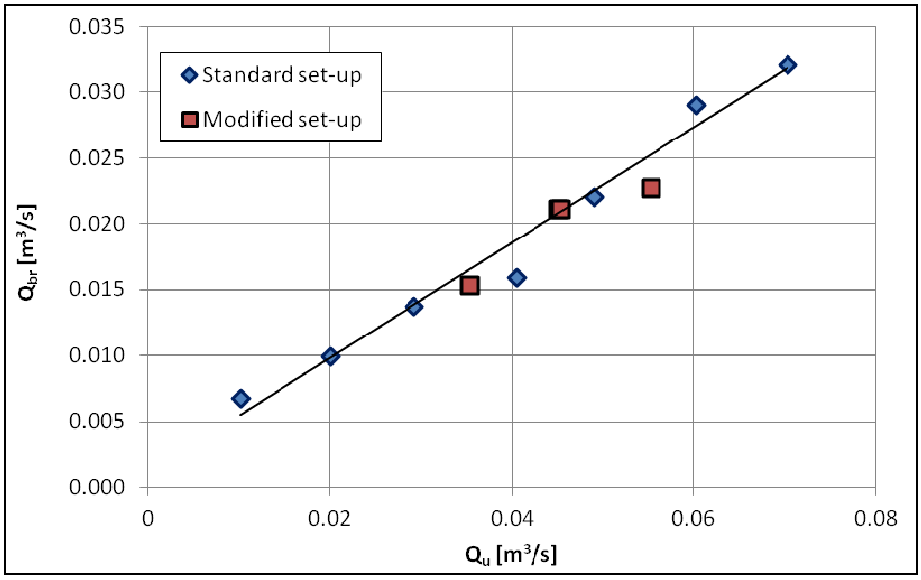

Figure 4.32: Q_{br} versus Q_u for each test at the final state.

The inflow discharge is not the only hydraulic feature important for the breach dynamics, but also the water levels in the river associated to the discharge are relevant to determine the hydraulic pressure on the levee. Anyway, the initial water level was always set at the levee crest during the present experiments: it was equal for each test and consequently it will not be considered in the following analyses.

Breach discharge seems to stay in a linear relation with the inflow: it is interesting to note that the dimensionless ratio Q_{br}/Q_u is almost constant for every test (see Figure 4.33) and it is around 50%. The only exception is represented by the first test (A1), which got a final ratio higher than the other tests. It is worth to remark that test A1 had the lowest values of the tested variables: test A1 had the lowest inflow discharge (around 10 l/s) and, consequently, experimental errors on the measured water levels and on the computed flow rates are significant for such small values of the inflow and of the breach discharge.

One can notice that tests B9 and C12 gave very similar discharge ratios: C12 test had almost the same inflow Q_u of B9 but it was the test in which two different breaches were triggered at the same time. The final outflow discharge through the two breaches of test C12 was equal to that one through the single breach of test B9. The response of the system river-breach in terms of fluid mass balance was the same for both tests, which had the same boundary conditions of upstream inflow and downstream sluice gate configuration. Figure 4.34 zooms in the two tests B9 and C12, in order to highlight the very similar value of the final result in terms of diverted breach discharge. Such a result was not found in previous studies of the analysed scientific literature.

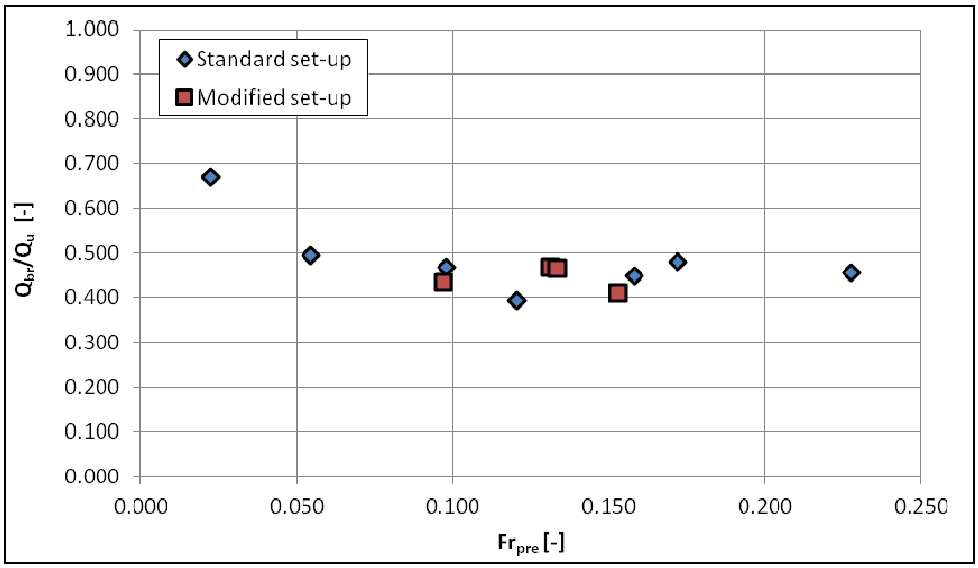

Figure 4.33: Q_{br}/Q_u versus Fr_{pre} for each test.

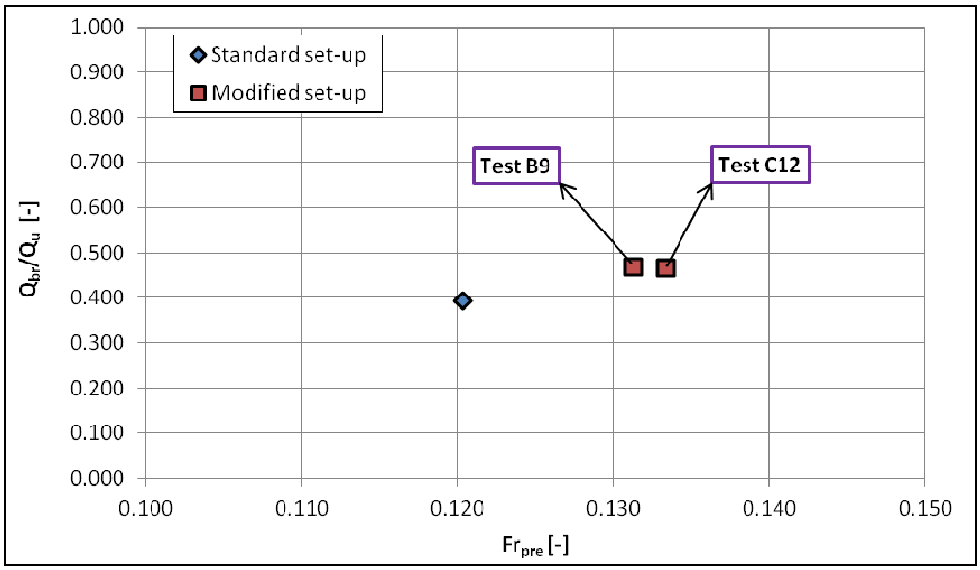

Figure 4.34: Discharge ratio Q_{br}/Q_u of the tests B9 (Q45.1Yg4.0S0.1%) and C12 (Q45.3Yg4.0S0.1%).

The breach discharge increases during the temporal development of the breaching process, with higher gradients during the first time steps and the tendency to achieve a final steady state (see Figure 4.35). The effect of drain removal operations is to accelerate the gain of the steady state. The drain removal allows for more vertical erosion of the breach channel so that the effective water head acting on the breach bottom is greater and it increases the breach discharge. It is likely that the system would have reached the final steady discharge only by means of the breach lengthening even if no drains had been removed: anyway, the breach discharge increases faster because of the vertical deepening compared with the lateral erosion, as the breach flow is basically given by the side weir law expressed by equation 4.5:

$$Q_{br} = \int_0^{L_{br}} C_{dbr} \cdot \sqrt{2g \cdot \left(h(x) - Z_{br}(x)\right)^3} \cdot dx \qquad (4.5)$$

With C_{dbr}: breach discharge coefficient [-]
h: water level acting on the breach [m]
Z_{br}: elevation of breach channel [m].

Fixed bed experiments show that for increasing length of the outflow structure (that is represented by the side weir, in fixed bed tests, and by the breach channel, in movable bed ones) the lateral discharge increases as well and a superior limit seems to exist in the order of $Q_{s,max} \approx 0.55 \cdot Q_u$, that is very similar to the discharge ratio found at the end of almost all the movable bed tests (see Figures 4.35 and 4.36).

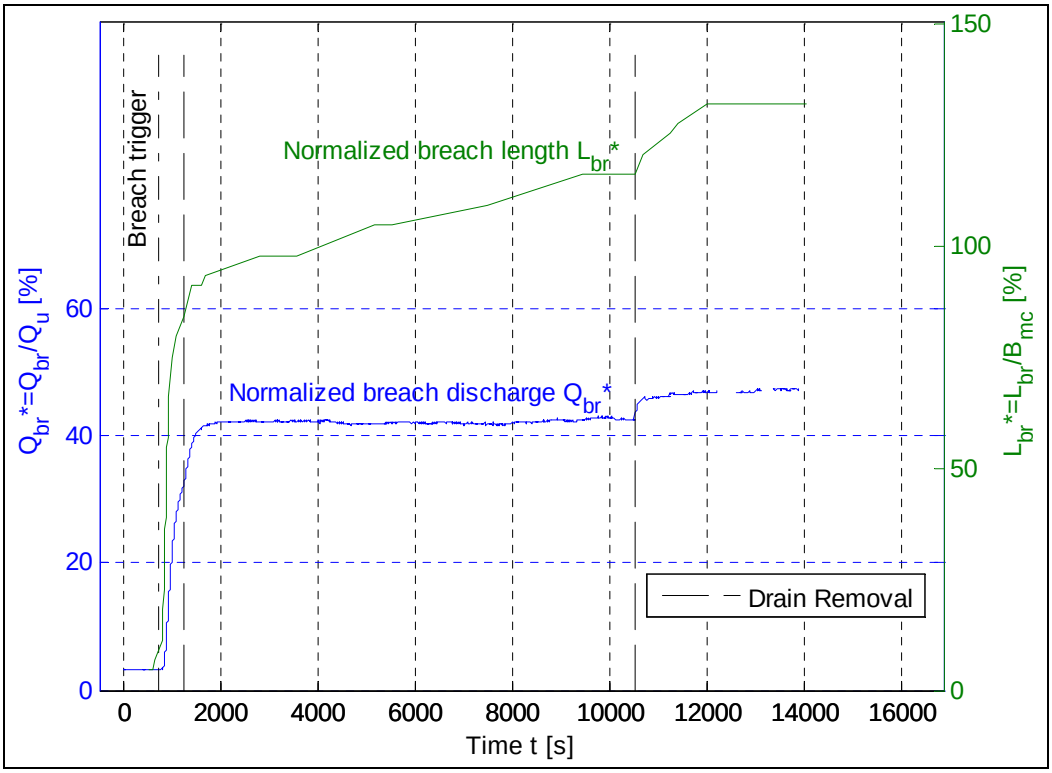

Figure 4.35: Temporal development of dimensionless breach discharge and of breach length (test A3 - Q29.2Yg2.2S0.1%).

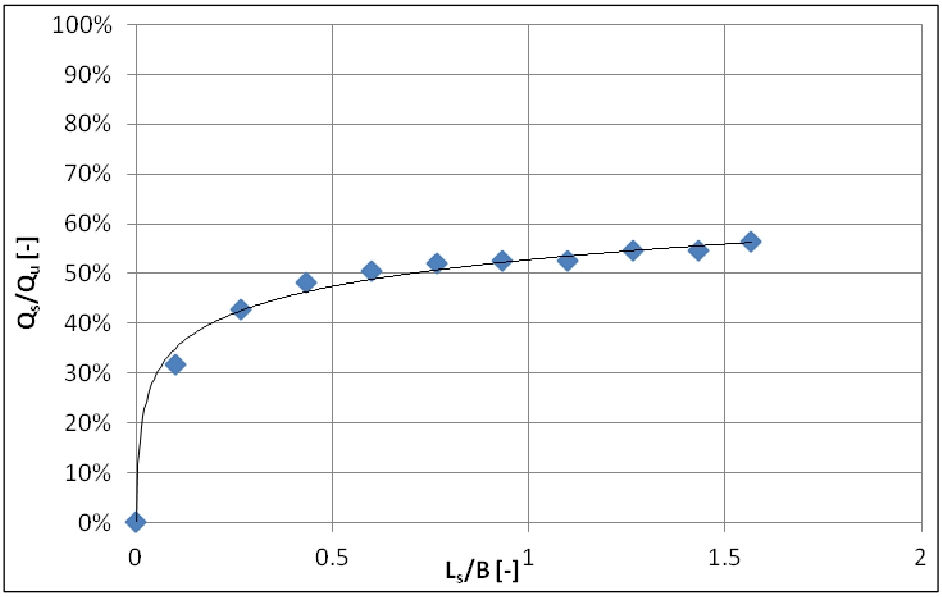

Figure 4.36: Side weir discharge over inflow discharge as a function of dimensionless side weir length for the fixed bed tests (B = 0.3 m, width of main channel in flume for fixed bed tests).

4.4.2 Analysis of breach length

The dependence of the breach final configuration to the inflow discharge is also shown by plot of Figure 4.37: the final breach length is linearly governed by the water discharge of the river, which is partially withdrawn by the breach itself.

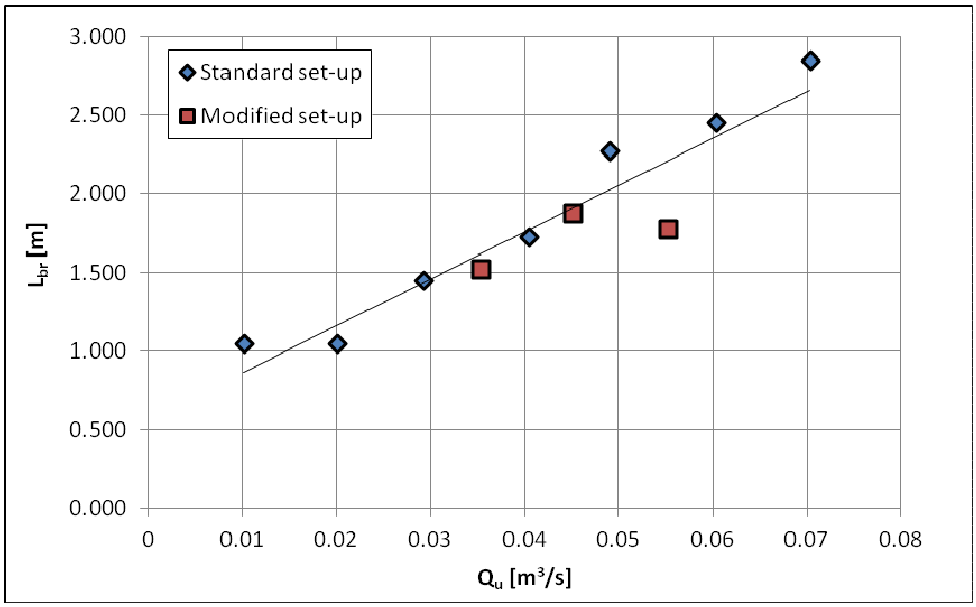

Figure 4.37: L_{br} versus Q_u at the end of each test.

Breach length and breach flow are connected each other, as Figure 4.38 depicts: breach flow acts like a side weir in a river and the lateral outflow is basically given by the side weir equation, in which the breach discharge is correlated with the breach length (equation 4.5), but it does not get a linear relationship, because the flow depth acting on the breach determines the outflow too.

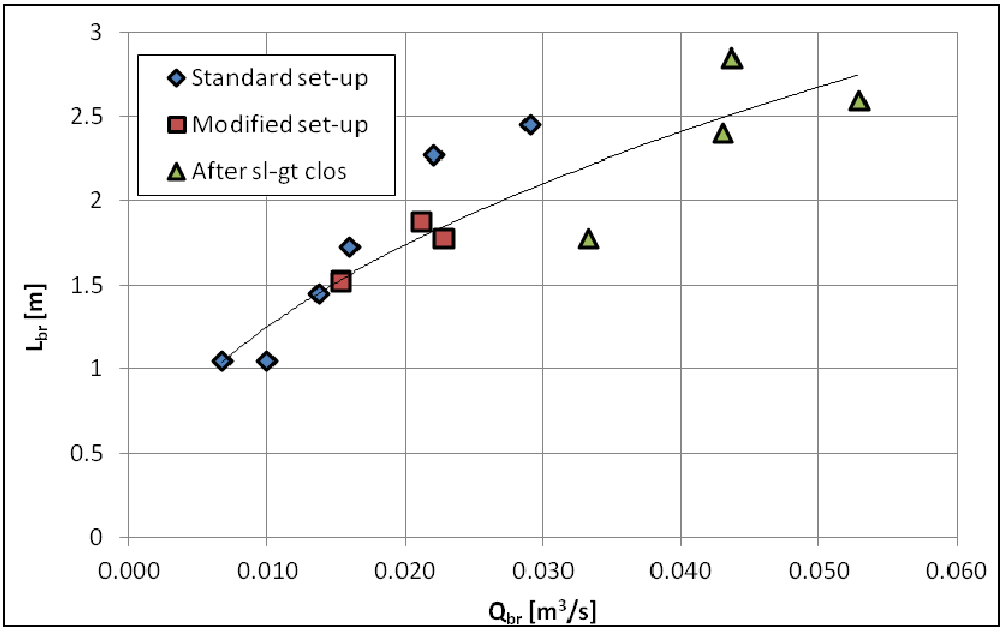

Figure 4.38: L_{br} versus Q_{br} for each test.

During the movable bed tests it was not possible to record the flow depth along the breach, but the water level profile was measured in the fixed bed tests. The lateral outflow discharge for the fixed bed tests can then be analysed together with the mean flow depth along the side weir and the length of the weir itself. Given equation 4.5, the lateral discharge Q_s can be made dimensionless by means of Q_s^*:

$$Q_s^* = Q_s / \left(\sqrt{2 \cdot g \cdot Y_{s,mean}^{\ 3}} \cdot B \right) \tag{4.6}$$

With $Y_{s,mean}$: mean water depth along side weir [m]
$B = 0.3$ m: width of main channel at free water surface [m]

Figure 4.39 shows that Q_s^* gets a linear relationship with respect to the side weir length L_s, as it was expected.

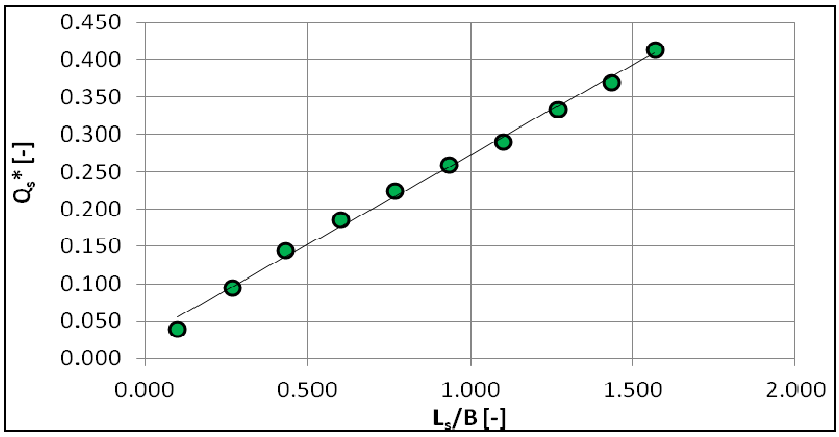

Figure 4.39: Side weir relationship for the fixed bed tests.

4.4.3 Analysis of river hydrodynamics

4.4.3.1 Flow depth and flow velocity

The understanding of river hydrodynamics is fundamental in order to explain how the system develops during each test. The fixed bed experiments are very useful to this aim, since the hydrodynamics of the flow in the main channel was well recorded for various side weir lengths. Figures 4.40 and 4.41 recall some results from the fixed bed experiments that are relevant for the following analysis.

Figure 4.40 shows the longitudinal profiles of the water depth in the main channel for several tests, i.e. for increasing side weir lengths which represent an increasing breach length. The plots show that, as the breach lengthens, water depth profile lowers in all the flume. The reach upstream the beginning of the side weir gets lower and lower flow depth until the flow almost crosses the critical depth (Y_{cr}). Flow depth increases along the side weir, but it has a first decreasing reach for the tests with the longest side weir lengths. The increasing behaviour is typical of a gradually varied subcritical flow, while a first supercritical reach is presumed when the flow depth decreases along the lateral outflow. The hydrodynamic features of the downstream reach, after the side weir, belong to an almost uniform subcritical flow, that is controlled by the downstream boundary condition. As a consequence, the mean flow velocity in the main channel increases going toward the breach beginning and then the flow slows down toward the downstream end of the breach (see Figure 4.41). The final water depth profile at the end of each movable bed tests was similar to the previously described situation: an example is given in Figure 4.42.

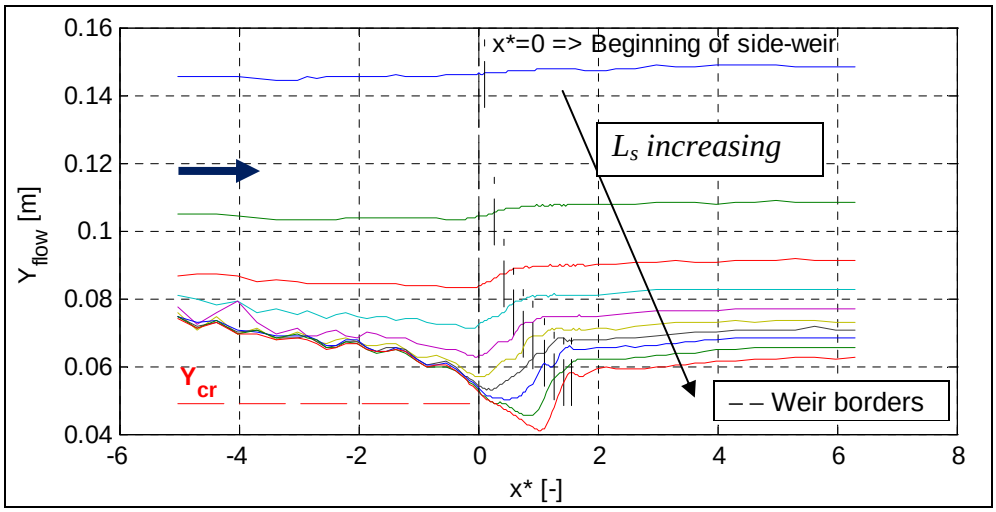

Figure 4.40: Flow depth profiles for the fixed bed tests.

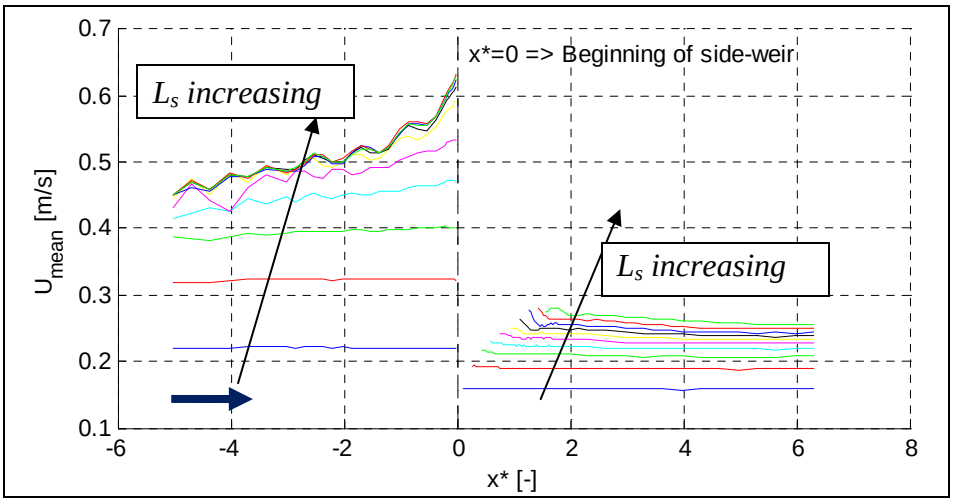

Figure 4.41: Flow velocity profiles for the fixed bed tests.

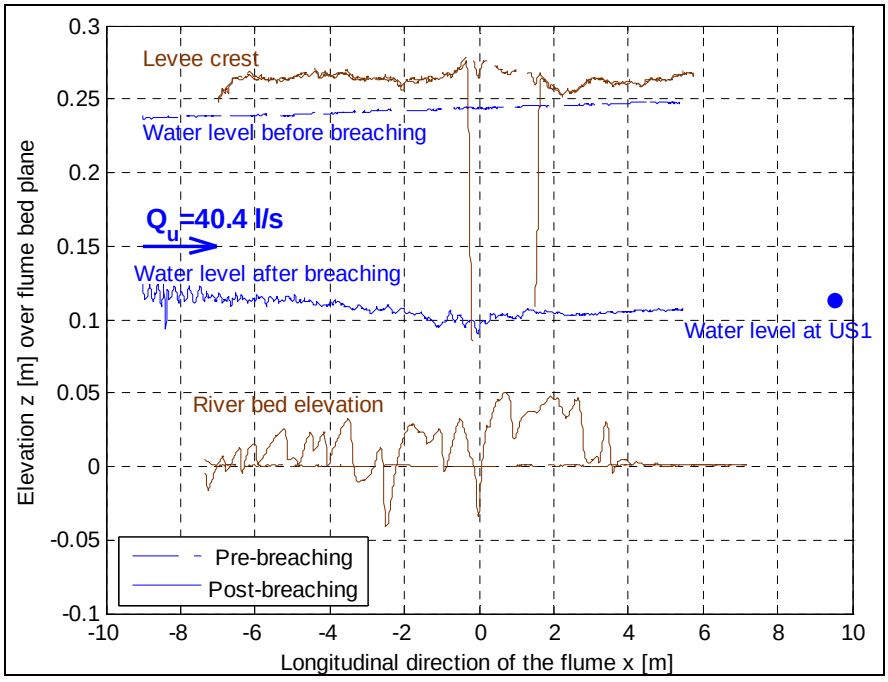

Figure 4.42: Water surface profiles before and after the breaching for test A4 (“Q40.4Yg3.4S0.1%”).

Some hydrodynamic features of the system for the movable bed tests were computed as referred to the end of the test. The recordings of water level and river bed morphology were elaborated and discretized along the breach channel, according to the scheme of Figure 4.31.

Flow features along the breach were calculated from the experimental data according to the following procedure. The breach channel is subdivided into N spatial intervals of equal length $\Delta x = 0.01$ m and the water surface level **h**, the river bed $\mathbf{Z_b}$ and the breach elevation $\mathbf{Z_{br}}$ were calculated at the middle point of each Δx. For each i-step, the following variables were computed:

- $Y_i = h_i - Z_{bi}$, flow depth at i-section in the main channel;
- $Y_{bri} = h_i - Z_{bri}$, flow depth at i-section acting on the breach.

The lateral outflow was calculated according the side weir equation (4.5), which needed a calibration to fit the final measured breach discharge. It was chosen to calibrate the effective flow depth acting on the breach by means of a calibration factor k, as multiplier of the mean breach bottom which for sure is an estimation with uncertainties due to the variability of the bed deformation at the breach site. The breach discharge coefficient was instead considered constant for each test, and it was assumed equal to the classical value for broad-crested weir ($C_{dbr} = 0.385$). The calibration function is then given by:

$$f(k) = \left| Q_{brmeas} - C_{dbr} \sum_{i=1}^{N} \Delta x \cdot \sqrt{2 \cdot g \cdot (h_i - k \cdot Z_{bri})^3} \right| \tag{4.7}$$

The calibration parameter k, which made the function f to get a local minimum value, ranged between 1.11 and 2.79 (Table 4.3) and it made the errors between the measured and the computed breach discharge to be less than 1% for all the analysed tests.

Table 4.3: Values of the calibration parameter k for movable bed tests.

	A					**B**				
	1	**2**	**3**	**4**	**5**	**6**	**7**	**8**	**9**	**10**
k [-]	1.11	1.22	1.19	1.57	1.17	1.20	1.11	2.79	1.76	2.02

The flow discharge are then calculated in the main channel along the flume for each i-position, since the flow outing from the breach is given by the calibrated side weir law. The longitudinal and transversal components of the flow in the main channel are calculated, from the continuity principle, according to the equations (4.8):

$$\begin{cases} U_{xi} = \dfrac{Q_{xi}}{A_i} = \dfrac{Q_u - \sum_{j=1}^{i} q_{br,j} \cdot \Delta x}{A_i} \\ U_{yi} = \dfrac{Q_{br,j}}{Y_i \cdot \Delta x} \end{cases} \tag{4.8}$$

The flow field at the breach site is affected by the lateral outflow and it gets important two-dimensional features, which make the transversal velocity U_y to get values in the order of the main flow velocity U_x. Figure 4.43 shows the results of such analysis for one movable bed test: the longitudinal component of velocity U_x decreases along the breach, due to the lateral outflow and as fixed bed analysis predicted, whereas the transversal component U_y increases, due to the combined effects of increased water level and river bed along the breach site.

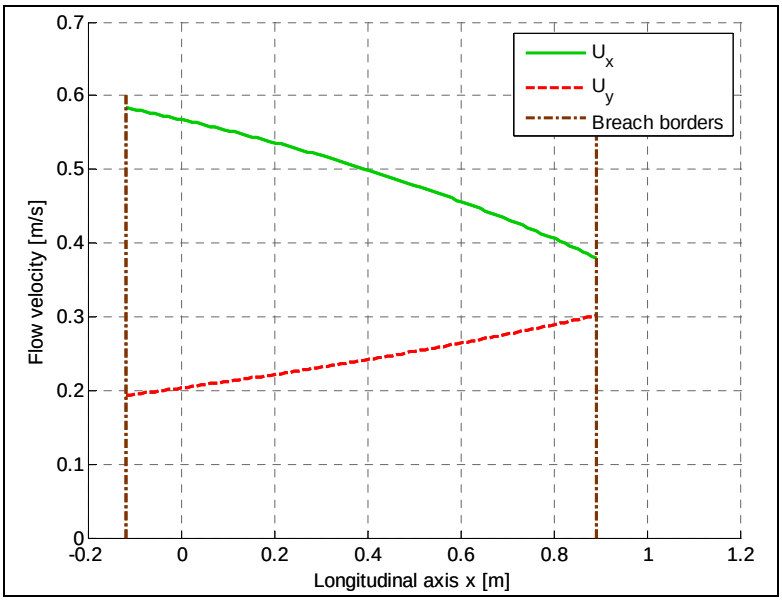

Figure 4.43: Components of flow velocity for test A3 ("Q29.2Yg2.2S0.1%").

4.4.3.2 Deflection angles

The fixed bed investigations showed that superficial streamlines turn toward the breach with increasing deflection angles θ: at the upstream corner of the breach, the flow is almost parallel to the main channel direction x, while deflection angle increases going toward the downstream corner, where flow deflection is maximum (see Figure 3.26). As a consequence, the flow velocity component toward the breach U_y gets higher importance at the downstream section of the breach instead of at the upstream section where there is almost only one component of the flow, U_x, as it was described by the previous analysis. Figure 4.44 depicts a sketch of the flow deflection.

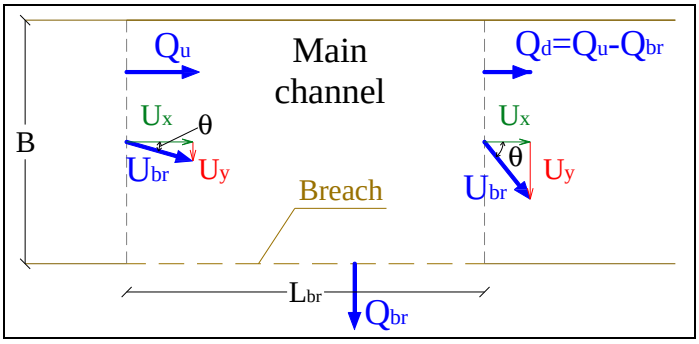

Figure 4.44: Sketch of the flow deflection at the breach site.

The deflection angle θ results from the combination of U_y and U_x and it is given by:

$$\theta = \tan^{-1}\left(\frac{U_y}{U_x}\right) \tag{4.9}$$

The previous analysis of flow velocity components allows to calculate the deflection angle along the centreline of the main channel. Figure 4.45 shows the results for test A3. The increase of the angle θ in the streamwise direction is clear, even if its values are not so high as they could be expected from fixed bed experiments. Anyway, the performed analysis is referred to the centreline of the main channel: it is likely that the deflection is stronger closer to the breach line.

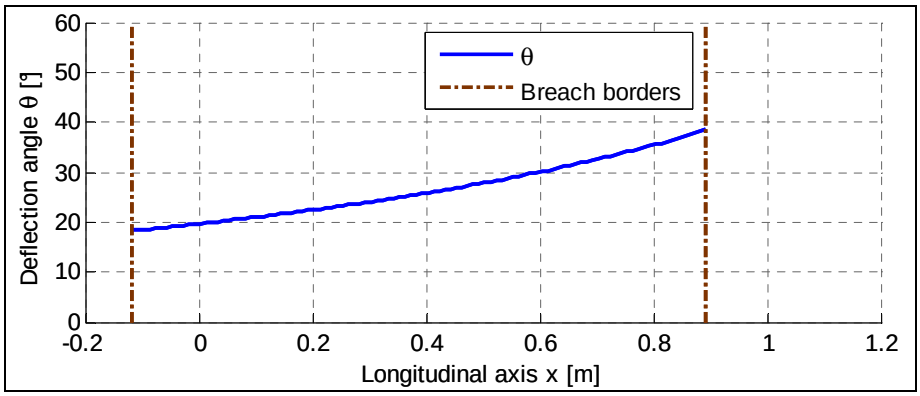

Figure 4.45: Deflection angles along the breach at the end of tests A3.

4.4.3.3 The De Marchi hypothesis

It is interesting to perform a preliminary verification of the application of the De Marchi (1934) hypothesis, which states that, along a side weir, the specific energy head of the main flow maintains a constant value. This hypothesis is commonly used by several authors dealing with side weir models and experiments (Montes, 1998; Borghei et al., 1999; Ranga Raju et al., 1979; May et al., 2003) and it was also verified for movable bed conditions (Paris et al., 2012). The levee breach resembles the situation of a flow over a side weir (Kamrath et al., 2006; Saucier et al., 2009; Oertel et al., 2011), but the constancy of specific energy head for this situation was not verified so far.

The energy balance of the main channel flow is applied between the up- and the downstream sections of the breach. According to the schematization depicted in Figures 4.31 and 4.46, the energy balance reads:

$$E_u = E_d + \Delta \tag{4.10}$$

With	$E = y + \alpha U^2/2g$	specific energy head [m]
	α	Coriolis coefficient (here assumed $\alpha = 1$)
	Δ	bed deformation between downstream and upstream [m]

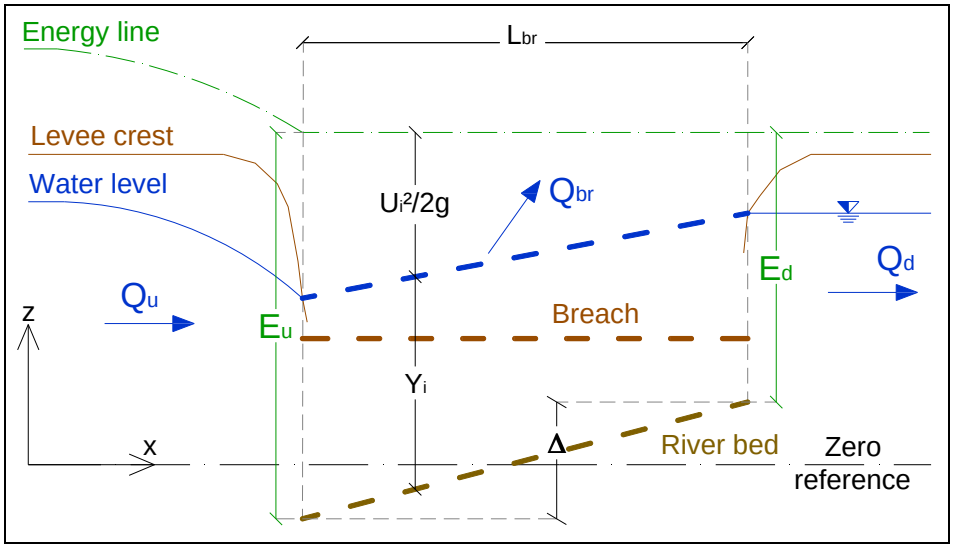

Figure 4.46: Scheme for specific energy head balance.

The specific energy head calculated at the end of each test is plotted in Figure 4.47: the most of the data (7 over 10 tests) satisfy the condition given by equation 4.10 within an error of ± 10%.

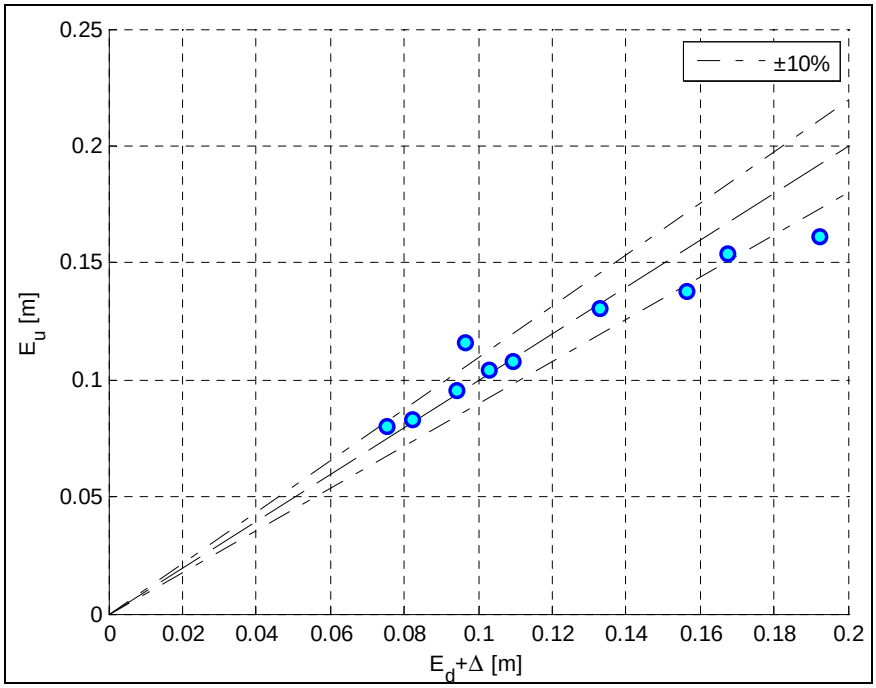

Figure 4.47: Specific energy head calculated at up- and downstream breach sections for the tests.

4.4.4 Analysis of sediment transport processes

The presence of the lateral outflow modified the river bed configuration in a quite evident way, as plots in Figures 4.20-21 and the picture of Figure 4.22 showed.

Figure 4.48 indicates that breach outflow affects linearly the river bed modification and this relation is plotted as function of breach discharge Q_{br} and river modification Δ_{max}. Test A1 and A2 had no river bed modification because of the too slight inflow discharge which did not mobilize the sediment particles in the flume.

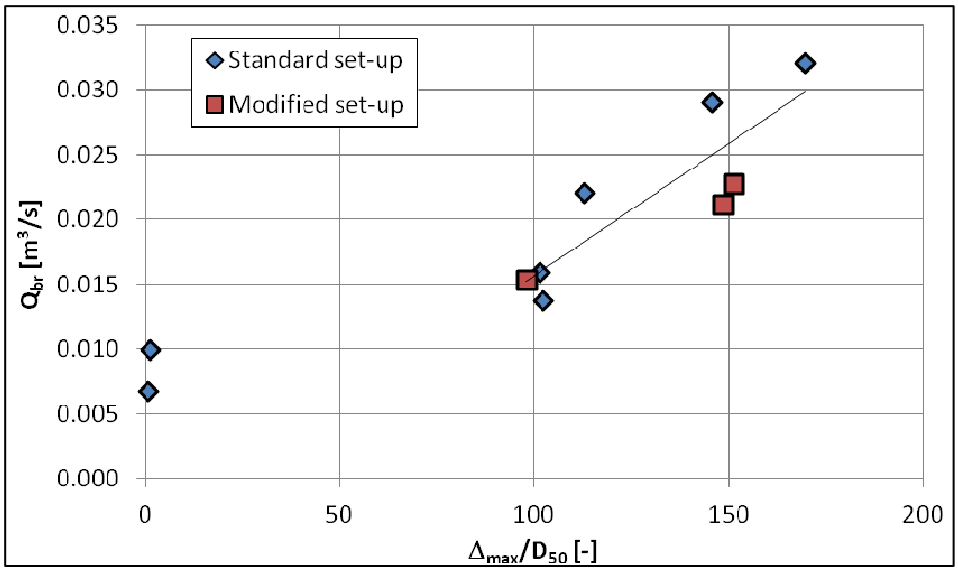

Figure 4.48: Q_{br} versus Δ_{max}/D_{50} for each test.

Bed deformation seems to have a quite important effect on the river-breach system, as already noticed by Bechi (2008) and Rosier (2007) in their experimental investigations about side weir in flume endowed with movable bed. The reason of such behaviour of the sediment transport in the river channel has to be explained by the hydrodynamics of the flow: during the breach formation and development more and more water flow discharges out of the breach. Flow upstream the breach is drawn by the outflow so that a drawdown water profile takes place with decreasing water depth along the channel and increasing flow velocity, since water discharge does not change (or, at least, it changes a little because of seepage flow). The acceleration of flow causes inception of sediment transport (since the shear stress increases with flow velocity) and sandy material starts to move from all the wetted perimeter, i.e., from the river bed and from the river side of the levee as well. Sediment transport from the levee slope causes erosion of the levee, while the river bed in the main channel is eroded if the sediment transport capacity of the flow is higher than the solid discharge provided at the flume entrance, that was zero in the present experiments. Motion of sandy materials in the main channel arranges itself as bed forms whose formation and development were clearly visible during the tests. It was noticed that sediment transport did not start at the beginning of the breaching phase, but after about 5 min from the breach triggering, i.e. after the time slot necessary to cause enough strong flow acceleration (see Figure 4.49).

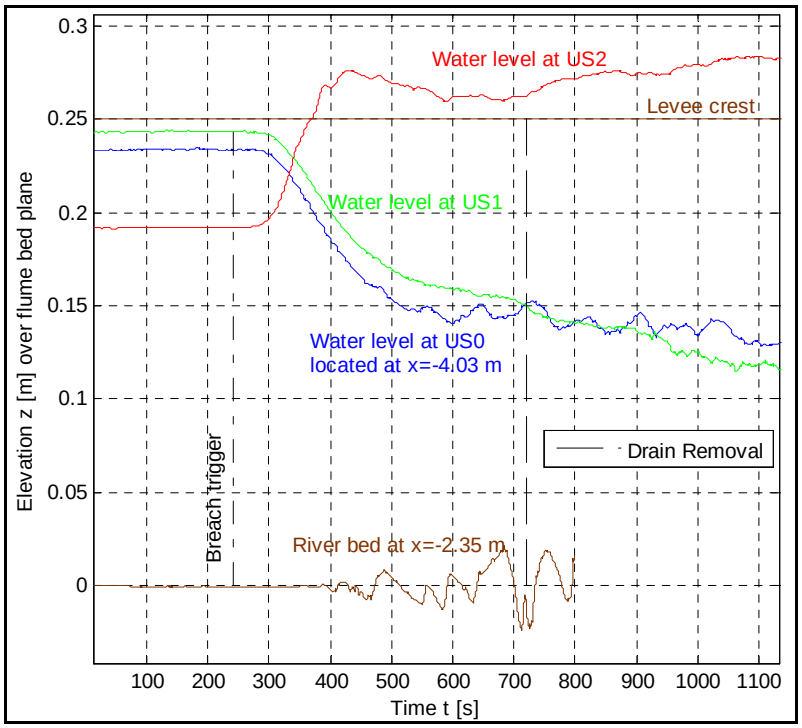

Figure 4.49: Temporal delay of river bed deformation for test B7 (“Q70.3Yg7.3S0.1%”).

Sediment transport is related to the shear stress τ acting on a granular material surface, and τ is correlated to the flow velocity, according to equation 4.11:

$$|\tau| = \gamma \cdot R \cdot S_f = \rho \cdot U_*^{\,2} = \rho \cdot \frac{|U|^2}{C_h^{\,2}} \qquad (4.11)$$

With γ specific weight of the water [N/m^3]
R hydraulic radius of the flow [m]
S_f energy slope [-]
U_* shear velocity [m/s]

$$|U| = \sqrt{U_x^{\,2} + U_y^{\,2}} \qquad \text{modulus of flow velocity [m/s]}$$

$$C_h = 5.75 \cdot \log_{10}\left(\frac{12 \cdot R}{2.5 \cdot D_{50}}\right) \qquad \text{Chézy coefficient [-]}$$

As flow velocity, τ has two components along the breach: τ_x and τ_y. The first one is responsible for the sediment transport along the river, it is maximum at the beginning of the breach because flow has its maximum velocity and it decreases downstream, since flow discharge decreases because of the lateral outflow. The general erosion of material upstream the breach is due to the increase of τ_x at upstream when the breach develops, while the deposition downstream is due to the decrease of τ_x along the breach.

The transversal component of shear stress τ_y governs the sediment transport through the breach. It gets more importance at the downstream end of the breach, where the flow curvature is pronounced. At the upstream breach section, the flow is more parallel to the levee alignment and, consequently, almost all the shear stress is directed in the longitudinal direction. At the downstream corner of the breach, the deflection is greater and the shear stress component is more directed toward the breach. The shear stress gets a more direct action on the downstream section of the breach compared with the upstream one: as a matter of fact, the breach was observed to develop mainly downstream.

The shear stress components are calculated as in equations 4.12 along the breach site, according to the elaboration made in Section 4.4.3:

$$\tau = \begin{cases} \tau_x = \dfrac{\rho}{C_h^{\,2}} \cdot |U| \cdot U_x \\ \tau_y = \dfrac{\rho}{C_h^{\,2}} \cdot |U| \cdot U_y \end{cases} \qquad (4.12)$$

Figure 4.50 shows the computed trend of the shear stress for test A3: it results that the longitudinal component of the shear stress decreases downstream, while the transversal component slightly increases, as previously predicted.

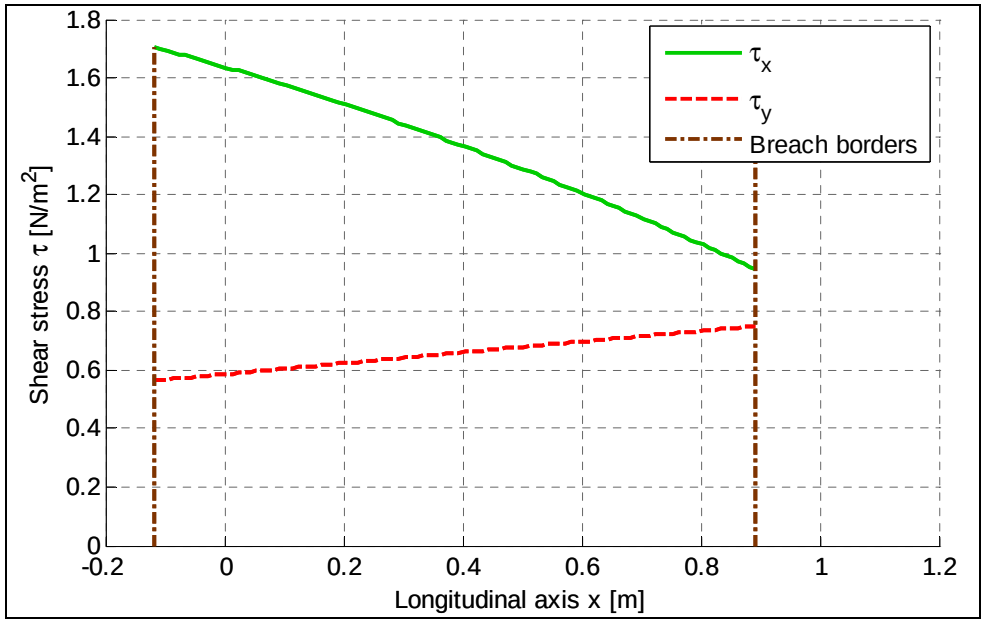

Figure 4.50: Shear stress components along the breach at the end of test A3.

The temporal trend of the shear stress was not known during the movable bed tests, but the fixed bed investigations can provide some useful complementary remarks.

At this point, it is useful to remind the fixed bed results. Figure 4.51 shows the trend of the total shear stress at the upstream and downstream section, for increasing side weir length: the shear stress τ_u tends to increase, due to the acceleration of the flow, while the downstream shear stress τ_d decreases and it is always lower than the upstream one. It can then be stated that the breach lengthening mobilizes bed materials at the beginning of the breach, the sediments are conveyed along (and partially through) the breach and they are finally deposited downstream the breach.

Moreover, a mean shear stress acting on the side weir in the outflow direction was calculated for each test, as in equation 4.13:

$$\tau_{sw,mean} = \rho \cdot \frac{\overline{U}_s^{\,2}}{C_h^{\,2}} = \frac{\rho}{C_h^{\,2}} \cdot \left(\frac{Q_s}{L_s \cdot \overline{Y}_s} \right)^2 \tag{4.13}$$

Figure 4.51 shows that the mean shear stress acting on the lateral weir decreases of one order of magnitude for longer side weirs and it tends to an asymptotic low value.

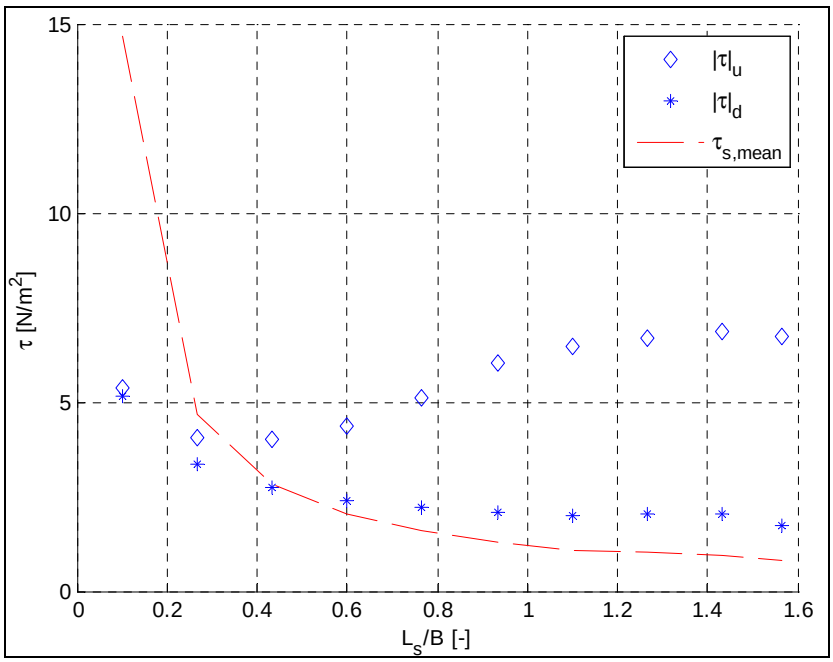

Figure 4.51: Shear stress at the side weir for the fixed bed tests.

The decreasing behaviour of the mean shear stress on the lateral weir may be compared with the recorded erosion rates of the movable bed tests. Breach lateral erosion was quite fast during the first 5-10 min from the triggering of the breach and then it slowed down toward low erosion rates. Breach erosion rates dL_{br}/dt were derived from breach length recordings: maximum erosion rate was in the order of 1-2 cm/s and then it decreased of one order of magnitude during the test (see Figure 4.52). The decrease of the erosion rate can be explained by means of the decrease of the mean stress acting on the breach channel as the breach lengthens. As a matter of fact, the soil erosion rate depends on the shear stress τ_{br} acting on the breach according to the excess shear stress equation:

$$\frac{dL_{br}}{dt} = a \cdot k_d \cdot (\tau_{br} - \tau_{cr})^b \tag{4.14}$$

With k_d: detachment coefficient [$m^3/(N \cdot s)$]
τ_{cr}: critical shear stress for inception of sediment transport [N/m^2]
a, b: coefficients of the excess shear stress equation [-]

The erosion rate can then be related to the mean shear stress acting on the side weir for different tests. Figure 4.53 plots the side weir shear stress and the breach erosion rate, for the decreasing portion of the curve, as function of the dimensionless length L (which is the side weir length, for the fixed bed tests, and the breach length, for the movable bed tests): the behaviour of the two curves is similar, even if they do not overlap, because coefficients of equation 4.14 and correction factors should be calibrated.

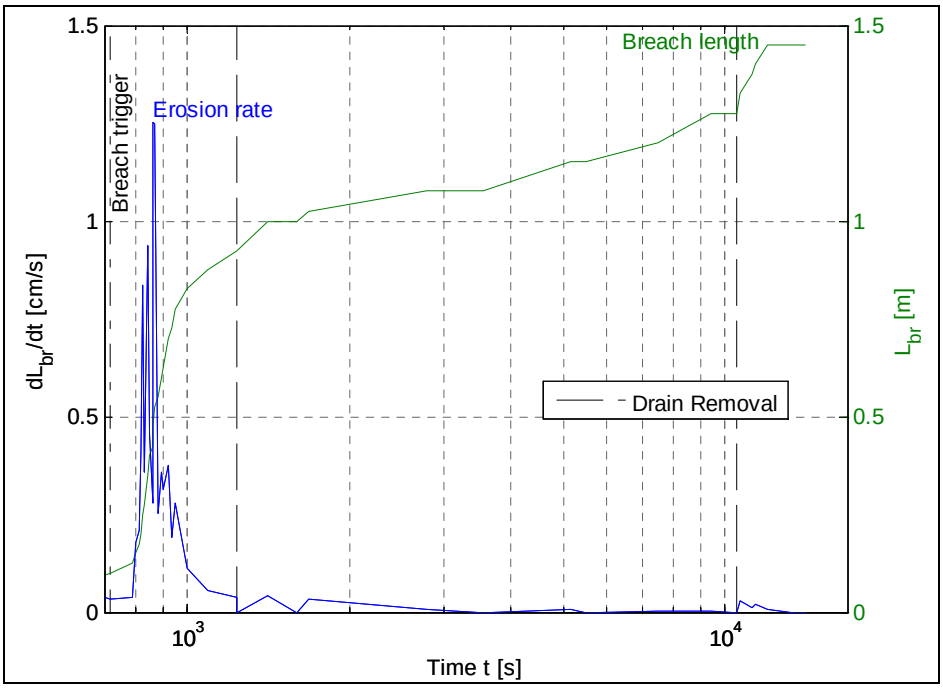

Figure 4.52: Temporal development of breach erosion rate and of breach length (test A3).

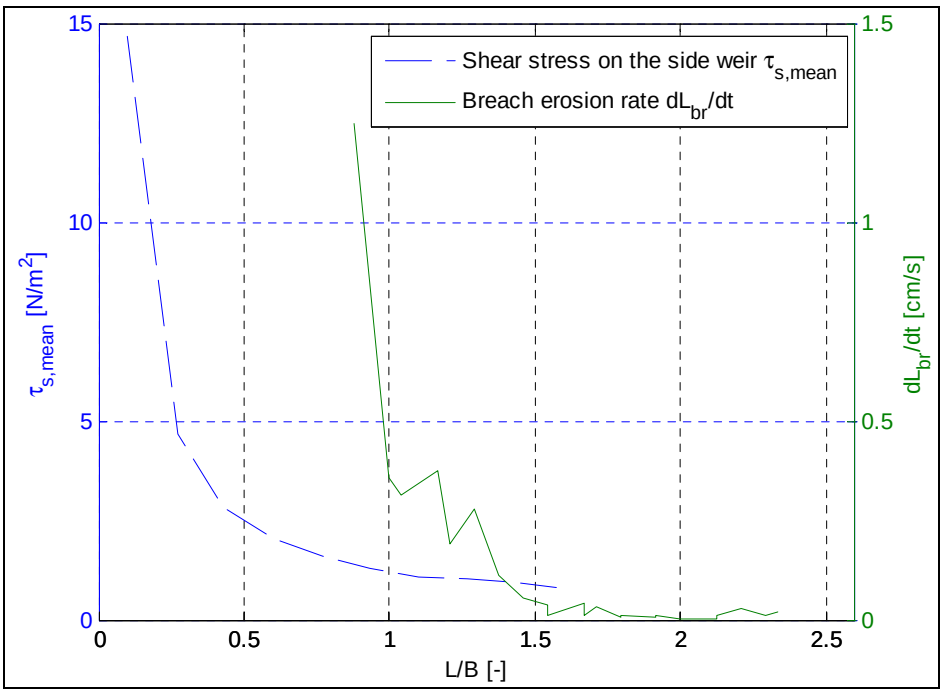

Figure 4.53: Comparison between shear stress on side weir and breach erosion rate.

4.4.5 Analysis of the breach morphology

Visual observations of the breach features at the up- and downstream sections seem to confirm the previous analysis about the shear stresses: the upstream breach section (Figure 4.54) resulted in a rounded shape and the marks of the accelerated flow passage remained on the sand surface, while downstream breach section (Figure 4.55) resulted in a more clear cut of the levee section with an almost vertical slope. Figure 4.56 shows clearly the different morphology of the breach at the upstream and downstream sections.

Figure 4.54: Upstream breach section (test A2 – "Q20.1Yg1.0S0.1%").

Figure 4.55: Downstream breach section (test A2 – "Q20.1Yg1.0S0.1%").

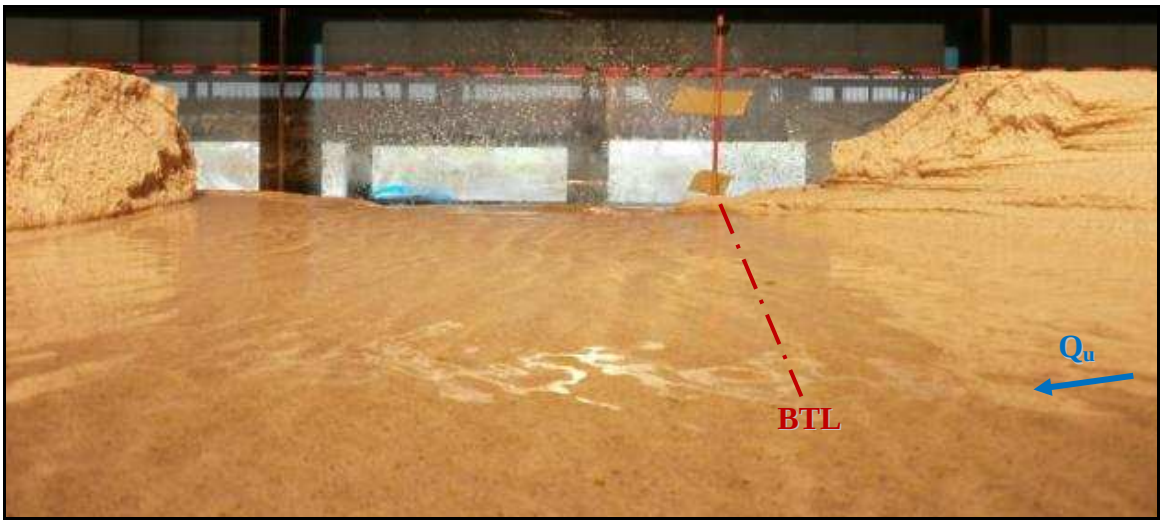

Figure 4.56: Frontal view of the breach (test A2 – "Q20.1Yg1.0S0.1%", inflow from right side).

Vertical wall of earth that formed at the edge of the breach at the downstream levee stub plays a key role in lengthening the breach: water erodes the levee toe and the material above it falls to form a vertical wall again (see Figure 4.57). The slumped material has to be removed before breach can lengthen furthermore and the removal action is exerted by the shear stress of the breach flow. The greater the velocity of the breach flow, the faster the flowing water will erode the edge of the levee stub and the faster the process of repeated wall formation will be. Cohesionless materials, such as the used sand, offer low resistance to the breach erosion action so that even weak shear stress could erode material from the downstream levee section.

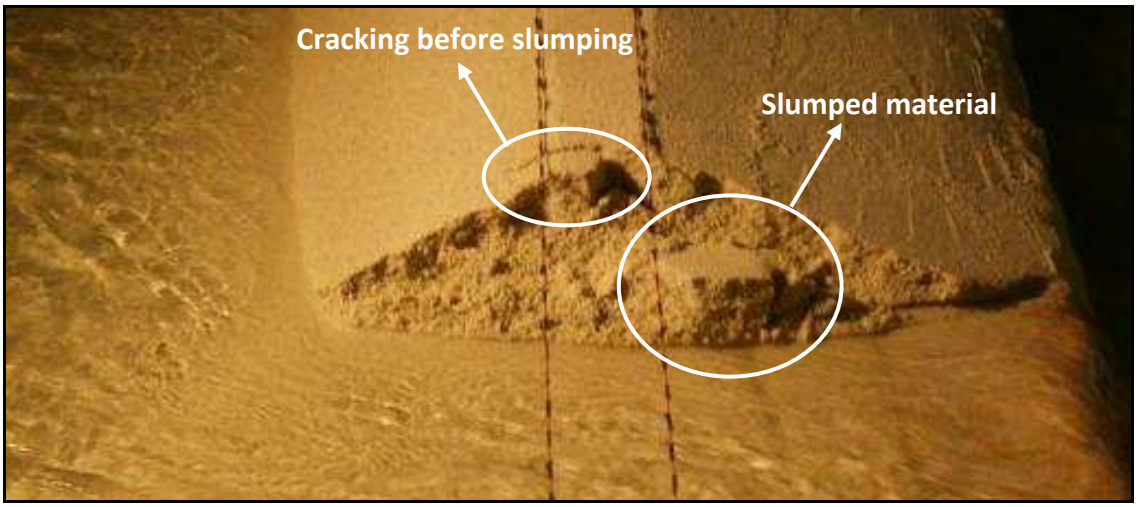

Figure 4.57: Mass failure at the downstream section of the breach.

Breach developed mainly downstream and this asymmetry can be explained by the presence of the river flow: test C11 showed how a dam breach develops both in the up- and downstream directions almost symmetrically, while the river flow field creates completely different loading conditions prevailing on the levee, as explained before, so that temporal development and final configuration of the breach will be different from the dam breach.

Breach channel was deeper toward the centre of the breach, but it did not deepen very much because the concrete wall limited the vertical erosion. The shape of the breach channel resembled the flow field acting over it: a kind of slight bend could be recognized turning from the main channel toward the breach.

The final shape of the breach was almost trapezoidal, with the lateral sides tilted of about 30-50° over the horizontal reference. Figure 4.58 points out the side slopes of the breach channel recorded at the end of each test and it results that the angles of the downstream side are usually greater than at the upstream side: this is another effect of the flow field, as already remarked.

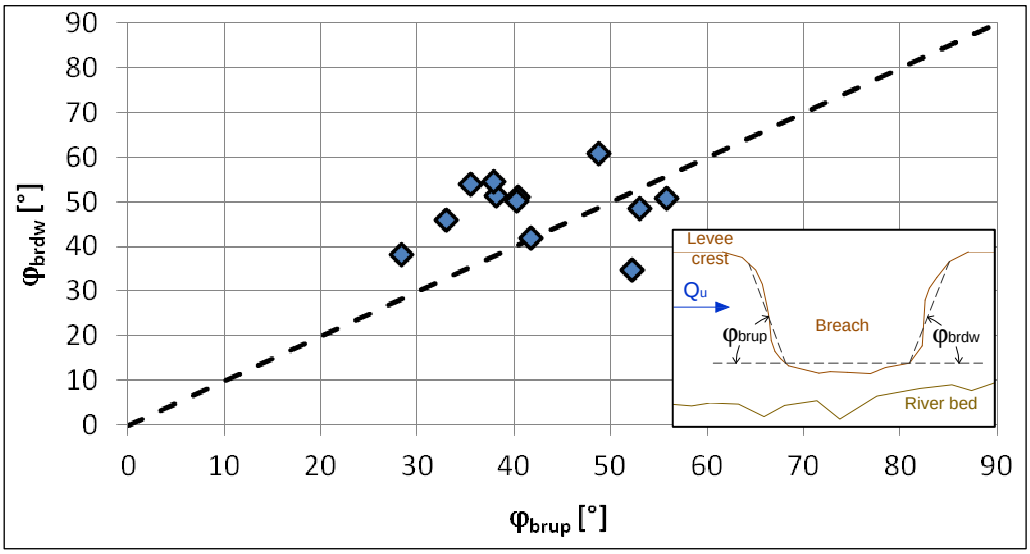

Figure 4.58: Slopes of the breach sides.

Finally, it is interesting to note that during test C12, the downstream breach developed faster than the upstream one (see Figure 4.28). This effect was likely due to two reasons: one of geotechnical origin and the other one of hydraulic origin. At the beginning, breach N°2 was eroded faster because it was triggered in a zone of the levee model whose material was not compacted since several weeks: as a matter of fact, the levee model was restored after each test only in the zone of the breach, while the remaining part of the levee, where breach N°2 was located, was not affected by breaching processes before that test. Erosion rates are dependent on the geotechnical properties of the levee, such as compaction degree, and the breach N°2 was eroded faster probably because of the difference in the compaction degree. As a consequence, the breach N°2 developed so fast that it drew down the water profile upstream it and this reduced the water depth prevailing on breach N°1. Since the downstream section is the most critical zone for the breach development, breach N°2 "controlled" breach N°1, whose development was quite slow until a drain was removed and some more water depth could start the erosive process again at the time t ≈ 3000 s (see Figure 4.28).

Numerical values of the main variables recorded and computed during the experimental tests are reported in Tables 4.4-4.5. It is worth to remember here the meaning of the variables reported into the Tables 4.4-4.5:

- Q_u: inflow discharge at the beginning of the flume
- Q_{br}: breach discharge measured at the end of the test
- $Q_{br\ post\ slgt}$: breach discharge measured at the end of the test, after the last closure of the downstream sluice gate (only for tests B7-B8-B9-B10)
- $L_{br\ u}$: breach length toward upstream at the end of the test
- $L_{br\ d}$: breach length toward downstream at the end of the test
- $L_{br\ tot}$: total breach length at the end of the test ($L_{br\ tot} = L_{br\ u} + L_{br\ d}$)

- $L_{br\ tot\ post\ slgt}$: total breach length at the end of the test, after the last closure of the downstream sluice gate (only for tests B7-B8-B9-B10)
- $h_{pre\ mean}$: mean water level along the flume before breaching
- $h_{br\ post\ mean}$: mean water level along the breach after breaching (end of test)
- $Fr_{pre\ mean}$: mean Froude number along the flume before breaching
- $Fr_{br\ post\ mean}$: mean Froude number along the breach after breaching (end of the test)
- $U_{x\ u}$: longitudinal component of flow velocity at the upstream section of the breach (computed as explained in Section 4.4.3)
- $U_{x\ d}$: longitudinal component of flow velocity at the downstream section of the breach (computed as explained in Section 4.4.3)
- $U_{y\ u}$: transversal component of flow velocity at the upstream section of the breach (computed as explained in Section 4.4.3)
- $U_{y\ d}$: transversal component of flow velocity at the downstream section of the breach (computed as explained in Section 4.4.3)
- $\tau_{x\ u}$: longitudinal component of shear stress at the upstream section of the breach (computed as explained in Section 4.4.4)
- $\tau_{x\ d}$: longitudinal component of shear stress at the downstream section of the breach (computed as explained in Section 4.4.4)
- $\tau_{y\ u}$: transversal component of shear stress at the upstream section of the breach (computed as explained in Section 4.4.4)
- $\tau_{y\ d}$: transversal component of shear stress at the downstream section of the breach (computed as explained in Section 4.4.4)
- Δ_{max}: maximum bed variation in the main channel along the breach
- Δ: bed variation in main channel along the breach ($\Delta = Z_{bd} - Z_{bu}$)
- $dL_{br}/dt_{\ max}$: maximum erosion rate recorded
- t_0: inception of breaching process
- t_{test}: total duration of the test

Table 4.4: Summary of main variables investigated in tests (part I).

Series	Test	Q_u	Q_{br}	Q_{br} post slgt	$L_{br\ u}$	$L_{br\ d}$	$L_{br\ tot}$	$L_{br\ tot}$ post slgt	h_{pre} mean	h_{br} post mean	Fr_{pre} mean	Fr_{br} post mean
		[m^3/s]	[m^3/s]	[m^3/s]	[m]	[m]	[m]	[m]	[m]	[m]	[-]	[-]
A	1	0.0101	0.0068	-	0.35	0.7	1.05	-	0.254	0.082	0.02	0.09
	2	0.0201	0.0100	-	0.225	0.825	1.05	-	0.252	0.093	0.05	0.20
	3	0.0292	0.0137	-	0.2	1.25	1.45	-	0.233	0.083	0.10	0.34
	4	0.0404	0.0159	-	0.25	1.475	1.73	-	0.246	0.103	0.12	0.43
	5	0.049	0.0221	-	0.225	2.05	2.28	-	0.239	0.086	0.16	0.59
B	6	0.0603	0.0290	-	0.25	2.2	2.45	-	0.256	0.095	0.17	0.67
	7	0.0703	0.0321	0.0437	0.125	1.725	1.85	2.85	0.238	0.110	0.23	0.73
	8	0.0353	0.0153	0.0333	0.275	1.25	1.53	1.78	0.252	0.093	0.10	0.39
	9	0.0451	0.0212	0.0431	0.275	1.6	1.88	2.40	0.250	0.117	0.13	0.42
	10	0.0552	0.0228	0.0529	0.25	1.525	1.78	2.60	0.266	0.106	0.15	0.60
C	11	0.0072	0.0153	-	0.225	0.275	0.50	-	0.245	-	0.01	-
	12	0.0453	0.0212	-	1.525	1.6	3.13	-	0.249	-	0.13	-

Table 4.5: Summary of main variables investigated in tests (part II).

Series	Test	$U_{x\ u}$	$U_{x\ d}$	$U_{y\ u}$	$U_{y\ d}$	$\tau_{x\ u}$	$\tau_{x\ d}$	$\tau_{y\ u}$	$\tau_{y\ d}$	Δ_{max}	Δ	dL_{br}/dt max	t_0	t_{test}
		[m/s]	[m/s]	[m/s]	[m/s]	[N/m^2]	[N/m^2]	[N/m^2]	[N/m^2]	[cm]	[cm]	[cm/s]	[min]	[min]
A	1	0.14	0.03	0.11	0.12	0.11	0.02	0.09	0.06	0.1	0.0	1.1	2	173
	2	0.25	0.12	0.14	0.15	0.31	0.09	0.17	0.11	0.1	0.0	2.5	2	182
	3	0.58	0.38	0.19	0.30	1.70	0.95	0.56	0.75	8.5	1.9	1.3	12	234
	4	0.51	0.40	0.09	0.17	1.12	0.81	0.20	0.34	8.4	3.1	1.7	3	121
	5	1.05	0.74	0.13	0.26	5.39	3.01	0.64	1.06	9.4	2.3	1.4	3	101
B	6	0.65	0.68	0.08	0.31	1.70	2.51	0.21	1.14	12.1	7.6	1.9	3	69
	7	0.60	0.78	0.07	0.35	1.35	3.20	0.16	1.42	14.1	10.3	1.3	4	52
	8	0.46	0.31	0.13	0.19	0.92	0.50	0.27	0.32	8.1	2.2	1.3	3	207
	9	0.43	0.38	0.07	0.14	0.72	0.70	0.11	0.26	12.3	5.6	1.4	3	174
	10	0.47	0.46	0.04	0.14	0.83	0.97	0.07	0.30	12.6	7.3	1.5	2	104
C	11	-	-	-	-	-	-	-	-	0.2	-	0.6	3	19
	12	-	-	-	-	-	-	-	-	7.3	-	1.9	-	95

4.5 Summary and concluding remarks

Twelve different experimental tests were performed in a large hydraulic flume (30 m long, 2 m wide and 0.8 m deep) of the laboratory of the Leichtweiß-Institute for Hydraulic Engineering and Water Resources of Braunschweig (LWI). The experiments were aimed to reproduce the phenomenon of breaching of a river levee. A sandy model of a river levee with trapezoidal shape (0.25 m high) was set longitudinally in the flume for a testing reach 15 m long and it was above a layer of sand which represented the river bed part (see Figure 4.2). A water discharge flowed into the flume parallel to the levee model and it was set steady, while the downstream water level was controlled by a sluice gate at the downstream end of the testing reach. Ten different combinations of inflow discharge and sluice gate opening defined the ten main tests, each one having an initial subcritical flow regime. Two further tests were conducted as limit cases: the case of dam breach with a static water level behind the levee and the case of two multiple breaches triggered during the same test.

The breaching of the levee was triggered under controlled conditions and the erosion evolved by overflowing of the levee. The breach evolution and the river hydro-morphodynamics were investigated and monitored until an almost steady state of the physical system was achieved. Basically, the hydrodynamics of the flow was observed by means of measures of water levels, flow discharge values and point velocity values, while the morphodynamics of river bed was acquired by bed profiler and the breach evolution was monitored by means of two cams.

For each test a steady flow was set before the breaching, then the breach was triggered and the breach formation and evolution were monitored until the end of the test. Water levels were recorded by means of ultrasonic sensors, inflow discharge was controlled by an electromagnetic flow meter, measures of the 3D components of the flow velocity were taken from time to time at various sections of the flume by means of an acoustic doppler profiler, the topography of the river bed was acquired at the beginning and at the end of each test by means of three ultrasonic sensors all along the testing reach, two high definition cams were installed on the flume in order to monitor the breach evolution.

The collected data were analysed, debugged and elaborated in order to create a consistent data-base, which was referred to a predefined spatial and temporal reference system. All the data were elaborated according to the same criteria explained in Sections 4.3 and 4.4.

Data elaborations allowed to get information about:

- Longitudinal profiles of water level, levee crest and bed elevation before the breaching and at the end of each test;
- Temporal development of water level at the three fixed locations of the ultrasonic sensors;
- Temporal development of breach discharge;
- Measurements of the three-dimensional components of the flow velocity at some locations for the duration of short time-slots during the breaching process;
- Spatial trend of flow velocity (both mean longitudinal and transversal components), deflection angle and shear stress (both longitudinal and transversal components);
- Breach development both in the up- and in the downstream directions;
- Temporal trend of the breach erosion rate;
- Morphology of the breach section at its finale state;

- Bed topography in the main channel before the breaching and at the end of the test and topography of the breach channel.

The data analysis allowed to get an insight of the investigated process from the point of view of hydrodynamic and morphodynamic mechanisms. The process understanding was integrated with the fixed bed experiments done on side weir flow, which gave a comparison in terms of hydraulic variables for increasing length of the lateral weir that spills out a part of the water discharge from the main channel.

The following main outcomes were achieved.

The physical system river-breach achieved a **steady final equilibrium** regarding the water flow balance, as the downstream discharge and the breach discharge achieved a stationary state, but it did not regarding the solid phase since a residual erosion rate continued eroding the levee. In fact, the temporal development of the water levels achieved an almost stationary state before the end of the tests, whose duration was in the order of 1-2 hours. The ratio between the final breach discharge and the inflow discharge was found to be almost equal for every test, around a value of 50%. The temporal trend of breach discharge was compared with results of the fixed bed experiments done for increasing side weir length: the comparison shows a similar increasing trend of the outflow until the value of 50%, which seems to be an asymptote. This finding was furthermore highlighted because it matched for the two-breaches case as well.

The **final breach length** is linearly governed by the water discharge of the river and breach discharge is strongly correlated with the breach length. The comparison with the fixed bed data allowed to verify that breach flow acts like a side weir in a river and the lateral outflow is basically given by the side weir equation.

The **river hydrodynamics** in the vicinity of the breach was analysed and a physical interpretation of the flow processes is given in terms of flow depths, flow velocities, flow angles and shear stresses.
The comparison with the fixed bed experiments confirms that the **flow depth** decreases all along the channel because of the lateral outflow and the profile along the breach is increasing as in case of subcritical flow. A direct measure of Froude regime was not possible, but no visible hydraulic jump seemed to be occurred, even if the fixed bed experiments showed that possible supercritical flows may take place for relevant lateral outflows and breach lengths. Nevertheless, hydraulic jumps are likely to be transitory phenomena in channels with movable bed (Grant, 1997), so that the high energy dissipation modifies the channel bed and hydraulic jump does not maintain a stable configuration.
The mean **flow velocity** increases upstream the breach and then decreases along it because of the lateral outflow. A computational analysis was performed in order to get the numerical values of the spatial trend of the longitudinal and transversal components of the flow velocity. The analysis was based on the application of the continuity equations both in longitudinal and transversal directions and on schematizing the water depth, the river bed and the breach bottom along the breach as linear trends between upstream and downstream sections. In agreement with a similar analysis performed for fixed bed tests, the longitudinal component of velocity decreases while the transversal one slightly increases along the breach. As a consequence, the **flow angles** should increase downstream, which is confirmed by the visual analysis of the breach morphology.
A preliminary verification about the applicability of the **De Marchi hypothesis** at the levee breaching situation was performed by applying the energy balance and taking into account the riverbed modifications: the most of the analysed data (seven over ten tests) satisfy the De Marchi condition within an error of ± 10%.

The flow processes analysis allowed to understand the morphodynamic and morphological processes, which were found to affect each other. The lateral outflow modified the river bed configuration and an evident mutual relationship between breach discharge Q_{br} and river modification Δ_{max} was found.
The **river bed** morphological configuration was explained by means of the analysis of the hydrodynamics, which was also supported by the fixed bed experiments.
Morphodynamic mechanisms acting in the riverbed were analysed in three main zones of the flume: upstream the breach site, at and near the breach, downstream the breach site.
The **sediment transport processes** were investigated by analysing the **shear stress** components along the breach by means of the previous computational analysis: the spatial trend at the final configuration shows the decreasing of the longitudinal shear stress and a slight increasing of its transversal component. This is in agreement with the trends found for each single fixed bed test and it explains the tendency to deposition of material downstream and the mainly downstream erosion of the breach.
In the zone upstream the breach site, the presence of the lateral outflow through the breach induced a strong flow acceleration (and flow depth decreasing) and the sediment transport in the main channel, which produced **erosion** of sediment. The erosion of the riverbed was extended quite far upstream, because all the upstream flow was accelerated toward the breach. The erosive action of the flow affected the riverside of the upstream levee as well.
In the zone downstream the breach, the mobilized sediments were deposited by the slowing down flow. The **bed aggradation** was evident close the downstream section of the breach, while the remaining downstream zone of the flume had no significant morphological modifications.
In front of the breach site, the riverbed elevation was constantly increasing because of the sediment deposition. The breach developed in an asymmetric way because of the presence of the river flow, which creates completely different conditions with respect to the dam breach case. Since the shear stress gets a more direct action on the downstream section of the breach compared with the upstream one, the breach was observed to develop mainly downstream. The flow processes explain also the **breach morphology**. The final shape of the upstream and downstream sections of the breach was depicted as the result of the shear stress components acting. Mass erosion mechanisms at the downstream section were qualitatively analysed.

The fixed bed tests were used to investigate the temporal behaviour of a single movable bed test: as the length of the lateral weir increases, the upstream shear stress increases (which means erosion of material), the downstream shear stress decreases (which leads to deposition) and the mean shear stress acting on the side weir dramatically reduces. The decreasing of the shear stress acting on the lateral weir is related to the reduction of the breach erosion rate: a strong correlation is found. As a matter of fact, the maximum erosion rate was in the order of 1-2 cm/s and it decreased of one order of magnitude during the test because of the decreasing of the shear stress acting on the breach channel (relation $dL_{br}/dt–\tau$).

Limit cases as **dam breach** and **two-breaches** were tested: the first one highlighted the difference with the river levee case, while in the second one the two breaches interacted each other and an explanation of the temporal trend of the two lengths concludes that the downstream breach controls the development of the upstream one.

The data collected within this experimental investigation, and here reported and explained, are among the few detailed data found in the literature regarding the levee breaching, since most of the works deal with dam breach cases. The data here reported, together with the integration provided by the fixed bed tests about the hydrodynamics of the flow, represent a very important data-base for any further experimental tests, which may want to investigate different condition of the experimental set-up, or for specific numerical models, which should be process-oriented in order to analyse the breaching process without strong assumptions

about the physics of the problem, that is by considering both the geotechnical processes affecting the levee and the river hydro-morphodynamics.

The experimental study highlighted a very complex phenomenon of mutual interaction between flow and morphological processes, which could be simulated only by a sophisticated process-oriented numerical model. The observed phenomena consist on a three-dimensional problem, which can properly be addressed only by a 3D model. A 2D movable bed model can be a relevant tool for a more realistic numerical simulation of the levee breach. Therefore, **further researches** are recommended toward a complete model which should couple the three-dimensional flow field, the river morphodynamics and the breach evolution. These three factors affect each other with mutual relationships and all determine the final configuration of the system river-breach. Existing breach development models can provide a starting point, but they should be adapted to the levee breach case to reproduce the particular features of that situation (e.g., the asymmetric development of the breach).
Finally, more **experimental investigations** are recommended in order to analyse the levee breach case. So far, almost the totality of experimental works about breaching have been conducted with reference to the case of dam embankment (i.e., without river flow). Further tests are urgently required to understand better and better how a breach in a river levee develops and to propose new and reliable formulations for the estimation of breach parameters (final breach length, peak breach discharge, …) on the basis of: river flow features, river channel geometry, geometrical and geotechnical properties of the levee. A further very interesting research would investigate the interaction between two simultaneous breaches by answering the following questions: how two levee breaches interact each other? How and which of the two govern the other one? Does a threshold distance between the breaches exist in order to make them independent between themselves?

5 Analytical flow modelling

The processes that cause a river levee to breach are very complex due to diverse interactions between water, soil and structure. As shown in Chapters 2, 3 and 4, these processes are highly influenced by the hydraulic loading and the river flow conditions prevailing in the vicinity of the breach site. Breach models found in literature are mainly developed for the dam break case, whose hydraulic boundary conditions greatly differ with respect to river levee case (Morris, 2009b; Roger et al., 2010). A new approach to the levee breach problem is elaborated which considers river flow dynamics as a key issue to achieve a better understanding of the breaching process. The features of the river flow are the main focus of this Chapter, which are analysed with reference to the "regime" phase of the breaching process (i.e., the last stage of the process when the breach is supposed to get a steady final equilibrium).

First, a general overview of the main features of the flow along the breach is presented, according to the theory of the steady gradually varied flows.

Second, an analytical model is developed on the basis of the De Marchi hypothesis for the side weir flow. The analytical model provides a tool for the interpretation of the main flow hydrodynamic features when a lateral outflow takes place in the main channel.

The application of the model to the collected experimental data and some real events is then performed in order to preliminary test the validity of the proposed analytical model.

5.1 Hydrodynamic features of the flow along the breach

When a breach develops in a river levee, a part of the flow discharge spills out through the gap in the lateral structure. The outflow progressively increases as the breach crest is lowered and its length is increased, and, consequently, the flow hydrodynamics in the vicinity of the breach site changes during the breaching process. The situation of a river levee breach resembles the case of a side weir built on one side of an open channel. As observed by various authors (Kamrath et al., 2006; Saucier et al., 2009; Oertel et al., 2011), the flow pattern through a levee during the breach growth closely resembles that of the flow over a compound, broad-crested side weir (see Figure 5.1).

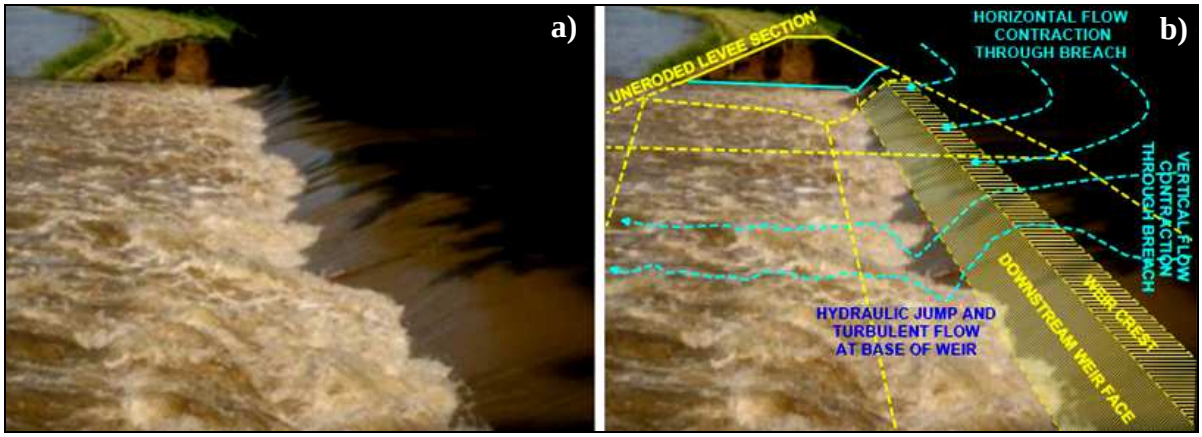

Figure 5.1: Similarity between a levee breach and a side weir: (a) unmodified photo, (b) photo with weir shape superposed (modified from Saucier et al., 2009).

Side weirs are hydraulic control structures used to divert flow from a main channel into a lateral channel when the water level in the main channel exceeds a specified limit, i.e. the weir crest p_s (see Figures 5.2-5.3-5.4). The structure is normally located on the side of the channel as a part of the channel bank and water discharges over it freely under gravity in the same way as for conventional weirs (May et al., 2003). Figures 5.2-5.3-5.4 show the plan view, the longitudinal section and the cross section of the main channel and they depict the main variables, whose description is reported in the "list of symbols" Section.

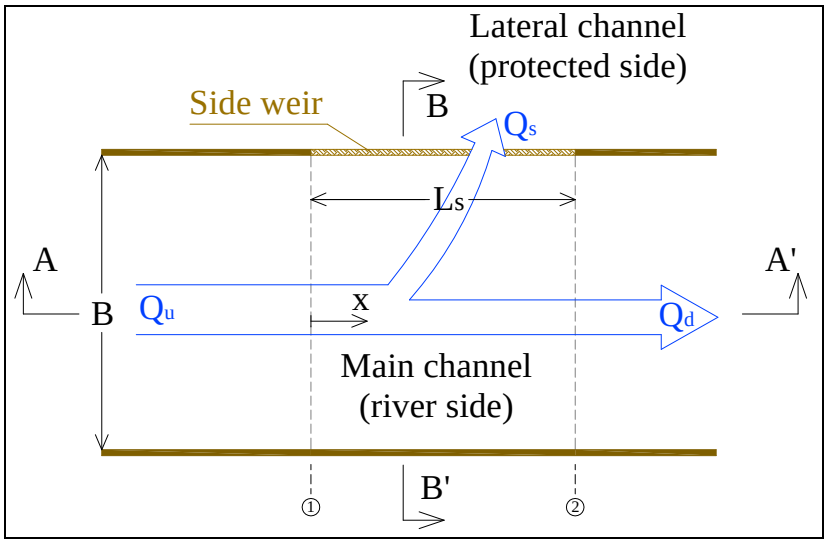

Figure 5.2: Side weir situation (plan view).

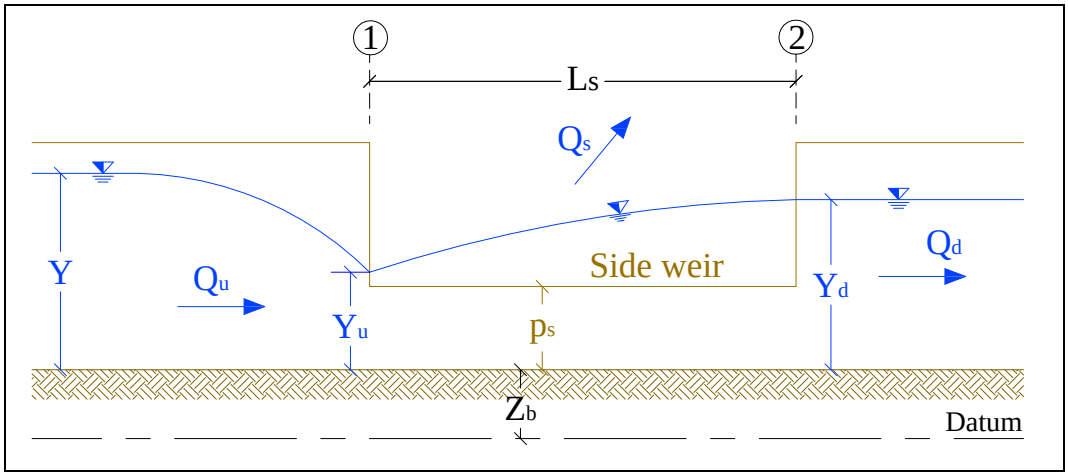

Figure 5.3: Side weir situation (longitudinal section A-A').

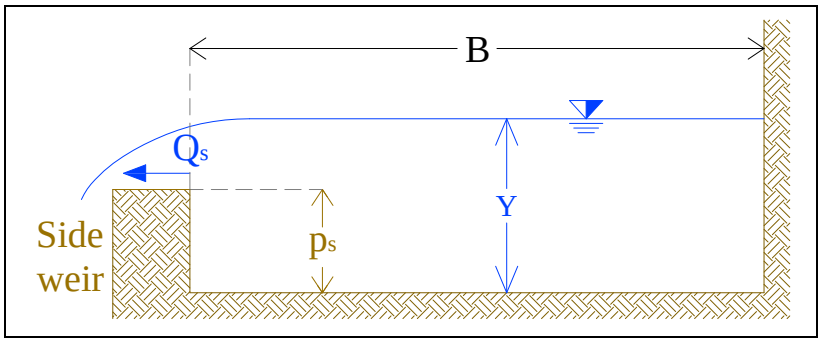

Figure 5.4: Side weir situation (cross section B-B').

The flow in the main channel along the side weir is a typical case of spatially (gradually) varied flow, which is defined as a non-uniform flow whose depth varies gradually along the channel because of water running out of the river (Chow, 1959). The diminution of water discharge causes disturbance in the energy and momentum balance of the flow and, as a result, the hydraulic behaviour of the flow is more complicated than for a flow with constant discharge.

As the discharge in the river decreases along the side weir, the water depth varies depending on the flow regime in the channel:

- For *subcritical flow*, the flow depth increases in the flow direction;
- For *supercritical flow*, the flow depth decreases downstream.

According to Borghei et al. (1999), the following main three types of flow profile may occur along the weir depending on the approach and the downstream water depth (see Figure 5.5):

a. *Subcritical flow profile*: the flow depth is greater than critical depth at the upstream section with subcritical flow in the weir section and water depth increasing along the weir (Figure 5.5a);

b. *Supercritical flow profile* at or near the entrance with supercritical flow in the weir section and depth of flow decreasing along the weir (Figure 5.5b);

c. *Critical flow profile* at the beginning of the weir section and subcritical flow in the downstream part, with a hydraulic jump occurring within the length of the weir (Figure 5.5c).

Other possible profiles may slightly differ from the three ones described above: for instance, the approach flow may be supercritical leading to profiles similar to types b and c, or the hydraulic jump may develop downstream the weir side (Chow, 1959; Montes, 1998).

The subcritical flow profile (type a) is the most common case encountered in practice (Montes, 1998; Borghei et al., 1999; Rosier, 2007) and it will be analysed in the following.

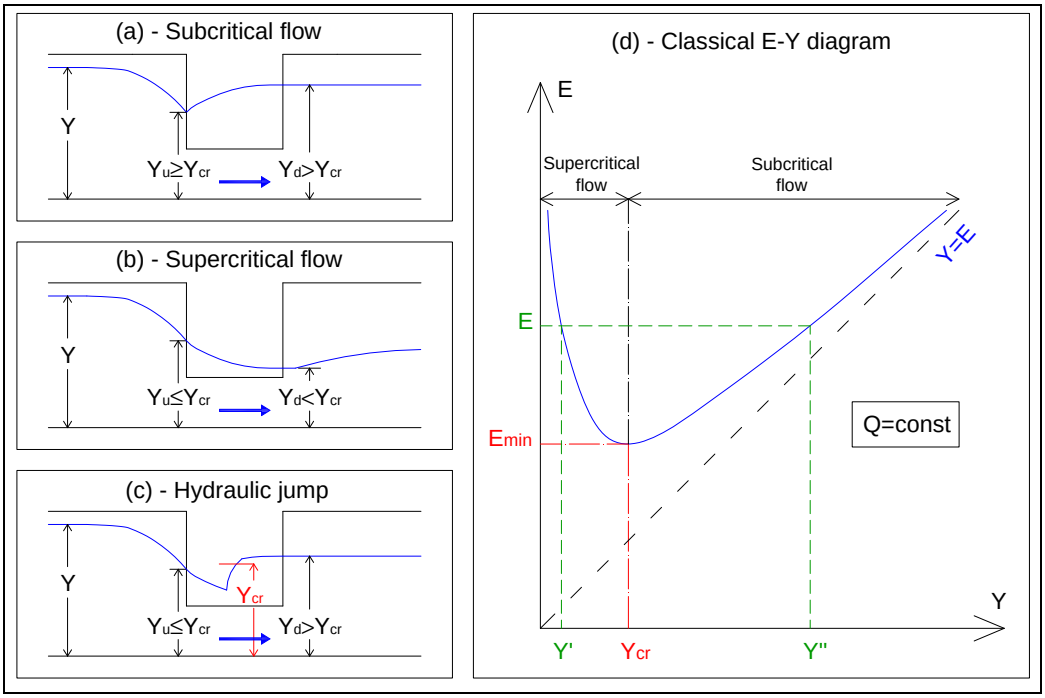

Figure 5.5: Water profiles in a channel along a side weir: (a) subcritical flow; (b) supercritical flow; (c) hydraulic jump; (d) E-Y diagram.

Figure 5.6 summarizes and explains graphically the hydraulic behaviour of the flow, given the usually assumed hypothesis of constant specific energy head E that will be discussed in the Section 5.2.

The downstream discharge Q_d can be given by two conjugate water depths: $Y_d' < Y_{cr}$ for supercritical flow and $Y_d'' > Y_{cr}$ for subcritical flow. If the flow is subcritical, the decrease of the discharge due to lateral outflow makes the water depth to rise along the weir (see curve Y-Q for a constant specific energy head E in Figure 5.6b). The rise of the water depth produces a decrease of the kinetic head $U^2/2g$ (see curve Y-E of Figure 5.6c) and the flow slows down in downstream direction.

The flow adopts an accelerated profile in the part upstream the side weir: it is a drawdown subcritical profile with depth decreasing downstream, which takes place in a channel with a mild slope. Due to the flow attraction through the side weir, the flow depth at the upstream cross section is progressively lowered as the lateral outflow increases (for instance because of a longer side weir). The upstream flow depth can decrease until the critical depth is encountered, which routes the inflow discharge Q_u with the minimum specific energy head E_{cr}.

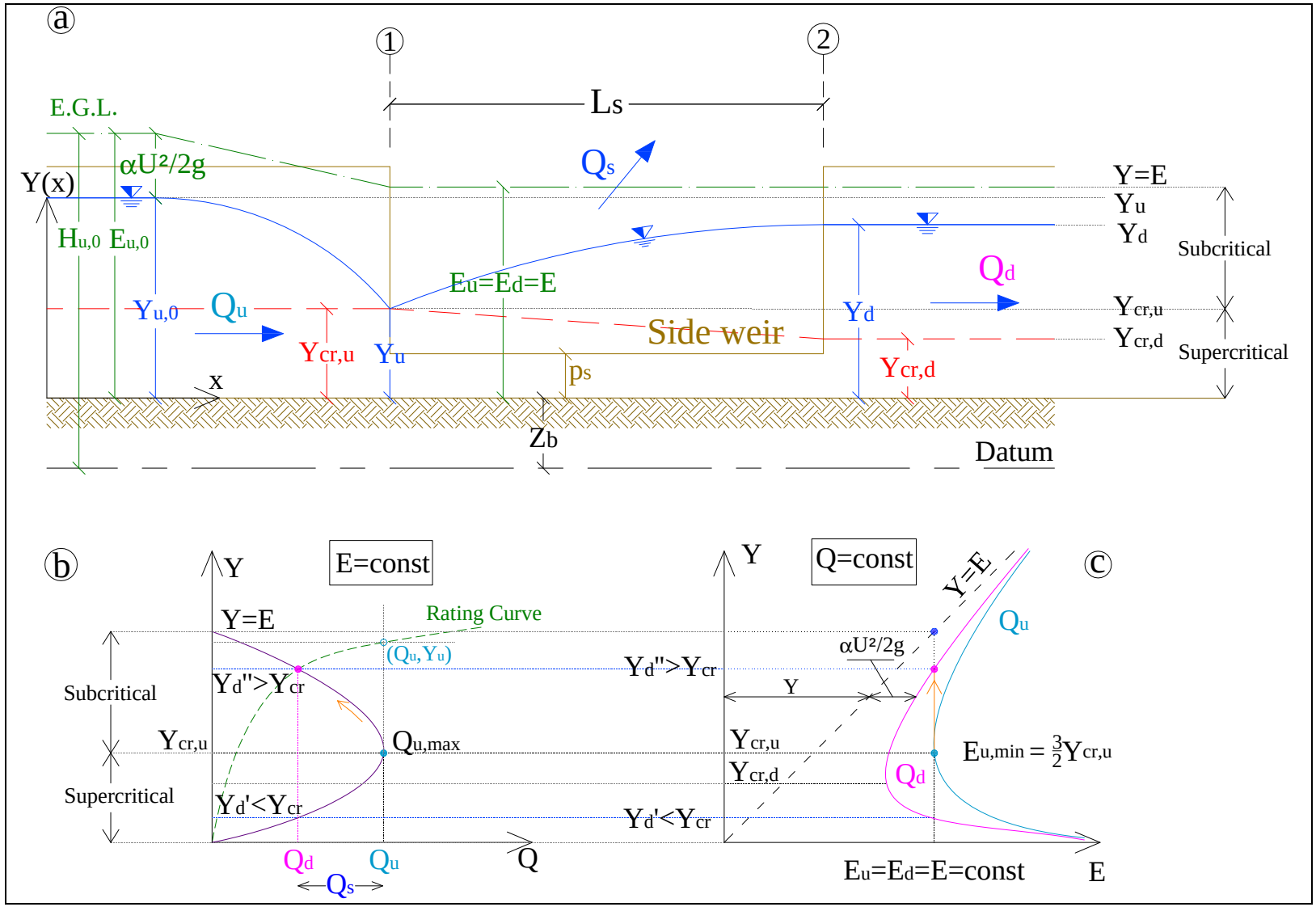

Figure 5.6: Overview of the hydraulic functioning of a side weir in case of subcritical flow: a) flow depth along the channel; b) Y-Q function; c) Y-E function.

5.2 The De Marchi's analytical model

The hydrodynamics of the flow in a river where a levee breach occurs is quite complex and it is surely endowed with three-dimensional features of the variables (e.g., flow velocity and bed geometry). Such a problem should be addressed by a complete 3D mobile bed unsteady flow model, based on the Navier-Stokes equations (NS), which can attempt to describe the physical system without introducing strong assumptions.

The general case of the flow of viscous and incompressible fluid is described by the Navier–Stokes equations and the continuity equation, which are derived from the momentum and mass conservation principles, respectively.

Although the Navier–Stokes equations describe all forms of flow, in practice they are useful for laminar flow only, while open channel flow is turbulent and random fluctuations of velocities and pressure are present. Since it is impossible to describe these fluctuations, the instantaneous value is expressed in terms of a time-averaged value and its random part (leading to the RANS, Reynolds Averaged Navier-Stokes equations) and the turbulent stresses have to be modelled (e.g., Boussinesq concept of the eddy viscosity).

The application of the full NS-equations allows to describe the three-dimensional features of the flow. However, the use of a 3D-NS model is not an easy task, since it requires sophisticated numerical techniques and significant computational power. Moreover, these equations need a turbulence model to be solved and some parameters will have anyway to be chosen/calibrated in order to fit every single situation considered.

Such a model would not be a handy tool, since it provides a very detailed behaviour of the flow field for specific channel geometries, flow parameters and boundary conditions, which may be less intuitive than results given by simpler models.

The three-dimensional equations can be simplified by means of mathematical operations of average of the variables in space. A two-dimensional model is obtained when the variables are integrated over the flow depth, hence neglecting their vertical components, while a one-dimensional model results from averaging the state variables on the cross-section. One-dimensional models are usually applied in river engineering, since a river has a predominant direction (the longitudinal one) along which the flow develops. Even if there are particular situations where 3D flow features are relevant (e.g., flow around bridge piers, side weir flows, …), a 1D model is a handy and useful tool to understand the main physical mechanisms acting on the system before performing a very detailed numerical analysis. Simplified models are easier to be implemented and they can lead to analytical demonstration of some characteristics of the investigated phenomena. Moreover, simple models are suggested as first step to understand complex phenomena whose behaviour is not well-known.

5.2.1 Mathematical formulation

The longitudinal rate of change of the water depth along a side weir can be predicted by applying the continuity equation coupled with the energy or momentum equation in the framework of one-dimensional steady flow.

The side weir flow model is developed under the assumptions of:

1. Steady spatially-varied flow;
2. One-dimensional flow;
3. Fixed bed conditions;

4. Small curvature of the flow (vertical variation in pressure remains hydrostatic);
5. Horizontal water surface across each cross-section in the main channel;
6. Critical flow depth at the side weir crest (with subcritical approaching flow and supercritical flow on the land side);
7. Applicability of a classical weir equation to the flow that spills over the side weir.

Some of these assumptions can apply better than other to the case of levee breach, especially regarding the *critical flow depth* at the weir crest (if no backwater effects from the protected side are considered) and the validity of a *side weir equation* for the lateral outflow calculation, as pointed out by Saucier et al. (2009). This assumption would be not completely fulfilled if tailwater on the protected land raises due to the flooding. In such a case, backwater effects may occur from the protected land, which limit the breach discharge. Nevertheless, side weir equation may be used as well, by considering a reduced discharge coefficient.

The *steady flow hypothesis* is applicable to the case of a levee breach if the time scale of the breaching process is much smaller than the time scale of the flood wave. Analysis under steady conditions is useful to investigate equilibrium conditions in the system.

On the other hand, *fixed bed* and *1D flow conditions* can conflict with a more realistic situation, in which the channel is endowed with movable bed and flow is 3D.

In the following elaborations, the breach is treated as a side weir of length L_s: the breach channel is considered to be rectangular as first approximation though a breach channel with rather trapezoidal shape commonly develops. The weir crest is taken at the main channel bottom ("zero height crest"), since field experience and laboratory investigations on dam embankments and river levees show that a breach primarily deepens until the levee toe and then it lengthens until it gets the final length (Hahn et al., 2000; Islam, 2012). The river reach along the breach is sketched as a straight prismatic channel with cross-section of constant rectangular shape of width B. The river bed, as well as the side weir, are considered to be not-erodible, i.e. the geometric boundary of the main channel is fixed.

The lateral outflow is analysed by means of the side weir theory. The one-dimensional equation for spatially-varied flow may be formulated in two alternative forms, depending on whether the derivation is based on energy or momentum conservation.

In the energy approach, the governing equations are the continuity and the energy equations:

$$\begin{cases} \dfrac{dE}{dx} = S_0 - S_f \\ \dfrac{dQ}{dx} = -q_s \end{cases} \tag{5.1}$$

where Q [m^3/s] is the discharge in the channel at a section x; q_s [m^2/s] is the discharge spilling through the side weir per unit length; E [m] is the specific energy head in the channel at a section x; S_0 [–] is the bed slope; S_f [–] is the energy gradient (or friction slope) and the local energy losses due to the overflow process are supposed to be negligible.

The specific energy head E at a section x is given by:

$$E(x) = Y(x) + \frac{\alpha(x)}{2g} \cdot \frac{Q^2(x)}{A^2(x)} \tag{5.2}$$

in which Y(x) [m] is the water depth profile in front of the lateral weir; g is the gravity acceleration [m/s^2]; α [–] is the Coriolis velocity distribution coefficient and A [m^2] is the wetted cross-section area.

By differentiating equation 5.2 and considering equations 5.1, and by using the classical weir equation for the spill flow, the following differential equations are written:

$$\begin{cases} \dfrac{dY(x)}{dx} = \dfrac{S_0 - S_f - \dfrac{\alpha(x)\cdot Q(x)}{g\cdot A^2(x)}\cdot\dfrac{dQ(x)}{dx} + \dfrac{\alpha(x)\cdot Q(x)}{g\cdot A^2(x)}\cdot\dfrac{\partial A(x)}{\partial x} - \dfrac{Q^2(x)}{2g\cdot A^2(x)}\cdot\dfrac{d\alpha(x)}{dx}}{1-\alpha(x)\cdot Fr^2(x)} \\ \dfrac{dQ(x)}{dx} = -q_s = C_d\cdot\sqrt{2g}\cdot\left(Y(x)-p_s\right)^{3/2} \end{cases} \tag{5.3}$$

where C_d [–] is the discharge coefficient assumed constant along the breach; B [m] is the wetted width of the cross-section (channel width at water surface); Fr [–] is the Froude number. The term ($Y–p_s$) represents the pressure head (without velocity head) above the weir crest.

Under the further assumptions of Coriolis coefficient α equal to unity and weir height p_s set to zero, equations 5.3 are simplified in:

$$\begin{cases} \dfrac{dY(x)}{dx} = \dfrac{S_0 - S_f - \dfrac{Q(x)}{g\cdot A^2(x)}\cdot\dfrac{dQ(x)}{dx}}{1-Fr^2(x)} \\ \dfrac{dQ(x)}{dx} = -q_s = C_d\cdot\sqrt{2g}\cdot\left(Y(x)\right)^{3/2} \end{cases} \tag{5.4}$$

The water profile along the side weir can be calculated by solving equations 5.4.

Equations 5.4 are ordinary differential equations of the first order, which describe the variation of the water profile Y(x) along the side-weir according to the principle of energy conservation. Equations 5.4 need one boundary condition to be solved: depending on whether the approaching flow at upstream section is subcritical or supercritical, a downstream or an upstream condition is assigned.

An analytical solution of the side weir problem was derived by De Marchi in 1934.

He stated that the specific energy head of the main flow can be assumed constant along the side weir, which is valid if the energy losses are negligible and the difference of the bed elevations at the up- and the downstream sections is small, so that the difference $S_0–S_f$ is negligible. Many authors (Subramanya and Awasthy, 1972; Borghei at al., 1999; Muslu, 2001; Rosier et al., 2008) followed the De Marchi hypothesis when modelling side weir with subcritical approaching flow even for movable bed conditions (Paris et al., 2012). According to the De Marchi assumption, the specific energy head E is assumed constant and the equations (5.4) are rewritten as:

$$\begin{cases} \dfrac{dY(x)}{dx} = -\dfrac{Q(x)\cdot Y(x)\cdot\dfrac{dQ(x)}{dx}}{g\cdot B^2\cdot Y^3(x) - Q^2(x)} \\ \dfrac{dQ(x)}{dx} = -q_s = -C_d\cdot\sqrt{2g}\cdot\left(Y(x)\right)^{3/2} \end{cases} \tag{5.5}$$

An analytical solution of equations (5.5) was found by De Marchi (1934) for subcritical flow, and it solves for the longitudinal axis x given the flow depth Y:

$$\begin{cases} \dfrac{C_d}{B}x = \Phi(Y,E) + C \\ \Phi(Y,E) = 2\sqrt{\dfrac{E-Y}{Y}} - 3\sin^{-1}\sqrt{\dfrac{E-Y}{E}} \end{cases} \tag{5.6}$$

where C is an integration constant determined from the boundary conditions.

The De Marchi solution of the side weir problem is simple to be applied, once the upstream and the downstream conditions are given. The upstream condition is represented by the inflow Q_u, whereas a rating curve is a common downstream condition.

The downstream flow rate Q_d is determined by the flow rating curve once the downstream flow depth Y_d is given. In such a way, the downstream specific energy head E_d is determined to be the energy E^* governing the process of the side weir flow.

Equations (5.6) can be solved from the downstream section in the upstream direction: an imposed variation of the flow depth Y gives the axis x where that variation occurs and the related flow discharge at that section is given by $Q(x) = B \cdot Y(x) \cdot \sqrt{2g\left(E^* - Y(x)\right)}$. The solving is performed until the Q_u is obtained, and then the flow depth profile Y(x) along the weir and its total length are gained.

Otherwise, the length of the weir can be directly calculated without solving for the whole depth profile, once the upstream flow depth Y_u is obtained from equation (5.7):

$$E^* = Y_u + \frac{Q_u^{\,2}}{2gA_u^{\,2}} \tag{5.7}$$

The length of the weir is then determined by the Φ-function:

$$L = x_d - x_u = \frac{B}{C_d} \cdot \left[\Phi\left(Y_d, E^*\right) - \Phi\left(Y_u, E^*\right)\right] \tag{5.8}$$

and the related outflow discharge Q_s is given by the difference between Q_u and Q_d:

$$Q_s = \int_0^L q_s \cdot dx = Q_u - Q_d = B \cdot \sqrt{2g} \cdot \left[Y_u \cdot \sqrt{(E^* - Y_u)} - Y_d \cdot \sqrt{(E^* - Y_d)}\right] \tag{5.9}$$

This is the classical analysis of the side weir flow by means of the De Marchi approach.

5.2.2 New form of the De Marchi solution

The described approach is generalized and developed in this thesis by introducing some dimensionless variables in the De Marchi solution.

Let us consider the dimensionless function Φ(Y, E) as a function of the Froude number in order to study its behaviour, that is plotted in Figure 5.7:

$$\Phi = Fr\sqrt{2} - 3\sin^{-1}\left(Fr\sqrt{\frac{1}{2+Fr^2}}\right) \tag{5.10}$$

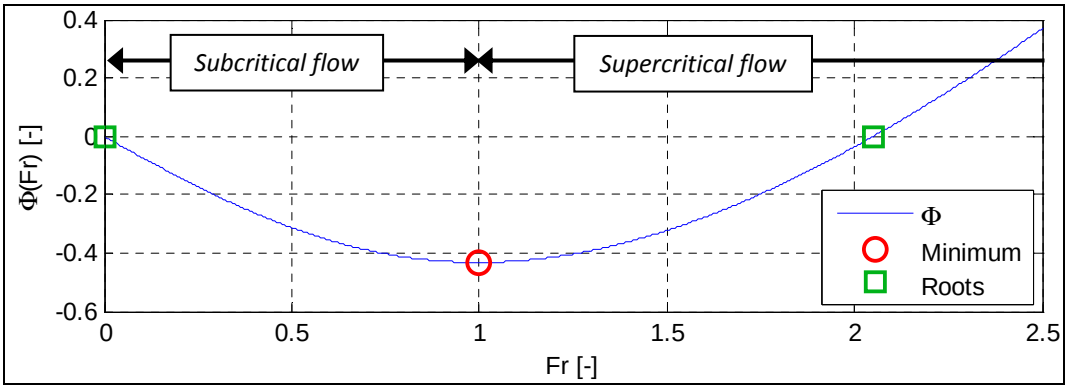

Figure 5.7: Φ as a function of Fr: roots and minimum detection.

The function Φ has a minimum for Fr = 1, which defines the critical state Y = Y_{cr}. Moreover, the function has two roots: one for Fr ≈ 2.052 and the other one for Fr→0. The first one is in the range of supercritical flows, whereas the second one is a border condition which is gained when the flow depth tends to equal the specific energy head. In the second case, the kinetic head is so low that almost no water flows along the channel. In the range of subcritical flows (0 < Fr < 1), Φ gets values between 0 and −0.4322.

Let us represent the breach situation by the two Froude numbers which identify the flow conditions in the main channel at the upstream (Fr_u) and downstream (Fr_d) sections of the breach. Fr_u and Fr_d identify in a dimensionless form the characteristics of the main channel flow incoming upstream and remaining downstream, respectively. Different zones of the "*Froude graph*" in the plane of the state variables Fr_u and Fr_d are distinguished (Figure 5.8).

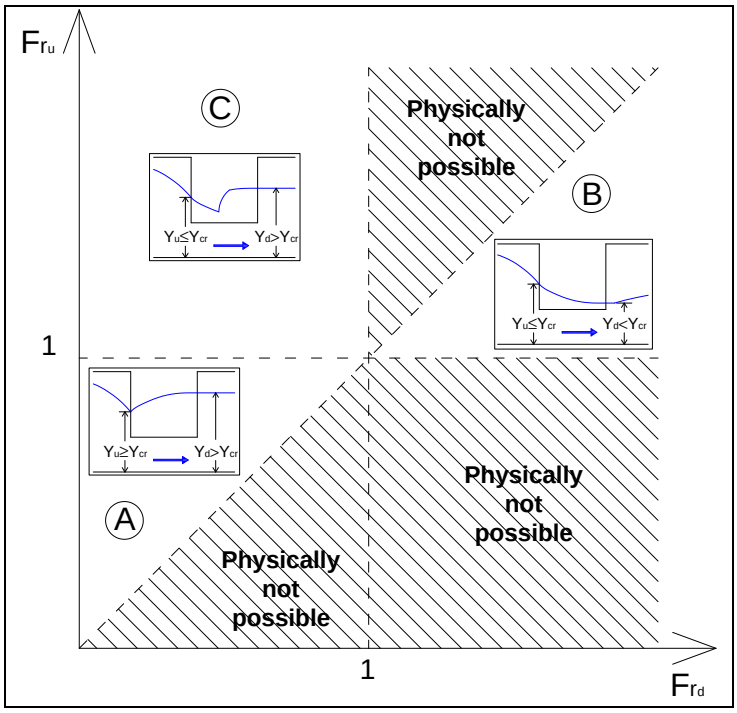

Figure 5.8: Side weir situation into "Froude graph": A) subcritical; B) supercritical; C) hydraulic jump.

The areas of Figure 5.8 are referred to the most common flow field conditions, which were already described in Figure 5.5:

- Zone A: the flow is subcritical along all the reach, with the upstream flow depth greater than the critical depth, the flow profile increasing downstream and the Froude number decreasing downstream;
- Zone B: the flow is supercritical along all the reach, with the upstream flow depth equal or lower than the critical depth, the flow profile decreasing downstream, and the Froude number increasing downstream;
- Zone C: the incoming flow is supercritical, but a hydraulic jump is encountered within the weir since a subcritical condition is imposed downstream.

The dashed zones identify flow combinations that are not physically possible: a subcritical flow before the weir will make the depth profile increasing and the flow velocity decreasing and, as a consequence, the downstream Froude number will be lower than the upstream one. In the same way, a supercritical approaching flow will develop towards greater values of Froude number downstream, except when a downstream control requires a depth larger than the critical one.

An analytical demonstration of such a behaviour is given by Montes (1998). For a rectangular section, the longitudinal variation of the Froude number is given by:

$$\begin{cases} \dfrac{dFr(x)}{dx} = \dfrac{d\left(\dfrac{Q(x)}{B\sqrt{g}\cdot Y^{3/2}(x)}\right)}{dx} \\ \dfrac{dY(x)}{dx} = \dfrac{-Fr^2(x)\dfrac{Y(x)}{Q(x)}\cdot\dfrac{dQ(x)}{dx}}{1-Fr^2(x)} \end{cases} \longrightarrow \frac{dFr(x)}{dx} = \frac{Fr(x)}{2Q(x)}\cdot\frac{dQ(x)}{dx}\cdot\left(\frac{2+Fr^2(x)}{1-Fr^2(x)}\right) \qquad (5.11)$$

In which the derivative dY/dx is given by a rearrangement of first equation of system 5.5.

This expression shows that there cannot be changes in the flow regime along the weir (at least for a main channel with rectangular section and fixed bed): since $dQ/dx < 0$, a channel with subcritical flow before the weir makes the Froude number to decrease ($dFr/dx < 0$) and then the flow remains subcritical. In the same way, a supercritical flow approaching the side weir remains supercritical with greater Froude numbers ($dFr/dx > 0$), except when a downstream subcritical flow is imposed in the main channel.

According to the assumption of subcritical flow up- and downstream the breach, the possible flow combinations within zone A are considered (in which $Fr_d \leq Fr_u \leq 1$).

The breach problem is solved as a function of the following dimensionless parameters:

- Flow depth ratio $r_Y = Y_d/Y_u$
- Discharge ratio $r_Q = Q_s/Q_u$
- Length ratio $r_L = L_s/B$

The solution is achieved by writing the governing principles of conservation of mass and energy balance in function of the dimensionless parameters.

Particularly, from the principle of constant specific energy head one gets (see Annex A for the mathematical demonstration):

$$r_Y = \frac{Y_d}{Y_u} = \frac{2+Fr_u^{\,2}}{2+Fr_d^{\,2}} \qquad (5.12)$$

From the continuity principle, it results:

$$r_Q = \frac{Q_s}{Q_u} = 1 - \frac{Fr_d}{Fr_u} r_Y^{\,3/2} \qquad (5.13)$$

And finally the length ratio is given by the De Marchi equation:

$$r_L = \frac{L_s}{B} = \frac{\Phi_d - \Phi_u}{C_d} \qquad (5.14)$$

where Φ is a function of Froude number, as in equation 5.10.

5.2.3 Model implementation in subcritical flow

The solution of the proposed model is solved for each admissible combination of Froude numbers (zone A in Figure 5.8). Any couple of considered Froude numbers can be obtained as a combination of different values of the imposed independent variables, which are: the main

channel geometry, the roughness, the bed slope, the input discharge, and the boundary conditions, i.e. the downstream rating curve.

The results of the model are shown by Figures 5.9-5.11 in terms of dimensionless parameters: the 45° line defines the condition of $Fr_u = Fr_d$, which occurs when no lateral outflow takes place in the channel ($Q_s = 0$). In such a situation the water depth and discharge upstream remain unchanged downstream and no lateral outflow occurs in the main channel ($r_Y = 1$, $r_Q = 0$, $r_L = 0$).

On the other hand, in the region where $Fr_u > Fr_d$ an outflow is possible, which makes the water depth increasing downstream ($r_Y > 1$) and the flow discharge decreasing ($r_Q > 0$) along the breach length ($r_L > 0$). This trend develops when Froude numbers is increasing upstream and decreasing downstream until, as a limit case, a critical state occurs in the upstream section ($Fr_u = 1$). A further limit is represented when no flow takes place downstream ($Fr_d = 0$), which is depicted in the upper left corner of the graphs. In that situation, r_Y tends to 1.5, r_Q to 1 and r_L to 1.1.

The maximum flow depth ratio is constant for a subcritical flow, since, in that limit case, the downstream depth is equal to the specific energy head E and the upstream depth equals the critical depth, which, for a rectangular channel, is $Y_{cr} = 2/3 \cdot E$. As a matter of fact: $(Y_d/Y_u)_{max} = E/(2/3 \cdot E) = 1.5$.

The ratio L_s/B expressed in equation (5.14) and plotted in Figure 5.11 is dependent on the value of the weir discharge coefficient C_d: different values and different methods for estimating C_d can be assumed. In the literature, there are a number of methods proposed for evaluating the discharge coefficient for side weir overflow (Borghei et al., 1999).

The theoretical analysis of the flow over a broad-crested weir states (Bélanger, 1849):

$$Y_{cr} = \frac{2}{3}(Y - p_s) = \sqrt[3]{\frac{q^2}{g}} \longrightarrow q = \left[\left(\frac{2}{3}\right)^{3/2} \cdot \frac{1}{\sqrt{2}}\right] \cdot \sqrt{2g(Y - p_s)^3}$$

which brings to the typical value of discharge coefficient for broad-crested weir

$$C_d = \left[\left(\frac{2}{3}\right)^{3/2} \cdot \frac{1}{\sqrt{2}}\right] = 0.385 \tag{5.15}$$

Preissler and Bollrich (1980) proposed the use of a reduced, constant overfall coefficient:

$$C_d = \frac{2}{3} \cdot \sigma \cdot C_w \tag{5.16}$$

with $\sigma = 0.95$ reduction factor and $C_w = [0.49 \div 0.51]$ weir coefficient.

Hager (1987) identified the discharge coefficient for a sharp-crested side weir of zero height as dependent on the approach Froude number Fr_u in the main channel:

$$C_d = \frac{2}{3} \cdot 0.485 \cdot \sqrt{\frac{2 + Fr_u^2}{2 + 3Fr_u^2}} \tag{5.17}$$

Kamrath et al. (2006) developed a *dike break formula* to calculate flow through a dike breach. They proposed the coefficient C_d to be a function of approaching Froude number and the ratio between the width of the floodplain b_{fp} at the river side and the breach length L_s:

$$C_d = \frac{2}{3} \cdot 0.577 \cdot \left\{ 0.1446 \cdot \ln\left[0.4 \cdot \sqrt{Fr_u} \cdot \left(\left(1.18 - \sqrt{Fr_u} \right) \cdot \frac{b_{fp}}{L_s} \right)^2 \right] + 0.6895 \right\} \quad (5.18)$$

Recently, Oertel et al. (2011) carried out investigations to determine the discharge coefficient for flat broad side weirs in river with subcritical conditions. They expressed the dependence of the discharge coefficient on the main channel's Froude number, the channel width and the weir length:

$$C_d = \frac{2}{3} \cdot \left\{ 0.05 \cdot \log\left[0.7 \cdot \sqrt{Fr_u} \cdot \left(1.44 - 2.4\sqrt{Fr_u} + Fr_u \right) \cdot \left(\frac{B}{L_s} \right)^2 \right] + 0.35 \right\} \quad (5.19)$$

The use of these C_d-functions into the proposed approach influences the value of r_L ratio (see equation 5.14), but it does not modify the general behaviour of the system. Table 5.1 lists the maximum ratio r_L found by applying some different C_d-functions: the upper limitation of L_s/B is still in the order of the river width. Note that the application of C_d-formulation proposed by Oertel et al. (2011) into the length ratio (equation 5.14) needs an iterative routine to be solved, since the L_s/B ratio is also implicitly included into the discharge coefficient. Equation 5.18 is not used for this analysis because the parameter b_{fp} is not defined in a rectangular main channel.

Table 5.1: r_L maximum values for different C_d methods.

C_d-method	**Equation**	**C_d-value**	**r_{Lmax}**
Theoretical broad-crested weir	Eq. 5.15	$C_d = 0.385$	1.12
Constant overfall coefficient	Eq. 5.16	$C_d = 0.317$	1.36
Zero height sharp-crested side weir	Eq. 5.17	$C_d = 0.323$, for $Fr_u=0$ $C_d = 0.250$, for $Fr_u=1$	1.73
River broad side weir	Eq. 5.19	$C_d = 0.166$, for $Fr_u \approx 0$ and $B/L=1/3$ $C_d = 0.150$, for $Fr_u=1$ and $B/L=1/3$ $C_d = 0.229$, for $Fr_u \approx 0$ and $B/L=3$ $C_d = 0.213$, for $Fr_u=1$ and $B/L=3$	2.86

The following outcomes were performed with $C_d = 0.385$, as typical value for broad-crested overflow weirs.

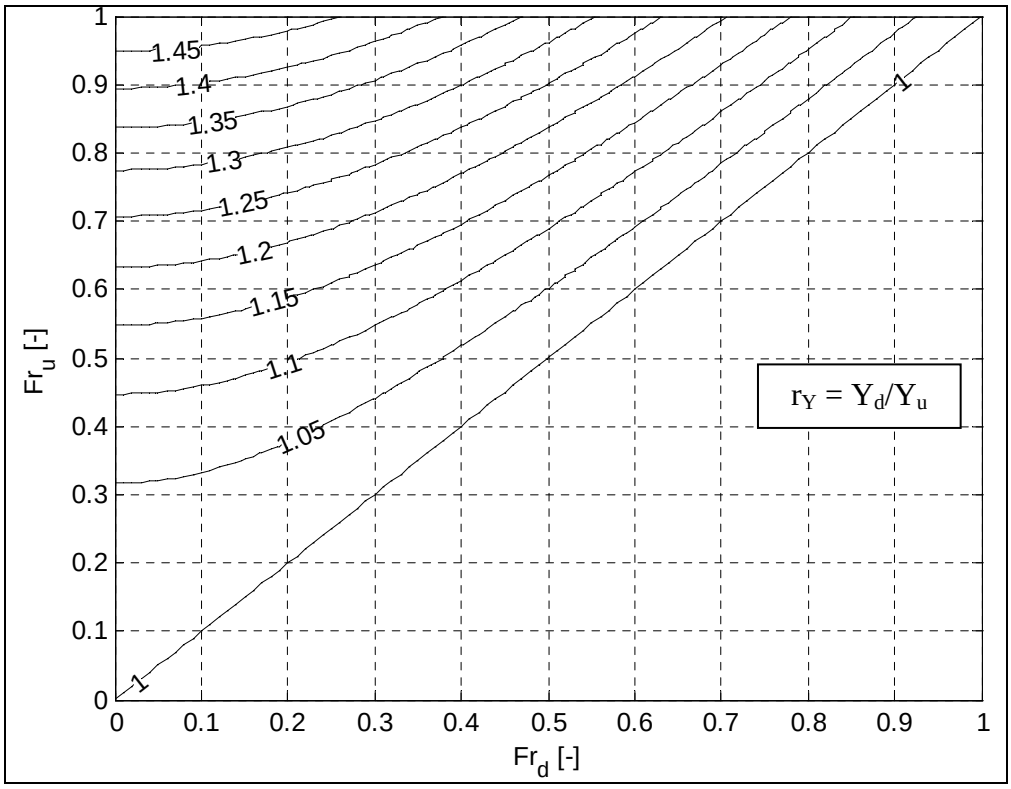

Figure 5.9: Flow depth ratio r_Y contours in the Froude graph.

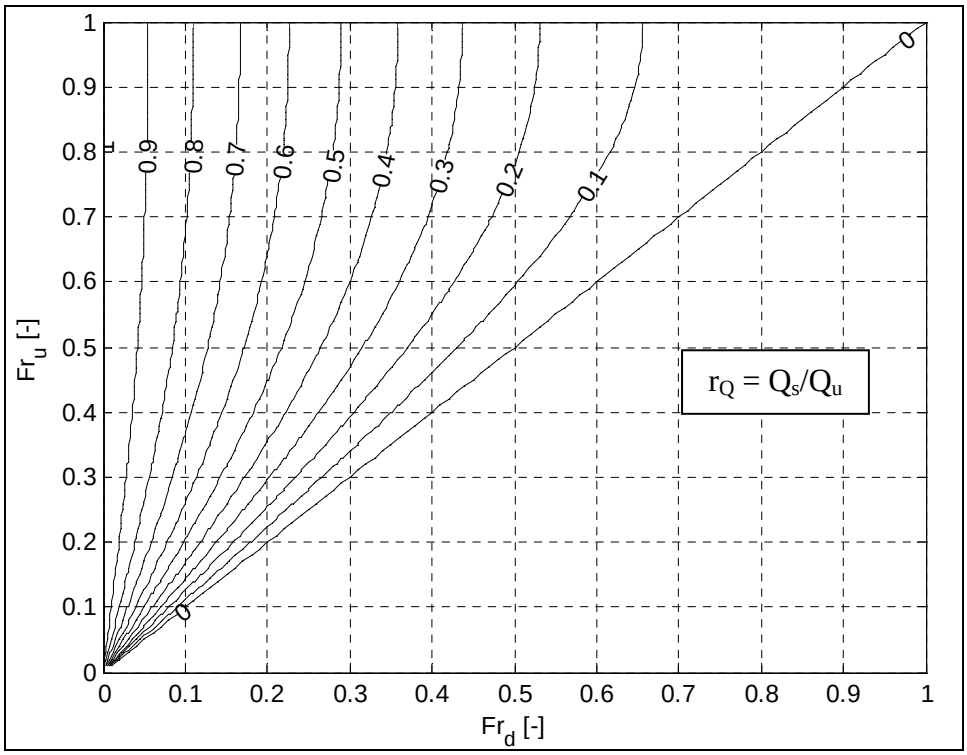

Figure 5.10: Discharge ratio r_Q contours in the Froude graph.

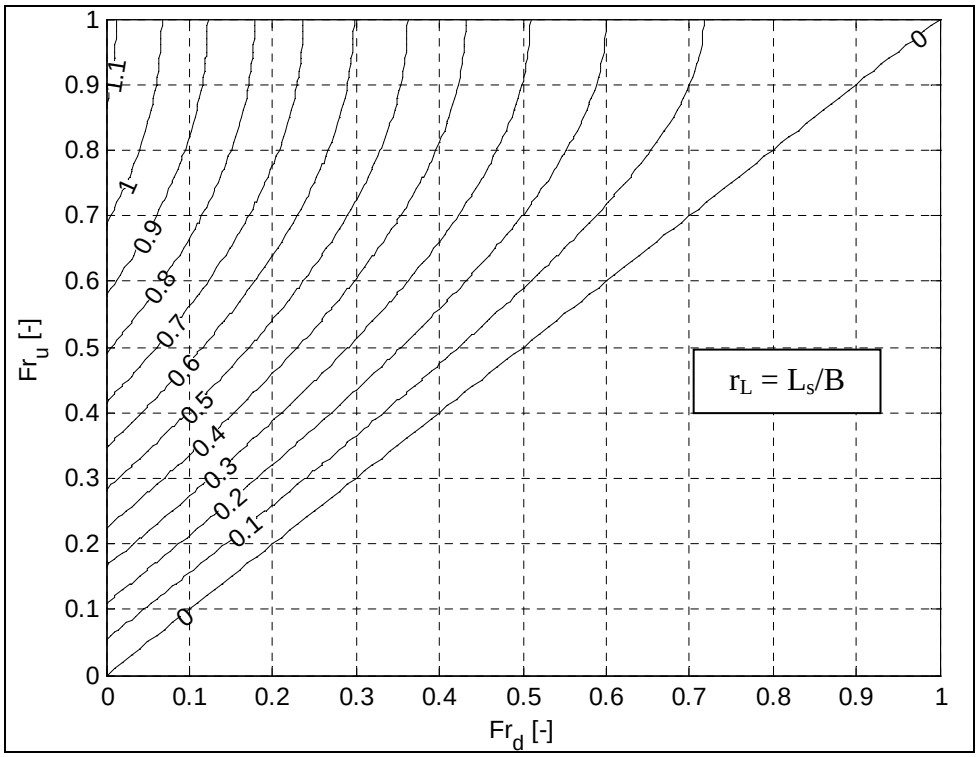

Figure 5.11: Length ratio r_L contours in the Froude graph.

Other dimensionless ratios between the variables predicted at the up- and downstream sections can be calculated:

- Flow velocity ratio $r_U = U_d/U_u = (1-r_Q)/r_Y$
- Shear stress ratio $r_\tau = \tau_d/\tau_u = r_U^2$

Figures 5.12 and 5.13 show that in case the lateral outflow takes place (region $Fr_u > Fr_d$), the mean flow velocity is reduced at the downstream section and, consequently the shear stress (proportional to the square of the mean flow velocity) also strongly decreases.

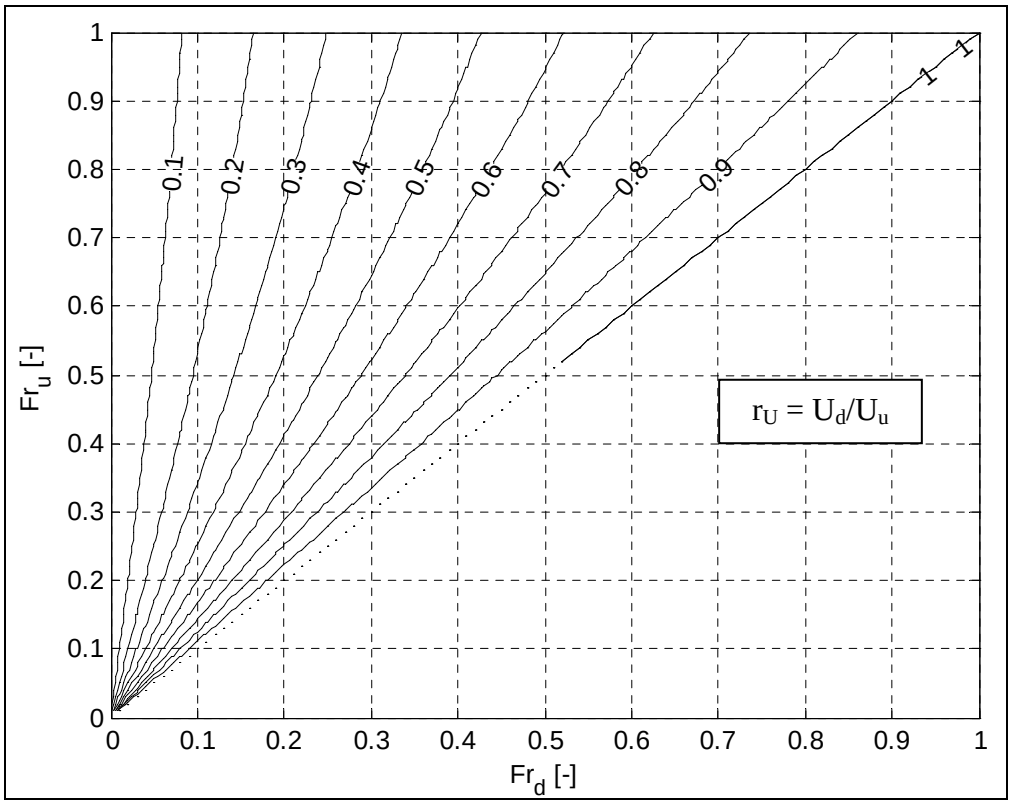

Figure 5.12: Flow velocity r_U contours in the Froude graph.

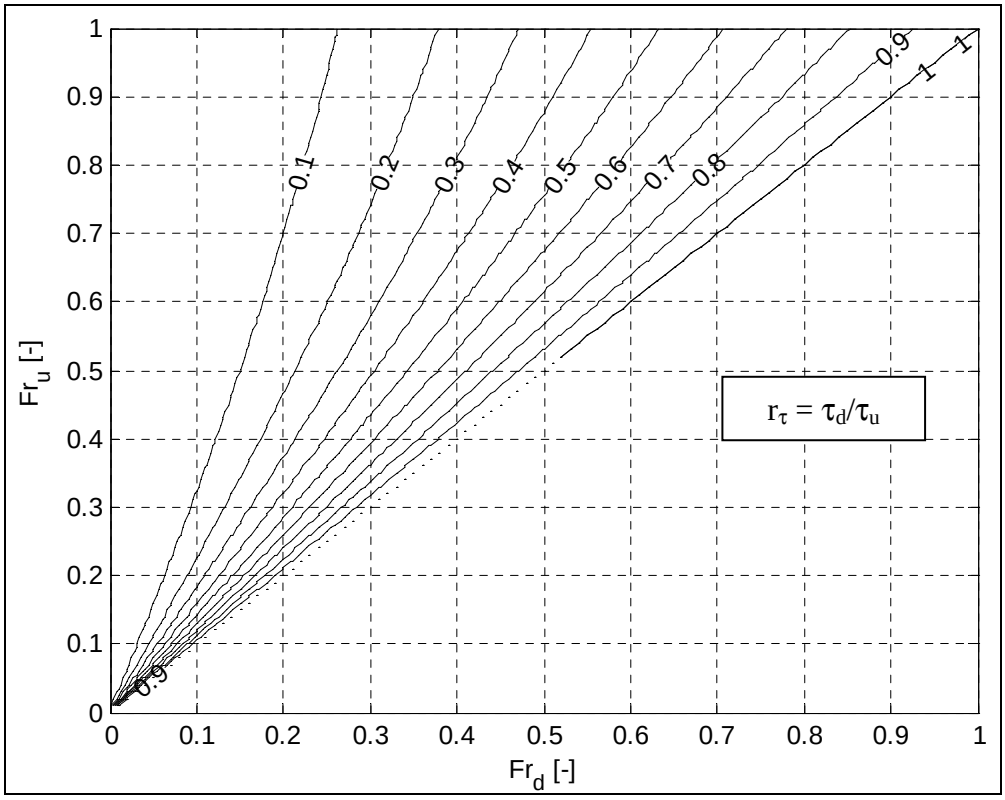

Figure 5.13: Shear stress r_τ contours in the Froude graph.

5.3 Application of the proposed model to laboratory and field data

5.3.1 Application to available laboratory data

The proposed analytical model is tested on available laboratory data in order to verify its validity in the range of the subcritical flows along side weirs.

Experimental data coming from laboratory measurements are compared with predicted values of the dimensionless ratios according to the proposed model. Basically, only the up- and the downstream Froude numbers are necessary to apply the model: the flow depth ratio r_Y, the discharge ratio r_Q and the length ratio r_L are calculated on the basis of those information.

Data reported into the Figures 5.14-5.16 are related to several experimental investigations, whose conditions are reported in Table 5.2.

Table 5.2: Main testing conditions of analysed laboratory data.

Laboratory test	**Reference**	**Side weir length [m]**	**Side weir height [m]**	**Inflow discharge [m^3/s]**	**Upstream Fr [–]**	**Downstream Fr [–]**
"El-Khashab & Smith"	El-Khashab and Smith (1976)	2.3	0.2	0.14	0.73	0.23
"Hager (1982)a"	Muslu et al. (2003)	1	[0.1÷0.2]	[0.039÷0.04]	[0.35÷0.87]	[0.18÷0.37]
"Hager (1982)b"	Yüksel (2004)	1	[0.1÷0.2]	[0.037÷0.039]	[0.29÷0.62]	0
"Hsu et al. (2002)*"	Hsu et al. (2002)	0.147 (lateral diversion)	0 (lateral diversion)	[0.003÷0.005]	[0.33÷0.77]	[0.14÷0.55]
"Present study (fixed bed)"	Michelazzo (2013)	[0.03÷0.47]	0	0.01	[0.22÷0.83]	[0.14÷0.51]

All the listed experiments were conducted in fixed bed main channels with rectangular cross section. The side weirs had rectangular shapes with different values of the length and of the height. Subcritical flow conditions were achieved during the tests. The data of series "Present study (fixed bed)" are part of the present PhD work and the related description is presented in Chapter 3. The data collected by Hsu et al. (2002) concern a flow regime different from the side weir situation: they are related to a lateral diversion, which is a rectangular channel departing from the main channel. The diversion had the same cross section geometry of the main channel and the connection angle was at 90 degrees. Lateral diversion data were analysed because they can provide some more insights about lateral outflow processes from a zero height sill, as this is the main focus of the present levee breach study. Anyway, these data were compared with the model regarding the flow depth and discharge ratios, whereas the length ratio was not analysed since the outflow of a lateral diversion can not be modelled by the side weir law.

Results presented in Figure 5.14-5.16 show that the proposed analytical model gives a good prediction of the flow conditions in terms of flow depth ratio and flow discharge ratio

within an error of ± 10%. The validity of De Marchi hypothesis is confirmed for lateral weir experiments as well as for lateral diversion tests. The ratio between the weir length and the main channel width is affected by higher errors (about ± 20%), which may be due to the estimation of the discharge coefficient C_d: the coefficient was set equal to a standard value of 0.385 for the first three tests regarding side weirs, while Hsu data and present-study-data were analysed by means of the Hager formulation (Hager, 1987), developed for side weirs of zero height.

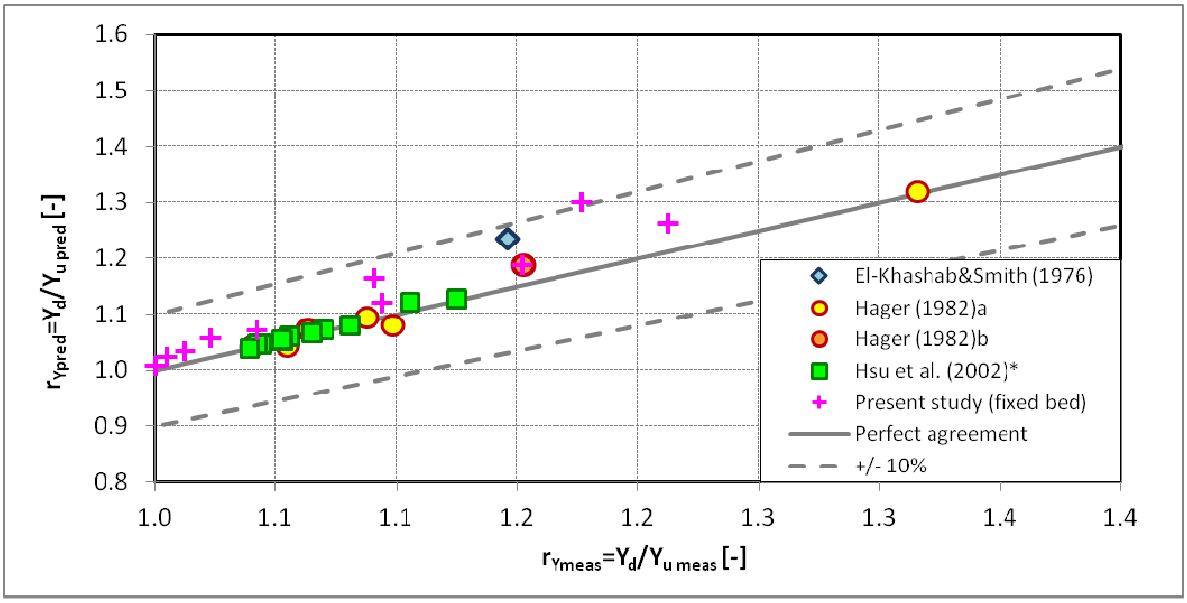

Figure 5.14: Comparison between measured and predicted depth ratios for laboratory data.

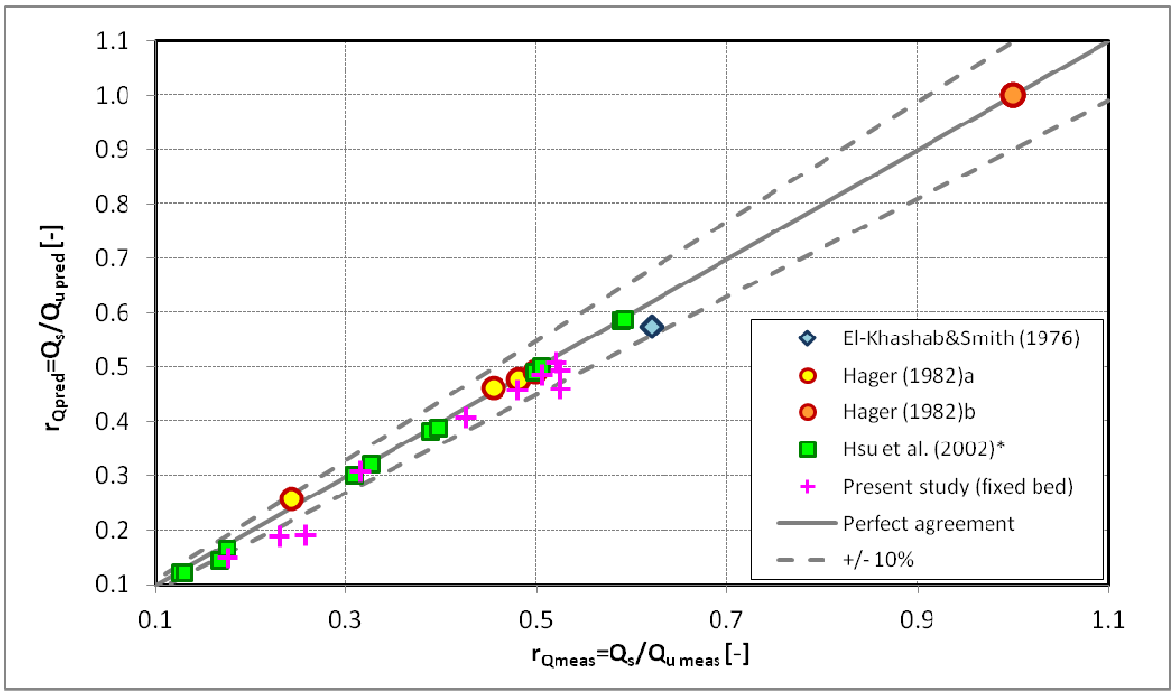

Figure 5.15: Comparison between measured and predicted discharge ratios for laboratory data.

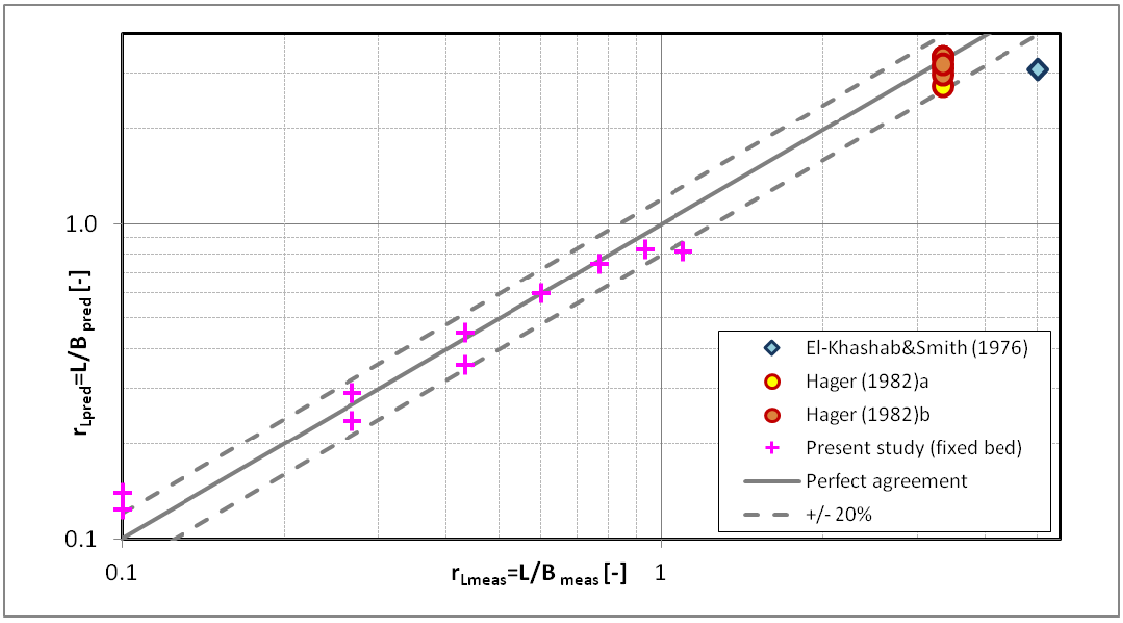

Figure 5.16: Comparison between measured and predicted length ratios for laboratory data.

5.3.2 Application to real river levee breach data

5.3.2.1 The context of real rivers

The proposed analytical model is applied to reproduce the steady one-dimensional features of the flow in a main channel when a lateral outflow takes place because a breach develops in the lateral levee. It is therefore relevant to extend the previous considerations to the context of real rivers in an attempt to apply the model for real levee breaches.

A uniform flow discharge in a river without any levee breach, and thus without any lateral outflow, is represented as a point on the 45° line in the Froude graph: i.e., the up- and the downstream Froude numbers coincide ($Fr_u = Fr_d$) since no outflow takes place and the flow regime is not modified from its initial state. On the other hand, when the levee is breached Fr_u differs from Fr_d, so that the point, which represents the flow condition up- and downstream, moves in the Froude graph. It is supposed that the levee crest is eroded until it reaches the toe level (that is the zero level at the main channel bottom in the present schematization) and that a rectangular side weir shape is formed which lengthens in time. As a result, the water depth decreases both at the up- and downstream section: the first one because of the flow acceleration, the second one because of the decreasing of the water discharge.

Now, it can be considered that the flow in the downstream part of the river is governed by the uniform rating curve of the channel itself, so that the variation of the Froude with the water depth is quite slight, i.e.:

$$Fr = \frac{U}{\sqrt{gY}} \approx C_h \sqrt{S_0} \qquad (5.20)$$

Where $C_h \approx 7.66 \cdot (Y/\kappa_r)^{1/6}$ is Chézy coefficient and κ_r [m] is the riverbed roughness.

Equation 5.20 shows that the variation of the Froude number with the flow depth for a uniform flow regime is small, since the uniform flow slope is constant and the resistance coefficient C_h changes only slightly with the flow depth. As a consequence, the downstream Froude should maintain an almost constant value for different lateral outflow scenarios, whereas the upstream Froude number increases: the state of the flow regime for increasing

breach length (and, consequently, for increasing lateral outflow discharge) is then represented as an almost vertical line in the Froude graphs, which starts from the "undisturbed" point (circle in Figures 5.17-5.18) that depends on the initial features (velocity U and depth Y) of the stream flow.

The initial value of the Froude number Fr_0 depends on the river flow features, such as the flood discharge, the channel geometry and roughness, the bed slope, and the boundary conditions (i.e., the downstream flow rating curve).

An estimation of Fr_0 can be obtained from equation 5.20 by considering different possible values of Chézy coefficient and bed slope. The Chézy coefficient for natural rivers in valley zones usually varies into the range (Yen, 2002): $C_h = [10 \div 20]$. If a typical mild slope is assumed ($S_0 = 0.5$ ‰), the Froude number range for a uniform subcritical flow results in:

$$Fr_{unif} = [0.22 \div 0.45]$$

Moreover, assuming the river to be in a regime condition, the hydraulic geometry relations are obtained by the flow regime theory (Singh, 2003):

$$\begin{cases} P = k_1 \cdot Q^c \\ Y = k_2 \cdot Q^d \end{cases} \tag{5.21}$$

Where: P = wetted perimeter [m] and k_1, k_2, c, d are parameters whose values were taken from Singh (2003).

If the river has a width B at the free surface much larger than the mean water depth Y, then $P \approx B$, and the two exponents c and d are set to the widely used values (c = 1/2, d = 1/3), the regime Froude number is achieved from equations (5.21):

$$Fr_{regime} = \frac{1}{\sqrt{g} \cdot k_1 \cdot k_2^{1.5}} \tag{5.22}$$

The parameters k_1 and k_2 usually vary as:

k_1 [-]	k_2 [-]
2.5	0.5
4.5	0.3

The Froude number at the "regime state" is then considered to vary in a range of:

$$Fr_{regime} = [0.36 \div 0.43]$$

The values found for Fr_{unif} and Fr_{regime} agree in defining a subcritical flow regime for a flood discharge in a valley embanked river. Particularly, the Froude number range of uniform flows includes that one of regime state, so that Fr_{unif} can be taken as initial "undisturbed" condition of the river flow. The Froude range is represented as highlighted area in Figures 5.17 and 5.18.

The arrow in Figures 5.17-5.18 shows a possible pattern of the flow regime during a breaching process (at successive times: $t_1 < t_2 < t_3$): downstream Froude number is almost constant if the downstream boundary condition is given by a uniform rating curve, while the upstream one increases as explained previously. The Froude graphs indicate that such a pattern has to be related with increasing breach discharge and increasing breach length, which is consistent with the physics of the phenomenon. The arrow represents a succession of steady states (according to the assumption of the model) so that flow features have to be considered in a regime state at each point of the line, whereas the transient processes are not modelled.

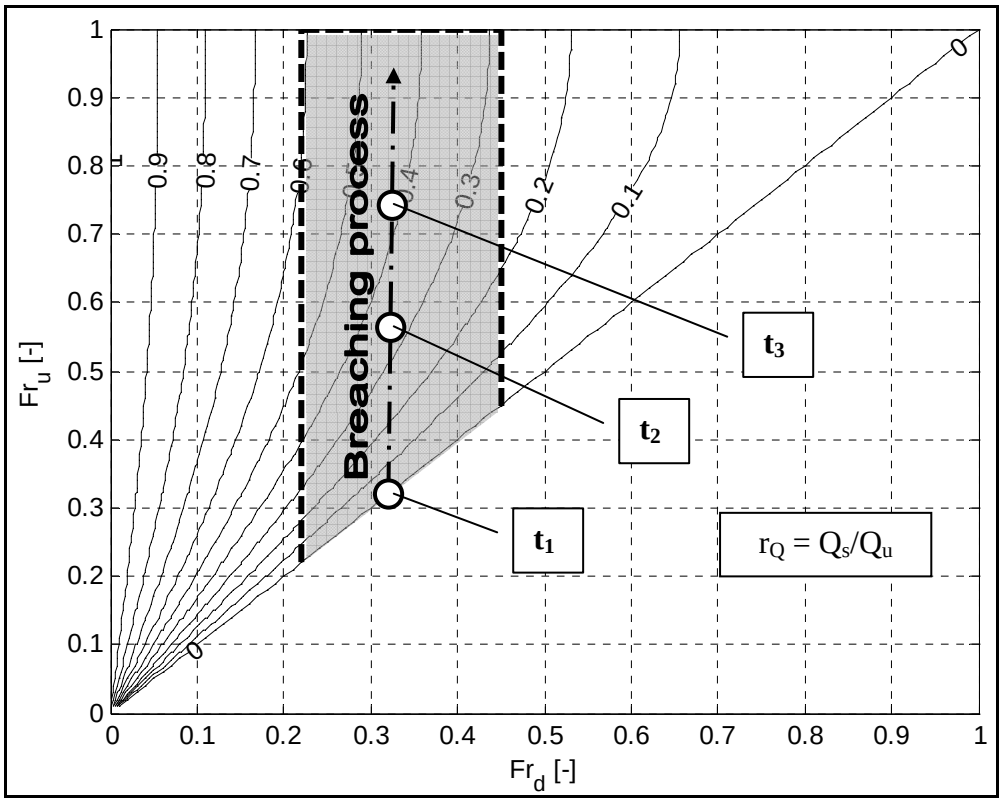

Figure 5.17: Flow regimes during breach opening in the Froude graph with discharge ratio r_Q contours.

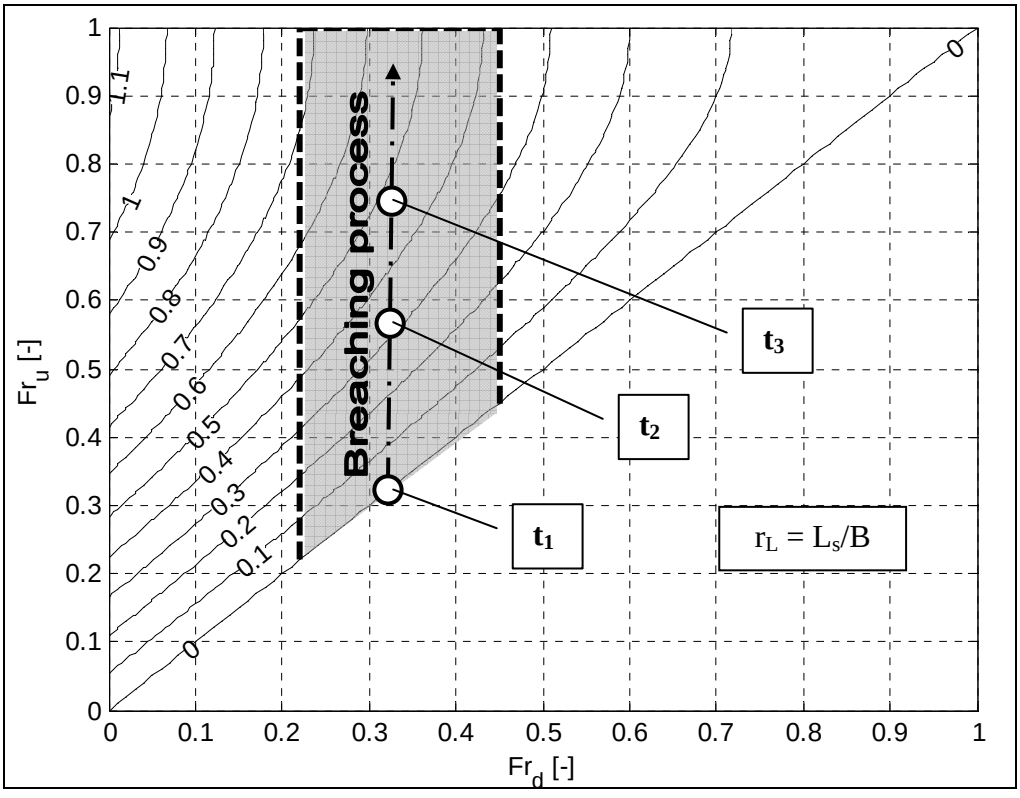

Figure 5.18: Flow regimes during breach opening in the Froude graph with length ratio r_L contours.

5.3.2.2 The levee breach of river Ombrone

The analysis described in Section 5.3.2.1 is applied to the real case of a levee breaching of the Ombrone Pistoiese river (Tuscany - Italy) in December 2009.

The Ombrone Pistoiese river broke a part of its right levee during the flood event of 25 December 2009. The river in the zone close to the breach is straight and regular and the geometry of its cross section is not very far from a rectangular shape. Figure 5.19 shows a plan view of the Ombrone river with location of the breach and Figure 5.22 shows the cross section at the breach site. Some pictures of the breach are reported in Figures 5.20-5.21, which were taken by the Land Reclamation Authority of Ombrone River.

Figure 5.19: Map of levee breach of Ombrone river (Tuscany – Italy).

Figure 5.20: Front view of the breach of Ombrone river (Tuscany – Italy) in December 2009.

Figure 5.21: Side view of the breach of Ombrone river (Tuscany – Italy) in December 2009.

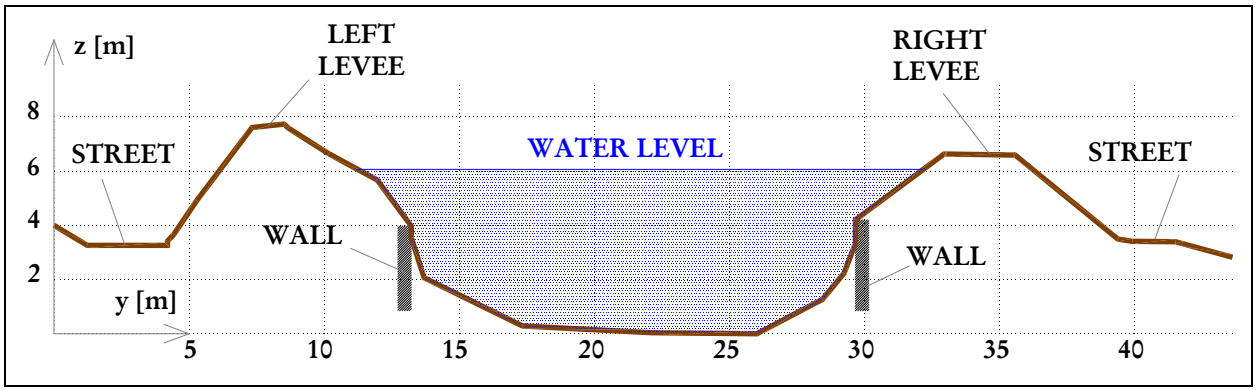

Figure 5.22: Cross-section of the Ombrone river at the breach site (water at flood level before breaching).

Quantitative data about the breach event were provided by the Civil Protection Regional Agency and by other local Water and Land Reclamation Authorities (such as "Consorzio di Bonifica Ombrone Pistoiese"). The following information were collected:

- The levee breach developed quite quickly in a time slot estimated in about 30-45 min and the failure mechanism was likely due to piping phenomena;
- The measured final length of the breach was of about 17 m and it developed until the elevation of a vertical wall, at the base of the right levee section;
- The peak of the outflow discharge was around 90 m^3/s while a water discharge of 192 m^3/s was flowing in the river with a water depth of about 6 m over the river bottom: these information were derived by means of hydrological analysis for the reconstruction of the flood hydrograph at the breach site (which was ungauged) from the nearest hydrometric gauging stations.

The main data of the event are summarized in Table 5.3:

Table 5.3: Flow features of the real breach event of Ombrone river.

River		**Breach**	
River flow discharge at breach time: **Q_u [m^3/s]**	Wetted width at cross-section at breach time: **B [m]**	Maximum breach discharge: **$Q_{br,max}$ [m^3/s]**	Final length of the breach: **L_{br} [m]**
192	21	90	17

The proposed model is applied in order to reproduce the characteristic ratios of the breach event on the basis of the previous information.

The breach event is simplified as follows:

- A steady discharge is considered to route in the channel (Q_u) and through the breach ($Q_{br,max}$) during all the breaching process;
- The breach is assumed to have a rectangular shape which lengthens until the recorded final length L_{br};
- The downstream boundary condition is governed by rating curve of uniform flow.

In order to apply the model, uniform flow rating curve is used to estimate the flow depth Y_0 at the flood peak before the breach started. Furthermore, flow depth at the downstream reach at the end of the breaching process Y_{dbr} is again achieved from the rating curve.

The upstream flow depth at the end of the breaching process Y_{ubr} is gained by imposing the De Marchi assumption that the specific energy head E (calculated by means of the flow features at the downstream section) is constant along the breach. As a consequence, the depth ratio r_Y of the flow is estimated.

The knowledge about the up- and downstream discharges and flow depths and the geometry of the cross-section allow to get the Froude numbers before the breaching (Fr_0), and after the breaching at the upstream (Fr_{ubr}) and downstream (Fr_{dbr}) sections.

The calculated dimensionless numbers are reported in Table 5.4:

Table 5.4: Dimensionless numbers of the real breach event of Ombrone river.

Initial Fr	**Upstream Fr**	**Downstream Fr**	**Discharge ratio**	**Depth ratio**	**Length ratio**
Fr_0	**Fr_{ubr}**	**Fr_{dbr}**	**r_{Qmeas}** = $Q_{br,max}/Q_u$	**r_{Ymeas}** = Y_{dbr}/Y_{ubr}	**r_{Lmeas}** = L_{br}/B
0.27	0.69	0.27	0.47	1.19	0.81

It can be noticed that the initial Froude defines a subcritical regime for the flood, which falls within the range indicated in Section 5.3.2.1. Moreover, the downstream Froude maintains almost the same value of the initial Fr_0, while the upstream Froude increases due to the lateral outflow. The behaviour of the system is represented as an almost vertical pattern in the Froude graph, which starts from the un-breached condition and ends at the final state. Figures 5.23-5.24-5.25 show the flow state pattern with the dimensionless ratios contours.

It has to be noticed that the pattern between the initial and final points is not reproduced by the model, which provides only the final variables at the steady state whereas their temporal development is not taken into account. In other words, the dash-dot line indicates the pattern that the flow features (at the up- and downstream sections close to the breach) may have assumed during the breaching process, but this information is actually unknown.

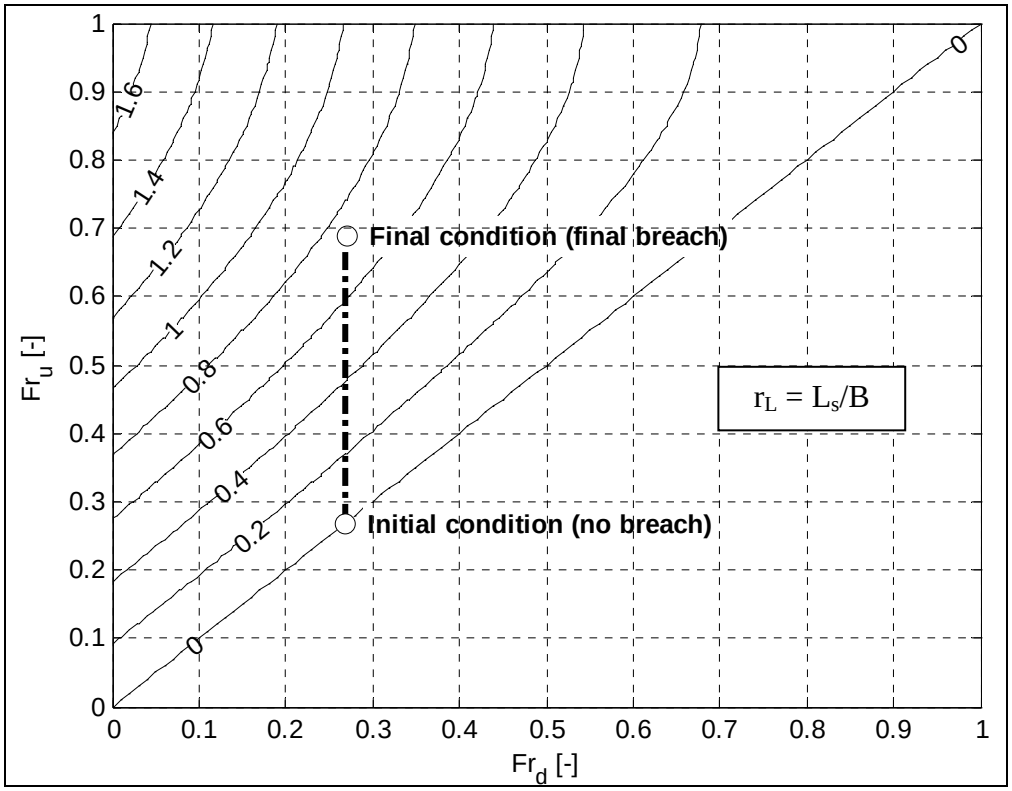

Figure 5.23: Ombrone breach event in the Froude graph with length ratio r_L contours.

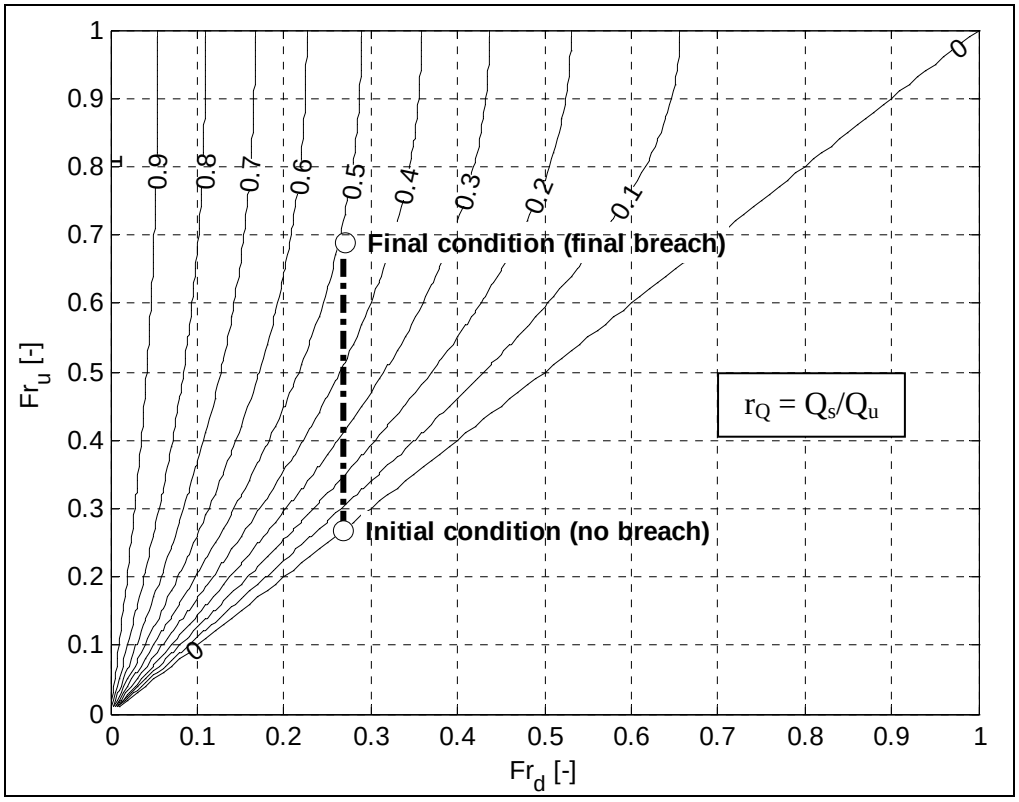

Figure 5.24: Ombrone breach event in the Froude graph with flow discharge ratio r_Q contours.

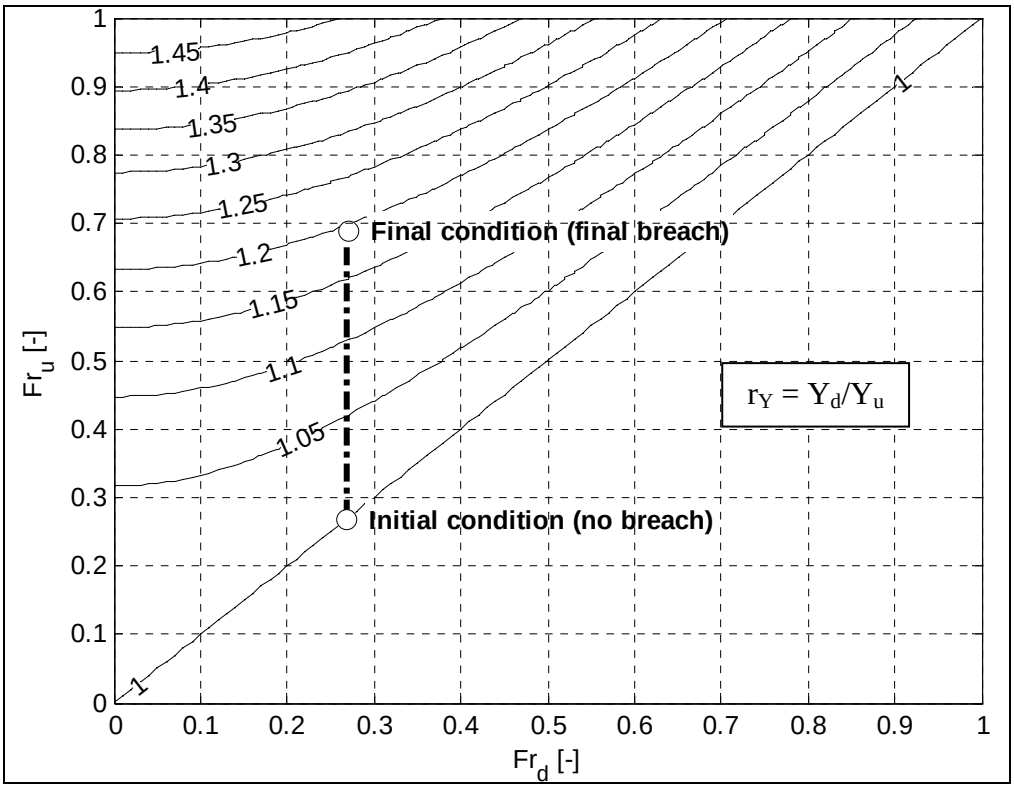

Figure 5.25: Ombrone breach event in the Froude graph with flow depth ratio r_Y contours.

The developed model predicts the dimensionless ratios, which are compared with the ones coming from the measured data in Table 5.5. The relative errors (*Err*) of the dimensionless ratios (r_x) are defined as:

$$\text{Err } r_x = \frac{r_{x\,meas} - r_{x\,pred}}{r_{x\,meas}}$$

Table 5.5: Comparison between measured and predicted ratios for the Ombrone breach event.

r_{Qmeas} [-]	r_{Qpred} [-]	Err r_Q [%]	r_{Lmeas} [-]	r_{Lpred} [-]	Err r_L [%]
0.47	0.49	- 4 %	0.81	0.73	+ 10 %

The comparison between measurement and model shows that, despite the simplicity of the model and the relevant assumptions made on the real phenomenon, the model prediction of the general behaviour of the hydrodynamics of the river flow is quite satisfactory. The predicted flow discharge ratio and length ratio result in errors less than ± 10% of the measured ratios.

However, there are a number of approximations introduced by the model that need to be discussed.

At first, the real process is not steady as in the model, but it is unsteady at least regarding the breach outflow hydrograph, the levee erosion and the flow depth variation in the main channel.

Moreover, the model does not consider movable bed conditions, while the strong acceleration of the flow due to the outflow likely modifies the river bed which can affect the outflow itself.

The proposed model considers a simplified rectangular shape both for the cross-section of the river and for the breach channel, although the real geometries are more complex (see Figures 5.20 and 5.21). Furthermore, the breach depth is considered to be at a zero level (i.e., at the bottom of the main channel), whereas it was rather at the vertical wall crest in the real case. The model does not consider the possible effect of the vertical wall on the breaching process, while it is likely that the wall did not allow the breach to deepen further: a deeper breach may have spilled greater discharge with a shorter final length than the measured one.

Another remark concerns the calculation of the final breach length, which is dependent on the side weir law. It is here assumed that the side weir equation is a realistic formulation for the breach case, which actually is stated by other authors (Saucier et al., 2009). The discharge coefficient C_d was here calculated according to the Hager (1987) formulation (see Section 5.2), which gave the best result in terms of relative error over the length ratio. Despite Hager formulation is proposed for sharp-crested weirs and the levee breach usually resembles a broad-crested weir, it fits real data better than other methods. According to that, this implies that other factors (e.g., bed morphology in river and breach channel) have greater influence on the outflow process from a breach than the difference in the method and conditions by means of which the discharge coefficient C_d is obtained, so that the formulation to calculate C_d for a levee breach flow has to chosen from case to case.

Despite all these remarks, the proposed model succeeded to reproduce properly the general features of the flow and of the breach. Moreover, it also provides a new insight into the river hydrodynamics during the breaching process.

5.3.3 Subcritical limitation of the breach features

The results obtained from the proposed analytical model come from a theoretical analysis referred to a simplified scheme of the physical system which is valid for the field of subcritical flows. As a matter of fact, the De Marchi assumption of constant specific energy head along the lateral outflow is adequate for subcritical flows, while it is not for supercritical flow regimes where greater energy losses take place. The proposed model can therefore be used to predict the behaviour of the river flow affected by a lateral outflow until the flow regime is subcritical.

The objective of this Section is the analysis of the *limit condition* of the model, defined as the change in the flow regime between subcritical and supercritical flow. This condition is investigated as possible *final state* of the flow regime during the breaching process, which, as explained in Section 5.3.2, causes an increasing of the upstream Froude number Fr_u toward the critical state. The aim of this analysis is to look at the range of application of the proposed model in order to give an indication about the admissible breach flow features in subcritical flow in terms of dimensionless ratios.

Two main assumptions are made within the current analysis:

i) The upstream Froude number Fr_u increases during the breaching process and it tends to the critical value ($Fr_u \rightarrow 1$);

ii) The downstream Froude number Fr_d keeps an almost constant value, which is related to the initial subcritical flow regime.

The proposed model is therefore used to analyse the *limit condition* at the subcritical-supercritical passage in the upstream cross-section. This is the situation in which the upstream flow depth decreases so much due to the lateral withdrawal that the critical depth is reached. In that situation, the maximum dimensionless ratios are achieved, whose values depend on the starting Froude number, as explained in Section 5.3.2.1.

If the Froude range of uniform flows is considered as initial Froude number, the following ranges of the dimensionless ratios are given as indicative values at the limit condition of subcritical flow for which the river flow and the breach features are predicted by the proposed model (Table 5.6 and Figure 5.26):

Table 5.6: Dimensionless ratios at the limit condition.

Fr_{ulim} [-]	Fr_{dlim} [-]	r_{Ylim} [-]	r_{Qlim} [-]	r_{Llim} [-]
1	0.22	1.46	0.61	1.68
1	0.45	1.36	0.28	0.76

The length ratio r_L is computed with the discharge coefficient C_d computed as Oertel formulation (see equation 5.19), which maximizes the length ratio.

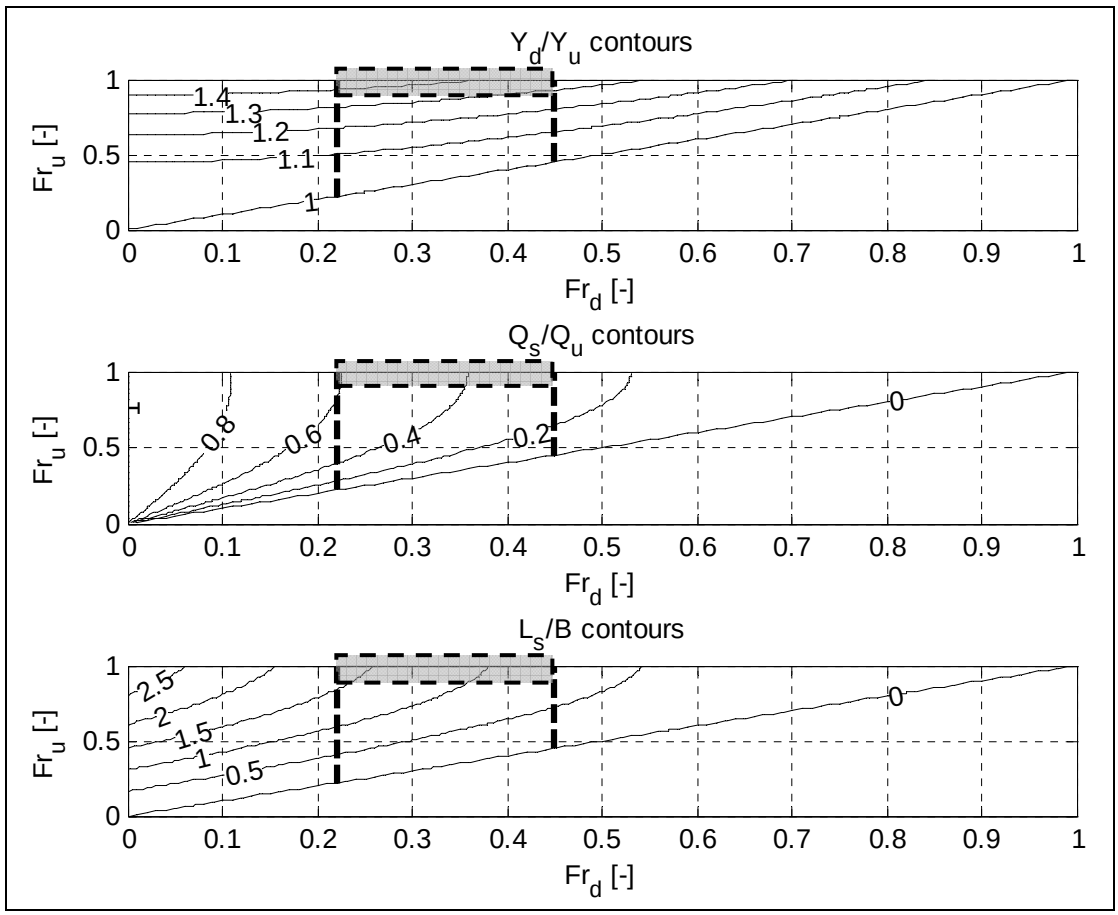

Figure 5.26: Dimensionless ratios at the limit condition for the assumed Froude range (highlighted area).

The proposed approach defines the *limit values* of the dimensionless ratios, which are compared with some experimental data and real events in order to preliminary verify its validity.

Unfortunately, no data concerning both breach and river flow characteristics were found in literature, except for the experimental data collected by Fujita and Tamura (1987) during their flume experiments on the process of breach enlargement and some data about the full-scale Chiyoda experimental channel (Shimada and Yokoyama, 2011). Anyway, the ten main experimental data about river levee breaching on movable bed presented in Chapter 4 are used.

Moreover, some field data were collected. A specific survey was carried out at several Water Authorities of Hungary and Italy and it allowed the collection of 29 field data in terms of mean river flood width B and final breach length L_{br} for the following rivers (Figure 5.27):

- Tisza river, Hungary (flood events in the period 1855-2001);
- Versilia river, Italy (1996 flood);
- Serchio river, Italy (2009 flood);
- Ombrone Pistoiese river, Italy (2009 flood);
- Calice river, Italy (2009 flood);
- Muson dei Sassi river, Italy (2009 flood);
- Bacchiglione river, Italy (2010 flood at Ponte S. Niccolò);
- Bacchiglione river, Italy (2010 flood at Caldogno).

Tisza river data were derived by the author under the supervision of Dr. Nagy of the University of Budapest (some details are in Nagy and Tóth, 2005), while data about Muson dei Sassi and Bacchiglione river were provided from University of Padova (see Viero et al., 2012 and 2013).

Data regarding the peak values of breach discharge and river discharge were also collected for 6 breach events regarding:

- Versilia river, Italy (1996 flood);
- Serchio river, Italy (2009 flood);
- Ombrone Pistoiese river, Italy (2009 flood);
- Muson dei Sassi river, Italy (2009 flood);
- Bacchiglione river, Italy (2010 flood at Ponte S. Niccolò);
- Bacchiglione river, Italy (2010 flood at Caldogno).

Collected data are presented in Figure 5.28.

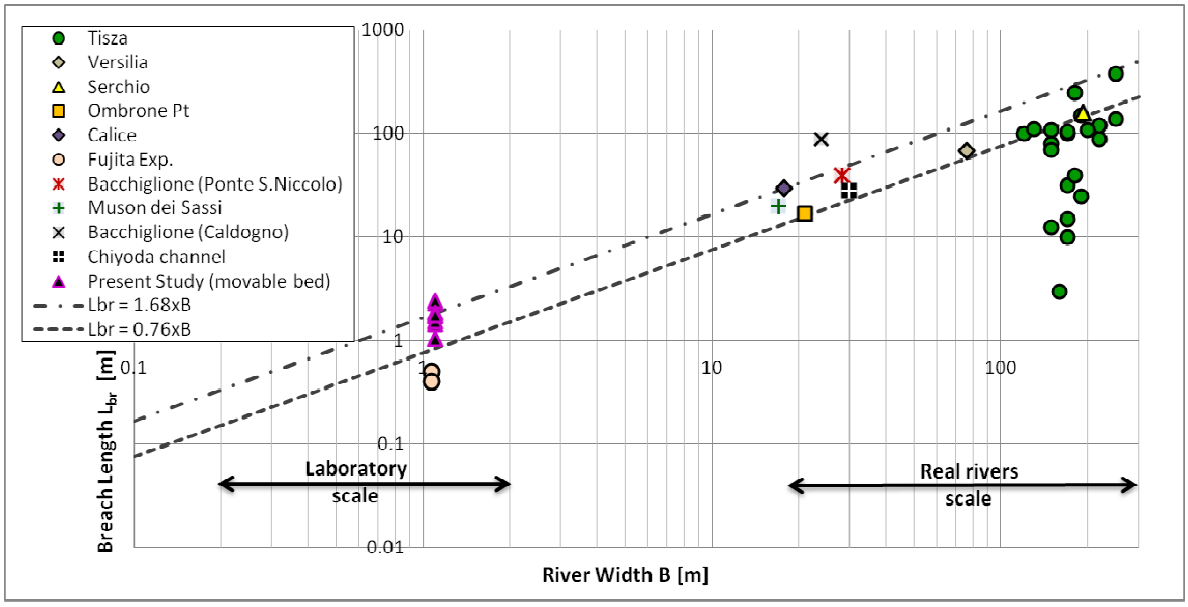

Figure 5.27: Comparison between final breach length and river flood width for experimental and real events data.

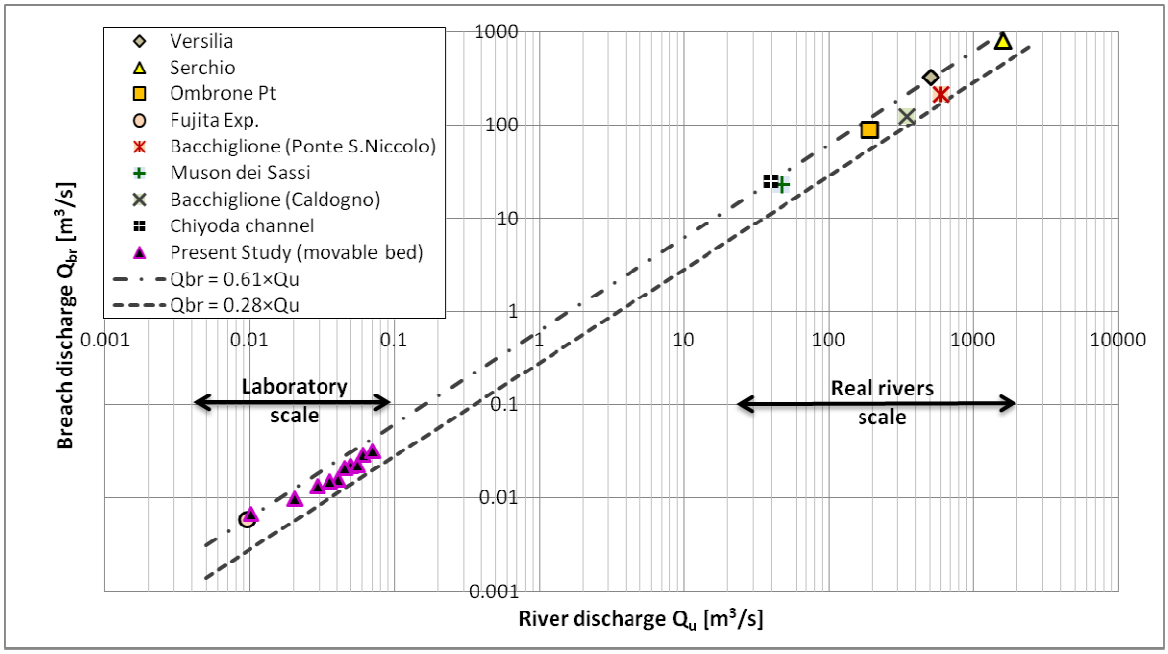

Figure 5.28: Comparison between peak breach and river discharge for experimental and real events data.

It can be noticed that the model predicts a range of values of breach features (L_{br} and Q_{br}) which is consistent with the collected data.

The final breach length is proportional to the river width and a part of the collected data are within the predicted range ($L_{br} = [0.76 \div 1.68] \cdot B$), even if a scatter is evident.

On the other hand, data regarding breach and river discharge are all within the foreseen range ($Q_{br} = [0.28 \div 0.61] \cdot Q_u$) and a quite strong relation seems to exist.

The larger scatter of data regarding the breach length is certainly due also to the dependance of this variable on other factors, as indicated by Nagy (2006). The geothecnical properties of the levee definitely play a key-role for the breaching dynamics and erosion rate, which is dependent on the resistence given by the material that forms the embankment. Also the dimensions and the geometry of the levee can influence the development of the breach and its lengthening, since the flow needs longer time to erode greater and larger levee sections. Moreover, the morphology of the river reach (straight, curved, …) can create different hydraulic conditions in the vicinity of the breach. The topographic conditions on the protected side may also affect the outflow process if backwater effects take place from the floodplain, which block the free flow through the breach. The failure mechanism may have an effect on the final breach length as well, as it is stated for dam-breach cases (Froehlich, 2008). Finally, flood emergency activity can limit the breach development, which is of course also time-dependent and it may need a time longer than the flood duration to completely develop.

Despite the collected data for different conditions and properties (regarding the size of the river and of the levee, the failure mechanism, the floodplain conditions, the geothecnical and geometrical properties of the levee, the scale of the flow rate which differs of five orders of magnitude between experimental and real event data), the relationship between peak breach discharge and river discharge at the breaching time seems to maintain the same trend, regarding the laboratory scale as well the real events. It is likely that the breach length is a more sensitive parameter to the listed factors instead of the breach discharge and that a kind of “equilibrium” is reached faster regarding the water flows in comparison with the final dimensions of the breach, as observed during the movable bed experiments (see Chapter 4).

5.4 Summary and concluding remarks

The breaching process of a river levee is quite complex and governed by the river flow conditions in the vicinity of the breach location. In this study, the river flow hydrodynamics has been analysed as a key issue to achieve a better understanding of the breaching process.

The flow features in the river have been analysed with reference to the theory of the side weir flow in the most common case of subcritical flow. The flow that develops along a side weir is analysed in order to get an overview of the river response to the outflow in terms of flow depth, flow velocity and water discharge.

The assumption of constant specific energy head in front of the lateral weir (De Marchi, 1934) is assumed to define an analytical solution of the equation of steady spatially-varied flow coupled with the classical weir equation. The calculation of the flow features (depth and discharge) in the main channel is therefore solved in a 1D fixed bed scheme.

The classical formulation of the De Marchi solution is analysed and rearranged in a dimensionless form, and a new analytical model is proposed to define the lateral outflow in terms of dimensionless ratios of the flow variables at the up- and downstream cross sections close to the side weir. The solution is easily performed once the boundary conditions, expressed in terms of Froude numbers at these two sections, are given (together with the river width and the discharge coefficient) and all the outflow process is explained as combination of the two Froude numbers in an original *Froude graph*.

The model is applied to laboratory data regarding experiments on side weirs of rectangular shapes with different values of the length and of the height, experiments conducted on zero height side weirs within the present PhD work, and experiments related to lateral diversions.

The results in terms of dimensionless ratios regarding flow depth, water discharge and side weir length show that:

- Flow depth and flow discharge ratios are predicted within an error of ± 10%;
- Length ratio is predicted within an error of ± 20%.

The applicability of the model assumptions to the context of real rivers is discussed and the representation of a real event is analysed into the Froude graphs. A realistic range of Froude numbers is considered and a likely pattern of the flow variables is represented into the Froude graphs: it is justified and discussed that the breaching event can be explained as a vertical pattern of the flow variables into the Froude graphs.

The proposed model is applied to a case of a real river breach: the Ombrone breach of 2009. The case study is presented and an interpretation of the event is given by means of the dimensionless model. The comparison between model and measured data shows that, despite the simplicity of the model and the relevant assumptions made on the real phenomenon (steady flow instead of unsteady flood wave; rectangular shape of river channel and breach channel instead of more compound forms; uniform flow as downstream boundary condition), the model predicts well the general behaviour of the hydrodynamics of the river flow. In particular:

- The measured flow discharge ratio r_Q is overestimated of 4%;
- The measured length ratio r_L is underestimated of 10%.

Finally, the proposed model is analysed for the *limit condition* of critical flow at the upstream section, which actually represents its limitation since it is based on the assumption of subcritical flows. The analysis of the limit condition allows to define a range of maximum

values that the dimensionless ratios may achieve during a breaching event, according to the proposed model.

The predicted range of dimensionless ratios regarding flow discharge and breach length are compared with a number of experimental and real event data collected at several Water Authorities of Hungary and Italy.

The model predicts a range of values of breach features (L_{br} and Q_{br}) which is consistent with the collected data: the ranges defined by the model contain most of data regarding breach length and the whole data regarding flow discharge.

Breach length data show a relevant scatter compared with the theoretical ranges, which is certainly due also to the dependance of this variable on other factors that the general model does not consider. The final configuration of the breach geometry depends on the geothecnical and geometrical properties of the levee, the morphology of the river reach, the topography of the protected side, the failure mechanism.

On the other hand, the predicted trend of the breach discharge in function of the river discharge explains the collected data in a real significant way: the data are all within the range [28% < r_Q < 61%] predicted by the proposed model at the limit condition, even if they are related to completely different conditions and to values ranging from laboratory scale to field scale.

It is concluded that the breach length is a more sensitive parameter to local factors instead of the breach discharge and that a kind of “equilibrium” is faster gained regarding the water flows in comparison with the final dimensions of the breach.

These results may have extremely important implications on both research and engineering practice, since they point out the existence of a strong (and maybe constant) relation between the river flow and the breach flow, which opens new research scenarios and possible practical applications in the field of flood risk mapping due to river levee breaching.

The proposed model therefore provides a useful, simple and intuitive insight into the hydrodynamics of the river flow affected by a lateral outflow. It is able to:

- Predict the longitudinal variation of water depth;
- Predict the longitudinal variation of flow discharge;
- Provide an analytical explanation of the breach hydrodynamics as one-dimensional flow;
- Describe the effects on the river flow in terms of dimensionless ratios between the flow variables (depth and discharge) at the up- and downstream sections of the lateral weir;
- Calculate the flow depth and water discharge ratios and the characteristics of the side weir (length over river width) as a function only of the boundary conditions expressed by the up- and downstream Froude numbers.

The model simplicity reflects its own limitations:

- *1D flow*: no vertical or transversal variations of the state variables can be predicted;
- *Steady flow*: no unsteady states are simulated;
- *Subcritical flow*: only flow regimes with Froude numbers less than unity are considered, while supercritical flows are not simulated;

- *Fixed bed*: the solid boundary of the river channel is not erodible, so that no erosion/deposition mechanisms can be simulated and no possible interaction between hydrodynamics and morphodynamics are taken into account.

Further improvements of the proposed model are recommended in order to make its results more realistic and to investigate other possible relationships between the physical variables of the river-breach system. For example:

- The implementation of other river section geometries (e.g., trapezoidal) may address more realistic situations usually encountered in rivers;
- The effect of movable bed by inserting a predefined configuration of the river bed on the basis of experimental results (as shown in Chapter 4), which may help in analysing the relation between breach flow and river morphology;
- The removal of the subcritical flow assumption by investigating other Froude numbers combinations into different areas of Froude graph (Figure 5.8) would be useful to extend the analysis of the assumed *limit condition*;
- The comparison with other experimental, field and real case data and with the results of more sophisticated numerical models (e.g., 2D or 3D models), in order to test the capability and reliability of the proposed model.

6 Conceptual model of a levee breaching

Levee breaching is associated with several complex interacting mechanisms in a quite complex system. The experimental and analytical works performed in the framework of this research primarily aim to analyse the "*river-breach system*" in order to improve the knowledge about the breaching process.

The ***fixed bed experiments*** have allowed us to analyse in detail the flow field in the vicinity of a side weir that simulates a fixed levee breach without considering the breach growth and the morphological changes in the river bed. The results provide an overview of the phenomena taking place in the fluid affected by a lateral outflow.

The ***movable bed experiments*** have, in addition, made possible to also analyse the mobility of the river bed and levee material as well as the geotechnical processes involved in the inception and development of the breach. The morphodynamic behaviour of the system was analysed by also considering the flow field recorded during in the fixed bed experiments. The process was investigated with the goal of looking for a steady final equilibrium.

The ***proposed analytical model*** that was applied to the laboratory data as well as to some real cases has enabled to provide a proper physical interpretation of the main hydrodynamic features of the processes involved.

The results of these three different types of investigations are brought together within this Chapter, in order to obtain a conceptual picture of the levee breaching in terms of a process-oriented analysis with a particular focus on the river flow. The obtained overall picture is expected to be very useful not only for this study, but also for any further laboratory, analytical, numerical and field studies on river levee breaching.

The breaching process induced by overtopping, that was described in Chapter 2 by means of a four-stages sequence (see Figure 2.8), is integrated into the temporal and spatial description of the hydro-morphodynamics of the river flow. The breaching initiated by overtopping, which was reproduced in the experimental investigations, is analysed. A straight river channel of constant cross-section and with movable bed is considered, which is delimited by a trapezoidal homogeneous earthen levee on one of its banks (and by a not-erodible structure, such as a flood wall, on the other side). It is assumed that the breaching starts during the passage of the peak of the flood wave which develops according to a time scale much greater than the time scale of the breaching process. In such a way, the theoretical final equilibrium of the breach should not depend on the decreasing of the water inflow associated with the flood attenuation. Moreover, no backwater effects are considered, i.e. the surrounding areas protected by the levee are flooded because of the breach, but the flood depth is such that it does not affect the breach flow from the river side.

6.1 Inception of the breaching (stage 1)

The initial state of the river flow before the breaching is determined by the river properties (channel geometry, bed slope, flow roughness), the water discharge flowing in the river $Q_u(t)$ and the boundary conditions (for instance, a downstream flow rating curve). The flood wave propagates downstream and a local uniform flow can be considered if no significant obstacles or geometry changes take place. Sediment transport can occur at high water discharge, but bed deformation is assumed to be negligible at the initial state, in order to better highlight the

next modifications. The initial state before breaching (stage 0) is depicted in Figure 6.1 and 6.2 as section and frontal view, respectively.

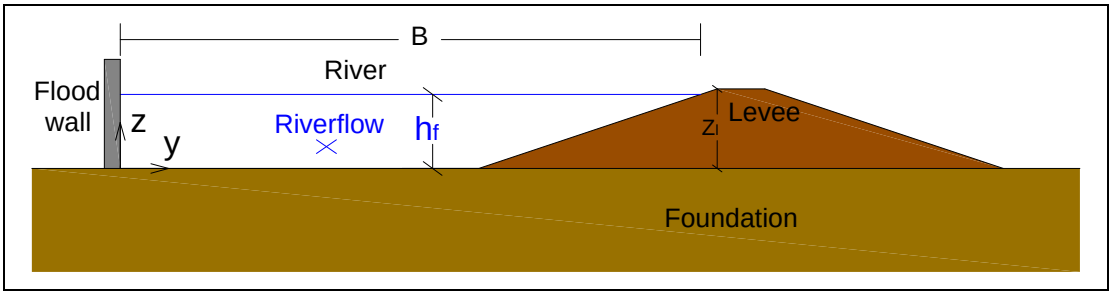

Figure 6.1: Stage 0: river flow situation before breaching (section view).

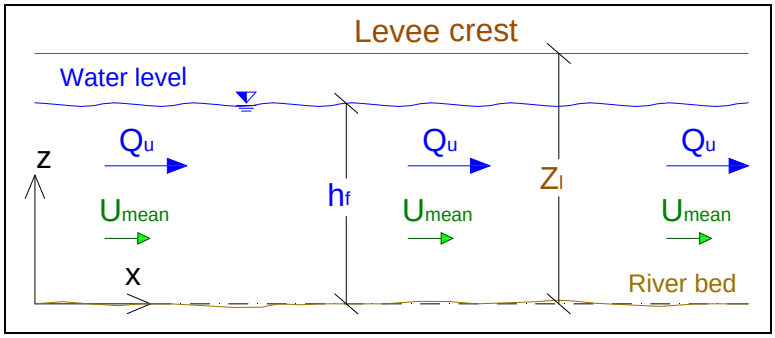

Figure 6.2: Stage 0: river flow situation before breaching (frontal view).

If the river section is no more able to convey all the water discharge downstream within its border, then water starts to overflow the levee where its crest is at the lowest point or where a local factor occurs, as, for instance, the backwater effect induced by the presence of a bridge. The first stage of the breaching phenomenon starts with an overflowing of the levee at the *Breach Trigger Location* (BTL) and the erosion of the protected side of the levee (Figures 6.3, 6.4 and 6.5).

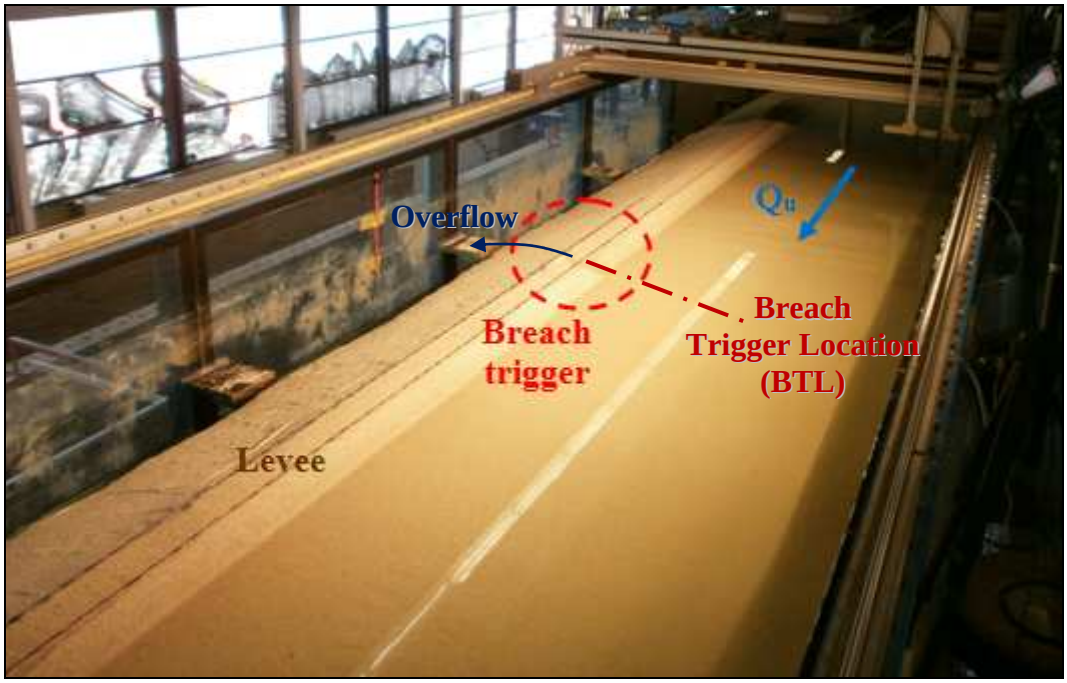

Figure 6.3: Stage 1 of test A3 (Q29.2Yg2.2S0.1%) of movable bed experiments with breach location.

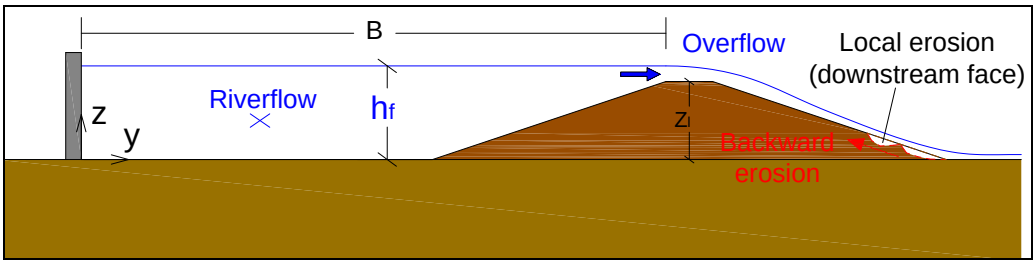

Figure 6.4: Stage 1 of breaching and river flow: overflow and local erosion of the levee (section view).

At this first stage, the river hydro-morphodynamics is slightly affected by the breaching phenomenon, because just a little portion of the flow discharge is spilled out (Figure 6.5), so that the upstream and downstream Froude numbers are almost equal. The overflow process is a distributed lateral outflow which is usually analysed by the overflow equation for broad crested weirs (equation 4.5).

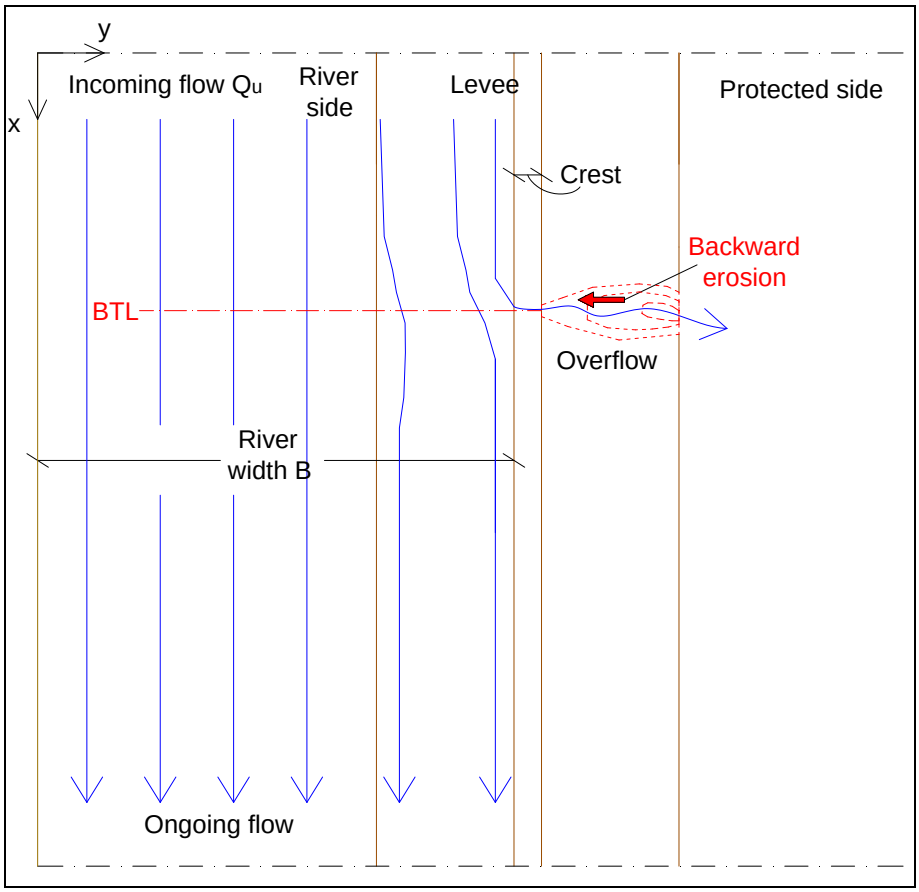

Figure 6.5: Stage 1 of breaching and river flow: overflow and local erosion of the levee (plan view).

6.2 Progressive erosion of downstream side (stage 2)

The erosion of the downstream side progresses backward toward the levee crest and the protected side of the levee is progressively washed away due to the water jet falling over the crest (Figure 6.6). This is a very important stage of the entire breaching process, since the levee crest is being lowered significantly until the breach channel is directly connected to the river: from that point on, the breaching will develop in an increasingly and uncontrolled way.

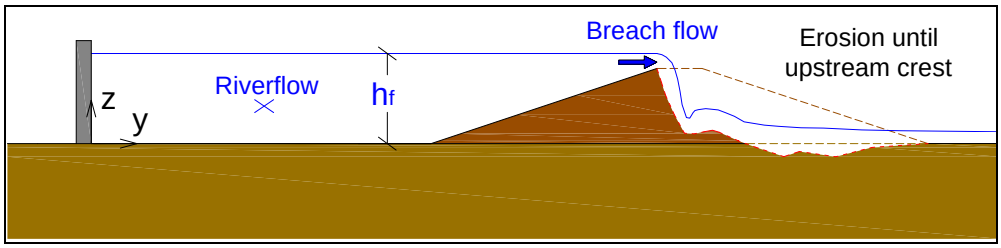

Figure 6.6: Stage 2 of breaching and river flow: backward erosion of protected side (section view).

During that stage, the breach channel develops to a single gully through the levee (in case of non-cohesive material) or as combined head cuts (in case of cohesive material), as explained in Chapter 2 (Figures 2.8, 2.9 and 2.10).

The breach flow rate is highly dependent on the effective water level prevailing at the breach, so that the deepening (vertical erosion) of the breach channel increases the overflow. The process then enhances itself: the lower is the levee crest, the greater is the lateral outflow which, as a consequence, has a stronger erosive action. The vertical erosion is the main mechanism which develops the breach channel at this stage, while the lengthening is slight and it gets importance during the third stage.

The river starts to "notice" the presence of the lateral outflow, but only the flow in the vicinity of the breach is affected, since the breach is still small. The water is attracted by the surface layers close to the levee crest in a way similar to the dam breaches: water is running over the breach and it follows a perpendicular pattern to the levee alignment. Moreover, the breach starts to lengthen because of two main erosion mechanisms: the *continuous erosive action* exerted by the flow and the *discontinuous mass failures* of material. The breach lengthens shortly both in the up- and downstream directions (symmetrical development) from the BTL during this stage (Figures 6.7, 6.8 and 6.9).

A small portion of the incoming flow is diverted by the breach (Q_{br} is a slight percentage of Q_u) and, anyway, it makes the downstream flow to decrease. In the usual case of subcritical flow regime and uniform flow rating curve as downstream boundary condition, the upstream Froude number Fr_u starts increasing because of the lateral outflow "attraction", while the downstream Froude number Fr_d almost keeps constant.

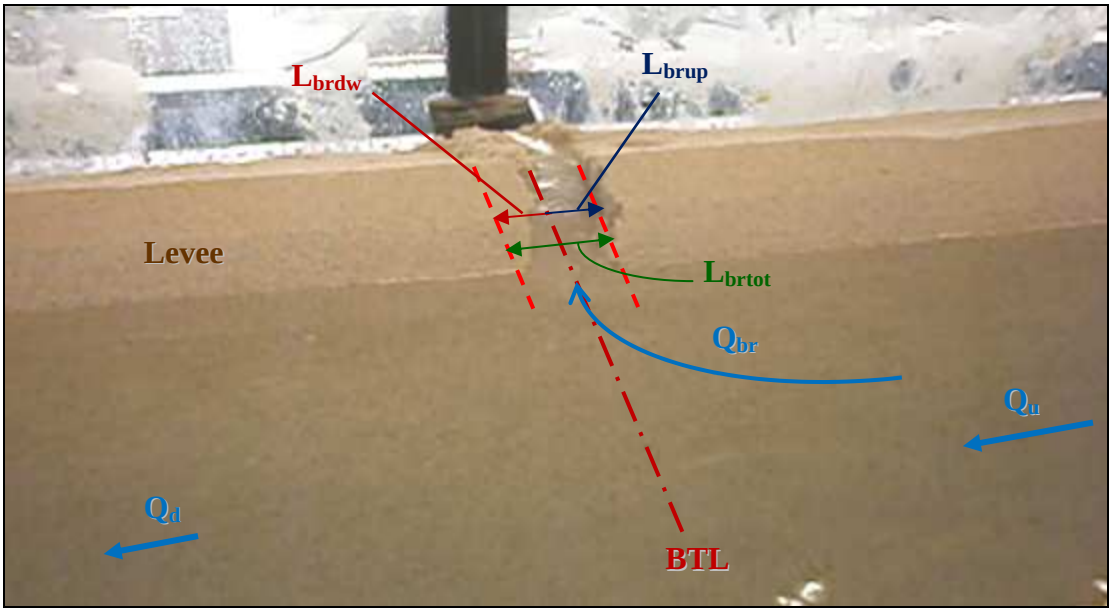

Figure 6.7: Breaching stage 2 during the movable bed experiments: almost symmetrical breach lengthening upstream (L_{brup}) and downstream (L_{brdw}).

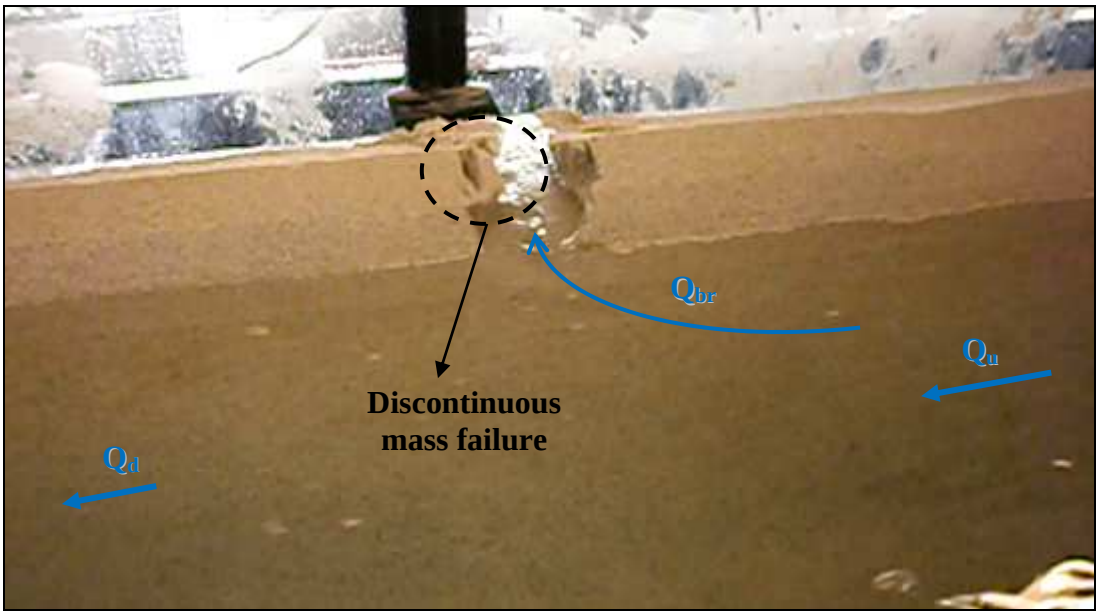

Figure 6.8: Breaching stage 2 during the movable bed experiments: discontinuous mass failure.

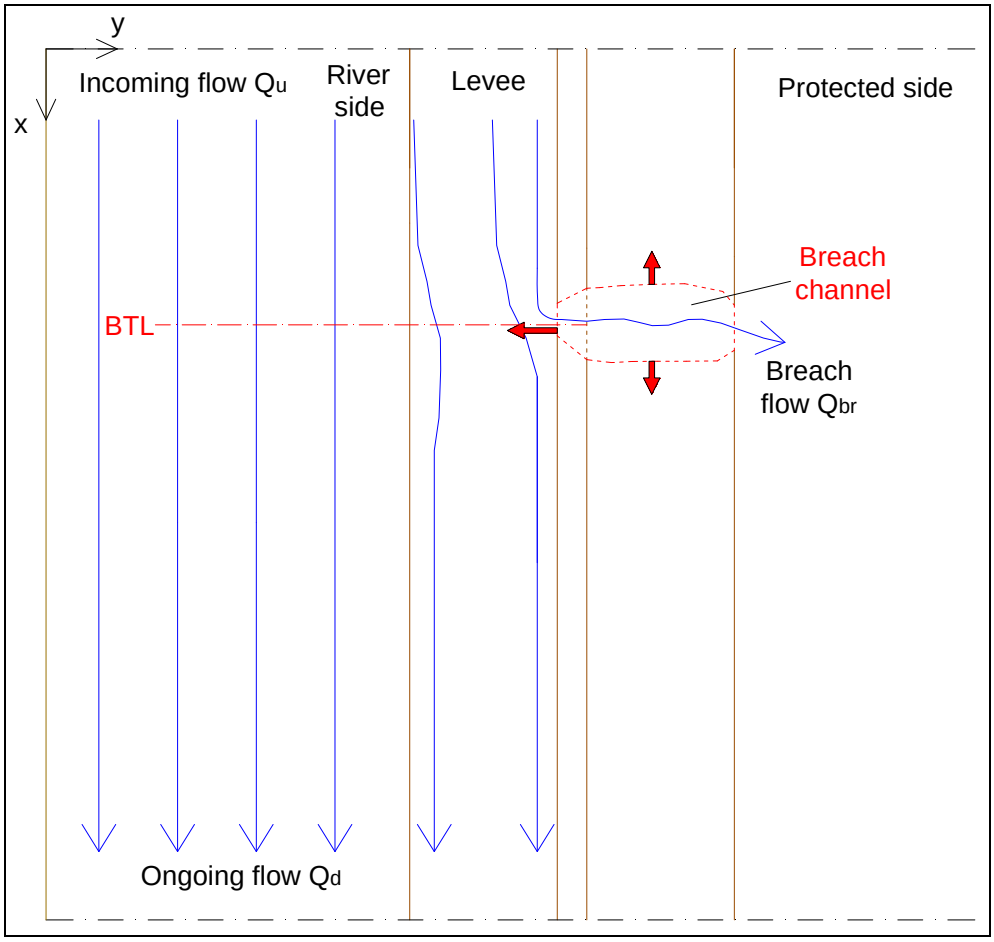

Figure 6.9: Stage 2 of breaching and river flow: symmetrical breach lengthening (plan view).

6.3 Progressive erosion of upstream side (stage 3)

The third stage concerns the erosion of the river side of the levee (see Figure 6.10). The levee crest is lowered and river floods the protected side increasingly. The breaching process is accelerated: the greater flow breach induces higher erosion rates, so that the levee section is progressively eroded and the breach lengthens faster, mainly downstream of the BTL. The peak erosion rate is reached during this stage, due to the quick increase of the flow rate through the breach. The erosion progresses upstream toward the river and the entrance of the breach channel is shaped as a curved "bell-mouth weir", which works as control weir of the flow.

The increasing of the breach features (size and discharge) provokes a disturbance in the flow field which influences an enlarging portion of the river channel.

A sequence of pictures of stage 3 recorded during one movable bed test is given in Figure 6.11, showing the development of the breach channel and flow. The pictures were taken during consecutive time steps ($t_1 < t_2 < t_3$): the increasing extension of the breach length, of the breach flow and of the bell-mouth weir are highlighted. The indication of the initial section of the breach (BTL) suggests that the breach developed mainly downstream, whose reason has to be looked for in the hydrodynamics of the river flow.

Figures 6.12-6.13-6.14 depict a plan view of the breaching development during stage 3. The breach channel is sketched together with direction of erosion (arrows) and flow streamlines. The river flow reacts quickly to the presence of the breach flow. Since the breach spills out more and more discharge, the entire upstream incoming flow is accelerated. The mean flow velocity of the river U_{mean}, and the longitudinal component of velocity U_x as well, increases while approaching the breach site (and the Froude number similarly), then it strongly slows down along the breach channel until the downstream section (Figures 6.13 and 6.14), due to the lateral loss of water and the increasing flow depth (decreasing of U_x up to 50%). On the other hand, the transversal flow velocity U_y (i.e., the component of the velocity directed toward the breach) increases toward downstream because of the increasing water level. These hydrodynamic mechanisms make the streamlines turning toward the breach with increasing deflection angles θ at the downstream section (see Figure 6.14): as a consequence, this is the more stressed section and the breach lengthens mainly toward downstream.

All these processes are also depicted in Figure 6.15, where the longitudinal cross-section is drawn during time evolution. The flow acceleration induced by the lateral outflow makes the upstream flow depth to decrease until the upstream section of the breach is reached. The flow depth increases along the breach, due to the subcritical regime of the flow, and then it tends to the downstream flow depth given by the boundary condition (as it is predicted by the side-weir theory). The asymmetry of the breach evolution is also highlighted with reference to the erosion length toward the upstream and the downstream direction, L_{brup} and L_{brdw} respectively. Moreover, the acceleration of the flow in the upstream reach increases the bed shear stresses, which mobilise the bed material and sediment transport starts with creation of bedforms (as ripples and dunes). The response of the solid phase to the disturbance given by the lateral outflow starts with some delay (time t_3, Figure 6.15): it is necessary that the breach has progressed enough to induce a sufficient flow velocity able to create a bed deformation.

At the end of the third stage, the levee section is completely eroded and a scour in the foundation has been initiated if allowed by the surrounding conditions (Figure 6.10). The breach has a gained significant length L_{br} which is in the order of the river width B and then it goes on lengthening during the fourth stage with lower erosion rates (one order of magnitude lower than the peak rate). The breach flow Q_{br} is a significant percentage of the river flow Q_u, in the order of 30% of Q_u, and it increases slower.

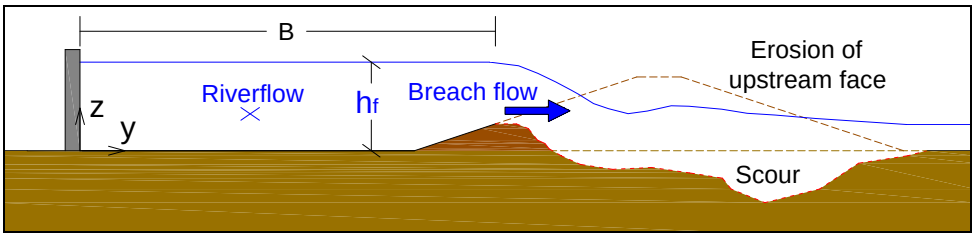

Figure 6.10: Stage 3 of breaching and river flow: erosion of upstream side (section view).

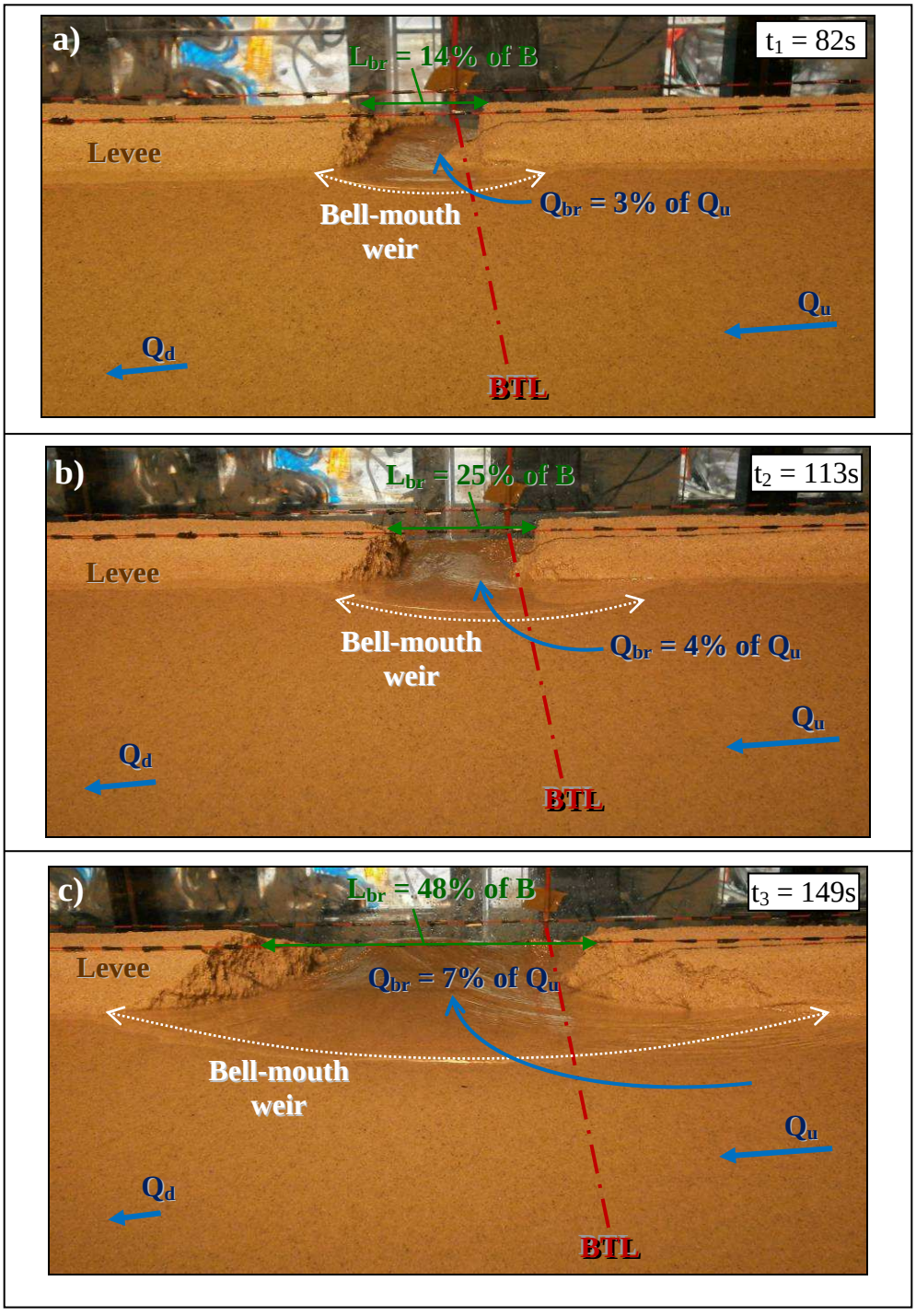

Figure 6.11: Photo series of stage 3 of breaching experiment A3 at three different times since breach trigger (t_0 = 0 s): a) t_1 = 82s; b) $t_2 = t_1 + 31$s; c) $t_3 = t_2 + 36$s.

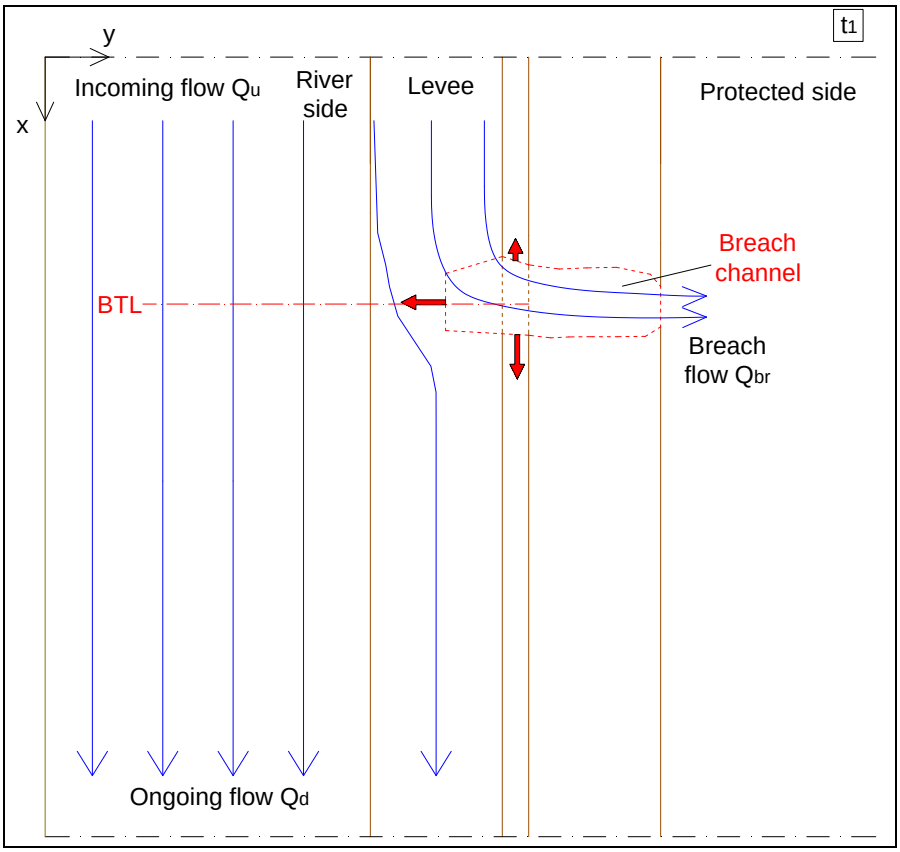

Figure 6.12: Sketch of stage 3 of breaching and river flow (time step t_1): breach development.

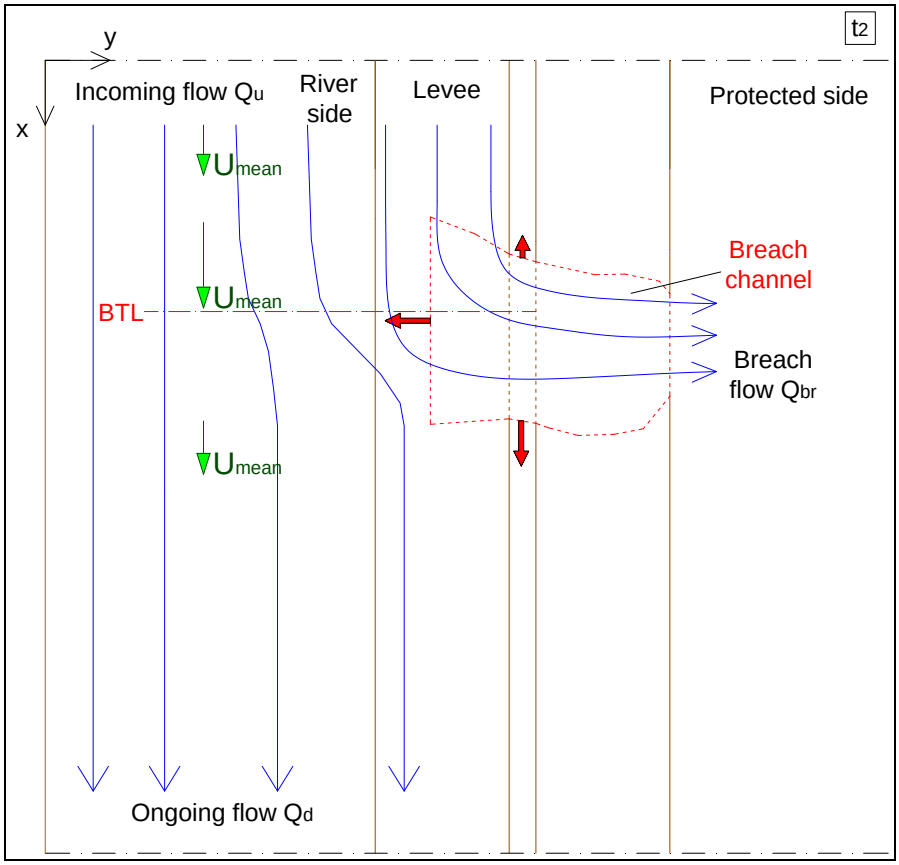

Figure 6.13: Sketch of stage 3 of breaching and river flow (time step t_2): mean flow velocity decreasing and breach development.

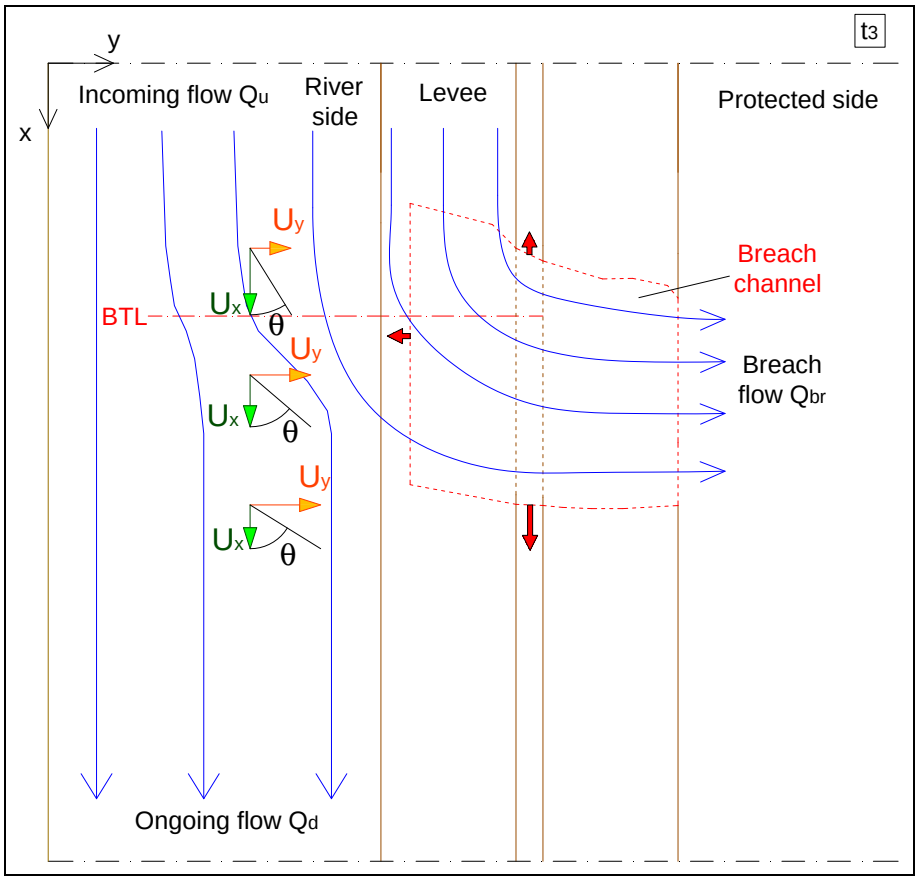

Figure 6.14: Sketch of stage 3 of breaching and river flow (time step t_3): 2D flow features at the breach location and breach development.

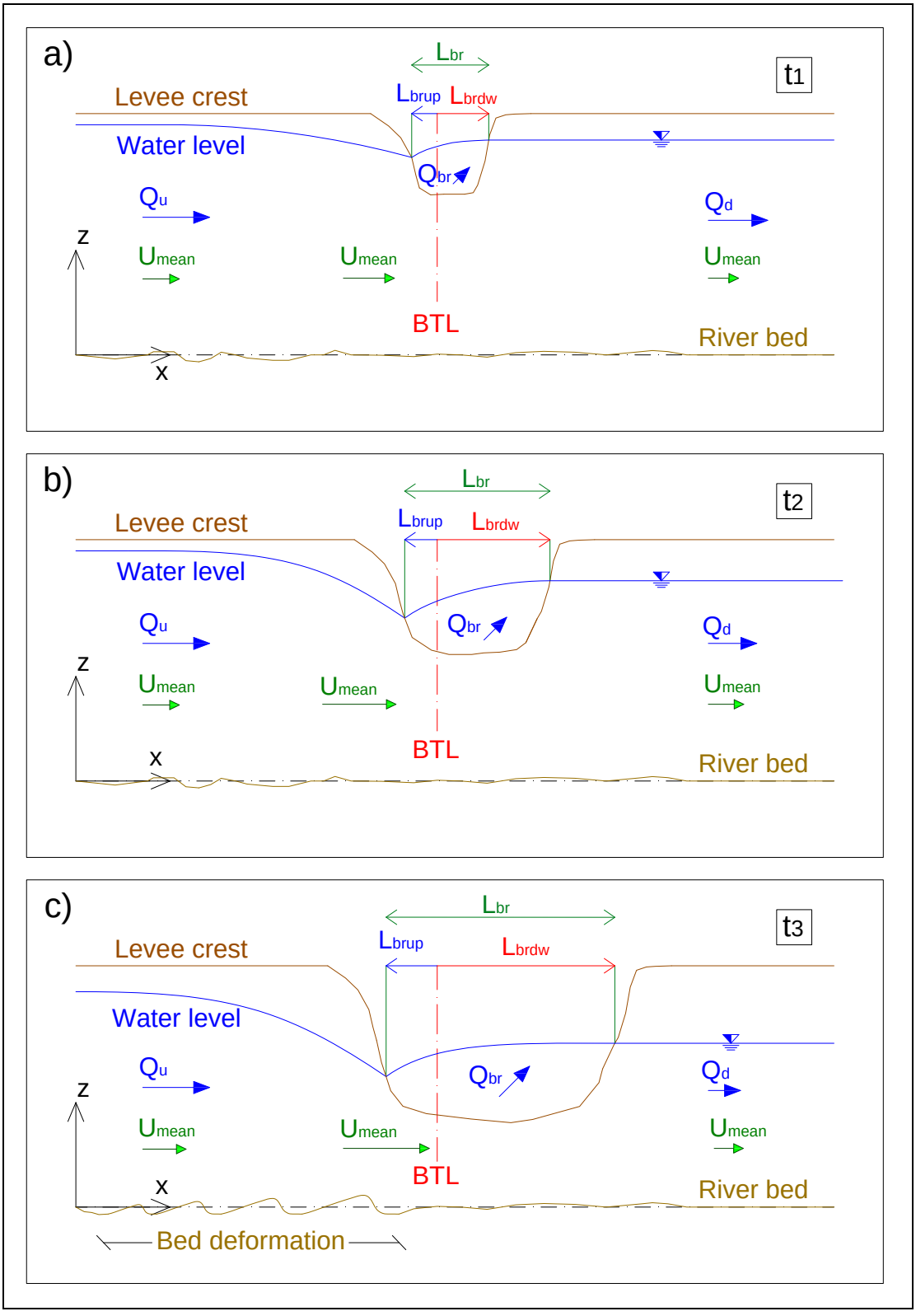

Figure 6.15: Evolution of breaching and river flow at different time steps of stage 3: a) water level decreasing and breach channel formation (t_1); b) water level decreasing and downstream breach development (t_2); c) water level decreasing, downstream breach development and river bed deformation (t_3).

6.4 Final breach configuration (stage 4)

The fourth breaching stage deals with the breach development until a final equilibrium is reached (see Figure 2.8f). Stage 4 is the longest of the four stages, during which the breach lengthens with lower erosion rates than in the previous stage. The breach gets a length in the order of the river width and, consequently, the river flow is increasingly more affected by the lateral outflow: several mechanisms of hydro-morphodynamic nature start to take place and they influence each other. The acceleration of the incoming flow toward the breach site continues to increase and the flow depth decreases. The lowest depth that the flow can reach is associated with the minimum specific energy head (at Fr = 1), i.e. the critical depth. The flow regime can theoretically be subcritical or supercritical along the breach. However, supercritical flows are usually unstable in small slope mobile bed channels, since the riverbed is modified by the flow until it gets a more stable configuration with the subcritical regime. As a consequence, the flow tends to achieve and maintain a high subcritical Froude number at the upstream section, while the water profile increases along the breach channel until the downstream section, where a subcritical Fr establishes according to the initial river flow conditions (before breaching) and to the downstream boundary condition.

The acceleration of the river flow induces a mobilization of material in the upstream part, associated with the increased bed shear stress τ and sediment transport capacity. If the incoming solid discharge is lower than the sediment transport capacity, the flow produces erosion of the river bed and of the levee at the river side slope. The mobilised material is then conveyed along the river resulting in significant bedforms (see Figure 6.16): a part can be deflected through the breach channel as bed or suspended load, while the remaining one is carried downstream. The lateral spill of water through the breach makes the longitudinal bed shear stress τ_x and the sediment transport capacity to reduce along the breach, so that the material is deposited and an aggradation of the river bed occurs. The sediment transport capacity in the main channel is still small at the remaining downstream part, so that no or small bed modifications take place there, as compared with the upstream part. Figure 6.17 shows a picture of the riverbed at the end of one experimental test, whereas a sketch is represented in Figure 6.18, where the maximum difference in height Δ_{max} between erosion (upstream the breach) and aggradation (at downstream part of the breach) is highlighted. The bed deformation is also underlined in the section view of sketches in Figure 6.19.

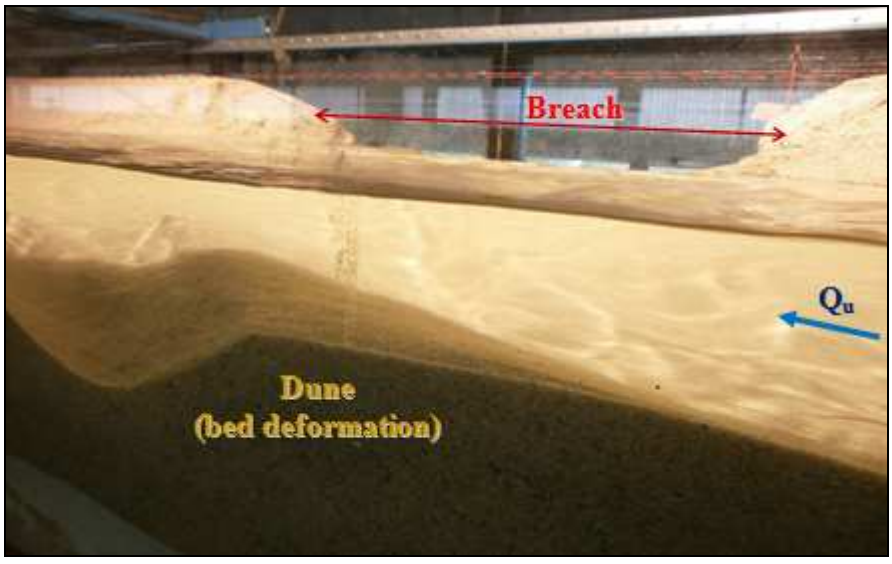

Figure 6.16: Dune formation during stage 4 of breaching experiment B8.

Figure 6.17: Bed deformation at the end of breaching experiment B8.

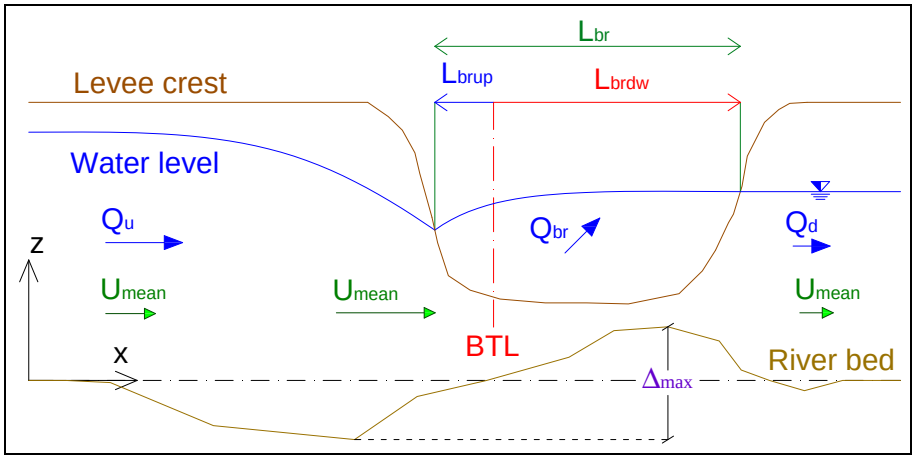

Figure 6.18: Longitudinal section of stage 4 of breaching process: riverbed deformation.

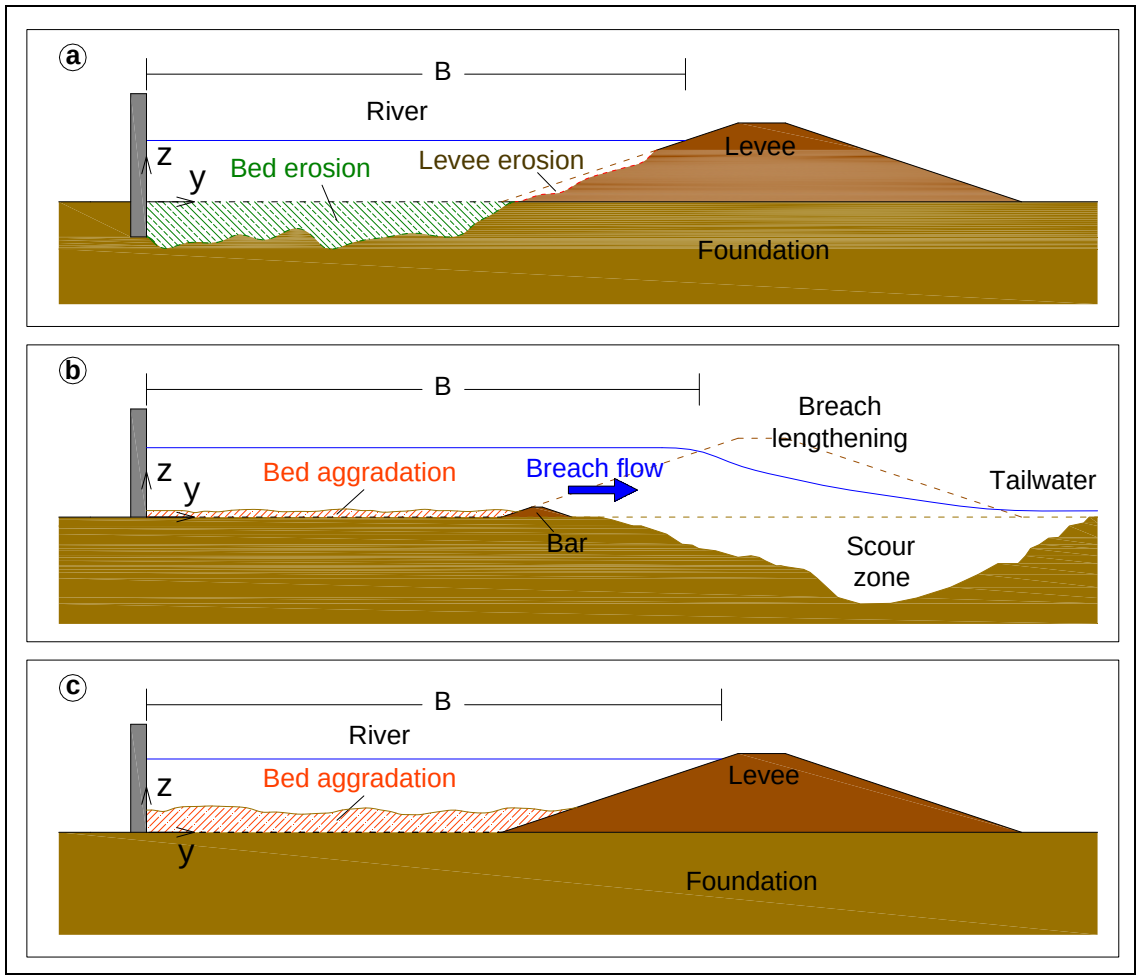

Figure 6.19: Stage 4 of breaching process at different cross-sections: a) erosion of river bed and of river side of levee at upstream zone; b) breach channel, breach flow and slight bed aggradation at the middle of the breach length; c) river bed aggradation at downstream zone.

The combined effect of flow deflection, flow velocity changes and river bed modification, makes the transversal shear stress τ_y to be higher at the downstream section: the shear stress τ gets a more direct action toward the downstream breach segment and, as a consequence, the breach develops asymmetrically mainly in the downstream direction. Another effect of the shear stress change is that the upstream breach section is rounded (high τ_x and low τ_y) while the downstream one results in a more clear cut (τ_x and τ_y similar). Figure 6.20 depicts the previously described situation.

Since the portion of the river flow affected by the breach is large and comparable to the river width, three-dimensional effects are induced in the flow field: a *dividing surface* distinguishes the flow going through the breach from the remaining one; a *helicoidal flow* may occur close to the levee starting at the downstream corner of the breach channel, which causes local erosion and deposition mechanisms; a *flow separation* zone can form on the opposite side of the breach, whose presence and size are likely dependent on the aspect ratio of the river flow (Y/B). These zones are depicted in Figure 6.20.

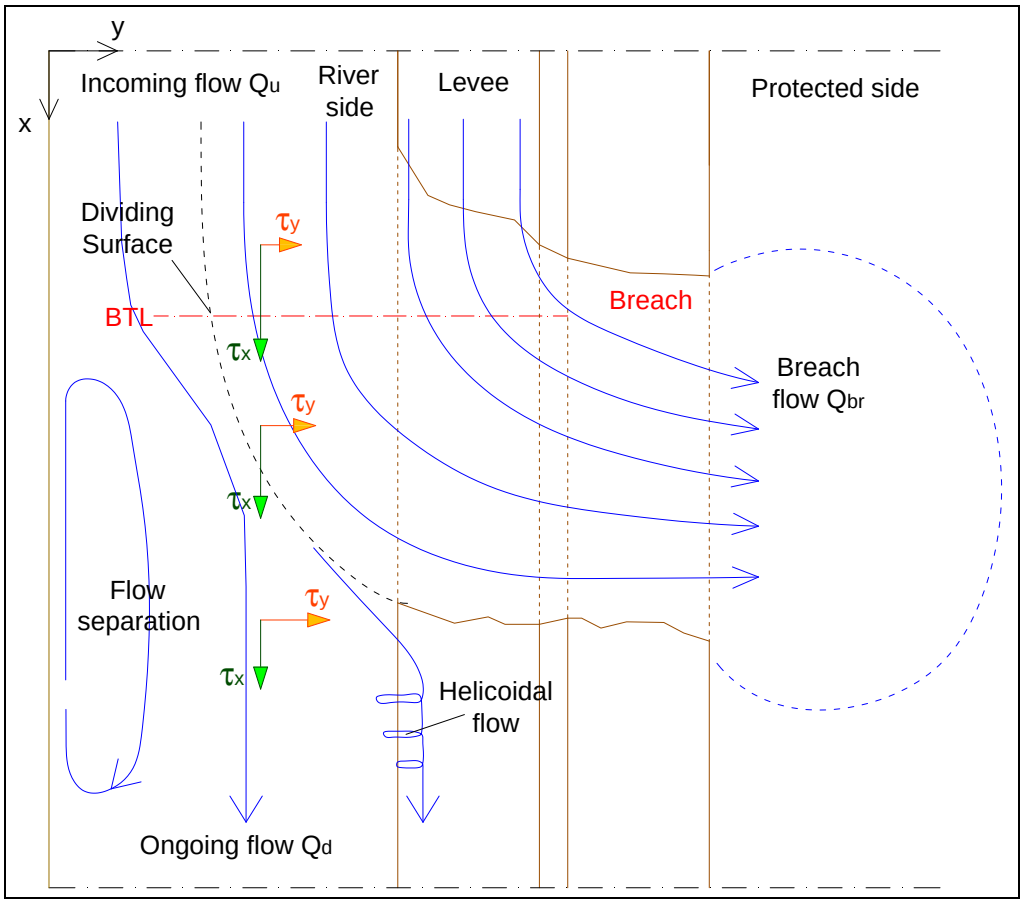

Figure 6.20: Stage 4 of breaching process (plan view): shear stress and three-dimensional effects.

The hydrodynamics and the morphodynamics interact and the entire river-breach system evolves in time: the flow field modifies the bed morphology which, as a consequence, affects the river hydrodynamics. The breach flow affects the acceleration of the incoming flow, which modifies the river bed (erosion upstream and aggradation downstream). The new bed configuration influences the hydraulic features in the river along the breach in terms of flow depth, flow velocity, hydraulic head acting over the breach and, consequently, the breach flow is affected by these morphodynamic mechanisms.

A strong correlation between breach outflow and bed deformation was found during the movable bed experimental tests (see Section 4.4.4): this may indicate that the riverbed deformation enhances the flow though the breach. At the same time, the breach lengthens but the water level acting on the breach decreases because of greater outflow and breach length. The erosion rate then decreases and the entire system tends towards an *equilibrium state*. Such an equilibrium is faster and easier achieved by the liquid phase than the solid phase, because water flow reacts at shorter time scales than sediment transport mechanisms, which also depend on further variables (sediment properties, geometric and geotechnical features of the levee, …).

The fourth breaching stage is then assumed to end when a steady equilibrium is achieved between incoming flow and breach flow, even if the breach geometry is not stable. The results found by the analytical modelling of Section 5.3.3 showed that the equilibrium lateral outflow is in the order of 50-60% of the incoming flow.

6.5 Summary of breaching stages 1-4

Breaching stages 1-4 as described above for a river levee are summarised in Figure 6.21 in terms of breach length, breach discharge and longitudinal erosion rate. Few information are given regarding the breach depth, because it was not observed during the movable bed experiments. However, a possible curve of the breach depth is proposed, on the basis of other works (Hahn et al., 2000; Shimada and Yokoyama, 2011; Islam 2012), in which the breach is observed to erode mainly vertically during the first stages and then to lengthen.

The first stage does not produce a significant increase of the breach features, which indeed takes place during the second stage. The breach accelerates its development during the third stage and, as a consequence, higher gradients of the variables are observed. The breaching process starts slowing down at the beginning of the fourth stage, during which the erosion rate decreases by one order of magnitude compared with the peak value achieved during stage 3. The breach continues lengthening while the breach discharge tends to get an equilibrium with the incoming flow.

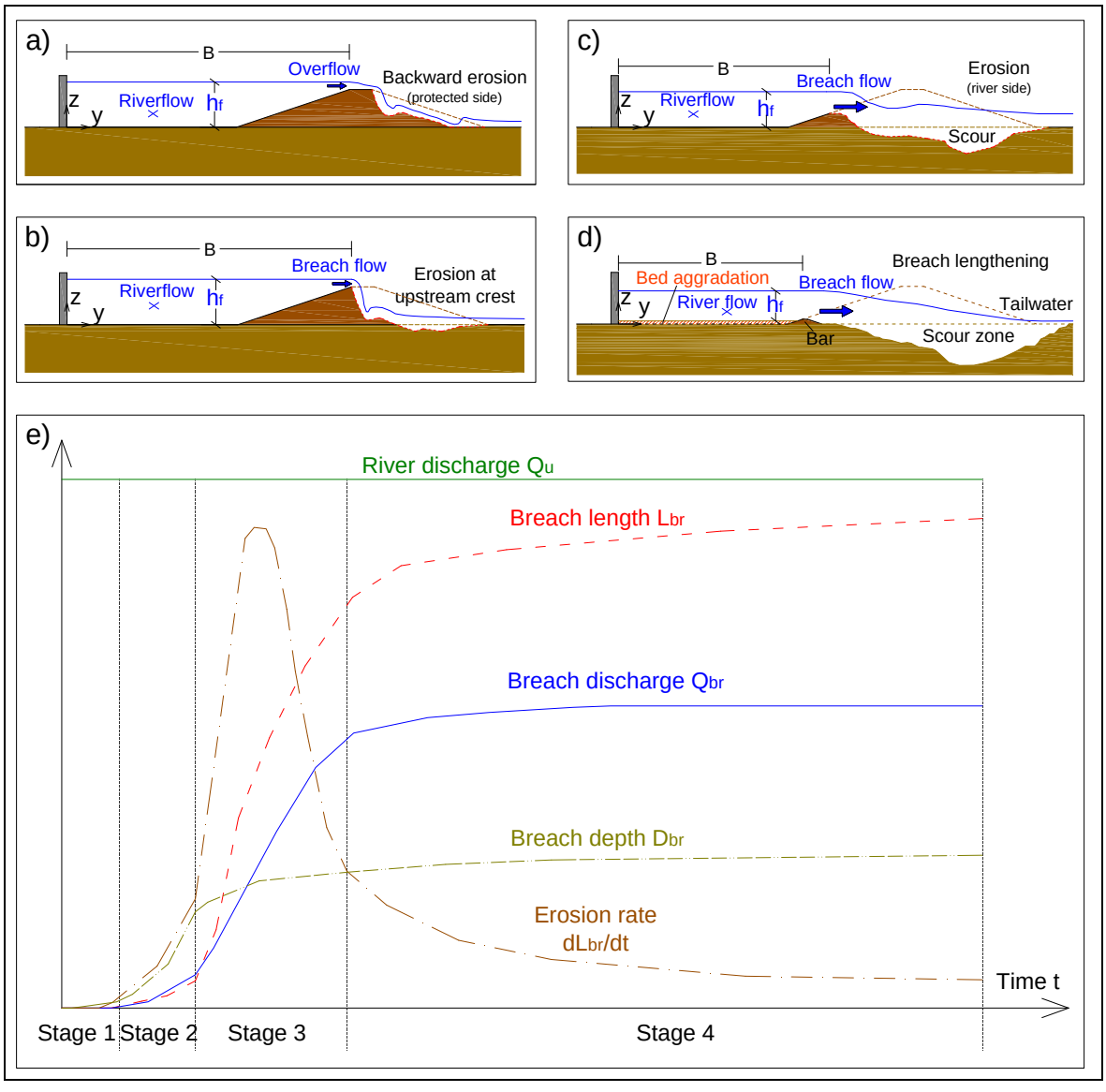

Figure 6.21: Qualitative trend of the breach features during the breaching process: a) Stage 1; b) Stage 2; c) Stage 3; d) Stage 4; e) Temporal trend of breach features.

Another qualitative description of the breaching process is given referred to the river flow in Figure 6.22. The four breaching stages are depicted within the "*Froude graph*" obtained by the analytical flow modelling, in which the breaching process is analysed as a lateral outflow that makes the river flow to change (see Section 5.3 for details). The flow modification is summarized in terms of boundary conditions, expressed as Froude numbers Fr_u and Fr_d at the up- and downstream sections of the breach site, respectively. The graph predicts the ratio between the lateral outflow and the incoming flow, given the two Froude numbers Fr_u and Fr_d.

At the beginning of the breaching, the breach discharge is so low that no significant effects on the river flow take place (breaching stage 1). As the breach develops, the incoming flow is accelerated, so that the upstream Froude number Fr_u increases. The breach flow is still small during breaching stage 2, because the levee crest is not eroded, and therefore the upstream Froude number Fr_u slightly increases. These effects are relevant when the breaching process speeds up, i.e. during breaching stage 3: the flow gets higher upstream velocities (and thus higher Fr_u) and the breach flow increases.

The river flow changes further during breaching stage 4, and the flow tends to maintain high Fr_u at the upstream section. The downstream Froude number Fr_d depends on the boundary condition: if a uniform flow rating curve is considered, the variation of Fr with the flow rate is negligible and the pattern of the breaching process in the Froude graph is almost vertical. It is worth to notice that, according to this schematization, the higher changes in the discharge ratio (Q_{br}/Q_u) are obtained during the third stage, while the last one deals with a lower and slower increase of the breach flow until the final equilibrium.

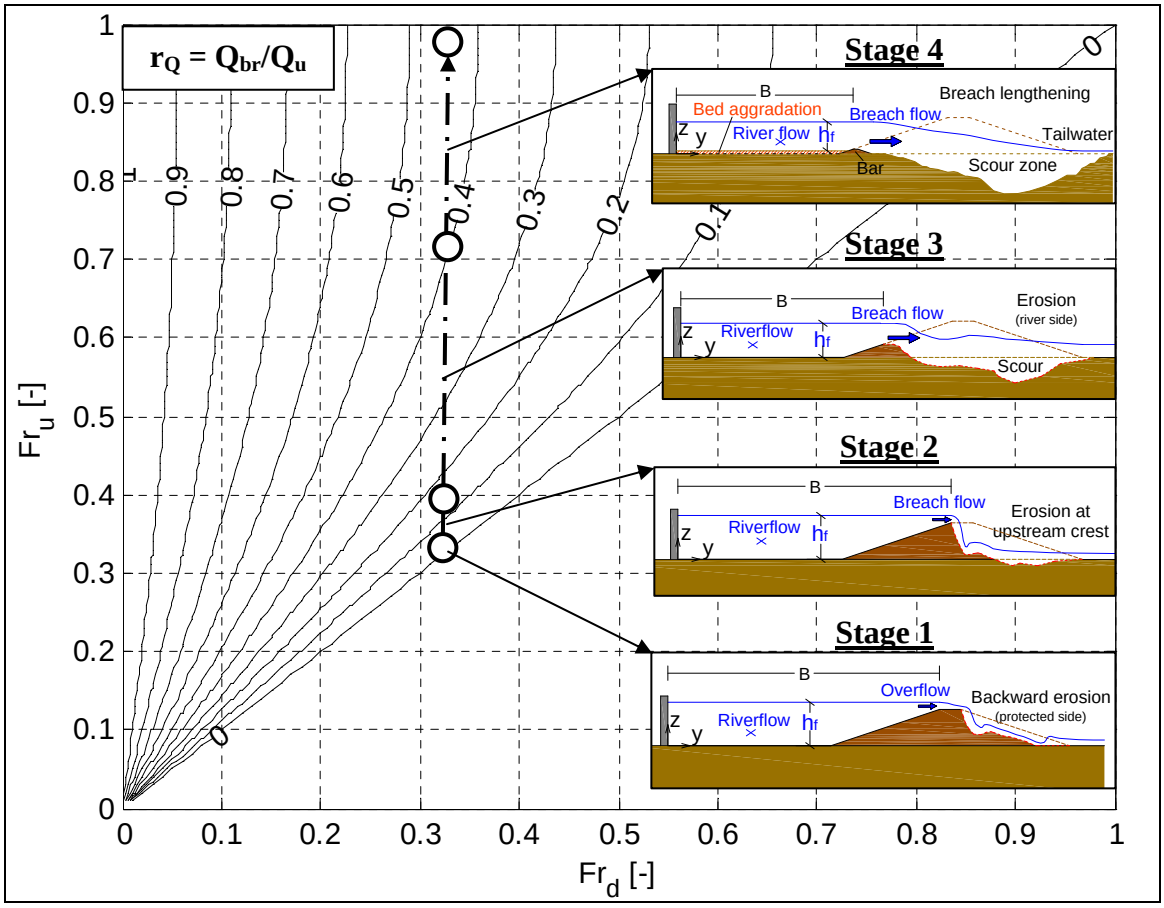

Figure 6.22: Interpretation of the breaching process in the "*Froude graph*" with Q_{br}/Q_u contours.

6.6 Summary and concluding remarks

A conceptual analysis of the levee breaching phenomenon has been considered in this Chapter. The classical four-stages process is reviewed and integrated with the description of the river flow features by means of the analyses given by the **fixed bed experiments**, the **movable bed experiments** and the **analytical model**.

A more complete and process-oriented description of the breaching process in river levees is obtained. The influence of the breach flow on the river hydro-morphodynamics is described in terms of hydraulic variables (as the Froude numbers at the up- and downstream sections) and of morphological modifications (river bed variation at the breach location).

A movable bed straight river channel of constant cross-section is considered, where a uniform flow discharge routes in steady state and subcritical regime. An earthen levee is assumed to delimit one side of the river and an initial overflowing is taken as trigger of the breaching process. No backwater effects from the floodplain into the river are taken into account.

In such conditions, the stage 1 of the breaching process causes an erosion of the protected side of the levee and the river flow is slightly affected by the breach discharge, that is an insignificant portion of the incoming flow Q_u until the levee crest is not lowered. The up- and downstream Froude numbers Fr_u and Fr_d are both almost equal to the initial value Fr_0, which is determined by the flow, the geometry and the boundary conditions acting in the river channel.

The breaching process achieves a critical point at the end of stage 2, when the levee crest is eroded until the river side: from that point on the protected side is directly linked to the river and the erosive action of the water flow encounters lower resistances. The breach channel forms through the levee by means of continuous erosive action and discontinuous mass failures. River flow is slightly affected only in the surface layers, so that breach lengthens both in the up- and downstream directions. Nevertheless, the river flow starts to be accelerated by the outflow "attraction" and the upstream Froude number Fr_u increases to some extent.

It has been explained how the breaching process becomes uncontrolled during the stage 3, due to the interaction between breach development and water flow: the erosion of the levee (mainly deepening and some lengthening) makes more flow discharge to out through the breach. This causes higher erosive actions which increase the breach size and, consequently, the breach flow. Peak erosion rate is detected during this stage.
The disturbance given by the breach flow propagates to the river flow, which is progressively affected by the lateral outflow and the flow field gets 2D features. The upstream zone of the river flow is accelerated toward the breach location, whereas longitudinal flow velocity U_x decreases along the breach toward the downstream zone because of the water spilling. The flow depth profile increases along the breach, due to the subcritical feature of the flow, and the transversal flow velocity U_y tends to increase. As a consequence, the flow deflection angle increases along the breach in the river, and the downstream section of the breach gets a more direct flow action: the breach then lengthens mainly downstream. The overall effect on the river flow is to increase the upstream Froude number Fr_u while the downstream Froude number Fr_d maintains an almost constant value that is given by the downstream boundary condition.

It has been highlighted the mechanism by which the river bed is modified by the flow acceleration. This effect mainly takes place during the stage 4 of the breaching process. The bed material is mobilized from the upstream part because of the increased shear stresses and then it is partially drawn out by the breach (transversal shear stress τ_y) and partially is carried

on in the river channel (longitudinal shear stress τ_x). The material is then deposited around the downstream section of the breach, since the longitudinal shear stress decreases along the breach. This morphodynamic modification results in a negative step of the river bed in the longitudinal direction, from the eroded bed upstream to the aggradated bed downstream, which is found to be strongly correlated with the breach discharge. Three-dimensional effects develop in the river flow because of the significant lateral outflow and they contribute to modify the riverbed morphology.

A final equilibrium is determined as the steady state in which the breach flow is in equilibrium with the incoming flow and the breach lengthens according to smaller erosion rates. The equilibrium values of the breach features are defined in relation with the river features: equilibrium breach flow is found to be in the order of 50% of the incoming flow, whereas the equilibrium breach length has a larger range of variability which anyway is in the order of the flood river width.

The breaching process is summarised in terms of the main breach features (temporal trend of L_{br} and Q_{br}) and of the response of the river in terms of Froude numbers Fr_u and Fr_d (in an original *Froude graph*).

The performed conceptual analysis may be used as framework of the river levee breaching phenomenon both for further scientific research and for engineering practice. In the field of practical applications, it can be extremely useful, for instance, to use the final equilibrium values of discharge ratio r_Q and length ratio r_L in order to preliminary assess the flood scenarios associated with levee breaches in rivers in the context of flood risk mapping.

Anyway, these results are limited to the considered assumptions, whose influence has to be further investigated:

- The analysis of the breaching initiated by piping by means of the same approach used in the overtopping case is recommended. Nevertheless, the last two stages of the breaching process (that are the most important ones in defining the flood consequences) are quite similar in both cases of overtopping and piping breaching, since they are both referred to the complete erosion of the majority of the levee section and to the progressive lengthening of the breach;
- Backwater effects from the floodplain have significant effects on the lateral outflow: they limit the breach flow and, consequently, the final breach length;
- Supercritical flows should be investigated in order to verify if the proposed approach is still valid and to check the existence of a similar equilibrium state.

7 Summary, conclusions and recommendations

7.1 Summary of key results

The key results achieved within the present work by means of two types of laboratory investigations and the analytical model are summarized below.

Fixed bed experiments with a side weir as an imposed breach allowed to investigate the effect of increasing side weir length on the hydraulic features of the flow field in the main channel in the vicinity of a lateral outflow. The increasing side weir length L_s induces the following effects:

- The upstream water level is decreased until the critical depth and velocity increases up to three times the mean velocity;
- The flow regime along the side weir is subcritical and it tends to be supercritical for longer side weirs;
- The downstream boundary condition has a great influence on the flow field in terms of flow regime, flow discharge and flow depth;
- The streamlines are deflected with increasing flow angles toward downstream (noticed by PTV technique and verified by computational analysis);
- Three-dimensional zones of the flow field take place around the outflow (for a length of L_s upstream and $2 \cdot L_s$ downstream): dividing surface, separation zone, helicoidal flow, reverse flow;
- The De Marchi assumption was verified for tests with relative weir lengths $L_s/B \leq 1.1$ and relative lateral discharge $Q_s/Q_u = 0.52$ within an error of ± 10%;
- The flow velocity U_x along the weir decreases by about 50% while the transversal velocity U_y increases;
- The shear stress τ along the weir decreases by more than 50% while the mean shear stress acting on the weir section decreases to an asymptotic low value by one order of magnitude for longer side weirs;
- Both the maximum discharge and momentum ratios (r_Q and r_M) are in the order of 50% – 60% which are reached for the longest weir;
- The upstream Froude number Fr_u increases with the side weir length because of flow acceleration while the downstream Froude number Fr_d slightly increases with the side weir length because of the effect of the downstream sluice gate;
- The aspect ratio of the side weir dramatically decreases.

Movable bed experiments with an initiated breach in a levee made of sand allowed to investigate the breach development and its effect on the evolution of the river sand bed. The following main outcomes were achieved:

- The physical system river-breach reached a steady final equilibrium regarding the water flow balance, and the ratio between the final breach discharge and the inflow discharge was found to be always around 50%;
- The final breach length is linearly governed by the water discharge of the river;

- The flow velocity components and deflection angle trends were found to be in agreement with the fixed bed computational analysis;
- The De Marchi assumption was verified for most of the analysed data (seven over ten tests) within an error of ± 10%;
- The lateral outflow Q_{br} and the river bed modification Δ_{max} were found to be strongly related;
- The main morphodynamic mechanisms observed in the riverbed were: erosion of the bed (upstream the breach site), aggradation of the bed (downstream the breach site), no or few modifications (remaining zone downstream the breach);
- The breach morphology was described as a result of the flow field acting at the up- and downstream breach sections;
- The breach development was found to be asymmetric (mainly directed downstream), with completely different dynamics compared to the dynamics of dam breaches. A physical explanation of such behaviour is given;
- The decreasing of the shear stress acting on the lateral weir is related to the reduction of the breach erosion rate.

An original ***1D analytical hydrodynamic model*** for the river flow along a breach was proposed. The model is based on the theory of side weirs and on the De Marchi hypothesis of constant specific energy head along the lateral outflow. The conventional formulation is rearranged in a new dimensionless form, in which the hydraulic system is described in terms of dimensionless ratios of the flow variables, at the up- and downstream cross sections close to the side weir. The influence of the boundary conditions is made explicit by introducing the dependence of the solution from the flow features at up- and downstream sections, expressed in terms of Froude numbers. By applying the improved model, the following results were obtained:

- A useful, simple and intuitive insight of the hydrodynamics of the river flow along a lateral outflow is provided;
- The longitudinal variation of water depth, flow discharge and flow velocity are well-predicted: the laboratory data (regarding side weirs and lateral diversions) are predicted within an error of ± 10% in terms of flow depth and flow discharge ratios and within an error of ± 20% in terms of length ratio;
- A real levee breach case (Ombrone river 2009) was reproduced within an error of less than ± 10% of the final values of the flow discharge ratio and the length ratio;
- The model was applied to the context of real rivers and it predicts a range of theoretical final values of breach features under the assumption that the flow remains subcritical. The predicted ranges are consistent with the collected real case and laboratory data.

An overall description of the observed phenomena is put together in order to give a conceptual picture of the levee breaching in the key of a process-oriented analysis with a particular focus on the river flow. This analysis integrates the present knowledge about the breaching of river levees, that is currently limited to the case of dam breaches without considering the river flow. The traditional four-stages process is reviewed by adding the description of the hydro-morphodynamics of the river flow.

7.2 Applicability of the results

This research study provides the necessary knowledge about the breaching process of river levees in order to support more realistic and more process-oriented approaches for the assessment of the breach features that can develop in a river levee.

The results from the improved analytical 1D model to the context of real rivers suggest that this research direction is appropriate. Preliminary evaluation of the breach length and the breach outflow can be made on the basis of the river and flow features. The performed analyses (together with the experimental observations) may be very useful to define a criteria for the evaluation of potential water volume that could outflow from the breach in case of failure, based on the theoretical limits found regarding the final length of the breach or the breach discharge. Instead of using statistics of breaches or dam case models, this might represent the first appropriate physical-based simple analytical approach to systematically map the flood hazard for levee breaching phenomena at large spatial scales.

Moreover, the laboratory results provide a sound and unique database for the development and validation of numerical models as well as for further laboratory investigations.

7.3 Future research

The results of the integrated analysis between laboratory experiments in fixed and movable bed and the analytical model are very promising, but they are affected by several limitations (according to the working assumptions) and by data uncertainties (regarding the experimental errors, and, particularly, the real case data) which allow to assess only preliminary outcomes.

As the existence of a steady final equilibrium of the river-breach system is not yet fully demonstrated, future research studies should focus more on the last stage of the breaching process by means of analytical, numerical and physical modelling.

In particular, the flow field observed during the laboratory tests may be further analysed with the proposed analytical model by introducing further new improvements such as:

- Implementation of different river section geometries (e.g., trapezoidal);
- Addition of the effect of movable bed by inserting a predefined modification of the river bed on the basis of the experimental results of Chapter 4;
- Removal of the subcritical flow assumption by investigating further combinations of Froude numbers at the up- and downstream sections.

In addition, the knowledge and data generated can be used for the development of more reliable numerical models which are capable to predict the 2D and 3D features of the flow field.

Moreover, an advanced numerical model for the river levee breaching fully coupled with a model to describe the evolution of the movable river bed should be developed in order to reproduce the asymmetric evolution of the breach and the mutual interaction between breach development and river hydro-morphodynamic evolution up- and downstream of the breach. The laboratory data obtained in the study (see Chapter 4) can be used for a systematic validation of the prospective model, but the final validation must be based on real case data.

The laboratory data collected in this study on the hydro-morphodynamics of the main flow and the erosion mechanisms during a levee breaching process are among the few experimental works on river levee breaches that focus on the specific case of river levees and that investigate the river flow field as main variable. Though detailed results have been achieved

(see Chapter 3 and 4), further laboratory investigations are recommended with both fixed bed with side weir as well as with movable bed and earthen embankment breaching.

Further fixed bed experiments are required in order to:

- Better specify the threshold between the subcritical and the supercritical flow in terms of side weir configuration (length, height) and discharge ratio;
- Define the existence, the location and the type of the hydraulic jump;
- Investigate the influence of the downstream boundary condition on the flow regime, since it highly affects the lateral outflow;
- Study the influence of the tailwater from the lateral channel;
- Set a predefined uniform rating curve as downstream boundary condition;
- Extend the collected data set for other configurations: longer side weirs, higher weir crests, different downstream conditions, further main channel characteristics (inflow, cross section dimensions, bed roughness).

Further movable bed experiments are necessary in order to verify the findings of the tests conducted with a single levee configuration, especially those related to the equilibrium value of the breach discharge over the river discharge ratio, for the following conditions:

- Different geometry and size of the levee model (side slopes, crest width, levee height, …);
- Different construction material for the levee model: cohesive material and a mix of cohesive and non-cohesive sediments;
- Geometry of the main channel with different width and, possibly, levee breach model in curved channel;
- Influence of the tailwater from the lateral channel;
- Removal of the vertical constraint in order to lead the breach to deepen freely;
- Influence of different downstream boundary conditions and a setting useful to impose a uniform rating curve;
- Setting of different inputs of solid discharge in order to study the influence of the sediment transport processes on the levee breaching (along main channel and through the breach);
- Different distances between the multiple breaches in order to study their interaction and the existence of a critical distance which can make one breach independent to the other.

References

Andrews, D.P., Coleman, S.E., Webby, M.G., and Melville, B.W. (1999). Noncohesive embankment failure due to overtopping flow. Proc., 28th Congress of the Int. Association for Hydraulic Research, Graz, Austria, 7.

Bechi, G. (2008). Numerical Modeling and Experimental Research on Side Weir Overflow. PhD Thesis. Engineering Faculty of Florence University.

Bélanger, J.B. (1849). Notes sur le Cours d'Hydraulique. (Notes on the Hydraulics Subject) Mém. Ecole Nat. Ponts et Chaussées (Paris, France).

Bligh, W.G. (1927). The Practical Design of Irrigation Works. Van Nostrand Co., New York.

Bonanni, Carli, Casarosa, Ceragioli, Dell'Aiuto, Della Maggesa, Forti, Matteoni, Pannocchia, and Sardi (2010). La rotta arginale del Serchio a Malaventre (frazione di Nodica) nel giorno di Natale 2009. Il Geologo, Periodico d'informazione dell'Ordine dei Geologi della Toscana, ANNO XXI - N. 79 marzo 2010.

Bor, A. (2008). Numerical modeling of unsteady and non-equilibrium sediment transport in rivers. A Thesis Submitted to The Graduate School of Engineering and Sciences of İzmir Institute of Technology.

Borghei, S.M., Jalili, M.R., and Ghodsian, M. (1999). Discharge coefficient for sharp-crested side weirs in subcritical flow. J. Hydraul. Eng., 125(10), 1051–1056.

Britton, Hanson, Cook, and Kadavy (2004). Breach Widening Observations from Earthen Embankment Tests. ASAE/CSAE Annual International Meeting.

Burchielli, S. (2010). Gli eventi del 25/12/2010 sul fiume Ombrone. Giornata di studio "Strutture arginali: vulnerabilità, monitoraggio, sicurezza". Firenze, 16/06/2010.

Chanson, H. (2004). The Hydraulics of Open Channel Flow: An Introduction. Butterworth-Heinemann, Oxford, UK, 2nd edition.

Chinnarasri, Tingsanchali, Weesakul, and Wongwises (2003). Flow Patterns and Damage of Dike Overtopping. International Journal of Sediment Research.

Chow, V.T. (1959). Open-Channel Hydraulics. McGraw-Hill, Inc.

Coleman, Andrews, and Webby (2002). Overtopping Breaching of Noncohesive Homogeneous Embankments. Journal of Hydraulic Engineering.

Covelli, C. (2006). Sulla formazione di brecce nei rilevati arginali: implicazioni relative alla protezione idraulica del territorio. PhD thesis, Università degli Studi di Napoli Federico II.

D'Eliso, C. (2007). Breaching of sea dikes initiated by wave overtopping. A tiered and modular modelling approach. PhD thesis in "Risk management on built environment".

De Marchi, G. (1934). Saggio di teoria di funzionamento degli stramazzi laterali. L'Energia Elettrica, 11, 849–860.

Dingman, S.L. (2009). Fluvial Hydraulics. Oxford University Press.

EXCIMAP (2007). Handbook on good practices for flood mapping in Europe. European exchange circle on flood mapping, available at:
http://ec.europa.eu/environment/water/flood_risk/flood_atlas/index.htm, 2007.

European Commission (2010). Risk assessment and mapping guidelines for disaster management. Commission Staff Working Paper, Brussels, 21.12.2010, SEC(2010) 1626 final.

El-Khashab, A., and Smith, K.V.H. (1976). Experimental investigation of flow over side weirs. J. Hydr. Div., ASCE, 102(9), 1255–1268.

Emiroglu, M.E., Agaccioglu, H., and Kayaa, N. (2011). Discharging capacity of rectangular side weirs in straight open channels. Flow Measurement and Instrumentation 22 (2011), 319–330.

Faeh, R. (2007). Numerical modeling of breach erosion of river embankments. Journal of Hydraulic Engineering, 133(9), 1000–1009.

Fell, Wan, Cyganiewicz, and Foster (2003). Time for Development of Internal Erosion and Piping in Embankment Dams. Journal of Geotechnical and Geoenvironmental Engineering.

Fell, R., and Wan, C.F. (2005). Methods for Estimating the Probability of Failure of Embankment Dams by Internal Erosion and Piping in the Foundation and from Embankment to Foundation. The University of New South Wales.

Foster, M.A., Fell, R., and Spannangle, M. (2000). The Statistics of Embankment Dam Failures and Accidents. Canadian Geotechnical Journal, Vol. 37, No. 5, pp. 1000-1024.

Fritz, H.M., and Hager, W.H. (1998). Hydraulics of Embankment Weirs. ASCE Journal of Hydraulic Engineering, Vol, 124, No. 9, pp. 963-971.

Froehlich, (2008). Embankment Dam Breach Parameters and Their Uncertainties. Journal of Hydraulic Engineering, ASCE.

Fujita, Y., and Tamura, T. (1987). Enlargement of Breaches in Flood Levees on Alluvial Plains. Journal of Natural Disaster Science, Vol. 9, No. 1, pp. 37-60.

Gilbert, P.A., and Miller, S.P. (1989). A Study of Embankment Performance During Overtopping. Technical Report GL-91-23, U.S. Army Corps of Engineers, Engineering Research and Development Center, 96 pp.

Gouldby, B.P., and Samuels, P.G. (2009). Language of risk: project definitions. FLOODsite Report T32-04-01.

Grant, G.E. (1997). Critical flow constrains flow hydraulics in mobile-bed streams: A new hypothesis. Water Resour. Res., 33(2), 349–358, 1997.

Hager, W.H. (1982). Die hydraulik von verteilkanälen. Teil 1-2, Mitteilungen der Versuchsanstalt für Wasserbau, Hydrologie und Glaziologie, No. 55-56, Zurich, Switzerland.

Hager, W.H., and Volkert, P.U., (1986). Distribution Channels. Journal of Hydraulic Engineering, ASCE, Vol. 112, No. 10, 1986, 935-952.

Hager, W.H. (1987). Lateral outflow over side weirs. J. H. Eng., ASCE, 113(4), 491–504.

Hahn, W., Hanson, G., and Cook, K.R. (2000). Breach Morphology Observations of Embankment Overtopping Tests. Proceedings of the 2000 Joint Conference on Water Resour Eng and Water Resour Plan & Manag, USA, Minneapolis, Minnesota, 2000.

Hanson, G.J., Cook, K.R., Hahn, W., and Britton, S.L. (2003a). Observed erosion processes during embankment overtopping tests. ASAE Paper No. 032066. ASAE St. Joseph, MI.

Hanson, G.J., Cook, K.R., Hahn, W., and Britton, S.L. (2003b). Evaluating Erosion Widening and Headcut Migration Rates for Embankment Overtopping Tests. 2003 ASAE Annual International Meeting.

Hanson, G.J, Cook, K.R., and Hunt, S.L. (2005). Physical Modeling of Overtopping Erosion and Breach Formation of Cohesive Embankments. Transactions of ASAE, Vol. 48, No. 5, pp 1783-1794.

Hanson, G.J. and Hunt, S.L. (2007). Lessons learned using laboratory jet testing method to measure soil erodibility of compacted soils. Journal of applied engineering in agriculture (ASABE), Vol. 23 (No. 3), pp. pp. 305-312.

Hanson, G.J., Robinson, K.M., and Cook, K.R. (2001). Prediction of headcut migration using a deterministic approach. Trans. ASAE 44(3): 525-531.

Hassan, Morris, Hanson, and Lakhal (2004). Breach formation: Laboratory and numerical modelling of breach formation. Association of State Dam Safety Officials Dam Safety Conference, 2004, Phoenix, Arizona, US, September 2004, 2004.

Horlacher, H.B., Bielagk, U., and Heyer, T. (2005). Analyse der Deichbrüche an der Elbe und Mulde während des Hochwassers 2002 im Bereich Sachsen. Research report 2005/09, Institut für Wasserbau und Technische Hydromechanik, Technische Universität Dresden, 82 pp.

Hsu, C.C., Tang, C.J., Lee, W.J., and Shieh, M.Y. (2002). Subcritical 90° equal-width open channel dividing flow. J Hydraul Eng, ASCE 2002; 128(7): 716–20.

IMPACT, (2001). Investigation of extreme flood processes and uncertainty.

IMPACT, (2004). Identifying Potential Breach Location.

International Federation of the Red Cross and Red Crescent (IFRC/RC) (2010). World Disasters Report 2010. Geneva 2010.

Islam, M.S., Okubo K., Muramoto, Y., and Morikawa, H. (1994). Experimental Study on Sedimentation over the Floodplain due to River Embankment Failure. Bulletin of the Disaster Prevention Research Institute, Kyoto University, 1994; 44:2, p. 69-92.

Islam, M.S., and Tsujimoto, T. (2011). Characteristics of Flood Disasters in Low Floodplain Along a Big River Due to Overflow Levee Breach. Int. J. of GEOMAT, Oct. 2011, Vol. 1, No. 1 (Sl. No. 1), pp., 56-63.

Islam, M.S. (2012). Study on levee breach and successive disasters in low-land through numerical and experimental approaches. PhD thesis. Nagoya university (Japan). http://hdl.handle.net/2237/17336.

Islam, M.S., and Tsujimoto T. (2012). Comparisons of Levee Breach and Successive Disasters in Floodplain between Bangladesh and Japan. International Conference on Modern Hydraulic Engineering.

Jalili, M.R., and Borghei, S.M. (1996). Discussion of 'Discharge coefficient of rectangular side weirs,' by Singh, Manivannan and Satyanarayana. J. Irrig. and Drain. Engrg., ASCE, 122(2),132.

Jonkman, S.N., and Vrijling J.K. (2008). Loss of life due to floods. J. Flood Risk Manage 2008; 1(1):43–56. http://dx.doi.org/10.1111/j.1753-318X.2008.00006.x.

Kamrath, P., Disse, M., Hammer, M., and Koengeter, J. (2006). Assessment of Discharge through a Dike Breach and Simulation of Flood Wave Propagation. Nat. Hazards 38, 63–78.

Khilar, K.C., Folger, H.S., and Gray, D.H. (1985). Model for piping-plugging in earthen structures. J. Geotech. Engrg., ASCE, 111(7), 833–846.

Lane, E.W. (1935). Security from Underseepage: Masonary Dams on Earth Foundation. Transactions ASCE, Vol. 100, pp. 1235-1272.

Liu, Z. (2001). Sediment transport.

Loat, R. (2009). Flood mapping in Europe – EXCIMAP. UNECE workshop on transboundary flood risk management. Geneva.

Macchione, and Rino (1999). Prediction capabilities of a simplified dam-breach model. Conference "Proceedings of the European Concerted Action of Dam-Break Modelling", Milan, 6-7 May, 1999.

MacDonald, T.C., and Langridge-Monopolis, J. (1984). Breaching Characteristics of Dam Failures. ASCE Journal of Water Resources, Vol. 110, No. 5, pp. 567-586.

May, R.W.P., Bromwich, B.C., Gasowski, Y., and Rickard, C.E. (2003). Hydraulic design of side weirs. Thomas Telford Publishing, London: p. 133.

Michelazzo, G. (2013). River Levee Breaching: Fixed Bed Laboratory Investigations. Internal report at Department of Civil and Environmental Engineering, University of Florence, Italy.

Michelazzo, G., and Oumeraci, H. (2013). River Levee Breaching: Movable Bed Laboratory Investigations. Berichte Leichtweiß-Institut für Wasserbau, Technische Universität Braunschweig, Nr. 1039, Braunschweig, Germany.

Mohamed A.A. Mohamed, Samuels, P.G., and Morris, M.W. (2002). Improving the Accuracy of Prediction of Breach Formation through Embankment Dams and Flood Embankments. Proc. of Int. Conf. On Fluvial Hydraulics, Louvain-la-Neuve, Belgium, 2002.

Montes, S. (1998). Hydraulics of open channel flow. Reston: ASCE Press, c1998.

Morris, M. (2009a). Breach initiation and growth: Physical processes. FLOODsite.

Morris, M. (2009b). Breaching Processes: A state of the art review. FLOODsite.

Morris, M. (2009c). Modelling Breach Initiation and Growth. FLOODsite.

Morris, Dyer, and Smith (2007). Management of flood embankments. A good practice review. Defra/Environment Agency.

Mous, B.C. (2010). Wave impact on grass covered outer slopes. MSc-thesis, Delft, Faculty of Civil Engineering & Geosciences.

Muslu, Y. (2001). Numerical analysis for lateral weir flow. J. Irrig. Drain. Eng., 127(4), 246–253.

Muslu, Y., Tozluk, H., and Yüksel, E. (2003). Effect of lateral water surface profile on side weir discharge. Journal of Irrigation and Drainage Engineering 129(5): 371–375.

Nagy, L. (2006). Estimating Dike Breach Length from Historical Data. Periodica Polytechnica, Serial Civil Engineering, Vol. 90, No. 2, pp. 125-139.

Nagy, L., and Tóth, S. (2005). Detailed technical report on the collation and analysis of dike breach data with regards to formation process and location factors. EU-IMPACT-Projekt, H-EURAua Ltd.

Neary, V.S., and Odgaard, A.J. (1993). Three-dimensional flow structure at open channel diversions. J. Hydr. Engrg., ASCE, 119(11), 1224–1230.

Neary, V.S., Sotiropoulos, F., and Odgaard, A.J. (1999). Three-dimensional numerical model of lateral-intake inflows. J. Hydraul. Eng., 125(2), 126–140.

Oertel, M., Carvalho, R.F., and Jansen, R.H.A. (2011). Flow over a rectangular side weir in an open channel and resulting discharge coefficients. Proceedings of the 34th World Congress of the International Association for Hydro-Environment Research and Engineering: 33rd Hydrology and

Water Resources Symposium and 10th Conference on Hydraulics in Water Engineering, Brisbane, Australia.

Ojha, Singh, and Adrian (2001). Influence of Porosity on Piping Models of Levee Failure. Journal of Geotechnical and Geoenvironmental Engineering.

Ozkan, S. (2003). Analytical Study on Flood Induced Seepage under River Levees. PhD thesis. Louisiana State University.

Paquier (2002). Sediment transport models used by Cemagref during Impact project. IMPACT Project.

Paris E., Solari, L., and Bechi, G. (2012). On the applicability of the De Marchi hypothesis for Side Weir Flow in the case of Movable Beds. Journal of Hydraulic Engineering. submitted May 2, 2011, accepted January 18, 2012, print January 20, 2012.

Pavlovsky, N.N. (1931). Seepage through earth dams. Instit. Gidrotekhnikii Melioratsii, Leningrad.

Powledge, G.R., Ralston, D.C., Miller, P., Chen, Y.H., Clopper, P.E., and Temple, D.M. (1989). Mechanics of Overflow Erosion on Embankments. II: Hydraulic and Design Considerations. ASCE Journal of Hydraulic Engineering, Vol. 115, No. 8, pp. 1056-1075.

Preissler, G., and Bollrich, G. (1980). Technical Hydromechanics. VEB, Berlin.

Preti, F., Paris, E. and Settesoldi, D. (1996). Evento alluvionale del 19 giugno 1996 in Versilia-Garfagnana: ricostruzione degli idrogrammi di piena. In: Convegno scientifico in occasione del trentennale dell'alluvione di Firenze: "La difesa dalle alluvioni"., Firenze, Italia, 4-5 novembre 1996, pp. 341-354.

Pugh, C.A. (1985). Hydraulic model studies of fuse plug embankments. REC-ERC-85-7. Bureau of Reclamation, D., Colarado.

Ranga Raju, K.G., Grupta, S.K., and Prasad, B. (1979). Side weir in rectangular channel. J. Hydr. Div., ASCE, 105(5), 547–554.

Regazzoni, P.L., Marot, D., Courivaud, J.R., Hanson, G., and Wahl, T. (2008). Soils Erodibility: A Comparison between the Jet Erosion Test and the Hole Erosion Test. Inaugural International Conference of the Engineering Mechanics Institute, Minneapolis, MN May 18-21, 2008.

Roger, S., Dewals, B.J., Erpicum, S., Schwanenberg, D., Archambeau, P., Köngeter, J., Pirotton, M., and Schüttrumpf, H. (2010). Hybrid modelling of dike-break induced flows. River Flow 2010, International Conference on Fluvial Hydraulics, Germany, Sep. 8-10, 2010.

Rosier, B. (2007). Interaction of a side weir overflow with bed-load transport and bed morphology in a channel. PhD Thesis, 3872, Ecole Polytechnique Fédérale de Lausanne EPFL, Switzerland.

Rosier, B., Boillat, J.L., and Schleiss, A.J., (2008). Outflow angle for side weirs in a channel with mobile bed at flood discharges. INTERPRAEVENT 2008 – Conference Proceedings, Vol. 1.

Saucier, Howard, and Tom (2009). Levee breach geometries and algorithms to simulate breach closure. U.S. Department of Homeland Security.

Sherard, J.L., Woodward, R.J., Gizienski, S.F., and Clevenger, W.A. (1963). Earth and Earth-Rock Dams. Engineering Problems of Design and Construction. John Wiley and Sons, Inc., NY.

Shields, A. (1936). Application of Similarity Principles and Turbulence Research to Bed-Load Movement. California Institute of Technology. Pasadena.

Shimada, T., and Yokoyama, H. (2011). Process of levee breach by overflow at the full scale Chiyoda experimental channel. American Geophysical Union, Fall Meeting 2011.

Silva-Araya, Alva-Solari, and Chaudhry (2010). Experimental Study of Levee Breach. 21st Century Watershed Technology: Improving Water Quality and Environment.

Singh, R., Manivannan, D., and Satyanarayana, T. (1994). Discharge coefficient of rectangular side weirs. J. Irrig. and Drain. Engrg., ASCE, 120(4), 814–819.

Singh, V.P. (2003). On the theories of hydraulic geometry. International Journal of Sediment Research, 18 (3), 2003, pp. 196-218.

Stanczak, G. (2008). Breaching of sea dikes initiated from the seaside by breaking wave impacts. Ph.D. thesis, Dissertation, Civil Engineering Faculty, Leichtweiß-Institut für Wasserbau, Technische Universität Braunschweig, University of Florence, 143 p.

Subramanya, K., and Awasthy, S.C. (1972). Spatially Varied Flow over Side Weirs. Journal of the Hydraulics Division, ASCE, Vol. 98, No. 1, 1972, 1-10.

Temple, D.M. (1992). Estimating flood damage to vegetated deep soil spillways. Applied Eng. in Agric. 8(2): 237-242.

Temple, D.M., Hanson, G.J., Neilsen, M.L. and Cook, K.R. (2005). Simplified breach analysis model for homogeneous embankments: Part 1, Background and model components. 25th Annual USSD Conference, Salt Lake City, Utah, USA, 6-10 June 2005, 2005.

Terzaghi, K. (1929). Effect of Minor Geologic Details on the Safety of Dams. Bulletin of American Institute of Mining and Metallurgical Engineers, Technical Publication 215, Class I, Mining Geology, No. 26, pp. 31-46.

Van Zyl, D., and Harr, M.E. (1981). Seepage Erosion Analysis of Structures. Proceedings of the Tenth International Conference on Soil Mechanics and Foundation Engineering, 15-19 June 1981, Stockholm, Part I, A.A. Balkema Publishers, The Netherlands, pp. 503-509.

Verheij, H. (2002). Time Dependent Breach Development in Cohesive Material. Internal Research Summary Report, Delft Hydraulics Laboratory.

Viero, D.P., D'Alpaos, A., Carniello, L. and Defina, A. (2012). Un modello idrodinamico accoppiato per la simulazione di rotte arginali in contesti fluviali. XXXIII Convegno Nazionale di Idraulica e Costruzioni Idrauliche, Brescia, 10-15 settembre 2012.

Viero D.P., D'Alpaos, A., Carniello, L., and Defina, A. (2013). Mathematical modeling of flooding due to river bank failure. Advances in Water Resources, 59, 82-94, doi:10.1016/j.advwatres.2013.05.011.

Visser, P.J. (1995). Application of sediment transport formulas to sand-dike breach erosion. Delft University of Technology, Delft, The Netherlands.

Visser, P.J. (1998). Breach growth in sand dikes. PhD Thesis. Delft University.

Von Thun, J.L., and Gillette, D.R. (1990). Guidance on Breach Parameters. Internal Technical Memorandum, United States Bureau of Reclamation, Denver, Colorado, pp.17.

Vorogushyn, S. (2008). Analysis of flood hazard under consideration of dike breaches. Dissertation Thesis. Mathematisch-Naturwissenschaftlichen Fakultät der Universität Potsdam.

Wahl, T.L. (1998). Prediction of embankment dam breach parameters, a literature review and needs assessment. Rep. No. DSO-98-004, Bureau of Reclamation, U.S. Department of the Interior, Denver, 60.

Wahl, T.L. (2004). Uncertainty of Predictions of Embankment Dam Breach Parameters. Journal of Hydraulic Engineering.

Wahl, Hanson, Courivaud, Morris, Kahawita, Mcclenathan, and Gee (2008a). Development of next-generation embankment dam breach models.

Wahl, Regazzoni, and Erdogan (2008b). Determining Erosion Indices of Cohesive Soils with the Hole Erosion Test and Jet Erosion Test. U.S. Dept. of the Interior, Bureau of Reclamation.

Xu, Y., and Zhang, L.M. (2009). Breaching Parameters for Earth and Rockfill Dams. Journal of Geotechnical and Geoenvironmental Engineering.

Yen, B.C. (2002). Open channel flow resistance. J. Hydraulic Engng. 128 (1), 20–39.

Yüksel, E. (2004). Effect of specific energy variation on lateral overflows. Flow Meas. Instrum., 15(5–6), 259–269.

Zech, Frazão, Spinewine and Grelle (2004). Dam-break induced flood modelling and sediment movement. IMPACT WP4 final scientific report.

Zenno, H., Iwasaki, T., Shimizu, Y., and Kimura, I. (2011). Computations of real scale experiment on levee breach with a 2D shallow flow model. Proceedings of the 34th World Congress of the International Association for Hydro- Environment Research and Engineering: 33rd Hydrology and Water Resources Symposium and 10th Conference on Hydraulics in Water Engineering. Barton, A.C.T.: Engineers Australia, 2011: 491-498.

Zhu, Y. (2006). Breach growth in clay dikes. Delft University of Technology, Delft, The Netherlands. PhD.

Annex A
Mathematical demonstration of the proposed analytical model

The dimensionless ratios presented in Section 5.2 describe the flow features of the side weir along a main channel of width B as a function of the up- and downstream flow conditions expressed by the relative Froude numbers. They result from the governing principles of conservation of the mass, the constancy of the specific energy head (according to the De Marchi hypothesis) and the De Marchi equation for lateral weirs.

In particular, the specific energy head E is written as:

$$E = Y\left(\frac{Y}{Y} + \frac{U^2}{2gY}\right) = Y\left(1 + \frac{Fr^2}{2}\right) \tag{A1}$$

The balance of the specific energy head E along the weir gives:

$$E_u = E_d \longrightarrow \frac{Y_u}{2}\left(2 + {Fr_u}^2\right) = \frac{Y_d}{2}\left(2 + {Fr_d}^2\right) \longrightarrow r_Y = \frac{Y_d}{Y_u} = \frac{2 + {Fr_u}^2}{2 + {Fr_d}^2} \tag{A2}$$

Moreover, the flow discharge is a function of the constant specific energy head E^*:

$$E^* = Y + \frac{Q^2}{2g(BY)^2} \longrightarrow Q = BY\sqrt{2g\left(E^* - Y\right)} \xrightarrow{2\left(E^* - Y\right) = Y \cdot Fr^2} Q = B\sqrt{g} \cdot Fr \cdot Y^{3/2} \tag{A3}$$

From the continuity principle it results:

$$Q_s = Q_u - Q_d \longrightarrow r_Q = \frac{Q_s}{Q_u} = 1 - \frac{Q_d}{Q_u} = 1 - \frac{B\sqrt{g} \cdot Fr_d \cdot {Y_d}^{3/2}}{B\sqrt{g} \cdot Fr_u \cdot {Y_u}^{3/2}} = 1 - \frac{Fr_d}{Fr_u} \cdot {r_Y}^{3/2} \tag{A4}$$

The length ratio is finally determined from equations 5.6:

$$r_L = \frac{L_s}{B} = \frac{\Phi_d - \Phi_u}{C_d} \tag{A5}$$

where the Φ function is:

$$\Phi(E, Y, p_s) = \frac{2E - 3p_s}{E - p_s}\sqrt{\frac{E - Y}{Y - p_s}} - 3\sin^{-1}\sqrt{\frac{E - Y}{E - p_s}} \tag{A6}$$

which, in the case of zero height crest (p_s = 0), can be expressed in terms of Froude number:

$$\Phi(E/Y) = 2\sqrt{\frac{E}{Y} - 1} - 3\sin^{-1}\sqrt{\frac{E/Y - 1}{E/Y}} \xrightarrow{E/Y = 1 + Fr^2/2} \Phi = Fr\sqrt{2} - 3\sin^{-1}\left(Fr\sqrt{\frac{1}{2 + Fr^2}}\right) \tag{A7}$$